ZIC2 TO *ALX1:* GENETIC REGULATORS FOR VERTEBRATE CRANIOFACIAL AND OCULAR MORPHOGENESIS

By

Baul Yoon

A dissertation submitted in partial fulfillment of

the requirements for the degree of

Doctor of Philosophy

(Genetics)

at the

UNIVERSITY OF WISCONSIN-MADISON

2020

Date of final oral examination: December 3, 2020

Final Oral Committee:

Yevgenya Grinblat, Associate Professor, Departments of Integrative Biology and Neuroscience

Francisco Pelegri, Professor, Department of Genetics

Antony Stretton, Emeritus Professor, Department of Integrative Biology

Xuehua Zhong, Associate Professor, Cellular and Molecular Biology Graduate Program

Acknowledgements

I thank my family members for their unconditional love and support to help and guide me during my PhD work.

Thanks to my wonderful PI, Jenya Grinblat, who has been mentoring me to be a successful scientist and expansively supporting my future career.

Thank you very much for the past and current members of the Grinblat lab – Nick Santistevan, Lauren Bluhm, Irina Sedykh, Fernando De la Torre, Carol Xu, Rosemary Rogers, Lindsey Toetz, and Ariel Cyrus – who have helped on my project. I also thank to Halloran lab members for supplying of reagents and helpful feedback and Liao lab members from the Harvard Medical School for collaboration and excellent discussions.

Thank you to my committee members Akihiro Ikeda, Francisco Pelegri, Antony Stretton, and Xuehua Zhong for their support and constructive feedback over the years.

I truly thank to campus community church members who have been constantly supporting and praying for me.

Lastly, I am deeply thankful to God who has provided me everything and given me the strength to finish my PhD work.

Table of Contents

Chapter I

Introduction

1. A brief overview of forebrain development/HPE

Vertebrate telencephalon can be generalized into two subdivisions, dorsally located pallium and ventral subpallium. Pallium and subpallium are both derived from the dorsal plate of the neural tube and give rise to cerebral cortex and basal ganglia, respectively (Grinblat and Lipinski, 2019; Moreno et al., 2009). The pallium changes its shape resulting in the formation of two lateral ventricles, which will become two cerebral hemispheres. Morphological change of the pallium is accomplished through a deep invagination of the dorsal telencephalic midline (Grinblat and Lipinski, 2019). The correct formation of the medial forebrain, a process highly susceptible to genetic and environmental factors, is required for central nervous system and craniofacial development.

In humans, holoprosencephaly (HPE) is the most common congenital forebrain malformation. HPE results from an incomplete division of the forebrain into two hemispheres. The incidence of HPE in living births and stillbirths is rare (1 in 10,000-20,000) but in conceptuses is prevalent (1 in 250) (Muenke and Beachy, 2000). Most HPE patients with cerebral defects also have retinal and/or craniofacial defects to various degrees, ranging from nothing abnormal besides development of a single incisor at the midline (mild) to facial clefts and cyclopia (severe). In many cases, HPE patients do not have neuroanatomic anomalies but have craniofacial defects, such as coloboma and facial cleft (coined as microform HPE) (Kruszka et al., 2015). Several studies have identified HPE-associated genes in humans and animal models; among these, mutations in *SHH,* sonic hedgehog, are the most common and mutations in *ZIC2*, a zinc-finger transcription factor, *SIX3*, a homeobox-containing gene, and *TGIF*, a homeobox transcription factor, are also commonly associated with HPE (Dubourg et

al., 2007; Kruszka et al., 2018; Nanni et al., 1999). Although *SHH*, *ZIC2*, *SIX3*, and *TGIF* are known to be common gene targets of mutations associated with HPE, the majority of cases in HPE patients do not have identified mutations (Dubourg et al., 2007; Dubourg et al., 2004; Roessler and Muenke, 2010). This suggests that the etiology of HPE is highly heterogenous, likely resulting from a combination of multiple environmental and/or genetic factors that have not been characterized.

2. Hh signaling

As *Hh* is the most common HPE-associated signaling pathway and HPE emerges with ventral midline malformation, ocular, and craniofacial defects, it is important to understand how an early source of Hh signaling contributes to the development of the craniofacial complex, which consists of the forebrain, eyes, and craniofacial cartilages. The subsequent sections focus on the role of Hh signaling for craniofacial complex development.

2.1 Hh signaling for medial forebrain development

In early embryos, the ventral midline formation is initially regulated by *Hh* secreted from axial mesendoderm, including the prechordal plate (PrCP) (Blaess et al., 2014; Chiang et al., 1996; Dale et al., 1997; Sagai et al., 2019). Removal of PrCP results in a failure of formation of cerebral and facial structures formed in the ventral midline, including the medial forebrain, reminiscent of human HPE (Aoto et al., 2009; Muenke and Beachy, 2000). A recent study has identified the novel forebrain enhancer (named SBE7), which regulates *Hh* expression in both ventral midline of the forebrain

and PrCP from mouse embryos. Mutations in SBE7 sequence cause abnormalities in the ventral midline of the forebrain similar to human HPE (Sagai et al., 2019). These studies suggest that PrCP is required for ventral midline specification.

Previous findings characterized that Hh signaling from PrCP contributes to ventral midline specification through inducing rostral diencephalic ventral midline, including hypothalamus, which serves as a secondary Hh signaling center (Dale et al., 1997; Szabo et al., 2009; Vieira et al., 2005; Zhao et al., 2012). *Hh* gradient produced from the hypothalamus is required for patterning anterior-posterior axis in the ventral midline of the hypothalamus (Zhao et al., 2012). SBE7, an upstream regulatory element of PrCP, and SBE2, an upstream regulatory element of the hypothalamus, are two transcriptional enhancers identified at the *Hh* locus that specifically mediate *Hh* expression in rostral brain (Jeong et al., 2008; Sagai et al., 2019; Zhao et al., 2012). SBE2 contains transcription binding sites for *sox2*, *sox3*, *six3*, and *six6*, which are required for *Hh* transcription in the hypothalamus (Jeong et al., 2008; Zhao et al., 2012). While the majority of HPE patients do not have mutations in the coding regions of HPE-associated genes, it is possible that the activity of brain enhancers is altered in some HPE patients which resulted from a poor binding of transcription factors at enhancers. Thus, it is important to investigate potential transcription binding sites in *Hh* enhancers further for understanding the molecular regulation of early Hh signaling from PrCP and hypothalamus and the etiology of HPE.

2.2 Hh signaling for eye morphogenesis

In vertebrates, eye morphogenesis begins when neural retina evaginates from the forebrain and is shaped into bilayered optic cups (Chow and Lang, 2001;

Fuhrmann, 2010). The optic cups are transiently connected with the medial forebrain via the optic stalk (Morcillo et al., 2006). Early Hh signaling from PrCP and later from the hypothalamus is required for establishing the optic stalk during ocular morphogenesis (Chiang et al., 1996; Masai et al., 2000; Zhao et al., 2012). Neural retina Hh-dependent activation of *pax2* in the optic stalk and repression of *pax6* in the retina is the main step of this process (Chiang et al., 1996; Ekker et al., 1995; Macdonald et al., 1995; Zhao et al., 2012). Loss of Hh signals from either PrCP or the hypothalamus results in reduced *pax2* induction, which in turn causes abnormal optic stalk formation (Aoto et al., 2009; Chiang et al., 1996; Zhao et al., 2012). At this point, the questions of why the restricted patterning of Hh signaling targets, such as *pax2* at the optic stalk and *pax6* at the retina, is required during ocular development and where *Hh* acts during this process need to be addressed.

Early Hh signaling for optic stalk formation is critical for the formation of hyaloid vasculature, which is required for retinal angiogenesis (Evans and Gage, 2005; Gage et al., 2005; Skarie and Link, 2009), because the optic stalk guides hyaloid vessel entry through the choroid fissure (Morcillo et al., 2006; Tao and Zhang, 2014). Once the hyaloid vessel enters, it starts to form the hyaloid loop around the lens and further branches within the lens to form the hyaloid network (Hartsock et al., 2014). *Hh* is required for formation of the hyaloid loop at the ventral surface of the lens through promoting vascular endothelium growth factor (VEGF)-mediated angiogenesis (Weiss et al., 2017). During retinal vasculature angiogenesis, *Hh* regulates vascular integrity through organizing tight junction proteins that stabilize retinal vasculature (Diaz-Coranguez et al., 2017) and contributes to forming a blood-retinal barrier (Pollock et al., 2020). Whether *Hh* contributes to hyaloid and retinal vasculature development

directly or indirectly is currently unknown.

Previous studies in Xenopus and zebrafish embryos show an early requirement of Hh signaling from the ventral midline for the development of anterior segment of the eyes (anterior segment), such as cornea and lens. In Xenopus, overexpression (Cornesse et al., 2005) or inhibition (Sasagawa et al., 2002) of Hh signaling results in abnormal lens formation. Likewise, in zebrafish, overexpression (Barth and Wilson, 1995; Ekker et al., 1995) or inhibition of Hh signaling shown in *cyclop* mutants (Ekker et al., 1995), *gli2* mutants (Karlstrom et al., 1999; Kondoh et al., 2000), and *smo* mutants (Dutta et al., 2005; Varga et al., 2001) results in aberrant lens formation. Interestingly, anterior pituitary placode derived from anterior neural ridge (Dutta et al., 2005; Eagleson et al., 1995), which serves as a telencephalic organizer that restricts *Hh* to ventral forebrain (Creuzet et al., 2006; Le Douarin et al., 2012), ectopically differentiates into lens in zebrafish *gli2* mutants and *smo* mutants (Dutta et al., 2005; Kondoh et al., 2000), suggesting that Hh signaling is required for restricting the anterior segment from the ventral forebrain.

Hh is also secreted from the retinal pigmented epithelium and retinal ganglion cells of the developing retina; however, unlike the early source of *Hh* secreted from PrCP and the hypothalamus, *Hh* from developing retina likely contributes to later eye morphogenesis. In the retina, *Hh* from retinal pigmented epithelium and retinal ganglion cells induce the proliferation and differentiation of Müller glial cells and photoreceptors (Neumann and Nuesslein-Volhard, 2000; Todd and Fischer, 2015). This process is accomplished through induction of *Hh* in other uncommitted cells and neuronal differentiation by *Hh* secreted from newly differentiated retinal ganglion cells (Neumann and Nuesslein-Volhard, 2000).

2.3 Hh signaling for craniofacial development

The process of vertebrate craniofacial morphogenesis includes the development of the palate and jaw cartilages of the pharyngeal arches, both of which are cranial neural crest derived. During palatogenesis, migrating cranial neural crest cells (CNCCs) condense at the oral ectoderm and differentiate into the palate (Eberhart et al., 2006; Swartz et al., 2011; Wada et al., 2005). The molecular mechanism of how cranial neural crest condenses at the oral ectoderm is currently unknown. *Hh* is expressed at the oral ectoderm in zebrafish, mouse, and chick embryos (Cordero et al., 2004; Eberhart et al., 2006; Miller et al., 2000) and oral ectoderm specification is regulated by *Hh* secreted from the ventral forebrain (Eberhart et al., 2006). Loss of Hh signaling from ventral forebrain and oral ectoderm leads to disruptive palatogenesis (Eberhart et al., 2006; Wada et al., 2005). Further molecular works revealed that palatogenesis is tightly regulated by Hh interaction with BMP (Bone Morphogeneic Protein) (Zhang et al., 2002) and FGF (Fibroblast growth factors) (Han et al., 2009; Rice et al., 2004).

Jaw cartilage development is also influenced by Hh signaling. Hh signaling from the oral ectoderm and pharyngeal endoderm is required for the survival of post migratory CNCCs and their differentiation to jaw cartilage (Billmyre and Klingensmith, 2015; Brito et al., 2006). Early disruption of Hh signaling results in disorganized anteriormost CNCC and anterior jaw defects while late disruption results in depleted CNCCs residing near the posterior arch (Schwend and Ahlgren, 2009). Zebrafish transplant analysis further revealed that not only pharyngeal endoderm but also CNCCs receive Hh signaling to ensure patterning pharyngeal arches and maintaining

Hh expression in the pharyngeal endoderm, respectively (Swartz et al., 2012).

3. Cranial neural crest for craniofacial complex development

The subsequent sections focus on CNCCs (Fig. 1), their contributions to craniofacial complex development, and the influence on their development by environmental factors, such as oxidative stress, and genetic factors, including *zic2* (which will be discussed in section 4.2).

3.1 Cranial neural crest

CNCCs are a group of migratory stem cells that originate in the anterior dorsal neural tube and migrate from the neural tube before its closure (Serbedzija et al., 1992). They give rise to several cell lineages that contribute to craniofacial complex development. In vertebrates, two different sources of CNCCs contribute to craniofacial complex development. CNCCs from the diencephalon and midbrain migrate anteriorly (coined as anterior cranial neural crest (aCNC)) and contribute to the development of anterior neural derivatives, such as the medial forebrain, optic stalk, retina, and anterior segment, while CNCCs from the hindbrain migrate in three separate streams caudally to the eyes and contribute to form jaw cartilages (Couly et al., 1993; Kish et al., 2011; Kontges and Lumsden, 1996).

3.2 Cranial neural crest contribution to medial forebrain development

Medial forebrain formation is regulated by aCNC. In avian embryos, aCNC

regulates *fgf8* transcription in the anterior neural ridge, a telencephalic organizer that restricts *Hh* expression to the ventral forebrain (Creuzet et al., 2006; Le Douarin et al., 2012). Disruption of aCNC formation and migration results in loss of *fgf8* in anterior neural ridge, ventrolateral expansion of *Hh*, and HPE (Aguiar et al., 2014; Creuzet et al., 2006). In mouse embryos, epithelial-to-mesenchymal transition (EMT) of aCNC to facial mesenchyme is required for the invagination of the dorsal forebrain midline, which will become the roof plate (Choe et al., 2014). These findings suggest that aCNC significantly contributes to the development of the medial forebrain; however, the molecular mechanism of how aCNC development regulates medial forebrain development remains poorly characterized.

3.3 Cranial neural crest contribution to ocular development

aCNC receives several signals from the eye. In zebrafish embryos with *chokh/eyeless* mutations, aCNC fails to migrate anteriorly but accumulates posteriorly in an unorganized fashion, indicating eyes provide important cues for aCNC migration (Langenberg et al., 2008). In the developing eyes, the optic stalk secretes platelet-derived growth factor (pdgf)-mediated cues to attract aCNC before migrating to its destination for differentiation (Eberhart et al., 2008). In addition, retinoic acid (RA) secreted from the eyes targets retinoic acid receptors (RARs) in aCNC. The interaction between RA and RARs is essential for ocular morphogenesis and, at the same time, regulates genes and signaling cascades present in aCNC (Ma and Lwigale, 2019; Matt et al., 2008).

During ocular morphogenesis, periocular neural crest, a subset of aCNC, forms around the optic cup (Langenberg et al., 2008; Williams and Bohnsack, 2015).

Once the optic cup is fully established, periocular neural crest migrates to the optic cup and subsequently differentiates into various cell types that are required for anterior segment development, such as corneal endothelium, keratocytes of corneal stroma, ciliary body, and iris stroma (Creuzet et al., 2005; Evans and Gage, 2005; Gage et al., 2005; Portal et al., 2019; Skarie and Link, 2009; Williams and Bohnsack, 2015). While *pitx2* and *foxc1* are the two most widely characterized genes that regulate periocular neural crest differentiation for anterior segment (Chawla et al., 2016; Evans and Gage, 2005; Hendee et al., 2018; Seo et al., 2017; Skarie and Link, 2009), periocular neural crests populated in anterior segment are, in fact, highly heterogenous (Van Der Meulen et al., 2020) and are tightly orchestrated by the interplays among many guidance molecules, such as *pax6* and TGF-beta signaling (Takamiya et al., 2020).

In addition to anterior segment, periocular neural crest differentiates into the muscle cells in the eyelid (Creuzet et al., 2005) and vascular pericytes of the hyaloid vasculature (Gage et al., 2005; Lupo et al., 2011; Trost et al., 2016; Trost et al., 2013), which stabilize and maintain the hyaloid vasculature for retinal angiogenesis (Saint-Geniez and D'Amore, 2004). In some animals, periocular neural crest differentiates into sclerotic cartilages (Creuzet et al., 2005; Thompson et al., 2010), which support the mechanical rigidity surrounding the eyeball and maintain an intraocular pressure for the retina to correctly perceive visual information (O'Quin et al., 2015; Seko et al., 2008). All these cell lineages are required for proper ocular development and vision.

Periocular neural crest also contributes to choroid fissure closure. Previous findings suggest that defective periocular neural crest formation or survival is associated with coloboma (Evans and Gage, 2005; Gestri et al., 2018; Lupo et al., 2011; McMahon et al., 2009). Hyaloid vasculature, derived from periocular neural crest

and lateral plate mesenchyme, has been characterized for its role for choroid fissure closure through facilitating the breakdown of basement membrane in the choroid fissure (James et al., 2016). However, zebrafish *cloche* mutants, which lack entire cephalic vasculature, exhibit normal choroid fissure closure (Dhakal et al., 2015), suggesting that hyaloid vasculature is dispensable for choroid fissure closure. Recent reports show that periocular neural crest possibly facilitates choroid fissure closure through regulating choroid fissure basement membrane proteins, such as nidogen (Bryan et al., 2020; Carrara et al., 2019). The underlying mechanism of how periocular neural crest controls choroid fissure closure remains unclear.

3.4 Cranial neural crest contribution to craniofacial development

In zebrafish, aCNC that migrated between the developing eyes differentiates into anterior neurocranium, which is functionally equivalent to the palate of mouse and human (Cusack et al., 2017; Dougherty et al., 2013; Swartz et al., 2011). aCNC that migrated from the anterior midbrain gives rise to the ethmoid plate while aCNC from the posterior midbrain differentiates into trabeculae span around ethmoid plates (Wada et al., 2005). Several growth factors and genes are necessary for aCNC migration, such as pdgf and alx1. aCNC-derived palatal precursors, which have pdgf receptors (Xu et al., 2005), are first recruited to the optic stalk via pdgf-mediated cues and then migrate onward to the oral ectoderm, another pdgf signaling center (Eberhart et al., 2008). If pdgf-mediated cues are disrupted, embryos develop with craniofacial defects, including facial cleft and craniofacial bone malformation (Eberhart et al., 2008; McCarthy et al., 2016). In both *in vivo* and *in vitro* analysis, *alx1* is required for aCNC migration (Dee et al., 2013; Pini et al., 2020). Because pre-migratory aCNC is

populated far away from the Hh source at the ventral forebrain, Hh signaling does not influence aCNC migration (Eberhart et al., 2006). However, Hh signaling is required for patterning of the oral ectoderm for aCNC condensation (Eberhart et al., 2006; Jeong et al., 2004; Wada et al., 2005).

CNCCs migrating caudally to the eyes interact with pharyngeal endoderm (Trainor and Krumlauf, 2001). Interestingly, pharyngeal arch patterning is normal in the absence of CNCCs (Veitch et al., 1999), suggesting a dispensable role of CNCCs for pharyngeal arch patterning. Instead, pharyngeal endoderm is required (Graham and Richardson, 2012). However, the interaction between CNCC and pharyngeal endoderm is required for patterning jaw cartilages derived from pharyngeal arches (Piotrowski and Nusslein-Volhard, 2000).

3.5. The impact of oxidative stress to cranial neural crest lineages.

Oxidative stress is triggered by environmental assaults, such as prenatal ethanol exposure and maternal diabetes. Prenatal ethanol exposure causes the production of reactive oxygen species (ROS) and disrupts the balance of intracellular redox state in the brain, which leads to DNA damage and aberrant gene expression (Brocardo et al., 2011; Dong et al., 2010; Lovely et al., 2017). Likewise, hyperglycemia for developing embryos increases the production of ROS leading to oxidative stress (Garcia-Sanz et al., 2017; Wang et al., 2015). As a result of excessive oxidative stress, newborn babies are often affected by congenital craniofacial complex malformations, such as fetal alcohol syndrome (FAS) and diabetic embryopathy (Castori, 2013; Lovely et al., 2017). The mechanism of how oxidative stress increases the susceptibility of congenital malformations in human embryos is poorly understood.

Maintaining the balance of oxidative state is critical for neural crest development because the neural crest is very sensitive to external oxidative stress (Sakai et al., 2016). Excessive oxidative stress reduces the production of antioxidative defense genes, such as *nrf2* (nuclear factor erythroid 2-related factor), in neural crest (Chen et al., 2013; Wentzel and Eriksson, 2011) and induces neural crest cell death (Chen et al., 2013; Wang et al., 2015). Because both craniofacial cartilage and the eyes are neural crest cell derived and form in proximity, craniofacial cartilage defects are often associated with anterior segment defects in some congenital disorders, such as Axenfeld-Rieger Syndrome (Volkmann et al., 2011; Williams and Bohnsack, 2015). However, the susceptibility of each neural crest lineages to oxidative stress varies. While cranial neural crest that gives rise to craniofacial cartilage is highly susceptible to oxidative stress, periocular neural crest that contributes to form anterior segment is much less affected as oxidative stress minimally affects *foxc1* and *pitx2*, two transcripts that are expressed in the anterior segment (Eason et al., 2017). This explains the rarity of ocular defects despite frequent craniofacial abnormalities found in FAS and diabetic embryopathy.

4. Zic2 for craniofacial complex development

Although craniofacial complex development is heavily influenced by aCNC migration and differentiation, little is known about the molecular mechanism of how aCNC function is regulated. The subsequent sections focus on *zic2*, a molecular regulator that controls neural crest and craniofacial complex development (Fig. 2).

4.1 Zic2

Zic, zinc finger in the cerebellum, proteins are a family of transcription factors that play essential roles in neurogenesis. The Zic family encodes five C_2H_2-type zinc finger domains, which are highly conserved in all multicellular animals (Aruga and Hatayama, 2018). Zic genes share a common ancestry with Gli proteins, Hh signaling mediators (Aruga and Hatayama, 2018), and physically and functionally interact with them as tested *in vitro* (Koyabu et al., 2001; Mizugishi et al., 2001).

Among these zic genes, *zic2* is a highly unique gene that contributes to forebrain and retinal development. *ZIC2* is the second most known HPE-associated gene. However, unlike other HPE-associated genes which are either linked with classical HPE, characterized by ventral midline defects, or midline inter-hemispheric (MIH) HPE, characterized by dorsal patterning defects, *ZIC2* mutations are associated with both classical and MIH HPE (Barratt and Arkell, 2018; Grinblat and Lipinski, 2019). In addition, *zic2* function in craniofacial complex development is highly conserved throughout vertebrates. In mouse, *Zic2* knockdown mice develop with HPE (Nagai et al., 2000). Zebrafish *zic2* morphants and mutants do not develop with HPE but exhibit coloboma and craniofacial defects (Sanek et al., 2009; Sedykh et al., 2017; Teslaa et al., 2013), which are subsets of HPE.

Although it is known that *zic2* function is highly important in craniofacial complex development, the molecular mechanisms of how *zic2* function regulates the neural crest and craniofacial complex lineages, including medial forebrain, retina, and craniofacial cartilages, need to be elucidated.

4.2 Zic2 function in neural crest development

At the early somite stages, *zic2* is one of the zic genes that is expressed in the neurectoderm which induces neural crest formation (Houtmeyers et al., 2013). *Zic2* function is critical for early neural crest development, such as production, induction and migration of neural crest cells (Elms et al., 2003). Defective *zic2* function, shown in *Zic2* mutant mice and zebrafish *zic2* morphants and mutants, leads to significant depletion of the neural crest population (Elms et al., 2003; Sedykh et al., 2017; Teslaa et al., 2013). At this point, it is unclear how *zic2* in the neurectoderm triggers neural crest induction.

Neural crest development is influenced by several signaling pathways along with *zic2*, such as canonical wnt and Hh signaling. Canonical wnt signaling has been known for its role in neural crest induction and proliferation (Garcia-Castro et al., 2002; Heeg-Truesdell and LaBonne, 2006; Ikeya et al., 1997). The interaction between *zic2* and canonical wnt signaling has been studied in both *in vivo* and *in vitro*. In zebrafish, *zic2a* is a downstream gene of canonical wnt signaling during neurulation (Nyholm et al., 2009). In human cell cultures, zic2 directly binds with the β-catenin/TCF4 complex, inhibiting canonical wnt signaling (Pourebrahim et al., 2011). Whether zic2-canonical wnt signaling interaction is required for early neural crest development remains unknown.

In zebrafish, *zic2* is activated by *Hh* and functions as a negative regulator of Hh signaling (Sanek and Grinblat, 2008; Sanek et al., 2009). *Zic2* and *Hh* likely interact together to regulate the patterning of neural crest, which subsequently contributes to craniofacial development, since *zic2a* overexpressed embryos develop with reduced *ptch2*, a Hh signaling inhibitor, expression in the ventral midline and craniofacial

defects (Teslaa et al., 2013) similar to those found in embryos with abrogated *Hh* function (Swartz et al., 2012; Wada et al., 2005). In xenopus embryos, Zic2 and Gli proteins function opposingly for neural crest development as Zic2 induces neural crest differentiation while Gli proteins restrict it (Brewster et al., 1998). While these studies suggest that *zic2* and Hh signaling interact each other to regulate the neural crest development, the molecular mechanism of *zic2*-Hh signaling interaction during neural crest development needs to be further explored.

The underlying mechanism of how zic2 regulates neural crest development is not clear until recently, when *zic2* is found to be required for the development of aCNC-derived frontonasal and periocular mesenchyme through activating *alx1*. In addition, *cldn11*a, the most significantly depleted gene in *zic2* mutants, is expressed anterior to the retina adjacent to choroid fissure, where frontonasal and periocular neural crests are populated; thus, it is a potential neural crest marker activated by *zic2* (Sedykh et al., 2017).

4.3 Zic2 function in craniofacial complex development

As *ZIC2* is one of the HPE-associated genes that are required for early forebrain and eye formation, it is important to understand how *zic2* function contributes to this process. Initially, *zic2* establishes Hh signaling in PrCP (Warr et al., 2008). Zic2 directly interacts with Smad2/3 in the Nodal signaling pathway for PrCP establishment (Houtmeyers et al., 2016). Once the ventral midline is specified via Hh signaling from PrCP and the hypothalamus, *Hh* transcriptionally activates *six3*, which is required for activating *Hh* in the ventral midline. Subsequently, *Hh* in the ventral midline activates several genes that are required for patterning the medial forebrain, such as *fgf8* and

nkx2.1 (Geng et al., 2008). Our lab previously identified that *zic2a* negatively modulates *six3b* transcription at the forebrain, which is essential for correct formation of the medial forebrain (Sanek et al., 2009).

With respect to ocular development, *zic2* function is required for optic stalk morphogenesis. Zebrafish *zic2* restricts *pax2a* transcription at the optic stalk and, if *zic2* function is disrupted, *pax2a* transcription is expanded to the medial forebrain and retina (Sanek et al., 2009; Sedykh et al., 2017). Other Hh signaling targets specifically expressed in the optic stalk, *vax1* and *vax2* (Take-uchi et al., 2003), are also negatively modulated by *zic2* (Sedykh et al., 2017). Together, these findings show that *zic2* acts as a negative regulator of Hh downstream targets at the optic stalk, which consequently marks a sharp boundary between medial forebrain and optic stalk and between retina and optic stalk. However, it is still unclear whether *zic2* directly regulates the optic stalk through modulating the transcription of *Hh* downstream targets, *pax2a*, *vax1*, and *vax2*, and whether *zic2* inhibition of *pax2a* expansion to the medial forebrain is required for separating the fate of the forebrain from that of the optic stalk.

5. Downstream effectors of zic2

Several important downstream effectors of *zic2* have been identified through RNA sequencing analysis (Chapter 2). The subsequent sections deal with brief introductions of *alx1* (Chapter 3, Appendix), *cldn11a* (Chapter 4), and *pax2a* (Chapter 4). The focus will be on the significance of these effectors for vertebrate craniofacial complex development.

5.1 Alx1

Alx1 is specifically expressed in neural crest cells for chondrogenesis and significantly downregulated in frontonasal and periocular mesenchyme in *zic2* mutants (Sedykh et al., 2017). *Alx1* (coined as *Cart-1*), a member of aristaless-like homeobox protein, was initially identified from a rat chondrosarcoma and is exclusively expressed in immature and condensed cranial mesenchymal cells that give rise to mature chondrocytes (Zhao et al., 1994; Zhao et al., 1993). *Alx1* function in craniofacial development is highly conserved throughout vertebrates. In humans, *ALX1* mutation is associated with frontonasal dysplasia (FND), severe orofacial facial cleft, and ocular defects, including extreme microphthalmia, anophthalmia, and coloboma (Pini et al., 2020). Burmese cats with *Alx1* mutation develop with FND and median facial cleft (Lyons et al., 2016). Mouse *Alx1* mutation does not fully recapitulate the craniofacial defects found in human or Burmese cats. Instead, *Alx1* mutant mice exhibit early neural tube defects (Zhao et al., 1996). In zebrafish, *alx1* morphants develop with both craniofacial defects and ocular defects, such as microphthalmia and retinal coloboma (Dee et al., 2013), while *alx1* mutants exhibit low penetrant craniofacial and ocular defects (Pini et al., 2020). Induced pluripotent stem cells (iPSCs) research and zebrafish studies identified a critical role of *alx1* during neural crest migration (Pini et al., 2020). These findings suggest that *alx1* regulates craniofacial and ocular development through regulating aCNC lineages.

Notably, *alx1* has been characterized for its requirement in EMT activation and collective cell migration through regulating snail, also known as zinc finger protein snai1. In sea urchin embryos, *alx1* is required for activating snail by inhibiting cadherin

transcription (Wu and McClay, 2007). In addition, alx1 forms a de-adhesion sub-circuit with twist and snail, downstream targets of *alx1*, and, at the same time, twist positively regulates alx1, forming a positive feedback loop mechanism for maintaining de-adhesion (Saunders and McClay, 2014). In human ovarian and lung cancer cells, *alx1* mediates EMT activation and promotes collective cell migration by regulating snail (Yao et al., 2015; Yuan et al., 2013). Although neural crest cells also migrate collectively (Szabo and Mayor, 2018; Szabo et al., 2016), whether *alx1* contributes to the collective migration of the neural crest is currently unknown.

Alx1 has two other alx gene family members: *Alx3* and *Alx4* (in zebrafish, three other genes: *alx3*, *alx4a*, and *alx4b*) (McGonnell et al., 2011). Each alx gene family member shares a similar homeodomain sequence with one another and is co-expressed at several domains including frontonasal mesenchyme and the neural-crest derivatives of branchial arches (Dee et al., 2013; Qu et al., 1999; ten Berge et al., 1998). Similar to *ALX1* mutation, *ALX3* and *ALX4* mutations are also associated with FND in humans, but with milder craniofacial deformities (Bertola et al., 2013; El-Ruby et al., 2018; Twigg et al., 2009). In mouse, a single mutation of *Alx1* or *Alx3* does not fully recapitulate ALX-related FND phenotypes in humans (Lakhwani et al., 2010; Zhao et al., 1996) whereas *Alx3; Alx4* double mutants and *Alx1; Alx4* double mutants exhibit midline fusion defects (Beverdam et al., 2001; Qu et al., 1999), suggesting functional compensation of the alx gene family during craniofacial complex development in mouse. In zebrafish, the role of other alx gene family members for craniofacial complex development has not been characterized and will be addressed in detail in chapter 3.

5.2 Cldn11

Similar to other claudin gene family, cldn11 is a tight junction protein that provides a primary barrier to protect against paracellular diffusion (Gow et al., 1999; Morita et al., 1999; Stevenson and Keon, 1998). *Cldn11* shares a structural similarity with other claudin genes which primarily form tight junctions in epithelial and endothelial cells. *Cldn11* is expressed in myelinating sheath in the CNS and in Sertoli cells in the testis. It is required for proliferation and migration of oligodendrocytes during myelination (Devaux and Gow, 2008; Morita et al., 1999; Tiwari-Woodruff et al., 2001). There is growing evidence that *cldn11* function is not restricted to oligodendrocytes in the CNS or Sertoli cells in testis. Prior to the formation of oligodendrocytes, *cldn11* is transiently expressed in mesenchymal cells adjacent to developing chondrocytes in rats (Bronstein et al., 2000). Along with other claudin gene family members and/or other tight junction proteins such as occludins, cldn11 maintains the blood-cerebrospinal fluid barrier (Kratzer et al., 2012; Whish et al., 2015; Wolburg et al., 2001), controls electric potential for hearing (Gow et al., 2004; Kitajiri et al., 2004), and forms a barrier between blood vessels and the testis (Su et al., 2009; Wessells et al., 2009).

In zebrafish, *cldn11* has two orthologs: *cldn11a* and *cldn11b*. *Cldn11a* expression has been initially reported in vascular endothelium (Cannon et al., 2013); however, we found that *cldn11a* is expressed in a domain anterior to the retina close to the choroid fissure, where periocular neural crest is expressed (Sedykh et al., 2017). C*ldn11a* is the most significantly downregulated gene in zic2 mutants (Sedykh et al., 2017), although the mechanism of how *cldn11a* is regulated by *zic2* is completely unknown. *Cldn11b* function and expression has not yet been reported. In chapter 4,

cldn11a and *cldn11b* function for ventral retinal morphogenesis will be discussed.

Recent findings uncover a novel and unexpected role of *cldn11* in collective cell migration, such as myelinating oligodendrocytes and cancer-associated fibroblasts, by maintaining the cell polarity (Karagiannis et al., 2014; Li et al., 2019). While it is unknown whether *cldn11* is required for collective neural crest migration, in tumor cells, *cldn11* is induced by snail, which is required for pre-migratory neural crest cells to depart from the neuroepithelium for migration (Hutchins and Bronner, 2019; Li et al., 2019).

5.3. Pax2

Pax2, a paired-box-containing gene, was first identified through its homology with *Drosophila* homeotic and segmentation genes (Dressler et al., 1990). *Pax2* expression is expressed in a number of embryonic lineages, such as in the developing excretory system (Dressler et al., 1990; Dressler and Douglass, 1992), neural tube (Nornes et al., 1990), midbrain-hindbrain boundary (MHB) (Puschel et al., 1992), and the junction between the retina and the optic stalk (Nornes et al., 1990; Puschel et al., 1992). In humans, *PAX2* mutation is associated with renal-coloboma syndrome, a combination of failure of choroid fissure closure and abnormal kidney formation (Sanyanusin et al., 1995a; Sanyanusin et al., 1995b).

During ventral retinal morphogenesis in mouse, *Pax2* expression is activated by FGF, BMP, and Hh signaling pathways. FGF promotes *pax2*, which is required for choroid fissure closure and optic disc specification for hyaloid vasculature entry and optic nerve outgrowth (Cai et al., 2013). BMP7, prior to Hh signaling, is required for

early optic disc formation by promoting generation and invasion of *pax2*-expressing cells to the optic stalk and ventral retina (Morcillo et al., 2006). The interaction between BMP7 and Hh is essential to promote *pax2* expression through relieving the repression of *pax2* by tlx, a repressor protein in the tailless transcription factor family (Sehgal et al., 2009).

Zebrafish *pax2a* is highly homologous to mouse *Pax2* (96% identity) and its expression is also very similar to mouse *Pax2* (Krauss et al., 1991; Puschel et al., 1992). In addition, its genomic structure is also conserved between humans and zebrafish (Lun and Brand, 1998; Sanyanusin et al., 1996). Similar to mouse, zebrafish ventral retinal morphogenesis is regulated by *Hh* (Macdonald et al., 1995; Varga et al., 2001). Ectopic *Hh* expression induces the expansion of *pax2a* at the optic vesicle and optic stalk (Ekker et al., 1995), while *pax2a* expression is lost at the optic stalk in the absence of *Hh* expression, as shown in smoothened mutants (Varga et al., 2001). Aberrant zebrafish *pax2a* function is characterized by the absence of MHB formation (also known as no isthmus/noi), failure of choroid fissure closure, aberrant hyaloid vasculature formation, and abnormal retinal ganglion axon departure from the eye (Kelly and Moon, 1995; Krauss et al., 1992; Lun and Brand, 1998; Macdonald et al., 1997; Pfeffer et al., 1998; Rowitch and McMahon, 1995; Sanek et al., 2009; Weaver et al., 2020). In chapter 4, the role of *pax2a* in ocular morphogenesis will be further elucidated and a novel role of *pax2a* for craniofacial development will be discussed.

While *zic2* has been characterized for its role in restricting *pax2a* transcription at the optic stalk (Sanek et al., 2009; Sedykh et al., 2017), the molecular mechanisms of how *pax2a* transcription is regulated during ventral retinal morphogenesis needs to be further investigated. In chapter 4, two novel genetic pathways regulating *pax2a*

transcription will be discussed.

Reference

Aguiar, D.P., Sghari, S., Creuzet, S., 2014. The facial neural crest controls fore- and midbrain patterning by regulating Foxg1 expression through Smad1 activity. Development 141, 2494-2505.

Aoto, K., Shikata, Y., Imai, H., Matsumaru, D., Tokunaga, T., Shioda, S., Yamada, G., Motoyama, J., 2009. Mouse Shh is required for prechordal plate maintenance during brain and craniofacial morphogenesis. Dev Biol 327, 106-120.

Aruga, J., Hatayama, M., 2018. Comparative Genomics of the Zic Family Genes. Adv Exp Med Biol 1046, 3-26.

Barratt, K.S., Arkell, R.M., 2018. ZIC2 in Holoprosencephaly. Adv Exp Med Biol 1046, 269-299.

Barth, K.A., Wilson, S.W., 1995. Expression of zebrafish nk2.2 is influenced by sonic hedgehog/vertebrate hedgehog-1 and demarcates a zone of neuronal differentiation in the embryonic forebrain. Development 121, 1755-1768.

Bertola, D.R., Rodrigues, M.G., Quaio, C.R., Kim, C.A., Passos-Bueno, M.R., 2013. Vertical transmission of a frontonasal phenotype caused by a novel ALX4 mutation. Am J Med Genet A 161A, 600-604.

Beverdam, A., Brouwer, A., Reijnen, M., Korving, J., Meijlink, F., 2001. Severe nasal clefting and abnormal embryonic apoptosis in Alx3/Alx4 double mutant mice. Development 128, 3975-3986.

Billmyre, K.K., Klingensmith, J., 2015. Sonic hedgehog from pharyngeal arch 1 epithelium is necessary for early mandibular arch cell survival and later cartilage condensation differentiation. Dev Dyn 244, 564-576.

Blaess, S., Szabo, N., Haddad-Tovolli, R., Zhou, X., Alvarez-Bolado, G., 2014. Sonic hedgehog signaling in the development of the mouse hypothalamus. Front Neuroanat 8, 156.

Brewster, R., Lee, J., Ruiz i Altaba, A., 1998. Gli/Zic factors pattern the neural plate by defining domains of cell differentiation. Nature 393, 579-583.

Brito, J.M., Teillet, M.A., Le Douarin, N.M., 2006. An early role for sonic hedgehog from foregut endoderm in jaw development: ensuring neural crest cell survival. Proc Natl Acad Sci U S A 103, 11607-11612.

Brocardo, P.S., Gil-Mohapel, J., Christie, B.R., 2011. The role of oxidative stress in fetal alcohol spectrum disorders. Brain Res Rev 67, 209-225.

Bronstein, J.M., Tiwari-Woodruff, S., Buznikov, A.G., Stevens, D.B., 2000. Involvement of OSP/claudin-11 in oligodendrocyte membrane interactions: role in biology and

disease. J Neurosci Res 59, 706-711.

Bryan, C.D., Casey, M.A., Pfeiffer, R.L., Jones, B.W., Kwan, K.M., 2020. Optic cup morphogenesis requires neural crest-mediated basement membrane assembly. Development 147.

Cai, Z., Tao, C., Li, H., Ladher, R., Gotoh, N., Feng, G.S., Wang, F., Zhang, X., 2013. Deficient FGF signaling causes optic nerve dysgenesis and ocular coloboma. Development 140, 2711-2723.

Cannon, J.E., Place, E.S., Eve, A.M., Bradshaw, C.R., Sesay, A., Morrell, N.W., Smith, J.C., 2013. Global analysis of the haematopoietic and endothelial transcriptome during zebrafish development. Mech Dev 130, 122-131.

Carrara, N., Weaver, M., Piedade, W.P., Vocking, O., Famulski, J.K., 2019. Temporal characterization of optic fissure basement membrane composition suggests nidogen may be an initial target of remodeling. Dev Biol 452, 43-54.

Castori, M., 2013. Diabetic embryopathy: a developmental perspective from fertilization to adulthood. Mol Syndromol 4, 74-86.

Chawla, B., Schley, E., Williams, A.L., Bohnsack, B.L., 2016. Retinoic Acid and Pitx2 Regulate Early Neural Crest Survival and Migration in Craniofacial and Ocular Development. Birth Defects Res B Dev Reprod Toxicol 107, 126-135.

Chen, X., Liu, J., Chen, S.Y., 2013. Over-expression of Nrf2 diminishes ethanol-induced oxidative stress and apoptosis in neural crest cells by inducing an antioxidant response. Reprod Toxicol 42, 102-109.

Chiang, C., Litingtung, Y., Lee, E., Young, K.E., Corden, J.L., Westphal, H., Beachy, P.A., 1996. Cyclopia and defective axial patterning in mice lacking Sonic hedgehog gene function. Nature 383, 407-413.

Choe, Y., Zarbalis, K.S., Pleasure, S.J., 2014. Neural crest-derived mesenchymal cells require Wnt signaling for their development and drive invagination of the telencephalic midline. PLoS One 9, e86025.

Chow, R.L., Lang, R.A., 2001. Early eye development in vertebrates. Annu Rev Cell Dev Biol 17, 255-296.

Cordero, D., Marcucio, R., Hu, D., Gaffield, W., Tapadia, M., Helms, J.A., 2004. Temporal perturbations in sonic hedgehog signaling elicit the spectrum of holoprosencephaly phenotypes. J Clin Invest 114, 485-494.

Cornesse, Y., Pieler, T., Hollemann, T., 2005. Olfactory and lens placode formation is controlled by the hedgehog-interacting protein (Xhip) in Xenopus. Dev Biol 277, 296-315.

Couly, G.F., Coltey, P.M., Le Douarin, N.M., 1993. The triple origin of skull in higher

vertebrates: a study in quail-chick chimeras. Development 117, 409-429.

Creuzet, S., Vincent, C., Couly, G., 2005. Neural crest derivatives in ocular and periocular structures. Int J Dev Biol 49, 161-171.

Creuzet, S.E., Martinez, S., Le Douarin, N.M., 2006. The cephalic neural crest exerts a critical effect on forebrain and midbrain development. Proc Natl Acad Sci U S A 103, 14033-14038.

Cusack, B.J., Parsons, T.E., Weinberg, S.M., Vieira, A.R., Szabo-Rogers, H.L., 2017. Growth factor signaling alters the morphology of the zebrafish ethmoid plate. J Anat 230, 701-709.

Dale, J.K., Vesque, C., Lints, T.J., Sampath, T.K., Furley, A., Dodd, J., Placzek, M., 1997. Cooperation of BMP7 and SHH in the induction of forebrain ventral midline cells by prechordal mesoderm. Cell 90, 257-269.

Dee, C.T., Szymoniuk, C.R., Mills, P.E., Takahashi, T., 2013. Defective neural crest migration revealed by a Zebrafish model of Alx1-related frontonasal dysplasia. Hum Mol Genet 22, 239-251.

Devaux, J., Gow, A., 2008. Tight junctions potentiate the insulative properties of small CNS myelinated axons. J Cell Biol 183, 909-921.

Dhakal, S., Stevens, C.B., Sebbagh, M., Weiss, O., Frey, R.A., Adamson, S., Shelden, E.A., Inbal, A., Stenkamp, D.L., 2015. Abnormal retinal development in Cloche mutant zebrafish. Dev Dyn 244, 1439-1455.

Diaz-Coranguez, M., Chao, D.L., Salero, E.L., Goldberg, J.L., Antonetti, D.A., 2017. Cell autonomous sonic hedgehog signaling contributes to maintenance of retinal endothelial tight junctions. Exp Eye Res 164, 82-89.

Dong, J., Sulik, K.K., Chen, S.Y., 2010. The role of NOX enzymes in ethanol-induced oxidative stress and apoptosis in mouse embryos. Toxicol Lett 193, 94-100.

Dougherty, M., Kamel, G., Grimaldi, M., Gfrerer, L., Shubinets, V., Ethier, R., Hickey, G., Cornell, R.A., Liao, E.C., 2013. Distinct requirements for wnt9a and irf6 in extension and integration mechanisms during zebrafish palate morphogenesis. Development 140, 76-81.

Dressler, G.R., Deutsch, U., Chowdhury, K., Nornes, H.O., Gruss, P., 1990. Pax2, a new murine paired-box-containing gene and its expression in the developing excretory system. Development 109, 787-795.

Dressler, G.R., Douglass, E.C., 1992. Pax-2 is a DNA-binding protein expressed in embryonic kidney and Wilms tumor. Proc Natl Acad Sci U S A 89, 1179-1183.

Dubourg, C., Bendavid, C., Pasquier, L., Henry, C., Odent, S., David, V., 2007. Holoprosencephaly. Orphanet J Rare Dis 2, 8.

Dubourg, C., Lazaro, L., Pasquier, L., Bendavid, C., Blayau, M., Le Duff, F., Durou, M.R., Odent, S., David, V., 2004. Molecular screening of SHH, ZIC2, SIX3, and TGIF genes in patients with features of holoprosencephaly spectrum: Mutation review and genotype-phenotype correlations. Hum Mutat 24, 43-51.

Dutta, S., Dietrich, J.E., Aspock, G., Burdine, R.D., Schier, A., Westerfield, M., Varga, Z.M., 2005. pitx3 defines an equivalence domain for lens and anterior pituitary placode. Development 132, 1579-1590.

Eagleson, G., Ferreiro, B., Harris, W.A., 1995. Fate of the anterior neural ridge and the morphogenesis of the Xenopus forebrain. J Neurobiol 28, 146-158.

Eason, J., Williams, A.L., Chawla, B., Apsey, C., Bohnsack, B.L., 2017. Differences in neural crest sensitivity to ethanol account for the infrequency of anterior segment defects in the eye compared with craniofacial anomalies in a zebrafish model of fetal alcohol syndrome. Birth Defects Res 109, 1212-1227.

Eberhart, J.K., He, X., Swartz, M.E., Yan, Y.L., Song, H., Boling, T.C., Kunerth, A.K., Walker, M.B., Kimmel, C.B., Postlethwait, J.H., 2008. MicroRNA Mirn140 modulates Pdgf signaling during palatogenesis. Nat Genet 40, 290-298.

Eberhart, J.K., Swartz, M.E., Crump, J.G., Kimmel, C.B., 2006. Early Hedgehog signaling from neural to oral epithelium organizes anterior craniofacial development. Development 133, 1069-1077.

Ekker, S.C., Ungar, A.R., Greenstein, P., von Kessler, D.P., Porter, J.A., Moon, R.T., Beachy, P.A., 1995. Patterning activities of vertebrate hedgehog proteins in the developing eye and brain. Curr Biol 5, 944-955.

El-Ruby, M., El-Din Fayez, A., El-Dessouky, S.H., Aglan, M.S., Mazen, I., Ismail, N., Afifi, H.H., Eid, M.M., Mostafa, M.I., Mehrez, M.I., Khalil, Y., Zaki, M.S., Gaber, K.R., Abdel-Hamid, M.S., Abdel-Salam, G.M.H., 2018. Identification of a novel homozygous ALX4 mutation in two unrelated patients with frontonasal dysplasia type-2. Am J Med Genet A 176, 1190-1194.

Elms, P., Siggers, P., Napper, D., Greenfield, A., Arkell, R., 2003. Zic2 is required for neural crest formation and hindbrain patterning during mouse development. Dev Biol 264, 391-406.

Evans, A.L., Gage, P.J., 2005. Expression of the homeobox gene Pitx2 in neural crest is required for optic stalk and ocular anterior segment development. Hum Mol Genet 14, 3347-3359.

Fuhrmann, S., 2010. Eye morphogenesis and patterning of the optic vesicle. Curr Top Dev Biol 93, 61-84.

Gage, P.J., Rhoades, W., Prucka, S.K., Hjalt, T., 2005. Fate maps of neural crest and mesoderm in the mammalian eye. Invest Ophthalmol Vis Sci 46, 4200-4208.

Garcia-Castro, M.I., Marcelle, C., Bronner-Fraser, M., 2002. Ectodermal Wnt function as a neural crest inducer. Science 297, 848-851.

Garcia-Sanz, P., Mirasierra, M., Moratalla, R., Vallejo, M., 2017. Embryonic defence mechanisms against glucose-dependent oxidative stress require enhanced expression of Alx3 to prevent malformations during diabetic pregnancy. Sci Rep 7, 389.

Geng, X., Speirs, C., Lagutin, O., Inbal, A., Liu, W., Solnica-Krezel, L., Jeong, Y., Epstein, D.J., Oliver, G., 2008. Haploinsufficiency of Six3 fails to activate Sonic hedgehog expression in the ventral forebrain and causes holoprosencephaly. Dev Cell 15, 236-247.

Gestri, G., Bazin-Lopez, N., Scholes, C., Wilson, S.W., 2018. Cell Behaviors during Closure of the Choroid Fissure in the Developing Eye. Front Cell Neurosci 12, 42.

Gow, A., Davies, C., Southwood, C.M., Frolenkov, G., Chrustowski, M., Ng, L., Yamauchi, D., Marcus, D.C., Kachar, B., 2004. Deafness in Claudin 11-null mice reveals the critical contribution of basal cell tight junctions to stria vascularis function. J Neurosci 24, 7051-7062.

Gow, A., Southwood, C.M., Li, J.S., Pariali, M., Riordan, G.P., Brodie, S.E., Danias, J., Bronstein, J.M., Kachar, B., Lazzarini, R.A., 1999. CNS myelin and sertoli cell tight junction strands are absent in Osp/claudin-11 null mice. Cell 99, 649-659.

Graham, A., Richardson, J., 2012. Developmental and evolutionary origins of the pharyngeal apparatus. Evodevo 3, 24.

Grinblat, Y., Lipinski, R.J., 2019. A forebrain undivided: Unleashing model organisms to solve the mysteries of holoprosencephaly. Dev Dyn 248, 626-633.

Han, J., Mayo, J., Xu, X., Li, J., Bringas, P., Jr., Maas, R.L., Rubenstein, J.L., Chai, Y., 2009. Indirect modulation of Shh signaling by Dlx5 affects the oral-nasal patterning of palate and rescues cleft palate in Msx1-null mice. Development 136, 4225-4233.

Hartsock, A., Lee, C., Arnold, V., Gross, J.M., 2014. In vivo analysis of hyaloid vasculature morphogenesis in zebrafish: A role for the lens in maturation and maintenance of the hyaloid. Dev Biol 394, 327-339.

Heeg-Truesdell, E., LaBonne, C., 2006. Neural induction in Xenopus requires inhibition of Wnt-beta-catenin signaling. Dev Biol 298, 71-86.

Hendee, K.E., Sorokina, E.A., Muheisen, S.S., Reis, L.M., Tyler, R.C., Markovic, V., Cuturilo, G., Link, B.A., Semina, E.V., 2018. PITX2 deficiency and associated human disease: insights from the zebrafish model. Hum Mol Genet 27, 1675-1695.

Houtmeyers, R., Souopgui, J., Tejpar, S., Arkell, R., 2013. The ZIC gene family encodes multi-functional proteins essential for patterning and morphogenesis. Cell Mol Life Sci 70, 3791-3811.

Houtmeyers, R., Tchouate Gainkam, O., Glanville-Jones, H.A., Van den Bosch, B., Chappell, A., Barratt, K.S., Souopgui, J., Tejpar, S., Arkell, R.M., 2016. Zic2 mutation causes holoprosencephaly via disruption of NODAL signalling. Hum Mol Genet 25, 3946-3959.

Hutchins, E.J., Bronner, M.E., 2019. Draxin alters laminin organization during basement membrane remodeling to control cranial neural crest EMT. Dev Biol 446, 151-158.

Ikeya, M., Lee, S.M., Johnson, J.E., McMahon, A.P., Takada, S., 1997. Wnt signalling required for expansion of neural crest and CNS progenitors. Nature 389, 966-970.

James, A., Lee, C., Williams, A.M., Angileri, K., Lathrop, K.L., Gross, J.M., 2016. The hyaloid vasculature facilitates basement membrane breakdown during choroid fissure closure in the zebrafish eye. Dev Biol 419, 262-272.

Jeong, J., Mao, J., Tenzen, T., Kottmann, A.H., McMahon, A.P., 2004. Hedgehog signaling in the neural crest cells regulates the patterning and growth of facial primordia. Genes Dev 18, 937-951.

Jeong, Y., Leskow, F.C., El-Jaick, K., Roessler, E., Muenke, M., Yocum, A., Dubourg, C., Li, X., Geng, X., Oliver, G., Epstein, D.J., 2008. Regulation of a remote Shh forebrain enhancer by the Six3 homeoprotein. Nat Genet 40, 1348-1353.

Karagiannis, G.S., Schaeffer, D.F., Cho, C.K., Musrap, N., Saraon, P., Batruch, I., Grin, A., Mitrovic, B., Kirsch, R., Riddell, R.H., Diamandis, E.P., 2014. Collective migration of cancer-associated fibroblasts is enhanced by overexpression of tight junction-associated proteins claudin-11 and occludin. Mol Oncol 8, 178-195.

Karlstrom, R.O., Talbot, W.S., Schier, A.F., 1999. Comparative synteny cloning of zebrafish you-too: mutations in the Hedgehog target gli2 affect ventral forebrain patterning. Genes Dev 13, 388-393.

Kelly, G.M., Moon, R.T., 1995. Involvement of wnt1 and pax2 in the formation of the midbrain-hindbrain boundary in the zebrafish gastrula. Dev Genet 17, 129-140.

Kish, P.E., Bohnsack, B.L., Gallina, D., Kasprick, D.S., Kahana, A., 2011. The eye as an organizer of craniofacial development. Genesis 49, 222-230.

Kitajiri, S.I., Furuse, M., Morita, K., Saishin-Kiuchi, Y., Kido, H., Ito, J., Tsukita, S., 2004. Expression patterns of claudins, tight junction adhesion molecules, in the inner ear. Hear Res 187, 25-34.

Kondoh, H., Uchikawa, M., Yoda, H., Takeda, H., Furutani-Seiki, M., Karlstrom, R.O., 2000. Zebrafish mutations in Gli-mediated hedgehog signaling lead to lens transdifferentiation from the adenohypophysis anlage. Mech Dev 96, 165-174.

Kontges, G., Lumsden, A., 1996. Rhombencephalic neural crest segmentation is preserved throughout craniofacial ontogeny. Development 122, 3229-3242.

Koyabu, Y., Nakata, K., Mizugishi, K., Aruga, J., Mikoshiba, K., 2001. Physical and functional interactions between Zic and Gli proteins. J Biol Chem 276, 6889-6892.

Kratzer, I., Vasiljevic, A., Rey, C., Fevre-Montange, M., Saunders, N., Strazielle, N., Ghersi-Egea, J.F., 2012. Complexity and developmental changes in the expression pattern of claudins at the blood-CSF barrier. Histochem Cell Biol 138, 861-879.

Krauss, S., Johansen, T., Korzh, V., Fjose, A., 1991. Expression of the zebrafish paired box gene pax[zf-b] during early neurogenesis. Development 113, 1193-1206.

Krauss, S., Maden, M., Holder, N., Wilson, S.W., 1992. Zebrafish pax[b] is involved in the formation of the midbrain-hindbrain boundary. Nature 360, 87-89.

Kruszka, P., Hart, R.A., Hadley, D.W., Muenke, M., Habal, M.B., 2015. Expanding the phenotypic expression of Sonic Hedgehog mutations beyond holoprosencephaly. J Craniofac Surg 26, 3-5.

Kruszka, P., Martinez, A.F., Muenke, M., 2018. Molecular testing in holoprosencephaly. Am J Med Genet C Semin Med Genet 178, 187-193.

Lakhwani, S., Garcia-Sanz, P., Vallejo, M., 2010. Alx3-deficient mice exhibit folic acid-resistant craniofacial midline and neural tube closure defects. Dev Biol 344, 869-880.

Langenberg, T., Kahana, A., Wszalek, J.A., Halloran, M.C., 2008. The eye organizes neural crest cell migration. Dev Dyn 237, 1645-1652.

Le Douarin, N.M., Couly, G., Creuzet, S.E., 2012. The neural crest is a powerful regulator of pre-otic brain development. Dev Biol 366, 74-82.

Li, C.F., Chen, J.Y., Ho, Y.H., Hsu, W.H., Wu, L.C., Lan, H.Y., Hsu, D.S., Tai, S.K., Chang, Y.C., Yang, M.H., 2019. Snail-induced claudin-11 prompts collective migration for tumour progression. Nat Cell Biol 21, 251-262.

Lovely, C., Rampersad, M., Fernandes, Y., Eberhart, J., 2017. Gene-environment interactions in development and disease. Wiley Interdiscip Rev Dev Biol 6.

Lun, K., Brand, M., 1998. A series of no isthmus (noi) alleles of the zebrafish pax2.1 gene reveals multiple signaling events in development of the midbrain-hindbrain boundary. Development 125, 3049-3062.

Lupo, G., Gestri, G., O'Brien, M., Denton, R.M., Chandraratna, R.A., Ley, S.V., Harris, W.A., Wilson, S.W., 2011. Retinoic acid receptor signaling regulates choroid fissure closure through independent mechanisms in the ventral optic cup and periocular mesenchyme. Proc Natl Acad Sci U S A 108, 8698-8703.

Lyons, L.A., Erdman, C.A., Grahn, R.A., Hamilton, M.J., Carter, M.J., Helps, C.R., Alhaddad, H., Gandolfi, B., 2016. Aristaless-Like Homeobox protein 1 (ALX1) variant associated with craniofacial structure and frontonasal dysplasia in Burmese cats. Dev Biol 409, 451-458.

Ma, J., Lwigale, P., 2019. Transformation of the Transcriptomic Profile of Mouse Periocular Mesenchyme During Formation of the Embryonic Cornea. Invest Ophthalmol Vis Sci 60, 661-676.

Macdonald, R., Barth, K.A., Xu, Q., Holder, N., Mikkola, I., Wilson, S.W., 1995. Midline signalling is required for Pax gene regulation and patterning of the eyes. Development 121, 3267-3278.

Macdonald, R., Scholes, J., Strahle, U., Brennan, C., Holder, N., Brand, M., Wilson, S.W., 1997. The Pax protein Noi is required for commissural axon pathway formation in the rostral forebrain. Development 124, 2397-2408.

Masai, I., Stemple, D.L., Okamoto, H., Wilson, S.W., 2000. Midline signals regulate retinal neurogenesis in zebrafish. Neuron 27, 251-263.

Matt, N., Ghyselinck, N.B., Pellerin, I., Dupe, V., 2008. Impairing retinoic acid signalling in the neural crest cells is sufficient to alter entire eye morphogenesis. Dev Biol 320, 140-148.

McCarthy, N., Liu, J.S., Richarte, A.M., Eskiocak, B., Lovely, C.B., Tallquist, M.D., Eberhart, J.K., 2016. Pdgfra and Pdgfrb genetically interact during craniofacial development. Dev Dyn 245, 641-652.

McGonnell, I.M., Graham, A., Richardson, J., Fish, J.L., Depew, M.J., Dee, C.T., Holland, P.W., Takahashi, T., 2011. Evolution of the Alx homeobox gene family: parallel retention and independent loss of the vertebrate Alx3 gene. Evol Dev 13, 343-351.

McMahon, C., Gestri, G., Wilson, S.W., Link, B.A., 2009. Lmx1b is essential for survival of periocular mesenchymal cells and influences Fgf-mediated retinal patterning in zebrafish. Dev Biol 332, 287-298.

Miller, C.T., Schilling, T.F., Lee, K., Parker, J., Kimmel, C.B., 2000. sucker encodes a zebrafish Endothelin-1 required for ventral pharyngeal arch development. Development 127, 3815-3828.

Mizugishi, K., Aruga, J., Nakata, K., Mikoshiba, K., 2001. Molecular properties of Zic proteins as transcriptional regulators and their relationship to GLI proteins. J Biol Chem 276, 2180-2188.

Morcillo, J., Martinez-Morales, J.R., Trousse, F., Fermin, Y., Sowden, J.C., Bovolenta, P., 2006. Proper patterning of the optic fissure requires the sequential activity of BMP7 and SHH. Development 133, 3179-3190.

Moreno, N., Gonzalez, A., Retaux, S., 2009. Development and evolution of the subpallium. Semin Cell Dev Biol 20, 735-743.

Morita, K., Sasaki, H., Fujimoto, K., Furuse, M., Tsukita, S., 1999. Claudin-11/OSP-based tight junctions of myelin sheaths in brain and Sertoli cells in testis. J Cell Biol 145, 579-588.

Muenke, M., Beachy, P.A., 2000. Genetics of ventral forebrain development and holoprosencephaly. Curr Opin Genet Dev 10, 262-269.

Nagai, T., Aruga, J., Minowa, O., Sugimoto, T., Ohno, Y., Noda, T., Mikoshiba, K., 2000. Zic2 regulates the kinetics of neurulation. Proc Natl Acad Sci U S A 97, 1618-1623.

Nanni, L., Ming, J.E., Bocian, M., Steinhaus, K., Bianchi, D.W., Die-Smulders, C., Giannotti, A., Imaizumi, K., Jones, K.L., Campo, M.D., Martin, R.A., Meinecke, P., Pierpont, M.E., Robin, N.H., Young, I.D., Roessler, E., Muenke, M., 1999. The mutational spectrum of the sonic hedgehog gene in holoprosencephaly: SHH mutations cause a significant proportion of autosomal dominant holoprosencephaly. Hum Mol Genet 8, 2479-2488.

Neumann, C.J., Nuesslein-Volhard, C., 2000. Patterning of the zebrafish retina by a wave of sonic hedgehog activity. Science 289, 2137-2139.

Nornes, H.O., Dressler, G.R., Knapik, E.W., Deutsch, U., Gruss, P., 1990. Spatially and temporally restricted expression of Pax2 during murine neurogenesis. Development 109, 797-809.

Nyholm, M.K., Abdelilah-Seyfried, S., Grinblat, Y., 2009. A novel genetic mechanism regulates dorsolateral hinge-point formation during zebrafish cranial neurulation. J Cell Sci 122, 2137-2148.

O'Quin, K.E., Doshi, P., Lyon, A., Hoenemeyer, E., Yoshizawa, M., Jeffery, W.R., 2015. Complex Evolutionary and Genetic Patterns Characterize the Loss of Scleral Ossification in the Blind Cavefish Astyanax mexicanus. PLoS One 10, e0142208.

Pfeffer, P.L., Gerster, T., Lun, K., Brand, M., Busslinger, M., 1998. Characterization of three novel members of the zebrafish Pax2/5/8 family: dependency of Pax5 and Pax8 expression on the Pax2.1 (noi) function. Development 125, 3063-3074.

Pini, J., Kueper, J., Hu, Y.D., Kawasaki, K., Yeung, P., Tsimbal, C., Yoon, B., Carmichael, N., Maas, R.L., Cotney, J., Grinblat, Y., Liao, E.C., 2020. ALX1-related frontonasal dysplasia results from defective neural crest cell development and migration. EMBO Mol Med, e12013.

Piotrowski, T., Nusslein-Volhard, C., 2000. The endoderm plays an important role in patterning the segmented pharyngeal region in zebrafish (Danio rerio). Dev Biol 225, 339-356.

Pollock, L.M., Perkins, B., Anand-Apte, B., 2020. Primary cilia are present on endothelial cells of the hyaloid vasculature but are not required for the development of the blood-retinal barrier. PLoS One 15, e0225351.

Portal, C., Rompolas, P., Lwigale, P., Iomini, C., 2019. Primary cilia deficiency in neural crest cells models anterior segment dysgenesis in mouse. Elife 8.

Pourebrahim, R., Houtmeyers, R., Ghogomu, S., Janssens, S., Thelie, A., Tran, H.T.,

Langenberg, T., Vleminckx, K., Bellefroid, E., Cassiman, J.J., Tejpar, S., 2011. Transcription factor Zic2 inhibits Wnt/beta-catenin protein signaling. J Biol Chem 286, 37732-37740.

Puschel, A.W., Westerfield, M., Dressler, G.R., 1992. Comparative analysis of Pax-2 protein distributions during neurulation in mice and zebrafish. Mech Dev 38, 197-208.

Qu, S., Tucker, S.C., Zhao, Q., deCrombrugghe, B., Wisdom, R., 1999. Physical and genetic interactions between Alx4 and Cart1. Development 126, 359-369.

Rice, R., Spencer-Dene, B., Connor, E.C., Gritli-Linde, A., McMahon, A.P., Dickson, C., Thesleff, I., Rice, D.P., 2004. Disruption of Fgf10/Fgfr2b-coordinated epithelial-mesenchymal interactions causes cleft palate. J Clin Invest 113, 1692-1700.

Roessler, E., Muenke, M., 2010. The molecular genetics of holoprosencephaly. Am J Med Genet C Semin Med Genet 154C, 52-61.

Rowitch, D.H., McMahon, A.P., 1995. Pax-2 expression in the murine neural plate precedes and encompasses the expression domains of Wnt-1 and En-1. Mech Dev 52, 3-8.

Sagai, T., Amano, T., Maeno, A., Ajima, R., Shiroishi, T., 2019. SHH signaling mediated by a prechordal and brain enhancer controls forebrain organization. Proc Natl Acad Sci U S A 116, 23636-23642.

Saint-Geniez, M., D'Amore, P.A., 2004. Development and pathology of the hyaloid, choroidal and retinal vasculature. Int J Dev Biol 48, 1045-1058.

Sakai, D., Dixon, J., Achilleos, A., Dixon, M., Trainor, P.A., 2016. Prevention of Treacher Collins syndrome craniofacial anomalies in mouse models via maternal antioxidant supplementation. Nat Commun 7, 10328.

Sanek, N.A., Grinblat, Y., 2008. A novel role for zebrafish zic2a during forebrain development. Dev Biol 317, 325-335.

Sanek, N.A., Taylor, A.A., Nyholm, M.K., Grinblat, Y., 2009. Zebrafish zic2a patterns the forebrain through modulation of Hedgehog-activated gene expression. Development 136, 3791-3800.

Sanyanusin, P., McNoe, L.A., Sullivan, M.J., Weaver, R.G., Eccles, M.R., 1995a. Mutation of PAX2 in two siblings with renal-coloboma syndrome. Hum Mol Genet 4, 2183-2184.

Sanyanusin, P., Norrish, J.H., Ward, T.A., Nebel, A., McNoe, L.A., Eccles, M.R., 1996. Genomic structure of the human PAX2 gene. Genomics 35, 258-261.

Sanyanusin, P., Schimmenti, L.A., McNoe, L.A., Ward, T.A., Pierpont, M.E., Sullivan, M.J., Dobyns, W.B., Eccles, M.R., 1995b. Mutation of the PAX2 gene in a family with optic nerve colobomas, renal anomalies and vesicoureteral reflux. Nat Genet 9, 358-

364.

Sasagawa, S., Takabatake, T., Takabatake, Y., Muramatsu, T., Takeshima, K., 2002. Axes establishment during eye morphogenesis in Xenopus by coordinate and antagonistic actions of BMP4, Shh, and RA. Genesis 33, 86-96.

Saunders, L.R., McClay, D.R., 2014. Sub-circuits of a gene regulatory network control a developmental epithelial-mesenchymal transition. Development 141, 1503-1513.

Schwend, T., Ahlgren, S.C., 2009. Zebrafish con/disp1 reveals multiple spatiotemporal requirements for Hedgehog-signaling in craniofacial development. BMC Dev Biol 9, 59.

Sedykh, I., Yoon, B., Roberson, L., Moskvin, O., Dewey, C.N., Grinblat, Y., 2017. Zebrafish zic2 controls formation of periocular neural crest and choroid fissure morphogenesis. Dev Biol 429, 92-104.

Sehgal, R., Sheibani, N., Rhodes, S.J., Belecky Adams, T.L., 2009. BMP7 and SHH regulate Pax2 in mouse retinal astrocytes by relieving TLX repression. Dev Biol 332, 429-443.

Seko, Y., Azuma, N., Takahashi, Y., Makino, H., Morito, T., Muneta, T., Matsumoto, K., Saito, H., Sekiya, I., Umezawa, A., 2008. Human sclera maintains common characteristics with cartilage throughout evolution. PLoS One 3, e3709.

Seo, S., Chen, L., Liu, W., Zhao, D., Schultz, K.M., Sasman, A., Liu, T., Zhang, H.F., Gage, P.J., Kume, T., 2017. Foxc1 and Foxc2 in the Neural Crest Are Required for Ocular Anterior Segment Development. Invest Ophthalmol Vis Sci 58, 1368-1377.

Serbedzija, G.N., Bronner-Fraser, M., Fraser, S.E., 1992. Vital dye analysis of cranial neural crest cell migration in the mouse embryo. Development 116, 297-307.

Skarie, J.M., Link, B.A., 2009. FoxC1 is essential for vascular basement membrane integrity and hyaloid vessel morphogenesis. Invest Ophthalmol Vis Sci 50, 5026-5034.

Stevenson, B.R., Keon, B.H., 1998. The tight junction: morphology to molecules. Annu Rev Cell Dev Biol 14, 89-109.

Su, L., Cheng, C.Y., Mruk, D.D., 2009. Drug transporter, P-glycoprotein (MDR1), is an integrated component of the mammalian blood-testis barrier. Int J Biochem Cell Biol 41, 2578-2587.

Swartz, M.E., Nguyen, V., McCarthy, N.Q., Eberhart, J.K., 2012. Hh signaling regulates patterning and morphogenesis of the pharyngeal arch-derived skeleton. Dev Biol 369, 65-75.

Swartz, M.E., Sheehan-Rooney, K., Dixon, M.J., Eberhart, J.K., 2011. Examination of a palatogenic gene program in zebrafish. Dev Dyn 240, 2204-2220.

Szabo, A., Mayor, R., 2018. Mechanisms of Neural Crest Migration. Annu Rev Genet

52, 43-63.

Szabo, A., Melchionda, M., Nastasi, G., Woods, M.L., Campo, S., Perris, R., Mayor, R., 2016. In vivo confinement promotes collective migration of neural crest cells. J Cell Biol 213, 543-555.

Szabo, N.E., Zhao, T., Zhou, X., Alvarez-Bolado, G., 2009. The role of Sonic hedgehog of neural origin in thalamic differentiation in the mouse. J Neurosci 29, 2453-2466.

Takamiya, M., Stegmaier, J., Kobitski, A.Y., Schott, B., Weger, B.D., Margariti, D., Cereceda Delgado, A.R., Gourain, V., Scherr, T., Yang, L., Sorge, S., Otte, J.C., Hartmann, V., van Wezel, J., Stotzka, R., Reinhard, T., Schlunck, G., Dickmeis, T., Rastegar, S., Mikut, R., Nienhaus, G.U., Strahle, U., 2020. Pax6 organizes the anterior eye segment by guiding two distinct neural crest waves. PLoS Genet 16, e1008774.

Take-uchi, M., Clarke, J.D., Wilson, S.W., 2003. Hedgehog signalling maintains the optic stalk-retinal interface through the regulation of Vax gene activity. Development 130, 955-968.

Tao, C., Zhang, X., 2014. Development of astrocytes in the vertebrate eye. Dev Dyn 243, 1501-1510.

ten Berge, D., Brouwer, A., el Bahi, S., Guenet, J.L., Robert, B., Meijlink, F., 1998. Mouse Alx3: an aristaless-like homeobox gene expressed during embryogenesis in ectomesenchyme and lateral plate mesoderm. Dev Biol 199, 11-25.

Teslaa, J.J., Keller, A.N., Nyholm, M.K., Grinblat, Y., 2013. Zebrafish Zic2a and Zic2b regulate neural crest and craniofacial development. Dev Biol 380, 73-86.

Thompson, H., Griffiths, J.S., Jeffery, G., McGonnell, I.M., 2010. The retinal pigment epithelium of the eye regulates the development of scleral cartilage. Dev Biol 347, 40-52.

Tiwari-Woodruff, S.K., Buznikov, A.G., Vu, T.Q., Micevych, P.E., Chen, K., Kornblum, H.I., Bronstein, J.M., 2001. OSP/claudin-11 forms a complex with a novel member of the tetraspanin super family and beta1 integrin and regulates proliferation and migration of oligodendrocytes. J Cell Biol 153, 295-305.

Todd, L., Fischer, A.J., 2015. Hedgehog signaling stimulates the formation of proliferating Muller glia-derived progenitor cells in the chick retina. Development 142, 2610-2622.

Trainor, P.A., Krumlauf, R., 2001. Hox genes, neural crest cells and branchial arch patterning. Curr Opin Cell Biol 13, 698-705.

Trost, A., Lange, S., Schroedl, F., Bruckner, D., Motloch, K.A., Bogner, B., Kaser-Eichberger, A., Strohmaier, C., Runge, C., Aigner, L., Rivera, F.J., Reitsamer, H.A., 2016. Brain and Retinal Pericytes: Origin, Function and Role. Front Cell Neurosci 10, 20.

Trost, A., Schroedl, F., Lange, S., Rivera, F.J., Tempfer, H., Korntner, S., Stolt, C.C., Wegner, M., Bogner, B., Kaser-Eichberger, A., Krefft, K., Runge, C., Aigner, L., Reitsamer, H.A., 2013. Neural crest origin of retinal and choroidal pericytes. Invest Ophthalmol Vis Sci 54, 7910-7921.

Twigg, S.R., Versnel, S.L., Nurnberg, G., Lees, M.M., Bhat, M., Hammond, P., Hennekam, R.C., Hoogeboom, A.J., Hurst, J.A., Johnson, D., Robinson, A.A., Scambler, P.J., Gerrelli, D., Nurnberg, P., Mathijssen, I.M., Wilkie, A.O., 2009. Frontorhiny, a distinctive presentation of frontonasal dysplasia caused by recessive mutations in the ALX3 homeobox gene. Am J Hum Genet 84, 698-705.

Van Der Meulen, K.L., Vocking, O., Weaver, M.L., Meshram, N.N., Famulski, J.K., 2020. Spatiotemporal Characterization of Anterior Segment Mesenchyme Heterogeneity During Zebrafish Ocular Anterior Segment Development. Front Cell Dev Biol 8, 379.

Varga, Z.M., Amores, A., Lewis, K.E., Yan, Y.L., Postlethwait, J.H., Eisen, J.S., Westerfield, M., 2001. Zebrafish smoothened functions in ventral neural tube specification and axon tract formation. Development 128, 3497-3509.

Veitch, E., Begbie, J., Schilling, T.F., Smith, M.M., Graham, A., 1999. Pharyngeal arch patterning in the absence of neural crest. Curr Biol 9, 1481-1484.

Vieira, C., Garda, A.L., Shimamura, K., Martinez, S., 2005. Thalamic development induced by Shh in the chick embryo. Dev Biol 284, 351-363.

Volkmann, B.A., Zinkevich, N.S., Mustonen, A., Schilter, K.F., Bosenko, D.V., Reis, L.M., Broeckel, U., Link, B.A., Semina, E.V., 2011. Potential novel mechanism for Axenfeld-Rieger syndrome: deletion of a distant region containing regulatory elements of PITX2. Invest Ophthalmol Vis Sci 52, 1450-1459.

Wada, N., Javidan, Y., Nelson, S., Carney, T.J., Kelsh, R.N., Schilling, T.F., 2005. Hedgehog signaling is required for cranial neural crest morphogenesis and chondrogenesis at the midline in the zebrafish skull. Development 132, 3977-3988.

Wang, X.Y., Li, S., Wang, G., Ma, Z.L., Chuai, M., Cao, L., Yang, X., 2015. High glucose environment inhibits cranial neural crest survival by activating excessive autophagy in the chick embryo. Sci Rep 5, 18321.

Warr, N., Powles-Glover, N., Chappell, A., Robson, J., Norris, D., Arkell, R.M., 2008. Zic2-associated holoprosencephaly is caused by a transient defect in the organizer region during gastrulation. Hum Mol Genet 17, 2986-2996.

Weaver, M.L., Piedade, W.P., Meshram, N.N., Famulski, J.K., 2020. Hyaloid vasculature and mmp2 activity play a role during optic fissure fusion in zebrafish. Sci Rep 10, 10136.

Weiss, O., Kaufman, R., Mishani, E., Inbal, A., 2017. Ocular vessel patterning in

zebrafish is indirectly regulated by Hedgehog signaling. Int J Dev Biol 61, 277-284.

Wentzel, P., Eriksson, U.J., 2011. Altered gene expression in rat cranial neural crest cells exposed to a teratogenic glucose concentration in vitro: paradoxical downregulation of antioxidative defense genes. Birth Defects Res B Dev Reprod Toxicol 92, 487-497.

Wessells, H., Sullivan, C.J., Tsubota, Y., Engel, K.L., Kim, B., Olson, N.E., Thorner, D., Chitaley, K., 2009. Transcriptional profiling of human cavernosal endothelial cells reveals distinctive cell adhesion phenotype and role for claudin 11 in vascular barrier function. Physiol Genomics 39, 100-108.

Whish, S., Dziegielewska, K.M., Mollgard, K., Noor, N.M., Liddelow, S.A., Habgood, M.D., Richardson, S.J., Saunders, N.R., 2015. The inner CSF-brain barrier: developmentally controlled access to the brain via intercellular junctions. Front Neurosci 9, 16.

Williams, A.L., Bohnsack, B.L., 2015. Neural crest derivatives in ocular development: discerning the eye of the storm. Birth Defects Res C Embryo Today 105, 87-95.

Wolburg, H., Wolburg-Buchholz, K., Liebner, S., Engelhardt, B., 2001. Claudin-1, claudin-2 and claudin-11 are present in tight junctions of choroid plexus epithelium of the mouse. Neurosci Lett 307, 77-80.

Wu, S.Y., McClay, D.R., 2007. The Snail repressor is required for PMC ingression in the sea urchin embryo. Development 134, 1061-1070.

Xu, X., Bringas, P., Jr., Soriano, P., Chai, Y., 2005. PDGFR-alpha signaling is critical for tooth cusp and palate morphogenesis. Dev Dyn 232, 75-84.

Yao, W., Liu, Y., Zhang, Z., Li, G., Xu, X., Zou, K., Xu, Y., Zou, L., 2015. ALX1 promotes migration and invasion of lung cancer cells through increasing snail expression. Int J Clin Exp Pathol 8, 12129-12139.

Yuan, H., Kajiyama, H., Ito, S., Yoshikawa, N., Hyodo, T., Asano, E., Hasegawa, H., Maeda, M., Shibata, K., Hamaguchi, M., Kikkawa, F., Senga, T., 2013. ALX1 induces snail expression to promote epithelial-to-mesenchymal transition and invasion of ovarian cancer cells. Cancer Res 73, 1581-1590.

Zhang, Z., Song, Y., Zhao, X., Zhang, X., Fermin, C., Chen, Y., 2002. Rescue of cleft palate in Msx1-deficient mice by transgenic Bmp4 reveals a network of BMP and Shh signaling in the regulation of mammalian palatogenesis. Development 129, 4135-4146.

Zhao, G.Q., Eberspaecher, H., Seldin, M.F., de Crombrugghe, B., 1994. The gene for the homeodomain-containing protein Cart-1 is expressed in cells that have a chondrogenic potential during embryonic development. Mech Dev 48, 245-254.

Zhao, G.Q., Zhou, X., Eberspaecher, H., Solursh, M., de Crombrugghe, B., 1993. Cartilage homeoprotein 1, a homeoprotein selectively expressed in chondrocytes.

Proc Natl Acad Sci U S A 90, 8633-8637.

Zhao, L., Zevallos, S.E., Rizzoti, K., Jeong, Y., Lovell-Badge, R., Epstein, D.J., 2012. Disruption of SoxB1-dependent Sonic hedgehog expression in the hypothalamus causes septo-optic dysplasia. Dev Cell 22, 585-596.

Zhao, Q., Behringer, R.R., de Crombrugghe, B., 1996. Prenatal folic acid treatment suppresses acrania and meroanencephaly in mice mutant for the Cart1 homeobox gene. Nat Genet 13, 275-283.

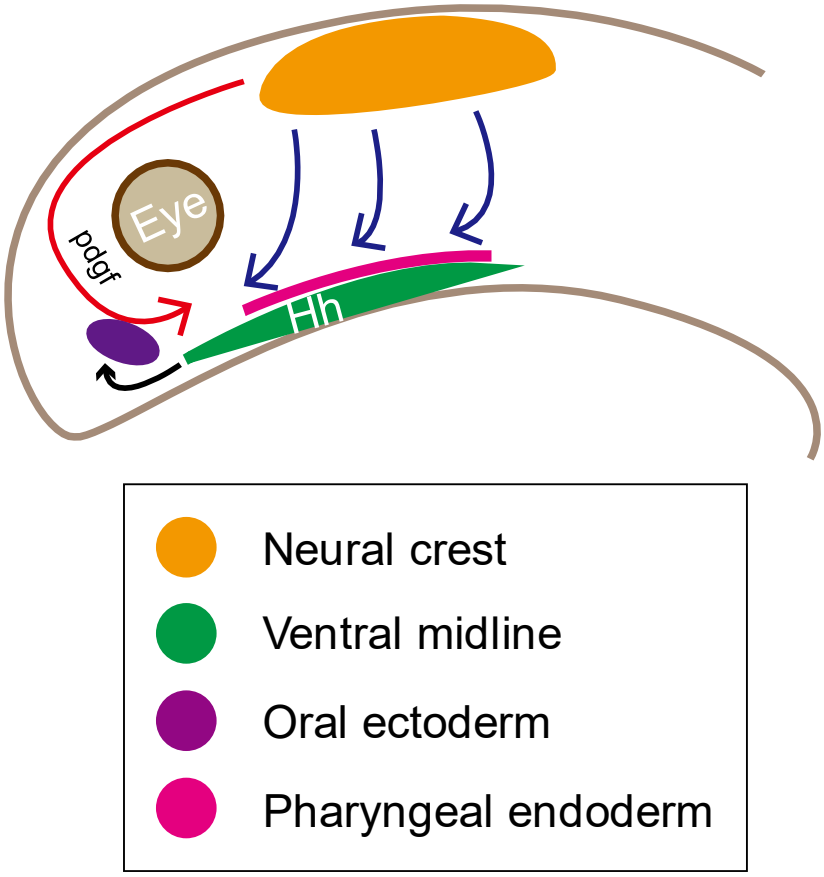

Figure 1. *Model representation of cranial neural crest migration*

Cranial neural crest migrating anterior to the eyes (aCNC) (Red arrow) receives the signal from the eyes, such as pdgf from the optic stalk, and then migrate onward to the oral ectoderm, which is induced by Hh signaling from the ventral midline. aCNC contributes to the development of anterior neural derivatives, ethmoid plate, and anterior segment of the eye.

Cranial neural crest migrating in three separate streams caudally to the eyes (Blue arrow) interacts with the pharyngeal endoderm and contributes to form jaw cartilages.

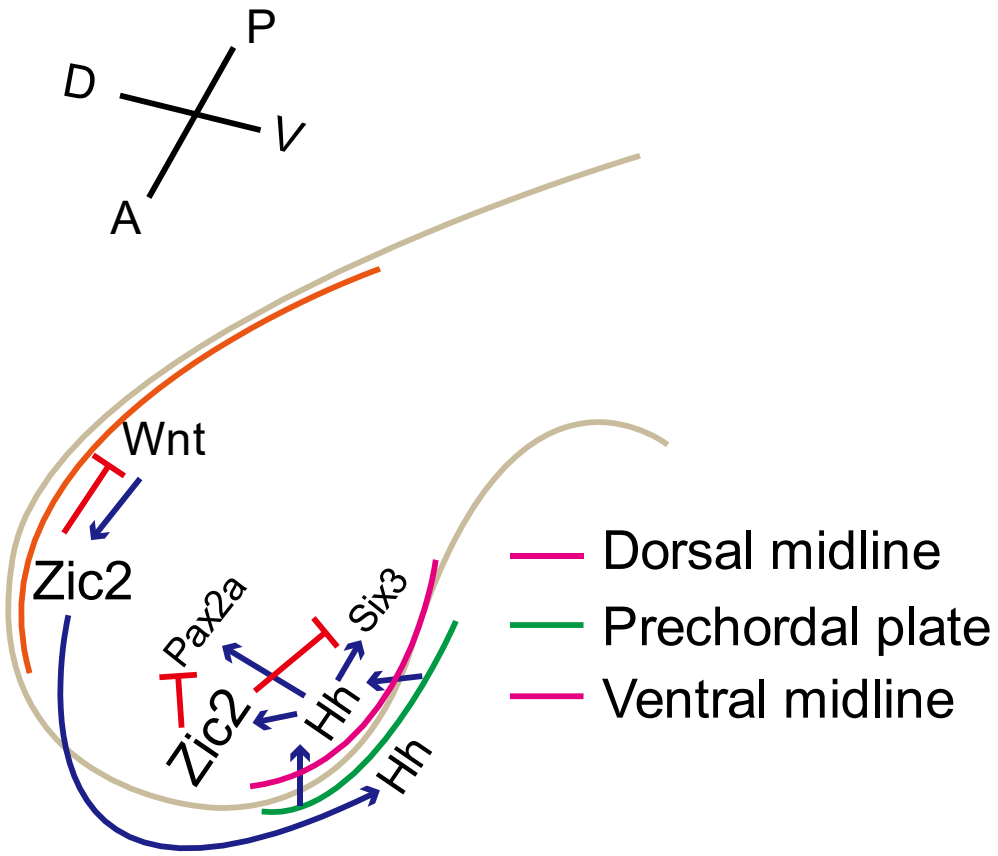

Figure 2. *Model representation of zic2 function in craniofacial complex development*

Wnt signaling in the dorsal midline induces telencephalic expression of *zic2* (Nyholm et al., 2009) and, conversely, *zic2* inhibits Wnt signaling (Pourebrahim et al., 2011). *Zic2* establishes Hh signaling in PrCP (Warr et al., 2008), which is required for further specification of ventral midline. Hh signaling from the ventral midline activates *zic2* and *pax2a* at the optic stalk and *six3* at ventral medial forebrain (Sanek et al., 2009). *Zic2* inhibits *pax2a* transcription at the optic stalk (Sanek et al., 2009; Sedykh et al., 2017) and negatively modulates *six3* transcription at ventral medial forebrain (Sanek et al., 2009).

Chapter II

Zebrafish zic2 controls formation of periocular neural crest and choroid fissure morphogenesis.

Sedykh, I., Yoon, B., Roberson, L., Moskvin, O., Dewey, C.N., Grinblat, Y., 2017. Zebrafish zic2 controls formation of periocular neural crest and choroid fissure morphogenesis. Dev Biol 429, 92-104.

Abstract

The vertebrate retina develops in close proximity to the forebrain and neural crest-derived cartilages of the face and jaw. Coloboma, a congenital eye malformation, is associated with aberrant forebrain development (holoprosencephaly) and with craniofacial defects (frontonasal dysplasia) in humans, suggesting a critical role for cross-lineage interactions during retinal morphogenesis. ZIC2, a zinc-finger transcription factor, is linked to human holoprosencephaly. We have previously used morpholino assays to show zebrafish zic2 functions in the developing forebrain, retina and craniofacial cartilage. We now report that zebrafish with genetic lesions in zebrafish zic2 orthologs, zic2a and zic2b, develop with retinal coloboma and craniofacial anomalies. We demonstrate a requirement for zic2 in restricting pax2a expression and show evidence that zic2 function limits Hh signaling. RNA-seq transcriptome analysis identified an early requirement for zic2 in periocular neural crest as an activator of alx1, a transcription factor with essential roles in craniofacial and ocular morphogenesis in human and zebrafish. Collectively, these data establish zic2 mutant zebrafish as a powerful new genetic model for in-depth dissection of cell interactions and genetic controls during craniofacial complex development.

Introduction

The key portion of the vertebrate eye, the neural retina, begins its development as an integral part of the forebrain primordium. It evaginates to form bilateral optic vesicles that connect to the forebrain via the optic stalks (OS). Optic vesicles then fold into cup-like structures that briefly remain open at the site adjacent to OS, termed the choroid fissure (Bazin-Lopez et al., 2015; Gestri et al., 2012; Kwan, 2014; Schmitt and

Dowling, 1994). The edges of the choroid fissure come together and fuse during normal development; failure of this process results in uveal coloboma, estimated to occur once in every 5,000 births (Williamson and FitzPatrick, 2014). Coloboma is a significant cause of congenital blindness, found in 3–11% of blind children (Onwochei et al., 2000). Despite its prevalence and debilitating consequences, the underlying molecular defects that cause coloboma are not well understood.

The choroid fissure forms in a complex environment that includes the adjacent forebrain and neural crest (NC)-derived mesenchymal cells on their way to becoming skeletal and vascular elements of the face and jaw. In zebrafish, NC cells that migrate in the anterior streams around the optic vesicle form the neurocranium (ethmoid plate and the trabeculae) (Schilling et al., 1999; Wada et al., 2005). The retina and OS signal to the anterior NC, directing it to its destinations (Eberhart et al., 2008; Kish et al., 2011; Swartz et al., 2011). There is emerging evidence for a reciprocal interaction, whereby NC cells signal back to the eye and brain (reviewed in (Bazin-Lopez et al., 2015; Gestri et al., 2012; Le Douarin et al., 2007). In humans, significant comorbidity has been reported between frontonasal dysplasia and coloboma (Wu et al., 2007), suggesting that NC plays a specific role in choroid fissure morphogenesis. The importance of this mechanism has only recently come to light and needs robust genetic models to be fully understood.

Dysregulation in several signaling pathways has been implicated in coloboma, with Hedgehog (Hh) signaling arguably the best characterized (Williamson and FitzPatrick, 2014). Disruption of Hh signaling also causes forebrain anomalies called holoprosencephaly (HPE)(Roessler et al., 1996; Roessler and Muenke, 2010), and facial dysmorphologies that range from hypertelorism (increased distance between

eye orbits) attributed to increased Hh signaling to orofacial clefting caused by Hh reduction (Brugmann et al., 2010; Gongal et al., 2011; Young et al., 2010). To understand how Hh signaling controls these processes, it is necessary to examine the downstream effectors of Hh signaling in each developmental context.

zic2, a member of the conserved Zic family of zinc-finger transcription factors, is one such effector. zic2 plays a key role in brain morphogenesis, as indicated by the high incidence of zic2 mutations in human patients with HPE (Brown et al., 2001; Brown et al., 1998; Ribeiro et al., 2012; Roessler et al., 2009; Solomon et al., 2010). Extensive studies in mouse and Xenopus have demonstrated essential roles for zic2 in early neural development, namely, neural crest specification and neural tube closure (Elms et al., 2004; Elms et al., 2003; Houtmeyers et al., 2016; Nagai et al., 2000; Nagai et al., 1997; Nakata et al., 1997, 1998; Nyholm et al., 2009; Teslaa et al., 2013; Warr et al., 2008; Ybot-Gonzalez et al., 2007). Zic2 is also required for specification of embryonic stem cells, where it functions as an enhancer-binding cofactor in concert with the Mbd3-NuRD chromatin remodeling complex (Luo et al., 2015). Later in development, zic2 function is required for correct migration of cortical neurons (Murillo et al., 2015), for cerebellar granular neuron differentiation (Frank et al., 2015) and as a key determinant of ipsilateral vs contralateral projection in retinal ganglion cells (Escalante et al., 2013; Garcia-Frigola et al., 2008; Herrera et al., 2003),. In hypomorphic zic2 mice, defective retinal morphogenesis has been reported, but not characterized (Herrera et al., 2003). The underlying mechanism of its functions during development have been elusive until recently, when zic2 was found to inhibit canonical Wnt signaling (Fujimi et al., 2012; Pourebrahim et al., 2011), and to control forebrain morphogenesis via a direct interaction with Smad2/3 in the Nodal signal transduction

pathway (Houtmeyers et al., 2016). To fully understand the mechanism of zic2 functions in the context of the developing embryo, it is essential that we dissect these functions further, and in more than one model organism.

Here we report that zebrafish with genetic lesions in zebrafish zic2 orthologs, zic2a and zic2b, develop with profound retinal and craniofacial anomalies, similar to those observed after transient depletion of zic2 by antisense morpholino oligos (Sanek et al., 2009; Teslaa et al., 2013). We show that zic2 function is required for the correct morphogenesis of the OS and for juxtaposing the edges of the fissure to allow its subsequent closure. We demonstrate a requirement for zic2 in restricting pax2a expression at the OS/ventral retina border, and show evidence of increased Hh signaling in the absence of zic2 function. Using RNA-seq-based transcriptome analysis, we confirm an early requirement for zic2 function in NC-derived pharyngeal and periocular neural crest, and identify a novel role for zic2 as a transcriptional activator of Alx1, a paired homeobox transcription factor with key functions in craniofacial and ocular morphogenesis in human and zebrafish embryos (Dee et al., 2013; Uz et al., 2010). Collectively, these data establish zic2 mutant zebrafish as a powerful new genetic model for in-depth dissection of the complex inter-lineage cell interactions and genetic controls during craniofacial complex development.

Materials and Methods

Zebrafish strains and embryo manipulation

Adult zebrafish were maintained according to established methods (Westerfield, 1993). All experimental protocols using zebrafish were approved by the University of Wisconsin Animal Care and Use Committee and carried out in accordance with the institutional animal care protocols. Embryos were obtained from natural matings and staged according to (Kimmel et al., 1995). The following mutant strains of zebrafish were used: zic2a^{GBT133} insertional mutant (Clark et al., 2011); zic2b^{UWt104} mutant, generated by TALEN mutagenesis in the course of the study; zic2b^{UW1127} and zic2b^{UW1116} mutants, generated by CRISPR/Cas9 mutagenesis in the course of this study. Double zic2 mutants were obtained by crossing zic2a^{GBT133}/+ zebrafish to each of the three zic2 mutant allele carriers; F1s were selected by RFP fluorescence to identify zic2a^{GBT133} carriers, which express RFP (Clark et al., 2011) and raised to adulthood. Adult zic2b+/− zebrafish were identified by PCR genotyping of genomic DNA extracted from tail clips.

Cyclopamine treatments were carried out as follows: cyclopamine (AdipoGen) was diluted in DMSO and added to E3 to final concentrations of 3uM or 4.5uM; final DMSO concentration was adjusted to 0.5%. Embryos were placed in E3 with cyclopamine or 0.5%DMSO for vehicle-only control. Treatments were started at 3hpf (before maternal-zygotic transition), 5 hpf or 6hpf. Embryos were moved to fresh E3

at 24 hpf and allowed to develop until 3–4 dpf, when they were assayed for retinal morphology.

Engineered nuclease mutagenesis and high-resolution melt analysis (HRMA)

Zic2b TALEN was designed and synthesized by the Mutation Generation and Detection Core (MGD) Facility, University of Utah to the following target left and right sites in exon 1, respectively: 5′-TCCTCTTGCGCAGCCGAGG-3′ and 5′-GGGGTGTTGTCCACTGGCCG-3.

Design of zic2b CRISPR site 5′-GGTGGAGTTAAAAGTGGAGC-3′ in exon1, mutagenesis and founder identifications were carried out as previously described (Sedykh et al., 2016), with the following HRMA primers pairs: TALEN site - 5′-TGGACAACACCCCATCTTCA-3′ and 5′-GGATGTTTGGAGAGCCGTGAT-3; CRISPR site - 5′-TATTCTGCGGCCGCTCTT3′ and 5′-GGAGTCGAATCCCCAAATC-3′.

Sequencing and PCR genotyping of zic2 mutant alleles

To determine zic2a genotype, DNA was extracted from individual embryos or adult fish and subjected to PCR with the following primers: gbt forward 5′-CCCCGTAATGCAGAAGAAGA-3′, gbt reverse 5′-GTCCAGCTTGATGTCGGTCT-3′,

wt forward and wt reverse 5′-ATTCATGGAGCCGTACTGGTTGTG-3′ and 5′-TGTTACTGGACGCAGGGCATCAGTT-3′. (see Supp. Fig. 2 for details).

Zic2b PCR fragments identified as mutant by HRMA were subcloned via TA cloning into pGEMT-Easy (Promega) and sequenced to characterize the mutations. Subsequently, PCR followed by Metaphor gel electrophoresis was used to efficiently genotype individual embryos and adult fish, HRMA primer sequence above were used for CRISPR allele genotyping. TALEN allele genotyping used 5′-GGACAACACCCCATCTTC-3′ and 5′-CGGGGAAAAGTAGGTGAC-3′ (Supp. Fig. 2).

RNA-seq transcriptome analysis

Embryos derived from a zic2a^{GBT133}/+; zic2b^{UW1127}/+ incross were sorted by presence or absence of coloboma. RNA was prepared from each individual embryo using the RNAEasy kit (Qiagen) according to (de Jong et al., 2010). cDNA libraries were prepared using the TruSeq stranded mRNA library preparation protocol with poly-A selection and sequenced on the Illumina HiSeq2500. Gene-level read counts were estimated from the raw sequencing data using RSEM v1.2.18 (Li and Dewey, 2011) and Bowtie v1.1.1 (Langmead et al., 2009). The gene set used consisted of all genes classified as protein coding or lincRNA within the Ensembl v77 annotation of the Zv9 assembly of the zebrafish genome. RSEM was run with option “–forward-prob 0” to take into account that the RNA-seq libraries were strand-specific. A matrix of gene-level counts from all libraries was compiled and analyzed for differential gene expression using the R statistical language and environment (R core team, 2014).

Specifically, the count matrix was first pre-normalized using the median normalization routine from the EBSeq v1.5.4 package (Leng et al., 2013). The normalized dataset was then filtered to exclude genes that did not show coverage of at least 10 counts in at least 1 library across the entire dataset. The edgeR v3.14.0 package, (Robinson et al., 2010) with internal normalization switched off, was subsequently applied to call for differential expression (DE). Genes with assigned value of False Discovery Rate (FDR) below 0.05 by edgeR were preliminarily selected. Since a) low-expressed genes tend to be artificially enriched in the list of genes called DE by statistical algorithms and b) DE genes expressed at higher levels have more biological relevance and follow-up potential, we applied an additional filter to the edgeR output by retaining genes that have expression exceeding a certain quantile (0.2) of genome-wide distribution of expression values in at least 60% of libraries representing the strain with a larger mean expression of that gene.

Immunohistochemistry, in situ hybridization, and alcian blue staining

Embryos were fixed in 4% paraformaldehyde (PFA) in PBS, or in 4% PFA/0.25% glutaraldehyde, 5mM EGTA, 0.2% TritonX-100, 1xPBS for optimal phalloidin staining. After PFA/glutaraldehyde fix, embryos were treated with 100mM sodium borohydride to reduce auto-fluorescence. Primary antibodies were detected fluorescently with Alexa-labeled goat anti-mouse or goat anti-rabbit secondary antibodies. Embryos were mounted in VectaShield and imaged on an Olympus IX81 inverted confocal microscope with the Fluoview 1000 confocal package, using a 60x water immersion

objective (NA 1.10), a 60x oil immersion objective (NA 1.35) or a 20x objective (NA 0.75).

Antibody/stain reagent	Source	Dilution
Rabbit anti-pax2a	GeneTex, cat# GTX128127	1:500
Mouse anti-acetylated tubulin	Sigma, T6793	1:400
Goat Anti-Mouse Alexa 488	Invitrogen, cat#A-11001	1:500
Goat Anti-Rabbit Alexa 568	Invitrogen, cat#A-11011	1:500
phalloidin Alexa 488 or 568	Molecular Probes, cat#A12379; A12380	1:100
DAPI	Molecular Probes, cat#D21490	1:5000

In situ hybridization was carried out as previously described (Gillhouse et al., 2004), using the following probes: pax2a (Hoyle et al., 2004); dlx2a (Akimenko et al., 1994); crestin (Luo et al., 2001); vax2 (Gross and Dowling, 2005); atoh7 (Masai et al., 2000). cldn11a was synthesized as a gBlocks® Gene Fragments (IDT) and TA-cloned into pGEMT-Easy (Promega). Full length alx1 cDNA was amplified from total mRNA of 24 hpf embryos by PCR with primers 5′-TTGAGACGAGGCCAGAGGAC-3′ and 5′-CCTGGCTCTGTGAATAATTACAAG-3′ primers using OneTaq One-Step RT-PCR kit (NEB), and TA-cloned into pGEMT-Easy (Promega). After WISH, embryos were mounted in 100% glycerol and imaged on Axioskop2 Plus (Zeiss) compound or Leica MZ FLIII stereo microscopes equipped with Leica DFC310 FX camera and LAS v4.0 software. For cartilage staining, zebrafish larvae were fixed at 5–6 dpf in 4%

paraformaldehyde and stained with Alcian Blue according to (Kimmel et al., 1998). Samples were flat-mounted in glycerol for imaging as described above.

Result

Zebrafish zic2 orthologs function redundantly during retinal and craniofacial morphogenesis

Zebrafish zic2 orthologs zic2a and zic2b, the only members of the Zic gene family duplicated in teleosts, reside on chromosomes 9 and 1, respectively. To build a genetic model of zic2-linked HPE in zebrafish, we set out to establish lines mutant at both loci. Toward this end, we obtained a mutagenic gene-trap insertion in the first coding exon of *zic*2a, zic2a^{gbt133}, isolated in a screen by Clark et al. (Clark et al., 2011) (Fig. S1). *zic*2a^{gbt133} homozygous embryos develop normally for the first 2 weeks (data not shown), likely due to functional redundancy with its ortholog, *zic*2b. We used targeted mutagenesis with TALEN and CRISPR/Cas9 to generate frame-shift alleles at two distinct sites in the first exon of the *zic*2b locus (see Materials and Methods for details). Three mutant alleles were isolated that contained a 27-nt insertion (zic2b^{1127}) or a 16-nt insertion (zic2b^{1116}) at the CRISPR target site, and a 4-nt deletion (zic2b^{t104}) at the TALEN target site (Fig. S1). *zic*2b homozygous mutants developed normally and were viable as adults despite the predicted absence of full-length zic2b protein; in contrast, ~5% of the embryos derived from a double heterozygous (*zic*2a+/−; *zic*2b+/−) incross exhibited retinal coloboma by 48 hpf (Fig. 1A–F; Table S1). The expected

proportion of *zic2a; zic2b* homozygous mutants (*zic2* mutants) is 6.25%. Affected embryos frequently presented with mild coloboma, defined here as a relatively small gap present in only one of the two retinae (Fig. 1B, G). Unexpectedly, a subset of embryos with coloboma exhibited periocular hemorrhage and edema, indicative of vascular deficits (Fig. 1C, F).

We next asked if the maternal function of zic2 played a role during retinal development by assessing embryonic phenotypes in progeny from a cross between *zic*2a+/−; ***zic2b−/−*** parents, 25% of which are predicted to be *zic2* mutants. 25% of these embryos exhibited coloboma by 2 dpf (Table S1); coloboma was primarily severe, i.e. bilateral with large ventral gaps (Fig. 1C, E, G), consistent with a requirement for maternal zic2b during retinal morphogenesis. To confirm that zic2 mutations were responsible for abnormal retinal morphogenesis, we genotyped representative embryos with and without coloboma individually (Fig. S2). This analysis showed that the majority of embryos with coloboma were zic2 mutants (going forward, we will refer to zic2 mutants derived from zic2b-/-mothers as MZ-zic2 mutants). Coloboma was also occasionally observed in maternally depleted embryos with one wildtype allele of zic2a (Fig 1H, I).

By 5 dpf, all embryos with coloboma exhibited profoundly hypoplastic craniofacial cartilages, both in the neurocranium and pharyngeal arches, and severe periocular and cranial edema (Fig. 2A, B; Table S2). Similar defects were observed in embryos produced by heterozygous parents and those from zic2a+/−; ***zic2b−/−*** parents (data not shown). Genotypic analysis revealed that this phenotype was restricted to zic2 mutants and embryos with one wildtype allele of zic2a (Fig. 2C,D). Collectively, these data clearly demonstrate a requirement for zygotic zic2 function in

the developing retina and craniofacial cartilages, and an early contribution of maternal zic2b function to retinal morphogenesis.

Zic2 restricts expression of pax2a in the optic stalk

We next asked if ventral retinal patterning and/or morphology were disrupted in zic2 mutants at 24 hpf, prior to the first appearance of overt coloboma. The choroid fissure and the OS are marked by patterned expression of several homeobox transcription factors, including *pax2a* (Macdonald et al., 1995; Mui et al., 2005; Take-uchi et al., 2003). We examined pax2a expression in zic2 embryos using whole mount in situ hybridization (WISH). Embryos derived from zic2a+/−;zic2b+/− parents exhibited normal expression of pax2a overall with the exception of the OS domain, which was mispatterned in 12% of the embryos (Fig. 3A, B). Post-hoc genotyping confirmed that all the embryos with mispatterned pax2a were homozygous for zic2b (Fig. 3C). All embryos with mispatterned pax2a exhibited aberrant ventral retina (Fig. 3D–F), i.e. were also zic2a^{gbt133} homozygous. We next applied confocal microscopy to examine distribution of the Pax2a epitope in 24 hpf MZ-zic2 mutants. Normal retina expressed Pax2a in the restricted portion of the retina adjacent to the choroid fissure (Fig. 3G). In MZ-zic2 mutants, retinal edges of the choroid fissure expressed Pax2a, but were separated by a large gap. The OS were abnormally wide and contained aberrantly high pax2a signal (Fig. 3H). We also noted an intense concentration of F-actin at the choroid fissure in normal siblings and an absence thereof in mutant retina, consistent with aberrant morphogenesis. These observations are consistent with our previous finding that pax2a is ectopically expressed in embryos transiently depleted

of zic2a (Sanek et al., 2009). When examined in ventral cross-sections, MZ-zic2 mutants exhibited aberrant expansion of Pax2a both in the ventral retina and in the pre-optic diencephalon contiguous with the OS (Fig. 3I, J). Pax2a-expressing diencephalon appeared dysmorphic, with thinner walls and larger lumen than the equivalent structure in the unaffected siblings (Fig. 3K, L). Collectively, these observations indicate an early requirement for zic2 function during morphogenesis of both the OS/choroid fissure boundary and the adjacent diencephalon.

Hedgehog growth factors secreted from the ventral diencephalic midline pattern the OS and retina, partitioning it into three domains: the OS, ventral retina and dorsal retina (Ekker et al., 1995; Lee et al., 2008a; Lupo et al., 2005; Schimmenti et al., 2003; Varga et al., 2001; Wang et al., 2015). Since pax2a requires Hh signaling for its expression, pax2a expansion in zic2 mutants may indicate aberrant levels of Hh or an aberrant downstream transcriptional response. Zebrafish that lack the functional Hh receptor *blowout/ptc*1 due to mutations show increased levels Hh signaling and develop with incompletely penetrant coloboma; this defect is efficiently rescued by exposure to low levels of cyclopamine, a small molecule that inhibits Hh signaling (Lee et al., 2008a). Cyclopamine treatment also rescues coloboma caused by knockdown of sox4 or sox11, transcription factors that function as inhibitory modulators of Hh signaling during retinal morphogenesis (Pillai-Kastoori et al., 2014; Wen et al., 2015). We reasoned that, if Hh signaling is expanded in zic2 mutants, inhibition of Hh signaling should reduce the penetrance and/or expressivity of coloboma. To test this prediction, we exposed progeny from *zic2a+/−; zic2b−/−* incrosses to low concentration of cyclopamine that was sufficient to rescue coloboma in *blowout/ptc*1 mutants (Lee et al., 2008a). When progeny from zic2a+/−; zic2b^{t104} parents were

exposed to cyclopamine during gastrulation and somitogenesis, they developed with significantly milder coloboma than their vehicle-treated siblings (Fisher Exact test, $p < 0.02$, Fig. 4A–E, Fig. S3). The overall morphology of the embryos was not affected at this cyclopamine concentration (3–4.5 μM). To test specificity of the rescue, we asked if cyclopamine rescue is allele-independent. Progeny from zic2a+/−; zic2b^{uw1116} parents exhibited significant alleviation of coloboma phenotype after cyclopamine treatment (Fisher Exact test, $p < 0.04$; Fig. 4E, Fig. S3). In contrast, cyclopamine did not significantly affect coloboma penetrance or expressivity in zygotic zic2 mutants (Fig. 4F, Fig. S3). These findings are consistent with the notion that Hh signaling is de-repressed in the absence of functional zic2 and that this de-repression contributes to retinal dysmorphology in zic2 mutants.

Zic2 function is required for neural crest-derived craniofacial lineage formation

We next set out to identify downstream effectors of zic2, i.e. genes whose transcription levels depend on zic2 function, using RNA-seq transcriptomic analysis (Fig. 5A). Embryos derived from *zic*2a+/−; *zic*2b+/− parents were sorted by coloboma at 25–28 hpf, when coloboma first manifests in zic2 mutants. RNA was isolated from individual embryos without pooling to increase the statistical power of analysis and subjected to high-throughput sequencing (see Materials and Methods for details). RNA-seq was performed on 10 samples in total, 5 normal and 5 with coloboma. One of the wild type samples was determined to be a mutant and excluded from further analysis. This approach identified a large set of 362 genes differentially expressed in zic2 mutants (199 increased and 169 reduced) (Table S3). We used the online

bioinformatics tool (Huang da et al., 2009) to sort the responsive gene list into categories based on tissue enrichment in zebrafish (ZFIN_ANATOMY). This analysis identified myotome/somite, craniofacial elements, and heart (enrichment scores 2.78, 2.24 and 1.71, respectively). Myotome/somite markers and heart markers were found primarily in the upregulated set, consistent with expression of zic2b in zebrafish somites (Toyama et al., 2004) and with the demonstrated function for mammalian Zic2 during myogenesis (Inoue et al., 2007; Pan et al., 2011). In contrast, craniofacial markers appeared among transcripts depleted in zic2 mutants. (Fig. 5A). This set included chondrogenic neural crest markers dlx1a, dlx2a, dlx4a and barx1, and xanthophore lineage markers aox5, gch2 and cax1 (references in Table S4). We have previously shown both lineages to be strongly dependent on zic2 function in morpholino assays (Teslaa et al., 2013). A small number of retinal markers were also reduced in zic2 mutants, namely, vax1 and vax2, Hh-regulated OS/ventral retina markers (Take-uchi et al., 2003), and atoh7, expressed in retinal ganglion cells (Masai et al., 2000). Notably, pax2a transcript levels were unchanged in zic2 mutants, perhaps because the mispatterning we have documented in Fig. 3 affects a small portion of its expression domain.

To validate these results, we used WISH on zic2 mutants and siblings. Dlx2a was specifically reduced in pharyngeal arch primordia at 24 hpf, but not in the tel- or diencephalon, in 6% of progeny from zic2a+/−;zic2b+/− parents (Fig. 5B–E), and this reduction was restricted to zic2b−/− embryos (Fig. 5F). Reduced expression of atoh7 and vax2 was also confirmed by WISH (Fig. S4).

Cldn11a, a tight junction component enriched in myelinating oligodendrocytes (Bronstein et al., 1997; Morita et al., 1999) was the most strongly depleted gene

identified by RNA-seq (Fig. 5A). In zebrafish, cldn11a expression has been reported in vascular endothelium (Cannon et al., 2013). In contrast, we found cldn11a expression to be restricted to a small group of cells anterior to the retina, in close proximity to the choroid fissure, at 24 hpf (Fig. 5G). Consistent with RNA-seq results, cldn11a expression was nearly abolished in zic2 mutants assayed by WISH (Fig. 5H). Notably, cldn11 transcription requires zic2 function in the differentiating mammalian cerebellar ganglion cells (Frank et al., 2015).

Zic2 controls transcription of alx1 in the periocular neural crest

One of the candidate targets of zic2 identified by RNA-seq, Alx1, is expressed in chondrogenic neural crest and functions during retinal and craniofacial cartilage morphogenesis. Homozygous mutations in *alx*1 are associated with profound frontonasal dysplasia and microophthalmia in humans (Bertola et al., 2013; Uz et al., 2010), and zebrafish alx1 morphants develop with hypoplastic craniofacial cartilages and coloboma (Dee et al., 2013). WISH analysis corroborated depletion of alx1 transcript in zic2 mutants (Fig. 6A,B). We examined expression of alx1 during normal development to verify its restriction to neural crest. At 16 hpf, alx1 was expressed in the frontonasal neural crest, which forms the facial skeleton (Couly et al., 2002; Langenberg et al., 2008) (Fig. 6C, D). alx1 was expressed in the periocular region at 24 and 36 hpf (Fig. 6E, F) and in the ethmoid plate anlagen at 48 hpf (Fig. 6F). alx1 was also expressed in the prospective swim bladder, but this domain did not appear to be affected in zic2 mutants (not shown).

To ask if alx1 depletion was indicative of a broader periocular mesenchyme deficit, we examined expression of *crestin*, an early general marker of neural crest (Langenberg et al., 2008) in MZ-zic2 mutants and siblings. We found the anterior stream of crestin-positive neural crest and its pharyngeal domain strongly reduced in zic2 mutants (Fig. 7A–E). In contrast, crestin-expressing cells in the trunk appeared unaffected (Fig. 7C, F).

Since crestin is not expressed in the ventral portion of periocular neural crest, we examined this NC population directly by high-resolution confocal imaging. MZ-zic2 mutants and their siblings were fixed at 24 hpf and stained for F-actin and DNA to visualize cell outlines and nuclei. In normal siblings, cells with mesenchymal appearance were observed in the periocular space adjacent to the choroid fissure; these were enriched in the proximal (closest to the OS) half of the optic cup (Fig. 8A–C). In contrast, the ventral periocular space was largely devoid of cells along the entire proximodistal axis of the mutant optic cup (Fig. 8D–F). Taken together, these data argue that zic2 plays a critical early role during periocular neural crest formation.

Discussion

The data presented here establish the first genetic model of zic-linked birth defects in zebrafish and extends our understanding of how zic2 coordinates development of the craniofacial complex comprised of brain, retina and craniofacial cartilages. We show that zebrafish zic2a and zic2b function redundantly to promote Hh-dependent retinal morphogenesis and demonstrate a requirement for both zygotic

and maternal zic2 in controlling morphogenesis of the optic stalk and retina, and to restrict pax2a expression in this region. This study confirms a key early role for zic2 in neural crest formation and identifies a homeobox transcription factor Alx1 as a novel effector of zic2 function in the periocular neural crest.

Where does zic2 function to control eye morphogenesis

Our transcriptome analysis identified an early requirement for zic2 function in a number of neural crest lineages, particularly in the cartilage precursors of the branchial arches and in periocular neural crest. Zebrafish zic2a and zic2b are predominantly expressed in the presumptive neural crest (Grinblat and Sive, 2001; Nyholm et al., 2007; Teslaa et al., 2013; Toyama et al., 2004); hence it is tempting to speculate that zic2 controls ventral retinal morphogenesis indirectly, via a primary function in neural crest. Alx1 is an attractive candidate effector of Zic2, since alx gene family members function in periocular neural crest to regulate retinal morphogenesis in human, mouse and zebrafish (Bertola et al., 2013; Dee et al., 2013; Lakhwani et al., 2010; Qu et al., 1999; Uz et al., 2010; Zhao et al., 1996).

Non-cell-autonomous roles for periocular neural crest in choroid fissure morphogenesis have been demonstrated in mouse mutants (Evans and Gage, 2005; Matt et al., 2008) and in zebrafish morpholino knockdowns (Lupo et al., 2011; McMahon et al., 2009). There is yet much to learn about the mechanisms of these cell interaction, e.g. which specific neural crest lineages are important, when and how they interact with the retina, and which genes direct these interactions.

Addressing these questions in robust mutant-based models will be essential going forward, yet such models are currently few and far between. The zic2 mutant zebrafish is an important step toward filling this gap.

Genetic removal of maternal zic2b enhances penetrance and expressivity of retinal coloboma in zic2 mutant embryos (Fig.1), suggesting a potential requirement for zebrafish zic2 function during gastrulation. Zic2a and 2b are expressed in the gastrula mesoderm (Drummond et al., 2013; Grinblat and Sive, 2001; Toyama et al., 2004), including the prechordal plate, which induces formation of the hypothalamus in the ventral diencephalon (Mathieu et al., 2002; Pera and Kessel, 1997; Rubenstein et al., 1998). The hypothalamus subsequently becomes an important source of Shh and is required for regionalization of the anterior diencephalon and optic fissure (Shimamura and Rubenstein, 1997; Zhao et al., 2012). It is therefore feasible that zic2 functions in the prechordal plate during gastrulation to promote ventral diencephalic/hypothalamic specification and the establishment of the hypothalamic signaling center. This hypothesis is supported by the partial rescue of coloboma by Hh inhibition in MZ-zic2 mutants. Notably, mouse zic2 promotes formation of the embryonic organizer during gastrulation (Barratt et al., 2014; Houtmeyers et al., 2016; Warr et al., 2008).

zic2a, but not zic2b, is also expressed in a restricted domain in the distal OS (Nyholm et al., 2007; Sanek et al., 2009; Toyama et al., 2004), where it may function to promote choroid fissure formation cell-autonomously. However, zic2b function should then be largely dispensable for normal retinal morphogenesis; this prediction is not born out by our results, which instead point toward a strict requirement for zic2b

and a somewhat relaxed requirement for zic2a function during retinal morphogenesis (Fig. 1).

zic2a and zic2b are also expressed in the retina itself, as is zic2 in higher vertebrates (Brown et al., 2003; Nagai et al., 1997; Toyama et al., 2004). While this expression begins relatively late, ~ 24 hpf, it may contribute to retinal morphogenesis cell-autonomously. The timing of the zic2 mutant deficits described here, which manifest by 24 hpf, argues against a cell-autonomous function of zic2 in the retina. However, the accumulated evidence in mouse models warrants a detailed examination of retinal function of zebrafish zic2 (Garcia-Frigola et al., 2008; Herrera et al., 2003; Lee et al., 2008b). zic2 mutants in combination with powerful methodologies available in zebrafish, e.g. transplant assays, tissue-specific transgenesis and high-resolution live imaging, provide a robust platform for testing these hypotheses efficiently in future studies.

What is the molecular mechanism of zic2 function in the developing retina?

Misregulation of PAX2 has been causally linked to coloboma in humans (reviewed in (Gregory-Evans et al., 2004) and in chick (Sehgal et al., 2008). Regardless of the cell type where zic2 exerts its primary function, it is likely that misregulation of pax2a in zic2 mutants demonstrated here and in zic2 morphants (Sanek et al., 2009) contributes to their retinal anomalies; for this reason, it will be important to ask if this mechanism is conserved in mouse models.

Our demonstration that cyclopamine exposure ameliorates zic2-linked coloboma supports, albeit indirectly, the idea that Hh signaling upregulation is responsible for retinal defects in zic2 mutants. pax2a, a target of Hh signaling, is mispatterned, but is not reduced overall in zic2 mutants. Likewise, upregulation of Hh signaling is not detectable at the level of whole-transcriptome gene expression of known direct targets of Hh at the diencephalic midline, ptc1 and nkx2.2 (Bergeron et al., 2008). These genes are also expressed normally in zic2 mutants when assayed by WISH (data not shown).

An alternate hypothesis, consistent with the apparent de-repression of Hh signaling in zic2 mutants posits that Zic2 regulates transcription of Hh pathway components in a small portion of the embryo, such that would not be detected by our whole-embryo transcriptome approach. For example, it is plausible that a sub-lineage of the periocular neural crest modulates Hh signaling by producing secreted Hh inhibitors or creating physical barriers for Hh diffusion. It is also possible that zic2 restricts pax2a transcription via a parallel, Hh-independent mechanism. If this were the case, cyclopamine acting through Hh signaling may counteract pax2a expansion in zic2 mutants, thereby alleviating severity of coloboma observed in MZ-zic2 mutants. Our data are also consistent with the possibility that zic2 controls cell movements of pax2a-expressing cells rather than pax2a transcription. While the apparent increase in the number of pax2a-positive cells in the mutant diencephalon (Fig. 3G–I) argues against this hypothesis, additional studies are needed to test these hypotheses.

We have likely missed important targets of zic2 in our whole-embryo transcriptome analysis. In other contexts, zic2 has been shown to directly modulate Nodal signaling and canonical Wnt signaling (Fujimi et al., 2012; Houtmeyers et al.,

2016; Murgan et al., 2015; Pourebrahim et al., 2011) and may function in this capacity in the developing zebrafish. Exciting recent data identify Zic2 as a key co-factor for chromatin remodeling in embryonic stem cells (Luo et al., 2015), and may function in this capacity in the developing embryos. Nonetheless, the broad-stroke approach taken here has correctly identified a number of cell lineages that depend on zic2 function, among them periocular neural crest, which is necessary for the formation and subsequent closure of the choroid fissure and whose migration is guided by the optic vesicle and by the optic stalks (Eberhart et al., 2008; Langenberg et al., 2008). Despite its limitations, this approach has led us to identify a strong candidate effector of zic2 function in retinal and craniofacial development, alx1. Going forward, RNA-seq to MZ-zic2 embryos at earlier stages of development will allow identification of a more complete and focused set of proximal zic2 targets and effectors.

How does this work inform our understanding of mammalian HPE and related disorders?

Loss-of-function alleles of ZIC2 are found in 10% of patients with the HPE (Brown et al., 2005; Solomon et al., 2010). zic2-linked HPE is unusual for two reasons. First, its penetrance in human patients is the highest of the common HPE-linked genes, 87%; by comparison, penetrance of HPE in patients with Shh mutations is only 36% (Solomon et al., 2012). Second, in contrast to Shh-linked HPE, facial structures of zic2-linked HPE patients are largely normal, although their cerebral morphology ranges from microform to severe alobar (Solomon et al., 2010). This suggests that the

developing human forebrain is very sensitive to reduction in ZIC2 levels during human embryogenesis (in contrast, duplication of the ZIC2-containing region does not disrupt human development (Jobanputra et al., 2012).

Mouse and zebrafish embryos are less sensitive to zic2 depletion, since they develop normally when heterozygous for loss-of-function alleles of zic2. Coloboma is the most obvious defect in zebrafish that lack zic2, but diencephalic deficits are also present, as indicated by dysmorphic preoptic diencephalon (Fig. 3), narrowing of forebrain midline in the MZ-zic2 mutants (Fig. 1) and reduction of ventral diencephalic marker expression in zic2 mutants (e.g. lhx6 and nkx2.1; Fig. S3). In contrast, homozygous zic2 mouse mutants develop with prominent forebrain defects (Elms et al., 2003; Nagai et al., 2000). Gongal et al (Gongal et al., 2011) have proposed that HPE and coloboma represent mild and severe aspects of the same phenotypic spectrum; by this token, it is likely that the overt differences between mouse and zebrafish mutant phenotypes reflect quantitative rather than qualitative differences in brain primordium architecture in teleosts vs mammals. This argument further emphasizes the need for in-depth analysis of zic2 functions in more than one model organism.

It is important to note that zic2 double mutant phenotypes largely, but not completely, replicate the phenotypes observed after morpholino-mediated knockdown of zic2a and zic2b individually. The biggest difference between the assays is observed in the anterior diencephalon, which forms normally in MZ-zic2 mutants (Fig. 3), but is disrupted in zic2a morphants (Sanek and Grinblat, 2008; Sanek et al., 2009; Teslaa et al., 2013). This difference may indicate genetic compensation by other members of the zebrafish Zic family that function during brain morphogenesis (Elsen et al.,

2008; Maurus and Harris, 2009; Winata et al., 2013) and retinal morphogenesis (Maurus and Harris, 2009). More generally, this study demonstrates the ability of closely related orthologs to compensate for each other's functions when disrupted chromosomally, but not via transient knockdown. These data will contribute to the collective efforts to understand the mechanisms that underlie the well-documented differences in outcomes of gene disruption through transient knockdown and chromosomal lesions in target genes (Kok et al., 2015; Rossi et al., 2015).

Collectively, our data identify a novel role for zic2 in frontonasal/periocular neural crest development and establish a new animal model of inherited coloboma with frontonasal dysplasia. These data suggest that ZIC2 mutations may contribute to human conditions other than HPE, e.g. frontonasal dysplasia. Human hereditary coloboma frequently presents unilaterally, an indication that modifiers (genetic or environmental) are important contributors to choroid fissure formation. We find that coloboma in zygotic zic2 mutants is incompletely penetrant and predominantly unilateral, making this model ideally suited for modifier screens to identify molecular pathways that interact with zic2. This model will also facilitate in-depth analysis of other key roles for zic2, e.g. their functions in post-mitotic neurons such as cerebellar granule neurons (Frank et al., 2015) and Cajal-Retzius cells (Escalante et al., 2013; Murillo et al., 2015) and its potential link to schizophrenia (Hatayama et al., 2011).

Acknowledgements

We are grateful to Abby Keller for establishing technical expertise in CRISPR mutagenesis, Kelsey Baubie and Lizzie Roehl for fish husbandry. We thank Steve Ekker for providing the zic2a^{gbt133} mutant zebrafish and Kristen Kwan for the gift of pax2a antibody. We also wish to thank David Grunwald for advice and support, the University of Utah Mutation Generation and Detection Core for TALEN design, and the University of Wisconsin Biotechnology Center DNA Sequencing Facility for providing sequencing facilities and services.

FUNDING

This work was supported by grants from the National Institutes of Health (EY022098-01) and American Heart Association (11GRNT7770002) to Y.G, and the Vilas Trust.

Reference

Akimenko MA, Ekker M, Wegner J, Lin W, Westerfield M. Combinatorial expression of three zebrafish genes related to distal-less: part of a homeobox gene code for the head. The Journal of neuroscience: the official journal of the Society for Neuroscience. 1994;14:3475–3486.

Barratt KS, Glanville-Jones HC, Arkell RM. The Zic2 gene directs the formation and function of node cilia to control cardiac situs. Genesis. 2014;52:626–635.

Bazin-Lopez N, Valdivia LE, Wilson SW, Gestri G. Watching eyes take shape. Current opinion in genetics & development. 2015;32:73–79.

Bergeron SA, Milla LA, Villegas R, Shen MC, Burgess SM, Allende ML, Karlstrom RO, Palma V. Expression profiling identifies novel Hh/Gli-regulated genes in developing zebrafish embryos. Genomics. 2008;91:165–177.

Bertola DR, Rodrigues MG, Quaio CR, Kim CA, Passos-Bueno MR. Vertical transmission of a frontonasal phenotype caused by a novel ALX4 mutation. American journal of medical genetics Part A. 2013;161A:600–604.

Bronstein JM, Micevych PE, Chen K. Oligodendrocyte-specific protein (OSP) is a major component of CNS myelin. Journal of neuroscience research. 1997;50:713–720.

Brown L, Paraso M, Arkell R, Brown S. In vitro analysis of partial loss-of-function ZIC2 mutations in holoprosencephaly: alanine tract expansion modulates DNA binding and transactivation. Human molecular genetics. 2005;14:411–420.

Brown LY, Kottmann AH, Brown S. Immunolocalization of Zic2 expression in the developing mouse forebrain. Gene expression patterns : GEP. 2003;3:361–367.

Brown LY, Odent S, David V, Blayau M, Dubourg C, Apacik C, Delgado MA, Hall BD, Reynolds JF, Sommer A, Wieczorek D, Brown SA, Muenke M. Holoprosencephaly due to mutations in ZIC2: alanine tract expansion mutations may be caused by parental somatic recombination. Human molecular genetics. 2001;10:791–796.

Brown SA, Warburton D, Brown LY, Yu CY, Roeder ER, Stengel-Rutkowski S, Hennekam RC, Muenke M. Holoprosencephaly due to mutations in ZIC2, a homologue of Drosophila odd-paired. Nature genetics. 1998;20:180–183.

Brugmann SA, Allen NC, James AW, Mekonnen Z, Madan E, Helms JA. A primary cilia-dependent etiology for midline facial disorders. Human molecular genetics. 2010;19:1577–1592.

Cannon JE, Place ES, Eve AM, Bradshaw CR, Sesay A, Morrell NW, Smith JC. Global analysis of the haematopoietic and endothelial transcriptome during zebrafish development. Mechanisms of development. 2013;130:122–131.

Clark KJ, Balciunas D, Pogoda HM, Ding Y, Westcot SE, Bedell VM, Greenwood TM, Urban MD, Skuster KJ, Petzold AM, Ni J, Nielsen AL, Patowary A, Scaria V, Sivasubbu S, Xu X, Hammerschmidt M, Ekker SC. In vivo protein trapping produces a functional expression codex of the vertebrate proteome. Nature methods. 2011;8:506–515.

Couly G, Creuzet S, Bennaceur S, Vincent C, Le Douarin NM. Interactions between Hox-negative cephalic neural crest cells and the foregut endoderm in patterning the facial skeleton in the vertebrate head. Development. 2002;129:1061–1073.

de Jong M, Rauwerda H, Bruning O, Verkooijen J, Spaink HP, Breit TM. RNA isolation method for single embryo transcriptome analysis in zebrafish. BMC research notes. 2010;3:73.

Dee CT, Szymoniuk CR, Mills PE, Takahashi T. Defective neural crest migration revealed by a Zebrafish model of Alx1-related frontonasal dysplasia. Human molecular genetics. 2013;22:239–251.

Drummond DL, Cheng CS, Selland LG, Hocking JC, Prichard LB, Waskiewicz AJ. The role of Zic transcription factors in regulating hindbrain retinoic acid signaling. BMC developmental biology. 2013;13:31.

Eberhart JK, He X, Swartz ME, Yan YL, Song H, Boling TC, Kunerth AK, Walker MB, Kimmel CB, Postlethwait JH. MicroRNA Mirn140 modulates Pdgf signaling during palatogenesis. Nature genetics. 2008;40:290–298.

Ekker SC, Ungar AR, Greenstein P, von Kessler DP, Porter JA, Moon RT, Beachy PA. Patterning activities of vertebrate hedgehog proteins in the developing eye and brain. Current biology : CB. 1995;5:944–955.

Elms P, Scurry A, Davies J, Willoughby C, Hacker T, Bogani D, Arkell R. Overlapping and distinct expression domains of Zic2 and Zic3 during mouse gastrulation. Gene expression patterns : GEP. 2004;4:505–511.

Elms P, Siggers P, Napper D, Greenfield A, Arkell R. Zic2 is required for neural crest formation and hindbrain patterning during mouse development. Developmental biology. 2003;264:391–406.

Elsen GE, Choi LY, Millen KJ, Grinblat Y, Prince VE. Zic1 and Zic4 regulate zebrafish roof plate specification and hindbrain ventricle morphogenesis. Developmental biology. 2008;314:376–392.

Escalante A, Murillo B, Morenilla-Palao C, Klar A, Herrera E. Zic2-dependent axon midline avoidance controls the formation of major ipsilateral tracts in the CNS. Neuron. 2013;80:1392–1406.

Evans AL, Gage PJ. Expression of the homeobox gene Pitx2 in neural crest is required for optic stalk and ocular anterior segment development. Human molecular genetics. 2005;14:3347–3359.

Frank CL, Liu F, Wijayatunge R, Song L, Biegler MT, Yang MG, Vockley CM, Safi A, Gersbach CA, Crawford GE, West AE. Regulation of chromatin accessibility and Zic binding at enhancers in the developing cerebellum. Nature neuroscience. 2015;18:647-656.

Fujimi TJ, Hatayama M, Aruga J. Xenopus Zic3 controls notochord and organizer development through suppression of the Wnt/beta-catenin signaling pathway. Developmental biology. 2012;361:220–231.

Garcia-Frigola C, Carreres MI, Vegar C, Mason C, Herrera E. Zic2 promotes axonal divergence at the optic chiasm midline by EphB1-dependent and - independent mechanisms. Development. 2008;135:1833–1841.

Gestri G, Link BA, Neuhauss SC. The visual system of zebrafish and its use to model human ocular diseases. Developmental neurobiology. 2012;72:302–327.

Gillhouse M, Wagner Nyholm M, Hikasa H, Sokol SY, Grinblat Y. Two Frodo/Dapper homologs are expressed in the developing brain and mesoderm of zebrafish. Developmental dynamics: an official publication of the American Association of Anatomists. 2004;230:403–409.

Gongal PA, French CR, Waskiewicz AJ. Aberrant forebrain signaling during early development underlies the generation of holoprosencephaly and coloboma. Biochimica et biophysica acta. 2011;1812:390–401.

Gregory-Evans CY, Williams MJ, Halford S, Gregory-Evans K. Ocular coloboma: a reassessment in the age of molecular neuroscience. J Med Genet. 2004;41:881–891.

Grinblat Y, Sive H. zic Gene expression marks anteroposterior pattern in the presumptive neurectoderm of the zebrafish gastrula. Developmental dynamics: an official publication of the American Association of Anatomists. 2001;222:688–693.

Gross JM, Dowling JE. Tbx2b is essential for neuronal differentiation along the dorsal/ventral axis of the zebrafish retina. Proceedings of the National Academy of Sciences of the United States of America. 2005;102:4371–4376.

Hatayama M, Ishiguro A, Iwayama Y, Takashima N, Sakoori K, Toyota T, Nozaki Y, Odaka YS, Yamada K, Yoshikawa T, Aruga J. Zic2 hypomorphic mutant mice as a schizophrenia model and ZIC2 mutations identified in schizophrenia patients. Scientific reports. 2011;1:16.

Herrera E, Brown L, Aruga J, Rachel RA, Dolen G, Mikoshiba K, Brown S, Mason CA. Zic2 patterns binocular vision by specifying the uncrossed retinal projection. Cell. 2003;114:545–557.

Houtmeyers R, Tchouate Gainkam O, Glanville-Jones HA, Van den Bosch B, Chappell A, Barratt KS, Souopgui J, Tejpar S, Arkell RM. Zic2 mutation causes holoprosencephaly via disruption of NODAL signalling. Human molecular genetics.

2016;25:3946–3959.

Hoyle J, Tang YP, Wiellette EL, Wardle FC, Sive H. nlz gene family is required for hindbrain patterning in the zebrafish. Developmental dynamics : an official publication of the American Association of Anatomists. 2004;229:835–846.

Huang da W, Sherman BT, Lempicki RA. Systematic and integrative analysis of large gene lists using DAVID bioinformatics resources. Nature protocols. 2009;4:44–57.

Inoue T, Ota M, Mikoshiba K, Aruga J. Zic2 and Zic3 synergistically control neurulation and segmentation of paraxial mesoderm in mouse embryo. Developmental biology. 2007;306:669–684.

Jobanputra V, Burke A, Kwame AY, Shanmugham A, Shirazi M, Brown S, Warburton PE, Levy B, Warburton D. Duplication of the ZIC2 gene is not associated with holoprosencephaly. American journal of medical genetics Part A. 2012;158A:103–108.

Kimmel CB, Ballard WW, Kimmel SR, Ullmann B, Schilling TF. Stages of embryonic development of the zebrafish. Developmental dynamics: an official publication of the American Association of Anatomists. 1995;203:253–310.

Kimmel CB, Miller CT, Kruze G, Ullmann B, BreMiller RA, Larison KD, Snyder HC. The shaping of pharyngeal cartilages during early development of the zebrafish. Developmental biology. 1998;203:245–263.

Kish PE, Bohnsack BL, Gallina D, Kasprick DS, Kahana A. The eye as an organizer of craniofacial development. Genesis. 2011;49:222–230.

Kok FO, Shin M, Ni CW, Gupta A, Grosse AS, van Impel A, Kirchmaier BC, Peterson-Maduro J, Kourkoulis G, Male I, DeSantis DF, Sheppard-Tindell S, Ebarasi L, Betsholtz C, Schulte-Merker S, Wolfe SA, Lawson ND. Reverse genetic screening reveals poor correlation between morpholino-induced and mutant phenotypes in zebrafish. Developmental cell. 2015;32:97–108.

Kwan KM. Coming into focus: the role of extracellular matrix in vertebrate optic cup morphogenesis. Developmental dynamics: an official publication of the American Association of Anatomists. 2014;243:1242–1248.

Lakhwani S, Garcia-Sanz P, Vallejo M. Alx3-deficient mice exhibit folic acid-resistant craniofacial midline and neural tube closure defects. Developmental biology. 2010;344:869-880.

Langenberg T, Kahana A, Wszalek JA, Halloran MC. The eye organizes neural crest cell migration. Developmental dynamics: an official publication of the American Association of Anatomists. 2008;237:1645–1652.

Langmead B, Trapnell C, Pop M, Salzberg SL. Ultrafast and memory-efficient alignment of short DNA sequences to the human genome. Genome biology.

2009;10:R25.

Le Douarin NM, Brito JM, Creuzet S. Role of the neural crest in face and brain development. Brain research reviews. 2007;55:237–247.

Lee J, Willer JR, Willer GB, Smith K, Gregg RG, Gross JM. Zebrafish blowout provides genetic evidence for Patched1-mediated negative regulation of Hedgehog signaling within the proximal optic vesicle of the vertebrate eye. Developmental biology. 2008a;319:10-22.

Lee R, Petros TJ, Mason CA. Zic2 regulates retinal ganglion cell axon avoidance of ephrinB2 through inducing expression of the guidance receptor EphB1. The Journal of neuroscience : the official journal of the Society for Neuroscience. 2008b;28:5910–5919.

Leng N, Dawson JA, Thomson JA, Ruotti V, Rissman AI, Smits BM, Haag JD, Gould MN, Stewart RM, Kendziorski C. EBSeq: an empirical Bayes hierarchical model for inference in RNA-seq experiments. Bioinformatics. 2013;29:1035–1043.

Li B, Dewey CN. RSEM: accurate transcript quantification from RNA-Seq data with or without a reference genome. BMC bioinformatics. 2011;12:323.

Luo R, An M, Arduini BL, Henion PD. Specific pan-neural crest expression of zebrafish Crestin throughout embryonic development. Developmental dynamics: an official publication of the American Association of Anatomists. 2001;220:169–174.

Luo Z, Gao X, Lin C, Smith ER, Marshall SA, Swanson SK, Florens L, Washburn MP, Shilatifard A. Zic2 is an enhancer-binding factor required for embryonic stem cell specification. Molecular cell. 2015;57:685–694.

Lupo G, Gestri G, O'Brien M, Denton RM, Chandraratna RA, Ley SV, Harris WA, Wilson SW. Retinoic acid receptor signaling regulates choroid fissure closure through independent mechanisms in the ventral optic cup and periocular mesenchyme. Proceedings of the National Academy of Sciences of the United States of America. 2011;108:8698–8703.

Lupo G, Liu Y, Qiu R, Chandraratna RA, Barsacchi G, He RQ, Harris WA. Dorsoventral patterning of the Xenopus eye: a collaboration of Retinoid, Hedgehog and FGF receptor signaling. Development. 2005;132:1737–1748.

Macdonald R, Barth KA, Xu Q, Holder N, Mikkola I, Wilson SW. Midline signalling is required for Pax gene regulation and patterning of the eyes. Development. 1995;121:3267-3278.

Masai I, Stemple DL, Okamoto H, Wilson SW. Midline signals regulate retinal neurogenesis in zebrafish. Neuron. 2000;27:251–263.

Mathieu J, Barth A, Rosa FM, Wilson SW, Peyrieras N. Distinct and cooperative roles for Nodal and Hedgehog signals during hypothalamic development. Development.

2002;129:3055-3065.

Matt N, Ghyselinck NB, Pellerin I, Dupe V. Impairing retinoic acid signalling in the neural crest cells is sufficient to alter entire eye morphogenesis. Developmental biology. 2008;320:140–148.

Maurus D, Harris WA. Zic-associated holoprosencephaly: zebrafish Zic1 controls midline formation and forebrain patterning by regulating Nodal, Hedgehog, and retinoic acid signaling. Genes & development. 2009;23:1461–1473.

McMahon C, Gestri G, Wilson SW, Link BA. Lmx1b is essential for survival of periocular mesenchymal cells and influences Fgf-mediated retinal patterning in zebrafish. Developmental biology. 2009;332:287–298.

Morita K, Sasaki H, Fujimoto K, Furuse M, Tsukita S. Claudin-11/OSP-based tight junctions of myelin sheaths in brain and Sertoli cells in testis. The Journal of cell biology. 1999;145:579–588.

Mui SH, Kim JW, Lemke G, Bertuzzi S. Vax genes ventralize the embryonic eye. Genes Dev. 2005;19:1249–1259.

Murgan S, Kari W, Rothbacher U, Iche-Torres M, Melenec P, Hobert O, Bertrand V. Atypical Transcriptional Activation by TCF via a Zic Transcription Factor in C. elegans Neuronal Precursors. Developmental cell. 2015;33:737–745.

Murillo B, Ruiz-Reig N, Herrera M, Fairen A, Herrera E. Zic2 Controls the Migration of Specific Neuronal Populations in the Developing Forebrain. The Journal of neuroscience : the official journal of the Society for Neuroscience. 2015;35:11266–11280.

Nagai T, Aruga J, Minowa O, Sugimoto T, Ohno Y, Noda T, Mikoshiba K. Zic2 regulates the kinetics of neurulation. Proceedings of the National Academy of Sciences of the United States of America. 2000;97:1618–1623.

Nagai T, Aruga J, Takada S, Gunther T, Sporle R, Schughart K, Mikoshiba K. The expression of the mouse Zic1, Zic2, and Zic3 gene suggests an essential role for Zic genes in body pattern formation. Developmental biology. 1997;182:299–313.

Nakata K, Nagai T, Aruga J, Mikoshiba K. Xenopus Zic3, a primary regulator both in neural and neural crest development. Proceedings of the National Academy of Sciences of the United States of America. 1997;94:11980–11985.

Nakata K, Nagai T, Aruga J, Mikoshiba K. Xenopus Zic family and its role in neural and neural crest development. Mechanisms of development. 1998;75:43–51.

Nyholm MK, Abdelilah-Seyfried S, Grinblat Y. A novel genetic mechanism regulates dorsolateral hinge-point formation during zebrafish cranial neurulation. Journal of cell science. 2009;122:2137–2148.

Nyholm MK, Wu SF, Dorsky RI, Grinblat Y. The zebrafish zic2a-zic5 gene pair acts downstream of canonical Wnt signaling to control cell proliferation in the developing tectum. Development. 2007;134:735–746.

Onwochei BC, Simon JW, Bateman JB, Couture KC, Mir E. Ocular colobomata. Survey of ophthalmology. 2000;45:175–194.

Pan H, Gustafsson MK, Aruga J, Tiedken JJ, Chen JC, Emerson CP., Jr A role for Zic1 and Zic2 in Myf5 regulation and somite myogenesis. Developmental biology. 2011;351:120-127.

Pera EM, Kessel M. Patterning of the chick forebrain anlage by the prechordal plate. Development. 1997;124:4153–4162.

Pillai-Kastoori L, Wen W, Wilson SG, Strachan E, Lo-Castro A, Fichera M, Musumeci SA, Lehmann OJ, Morris AC. Sox11 is required to maintain proper levels of Hedgehog signaling during vertebrate ocular morphogenesis. PLos genetics. 2014;10:e1004491.

Pourebrahim R, Houtmeyers R, Ghogomu S, Janssens S, Thelie A, Tran HT, Langenberg T, Vleminckx K, Bellefroid E, Cassiman JJ, Tejpar S. Transcription factor Zic2 inhibits Wnt/beta-catenin protein signaling. The Journal of biological chemistry. 2011;286:37732–37740.

Qu S, Tucker SC, Zhao Q, deCrombrugghe B, Wisdom R. Physical and genetic interactions between Alx4 and Cart1. Development. 1999;126:359–369.

Ribeiro LA, Roessler E, Hu P, Pineda-Alvarez DE, Zhou N, Jones M, Chandrasekharappa S, Richieri-Costa A, Muenke M. Comparison of mutation findings in ZIC2 between microform and classical holoprosencephaly in a Brazilian cohort. Birth defects research Part A, Clinical and molecular teratology. 2012;94:912–917.

Robinson MD, McCarthy DJ, Smyth GK. edgeR: a Bioconductor package for differential expression analysis of digital gene expression data. Bioinformatics. 2010;26:139–140.

Roessler E, Belloni E, Gaudenz K, Jay P, Berta P, Scherer SW, Tsui LC, Muenke M. Mutations in the human Sonic Hedgehog gene cause holoprosencephaly. Nature genetics. 1996;14:357–360.

Roessler E, Lacbawan F, Dubourg C, Paulussen A, Herbergs J, Hehr U, Bendavid C, Zhou N, Ouspenskaia M, Bale S, Odent S, David V, Muenke M. The full spectrum of holoprosencephaly-associated mutations within the ZIC2 gene in humans predicts loss-of-function as the predominant disease mechanism. Human mutation. 2009;30:E541-554.

Roessler E, Muenke M. The molecular genetics of holoprosencephaly. American journal of medical genetics Part C, Seminars in medical genetics. 2010;154C:52–61.

Rossi A, Kontarakis Z, Gerri C, Nolte H, Holper S, Kruger M, Stainier DY. Genetic compensation induced by deleterious mutations but not gene knockdowns. Nature. 2015;524:230–233.

Rubenstein JL, Shimamura K, Martinez S, Puelles L. Regionalization of the prosencephalic neural plate. Annual review of neuroscience. 1998;21:445–477.

Sanek NA, Grinblat Y. A novel role for zebrafish zic2a during forebrain development. Developmental biology. 2008;317:325–335.

Sanek NA, Taylor AA, Nyholm MK, Grinblat Y. Zebrafish zic2a patterns the forebrain through modulation of Hedgehog-activated gene expression. Development. 2009;136:3791–3800.

Schilling TF, Concordet JP, Ingham PW. Regulation of left-right asymmetries in the zebrafish by Shh and BMP4. Developmental biology. 1999;210:277–287.

Schimmenti LA, de la Cruz J, Lewis RA, Karkera JD, Manligas GS, Roessler E, Muenke M. Novel mutation in sonic hedgehog in non-syndromic colobomatous microphthalmia. American journal of medical genetics Part A. 2003;116A:215–221.

Schmitt EA, Dowling JE. Early eye morphogenesis in the zebrafish, Brachydanio rerio. The Journal of comparative neurology. 1994;344:532–542.

Sedykh I, TeSlaa JJ, Tatarsky RL, Keller AN, Toops KA, Lakkaraju A, Nyholm MK, Wolman MA, Grinblat Y. Novel roles for the radial spoke head protein 9 in neural and neurosensory cilia. Scientific reports. 2016;6:34437.

Sehgal R, Karcavich R, Carlson S, Belecky-Adams TL. Ectopic Pax2 expression in chick ventral optic cup phenocopies loss of Pax2 expression. Dev Biol. 2008;319:23–33.

Shimamura K, Rubenstein JL. Inductive interactions direct early regionalization of the mouse forebrain. Development. 1997;124:2709–2718.

Solomon BD, Bear KA, Wyllie A, Keaton AA, Dubourg C, David V, Mercier S, Odent S, Hehr U, Paulussen A, Clegg NJ, Delgado MR, Bale SJ, Lacbawan F, Ardinger HH, Aylsworth AS, Bhengu NL, Braddock S, Brookhyser K, Burton B, Gaspar H, Grix A, Horovitz D, Kanetzke E, Kayserili H, Lev D, Nikkel SM, Norton M, Roberts R, Saal H, Schaefer GB, Schneider A, Smith EK, Sowry E, Spence MA, Shalev SA, Steiner CE, Thompson EM, Winder TL, Balog JZ, Hadley DW, Zhou N, Pineda-Alvarez DE, Roessler E, Muenke M. Genotypic and phenotypic analysis of 396 individuals with mutations in Sonic Hedgehog. Journal of medical genetics. 2012;49:473–479.

Solomon BD, Lacbawan F, Mercier S, Clegg NJ, Delgado MR, Rosenbaum K, Dubourg C, David V, Olney AH, Wehner LE, Hehr U, Bale S, Paulussen A, Smeets HJ, Hardisty E, Tylki-Szymanska A, Pronicka E, Clemens M, McPherson E, Hennekam RC, Hahn J, Stashinko E, Levey E, Wieczorek D, Roeder E, Schell-Apacik CC, Booth CW,

Thomas RL, Kenwrick S, Cummings DA, Bous SM, Keaton A, Balog JZ, Hadley D, Zhou N, Long R, Velez JI, Pineda-Alvarez DE, Odent S, Roessler E, Muenke M. Mutations in ZIC2 in human holoprosencephaly: description of a novel ZIC2 specific phenotype and comprehensive analysis of 157 individuals. Journal of medical genetics. 2010;47:513–524.

Swartz ME, Sheehan-Rooney K, Dixon MJ, Eberhart JK. Examination of a palatogenic gene program in zebrafish. Developmental dynamics: an official publication of the American Association of Anatomists. 2011;240:2204–2220.

Take-uchi M, Clarke JD, Wilson SW. Hedgehog signalling maintains the optic stalk-retinal interface through the regulation of Vax gene activity. Development. 2003;130:955-968.

Teslaa JJ, Keller AN, Nyholm MK, Grinblat Y. Zebrafish Zic2a and Zic2b regulate neural crest and craniofacial development. Developmental biology. 2013;380:73–86.

Toyama R, Gomez DM, Mana MD, Dawid IB. Sequence relationships and expression patterns of zebrafish zic2 and zic5 genes. Gene expression patterns: GEP. 2004;4:345-350.

Uz E, Alanay Y, Aktas D, Vargel I, Gucer S, Tuncbilek G, von Eggeling F, Yilmaz E, Deren O, Posorski N, Ozdag H, Liehr T, Balci S, Alikasifoglu M, Wollnik B, Akarsu NA. Disruption of ALX1 causes extreme microphthalmia and severe facial clefting: expanding the spectrum of autosomal-recessive ALX-related frontonasal dysplasia. American journal of human genetics. 2010;86:789–796.

Varga ZM, Amores A, Lewis KE, Yan YL, Postlethwait JH, Eisen JS, Westerfield M. Zebrafish smoothened functions in ventral neural tube specification and axon tract formation. Development. 2001;128:3497–3509.

Wada N, Javidan Y, Nelson S, Carney TJ, Kelsh RN, Schilling TF. Hedgehog signaling is required for cranial neural crest morphogenesis and chondrogenesis at the midline in the zebrafish skull. Development. 2005;132:3977–3988.

Wang X, Lupo G, He R, Barsacchi G, Harris WA, Liu Y. Dorsoventral patterning of the Xenopus eye involves differential temporal changes in the response of optic stalk and retinal progenitors to Hh signalling. Neural development. 2015;10:7.

Warr N, Powles-Glover N, Chappell A, Robson J, Norris D, Arkell RM. Zic2-associated holoprosencephaly is caused by a transient defect in the organizer region during gastrulation. Human molecular genetics. 2008;17:2986–2996.

Wen W, Pillai-Kastoori L, Wilson SG, Morris AC. Sox4 regulates choroid fissure closure by limiting Hedgehog signaling during ocular morphogenesis. Developmental biology. 2015;399:139–153.

Westerfield M. The zebrafish book : a guide for the laboratory use of zebrafish

(Brachydanio rerio) M Westerfield; Eugene, OR: 1993.

Williamson KA, FitzPatrick DR. The genetic architecture of microphthalmia, anophthalmia and coloboma. European journal of medical genetics. 2014;57:369–380.

Winata CL, Kondrychyn I, Kumar V, Srinivasan KG, Orlov Y, Ravishankar A, Prabhakar S, Stanton LW, Korzh V, Mathavan S. Genome wide analysis reveals Zic3 interaction with distal regulatory elements of stage specific developmental genes in zebrafish. PLoS genetics. 2013;9:e1003852.

Wu E, Vargevik K, Slavotinek AM. Subtypes of frontonasal dysplasia are useful in determining clinical prognosis. American journal of medical genetics Part A. 2007;143A:3069–3078.

Ybot-Gonzalez P, Gaston-Massuet C, Girdler G, Klingensmith J, Arkell R, Greene ND, Copp AJ. Neural plate morphogenesis during mouse neurulation is regulated by antagonism of Bmp signalling. Development. 2007;134:3203–3211.

Young NM, Chong HJ, Hu D, Hallgrimsson B, Marcucio RS. Quantitative analyses link modulation of sonic hedgehog signaling to continuous variation in facial growth and shape. Development. 2010;137:3405–3409.

Zhao L, Zevallos SE, Rizzoti K, Jeong Y, Lovell-Badge R, Epstein DJ. Disruption of SoxB1-dependent Sonic hedgehog expression in the hypothalamus causes septo-optic dysplasia. Developmental cell. 2012;22:585–596.

Zhao Q, Behringer RR, de Crombrugghe B. Prenatal folic acid treatment suppresses acrania and meroanencephaly in mice mutant for the Cart1 homeobox gene. Nature genetics. 1996;13:275–283.

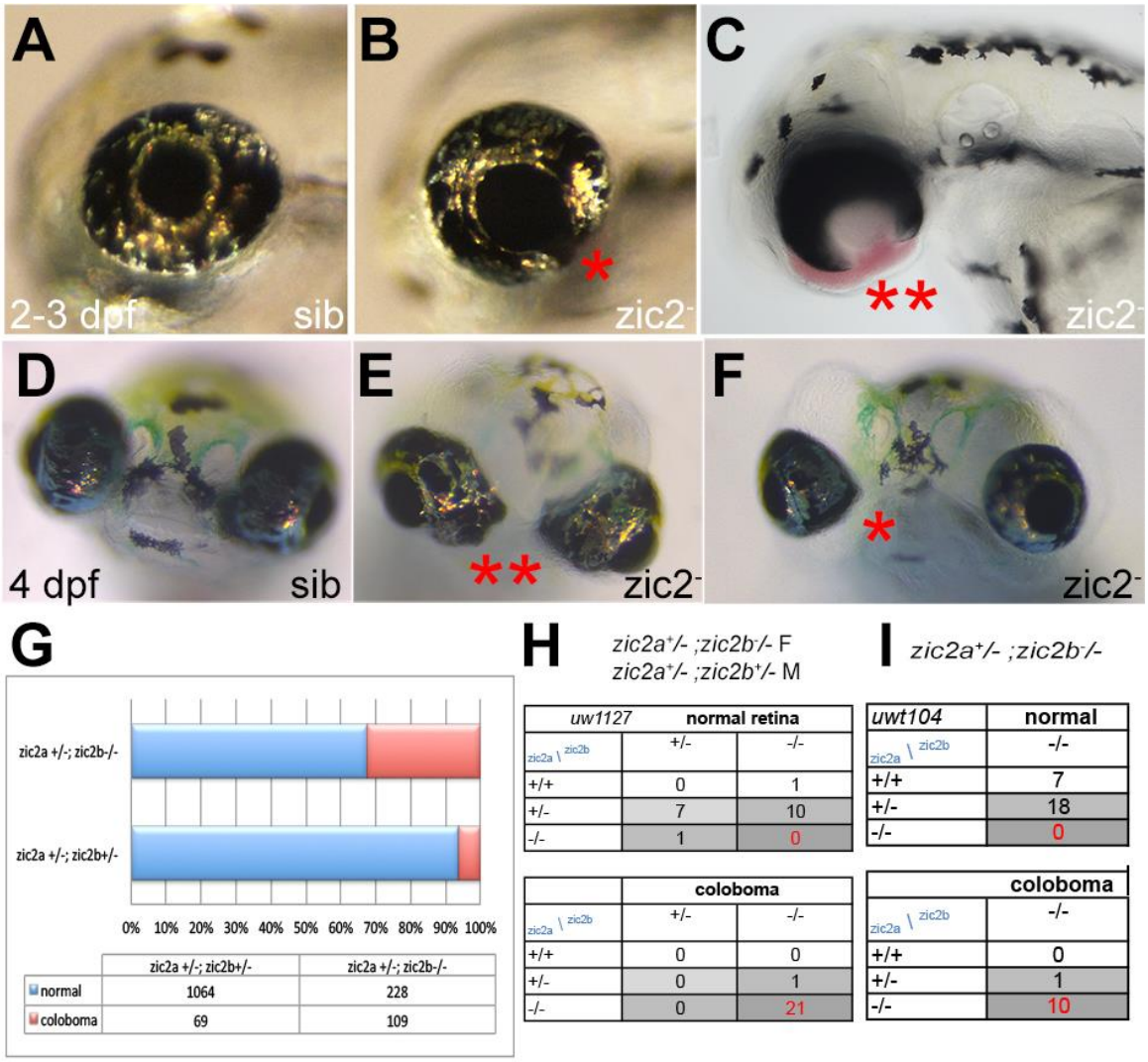

Figure 1. *Zebrafish Zic2 is required during retinal morphogenesis*

A: normal retinal morphology. B: retina exhibiting mild coloboma (*). C: retina exhibiting severe coloboma with periocular hemorrhaging (**). D: normal retinal morphology. E: bilateral coloboma in a severely affected embryo (**). F: mild, unilateral coloboma in an affected embryo. G: Penetrance and expressivity of coloboma is increased in progeny that lack maternal zic2b, derived from zic2a$^{gbt133/+;}$ zic2b$^{t104/}$zic2b^{t104} parents, compared to those from double heterozygous (zic2a^{gbt133}/+; zic2b^{t104}/+) parents (see Table S1 for details). H, I: Both CRISPR- and TALEN-induced mutant alleles of zic2b are tightly associated with coloboma in MZ-zic2 embryos. Embryos in A–C are at 2–3

dpf, shown in lateral views, anterior to the left. Embryos in D–F are at 4 dpf, shown in anterior views, dorsal at the top.

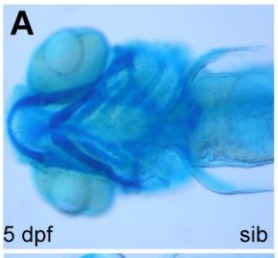

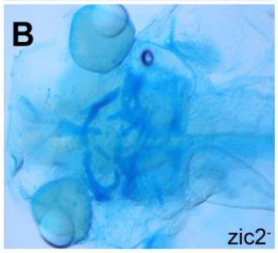

C

zic2a⁺/- ;zic2b⁺/-

uw1116	normal CF cartilage		
zic2a \ zic2b	+/+	+/-	-/-
+/+	0	2	2
+/-	0	4	3
-/-	0	0	0

	aberrant CF cartilage		
zic2a \ zic2b	+/+	+/-	-/-
+/+	0	0	0
+/-	2	0	1
-/-	0	0	5

D

zic2a⁺/- ;zic2b⁻/-
zic2a⁺/- ;zic2b⁺/-

uw1127	normal CF cartilage	
zic2a \ zic2b	+/-	-/-
+/+	0	0
+/-	6	4
-/-	1	0

	aberrant CF cartilage	
zic2a \ zic2b	+/-	-/-
+/+	0	0
+/-	0	8
-/-	0	14

Figure 2. *Zebrafish Zic2 is required for craniofacial cartilage development*

A: normal neurocranium and branchial arches. B: hypoplastic, disorganized craniofacial cartilages in a zic2 mutant. C: Craniofacial defects are enriched in zic2 mutants derived from double heterozygous parents. D: In embryos that lack maternal zic2b, craniofacial defects are observed in zic2 mutants and in embryos with one wildtype copy of zic2a. Cartilage was visualized by staining with Alcian Blue. Embryos at 5 dpf are shown in ventral views, anterior to the left.

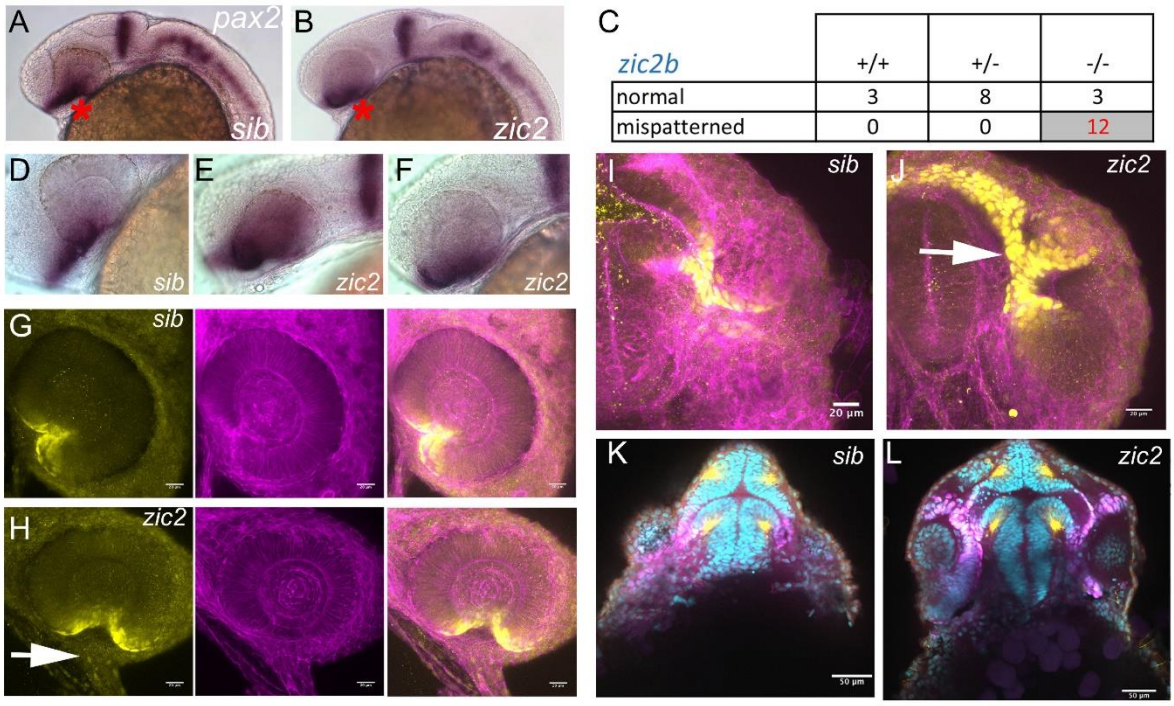

Figure 3. *Pax2a expression is aberrant in MZ-zic2 mutants at 1 dpf.*

Pax2a expression at 1 dpf was visualized in embryos derived from zic2a^{gbt133}/+; zic2b$^{uw1116/+}$ parents using WISH (A–F) or in progeny of zic2a^{gbt133}/+; zic2b^{uwt104} parents using immunohistochemistry (G–L). A: normal pax2a expression in the ventral retina (*). B: mispatterned pax2a expression (*) was observed in 12 out of 103 embryos (12%, 2 expts.). C: Only zic2b homozygous embryos exhibit pax2a mispatterning. zic2a genotype was not tested because PCR genotyping was not robust after WISH. D–F: Embryos with mispatterned pax2a expression also exhibit coloboma, indicative of homozygosity for zic2a^{gbt133}. G, H: confocal stacks through representative retina of normal (G) and zic2 mutant (H) retina. I, J: confocal stacks through the ventral aspects of a normal (I) and zic2 mutant (J) diencephalon and retina. Arrowheads in H, J point to the aberrant optic stalk. In G–J, yellow = Pax2a, magenta = F-actin cytoskeleton visualized by phalloidin. K, L: single confocal sections through representative normal (K) and zic2 mutant (L) embryos, imaged ventrally at the level of choroid fissure.

magenta = Pax2a; yellow = acetylated tubulin; cyan = nuclei visualized by DAPI. Embryos are shown in lateral views, anterior to the left (A–F) or anterior to the right (G, H); in ventral views with anterior at the top (I–L).

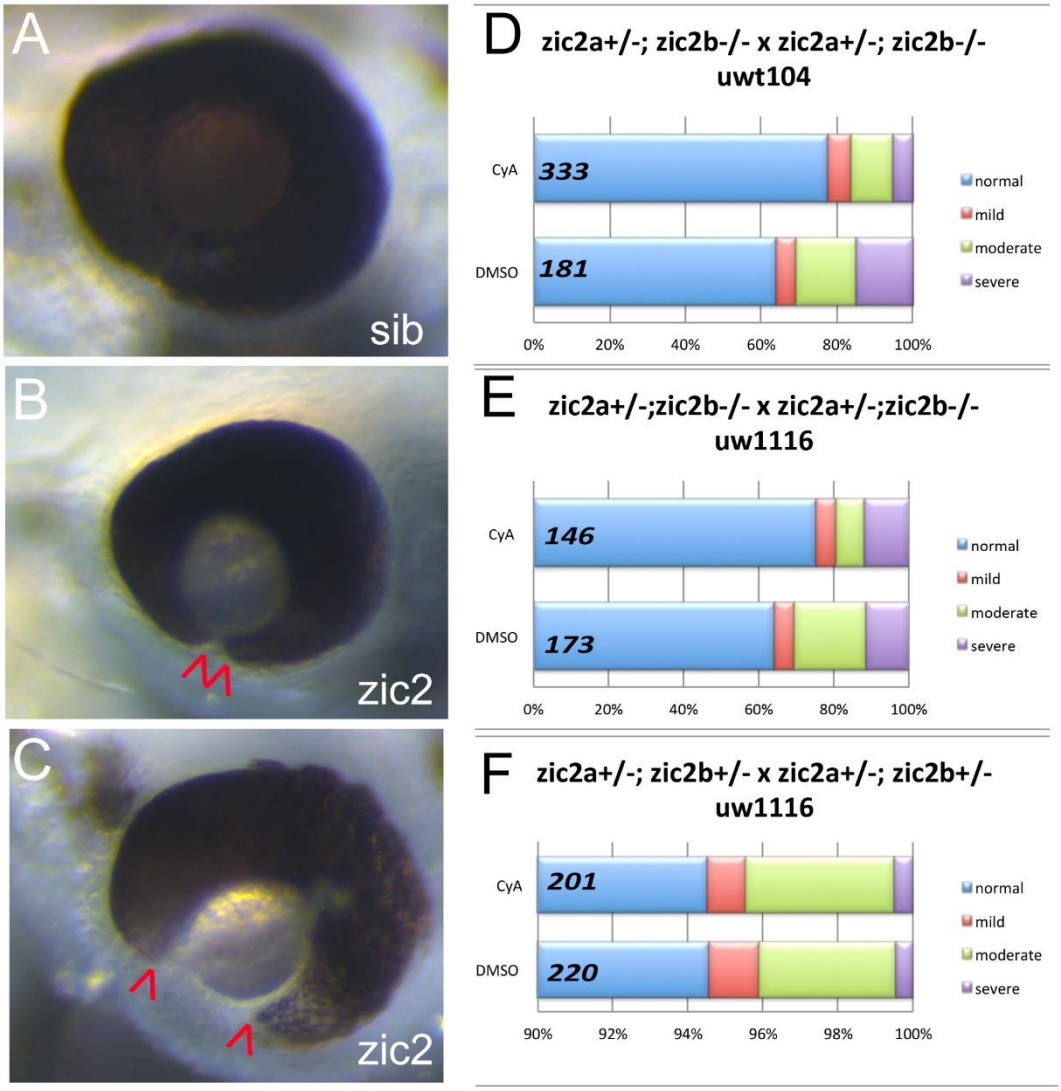

Figure 4. *Cyclopamine treatment reduces frequency and severity of coloboma in zic2 mutants*

A: normal retinal morphology; B: retina with mild coloboma; C: retina with moderate coloboma. D: Embryos were derived from zic2a^{gbt133}/+; zic2b^{t104} parental crosses and exposed to 3 or 4.5 μM cyclopamine (CyA) from 3–5 hpf until 24–26 hpf. In CyA-treated groups (3 expts; Fig. S3A), the proportion of embryos with coloboma was reduced significantly compared to vehicle-treated control siblings (Fisher's Exact test, $P < 0.001$). Proportion of severely affected embryos among all embryos with coloboma was also decreased in CyA-treated siblings (Fisher Exact test, $p<0.02$). E: Embryos

were derived from zic2a^{gbt133}/+; zic2b^{uw1116} parents and treated starting at 3 hpf with 4.5 uM Cya. CyA-treated groups exhibited reduction in coloboma penetrance (Fisher's Exact test $p<0.04$) compared to vehicle-treated control siblings (2 expts; Fig. S3B). F: Embryos were derived from zic2a^{gbt133}/+; zic2b^{uw1116}/+ parents and treated as in D with 4.5 uM CyA or vehicle starting at 3 hpf. Proportion of embryos with coloboma was not affected by exposure to cyclopamine (2 expts). Embryos with unilateral mild coloboma were scored as "mild"; embryos with bilateral mild coloboma were scored as "moderate", and embryos with bilateral moderate coloboma were scored as "severe".

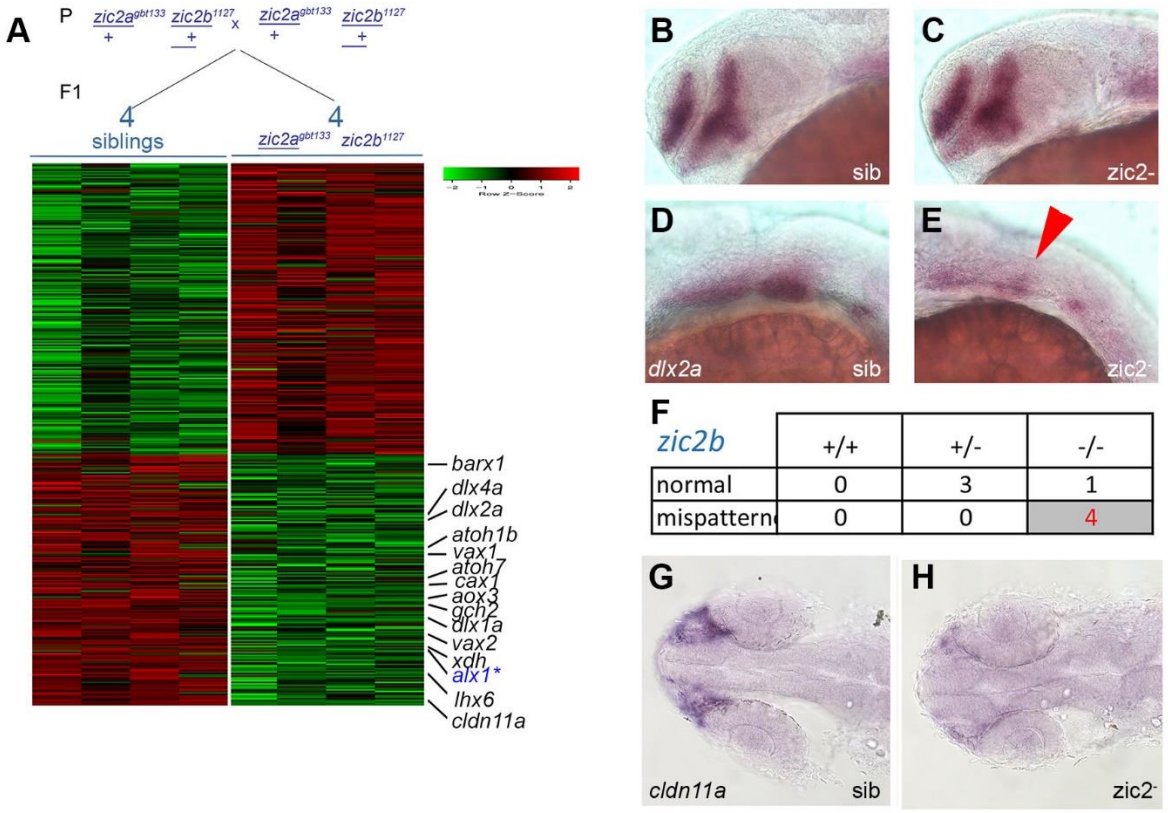

Figure 5. *RNA sequencing transcriptome analysis identifies a set of Zic2-dependent targets*

A: Embryos derived from zic2a^{gbt133}/+; zic2b^{1127}/+ parents were sorted by presence or absence of coloboma into zic2 mutants and sibling groups, respectively. RNA extracted from individual embryos (4 wildtype and 5 with coloboma) was used to prepare cDNA libraries for illumina high-throughput sequencing. Genes with assigned value of False-Discovery Rate below 0.05 were preliminarily selected. The heat-map color represents relative expression levels of differentially expressed genes; 4 out of 5 coloboma-representing libraries are shown to maintain visual balance with the 4 normal sibling samples. B, C: Representative sibling and zic2 mutant embryos derived from zic2a^{gbt133}/+;zic2b^{uw1116}/+ parents show normal dlx2a expression by WISH in the telencephalon and diencephalon. D: normal dlx2a expression in branchial arch

primordia. E: depleted branchial arch dlx2a expression (arrowhead) was observed in 7 out of 127 (6%, 3 expts.) of embryos from this cross. F: Only zic2b− homozygotes exhibited dlx2a reduction in branchial arch primordia. G: normal cldn11a expression adjacent to the optic stalk of embryo with normal retinal morphology. H: depleted cldn11a expression in zic2 mutant with coloboma. Embryos in B – E are shown in lateral views, anterior to the left. Embryos in G and H are shown in dorsal views, anterior to the left.

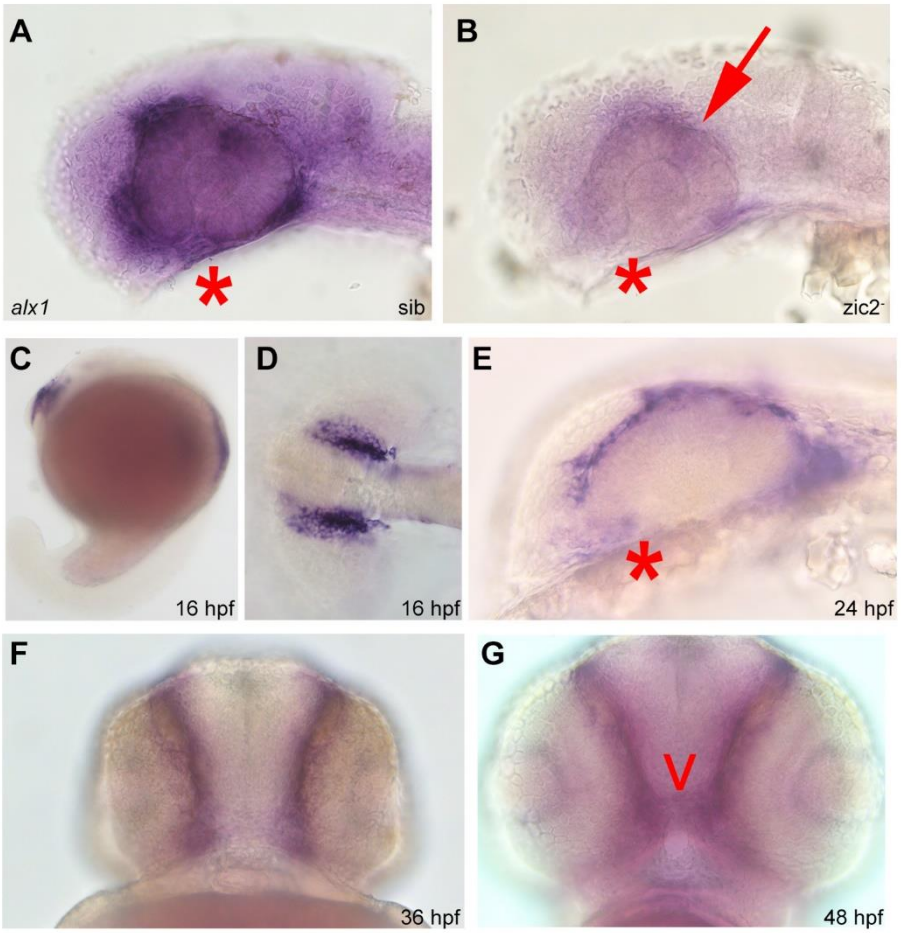

Figure 6. *Alx1 is a novel target of zic2 in the periocular neural crest*

Embryos derived from zic2a^{gbt133}/+; zic2b^{t104}/zic2b^{t104} parents were stained for alx1 expression by WISH. A: normal expression in periocular mesenchyme of sibling embryo. B: depleted expression in zic2 (arrow) in mutant embryo (39 out of 112 total, 2 expts). C–G: wild type embryos stained for alx1 expression by WISH. C–D: alx1 is expressed in frontonasal neural crest at 16 hpf. E, F: alx1 is expressed in periocular mesenchyme (*) at 24 hpf and 36 hpf. G: alx1 is expressed in the ethmoid plate (arrowhead) at 48 hpf. Embryos in A, B, C, and E are shown in lateral views, anterior to the left. Embryo in D is shown dorsally, anterior to the left. Embryos in F and G are shown in anterior views, ventral at the top.

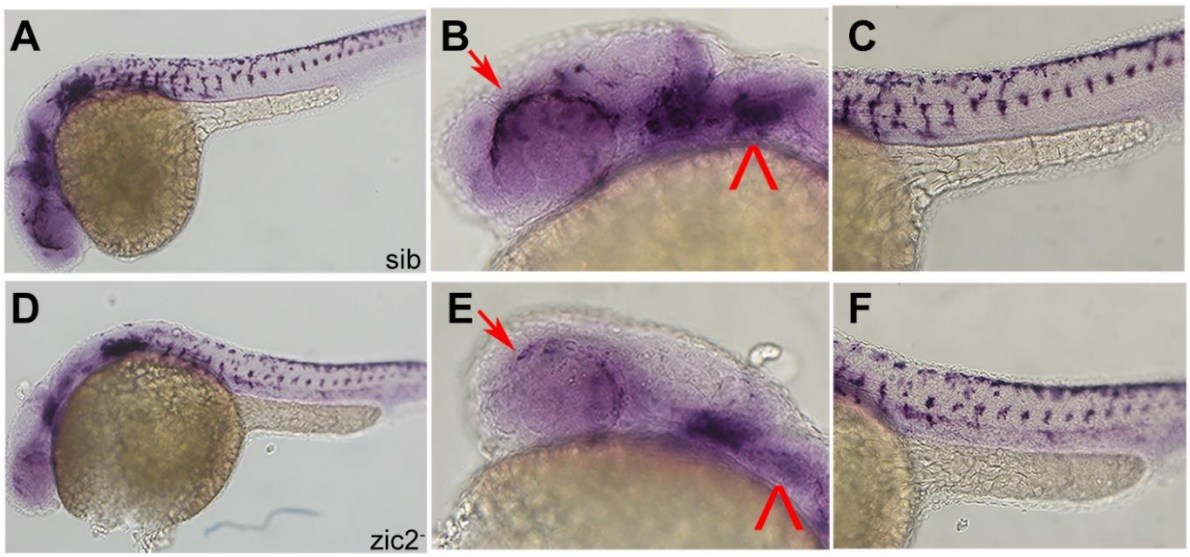

Figure 7. *Frontonasal and pharyngeal neural crest is depleted in MZ-zic2 mutants*

A–C: normal crestin expression in frontonasal and pharyngeal neural crest. D–F: depleted crestin expression in 14 of 55 embryos from a zic2a^{gbt133}/+; zic2b^{t104}/zic2b^{t104} incross. Arrows point to periocular neural crest. Arrowhead points to pharyngeal arch expression. Embryos are shown in lateral views, anterior to the left.

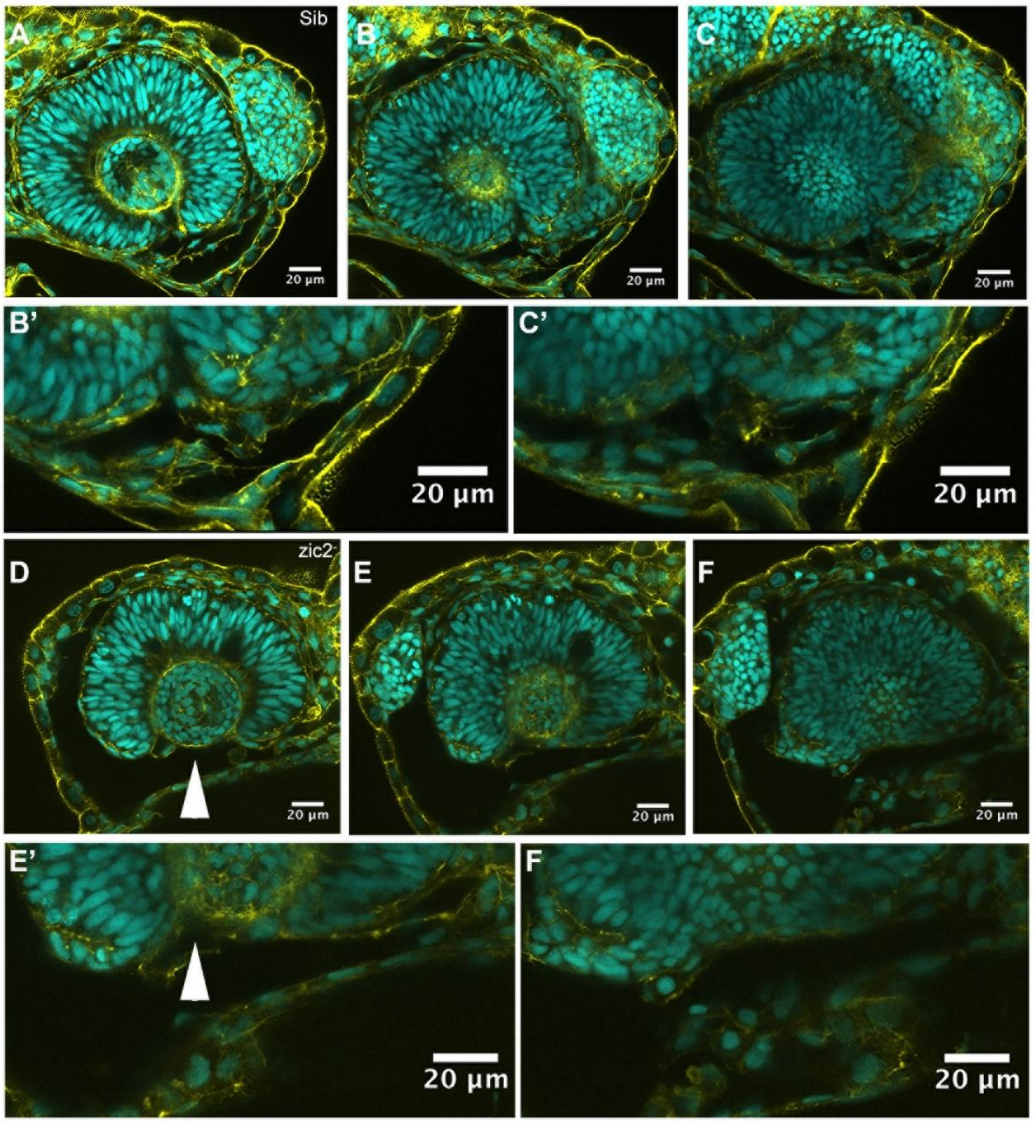

Figure 8. *Ventral periocular neural crest is depleted in MZ-zic2 mutants*

Single confocal sections through optic cups of embryos derived from zic2a^{gbt133}/+; zic2b^{uw1116}/zic2b^{uw1116} parents. A–C′: embryo with normal retinal morphology. D–F′: embryo with coloboma. Embryos were imaged in lateral mounts. Cyan = nuclei visualized by DAPI; yellow=F-actin cytoskeleton visualized by phalloidin. Arrowheads point to aberrant gap in the ventral retina (coloboma). Embryos are shown in lateral views, anterior to the right (A–C) or anterior to the left (E–G). B′, C′, E′, F′ are enlarged from B,C,E and F, respectively.

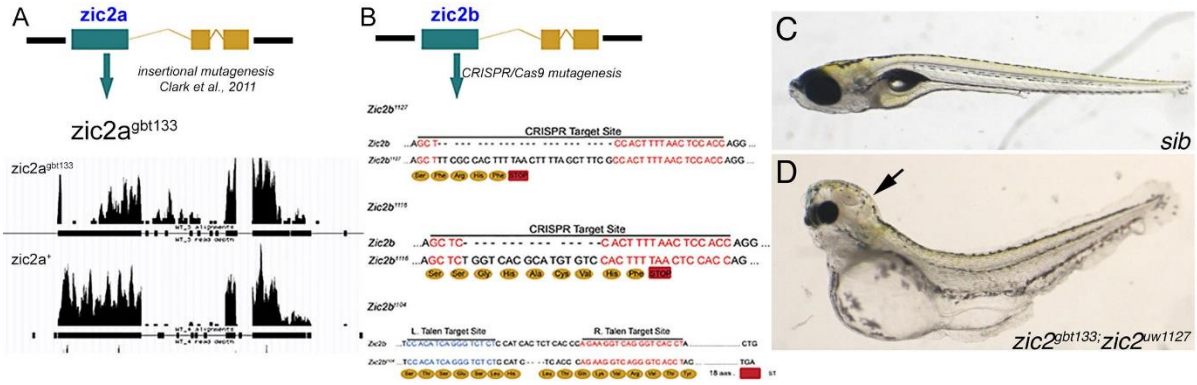

Supplementary Figure 1. *Generation and characterization of mutant alleles at zic2a and zic2b loci.*

A: zic2agbt133 was identified in an insertional mutagenesis screen (Clark et al., 2011). This insertion in the first coding exon of zic2a, near the N-terminus of the predicted open reading frame of zic2a. This allele is predicted to be a functional null. Tracks from individual embryos deep-sequenced on the Illumina platform show that the insertional allele inhibits transcription of the first coding exon of zic2a. B: CRISPR and TALEN nucleases were designed to target different sites in the first coding exon of zic2b.Two mutant alleles of zic2b were generated using CRISPR mutagenesis (uw1127 and uw1116). A third allele of zic2b was generated using TALEN mutagenesis (uwt104). Uwt104 and uw1116 cause frameshifts; uw1127 is an in-frame insertion that contains a translational termination codon. All three alleles encode truncated proteins that do not contain the ultra-conserved zinc binding domains. C: normal 5 dpf sibling and D: zic2 mutant with cerebral edema (arrow) from a zic2 heterozygous carrier incross.

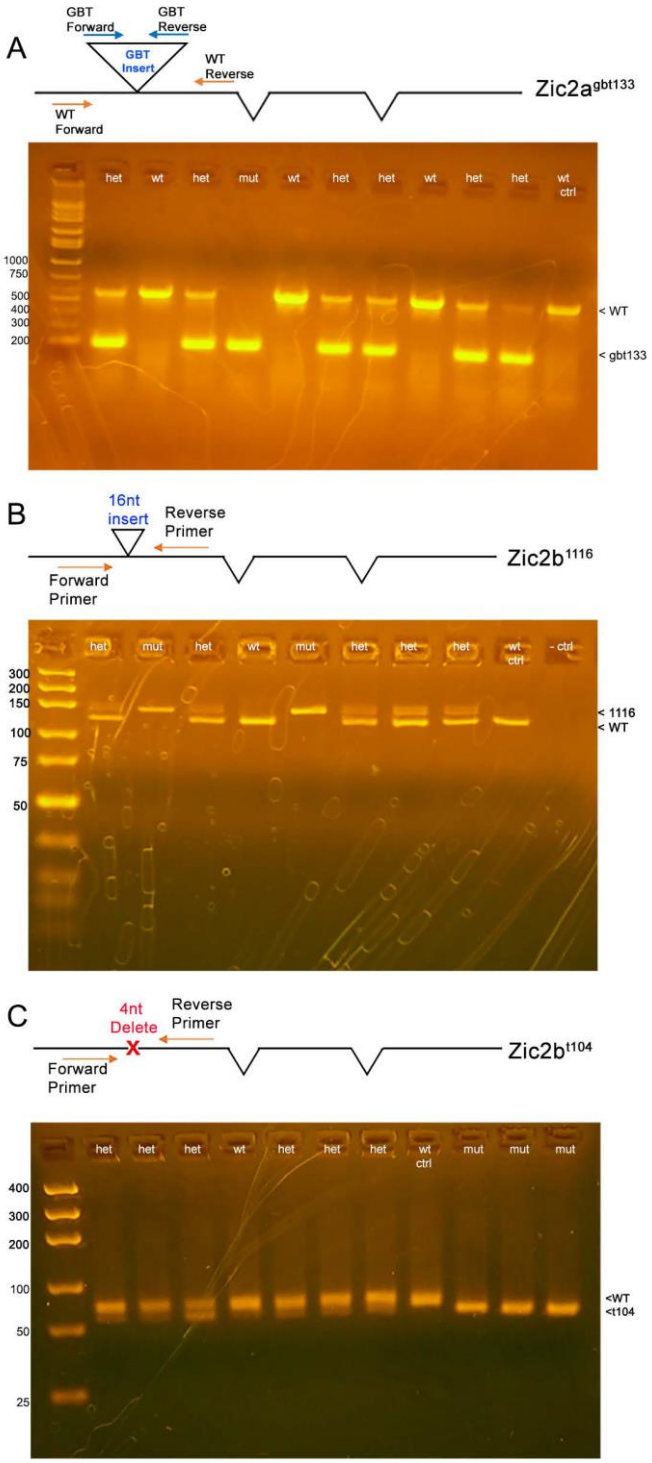

Supplementary Figure 2. *PCR genotyping assays used to identify zic2a and zic2b mutant alleles.*

A: Two sets of primers were used to identify the viral insertion in zic2a^{gbt133}. gbt forward

and reverse primers amplify a 202 nt band in carriers only. wt forward and reverse primers amplify a 582 nt band from the wildtype allele of zic2a.

B: zic2b(crispr) forward and reverse primers amplify a 134 nt fragment from the wild type allele, and a 150 nt fragment from the zic2b^{1116} allele.

C: zic2b(talen) forward and reverse primers amplify 78 nt and 82 nt fragments from zic2b^{t104} and wild type alleles, respectively.

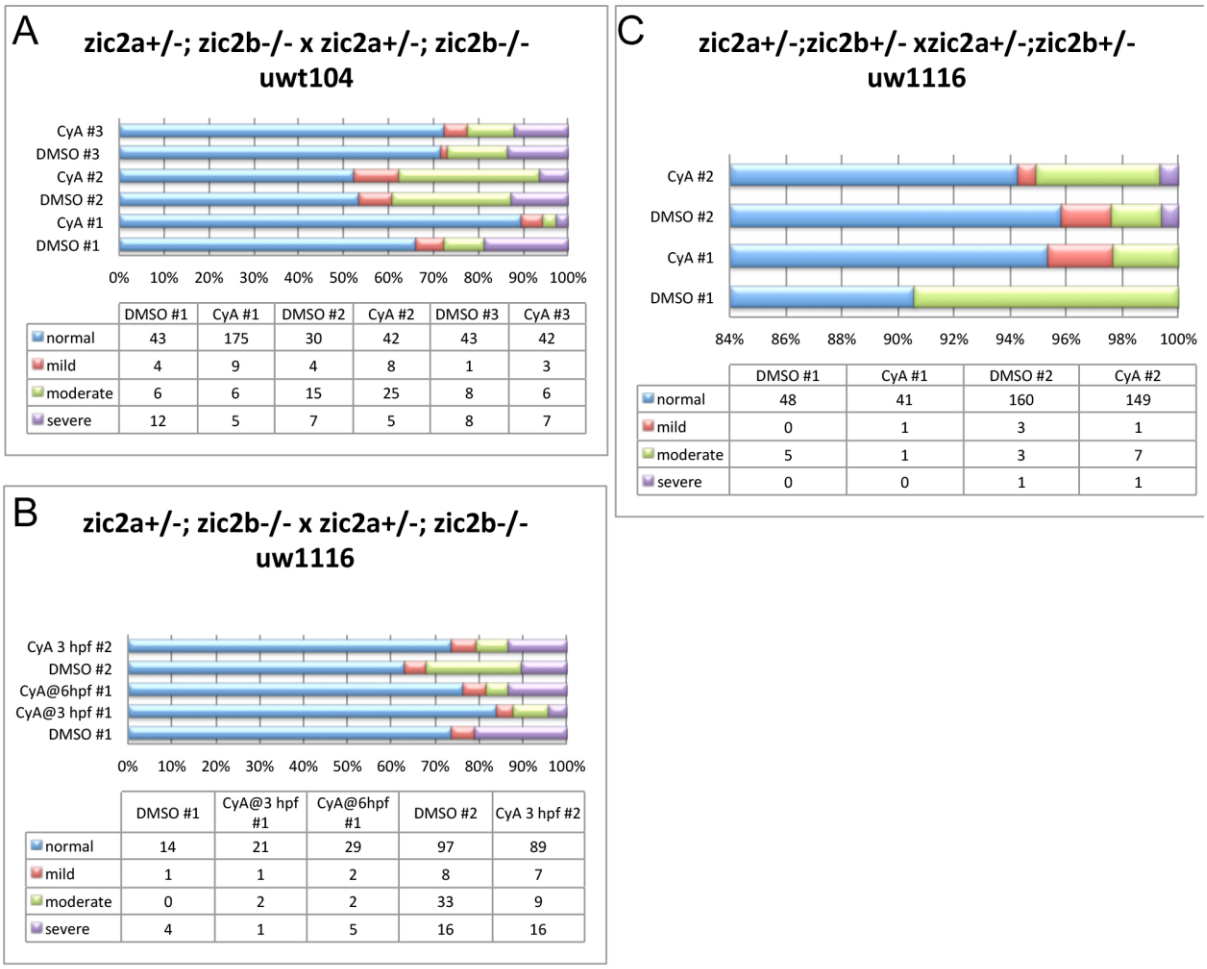

Supplementary Figure 3. *Results of cyclopamine treatments of zic2 mutant embryos.*

A: Embryos were derived from three independent zic2a^{gbt133}/+; zic2b^{t104} parental crosses. Each clutch was divided into two groups, one treated with 3 or 4.5 μM cyclopamine and the other with vehicle control, starting at 3-5 hpf. Drug was removed at 24 – 26 hpf. At 3 dpf, retinal morphology was scored blind to treatment condition. B: Embryos were derived from zic2a^{gbt133}/+; zic2b^{uw1116} parents. Each clutch was divided into three groups, treated as follows: vehicle only added at 3 hpf; 4.5 μM cyclopamine

added at 3 hpf; and 4.5 μM added at 6 hpf. C: Embryos were derived from zic2a^{gbt133}/+; zic2b^{uw1116}/+ parents and treated as in A. In all experiments, embryos with unilateral mild coloboma were scored as “mild”; embryos with bilateral mild coloboma were scored as “moderate”, and embryos with bilateral moderate coloboma were scored as “severe.”

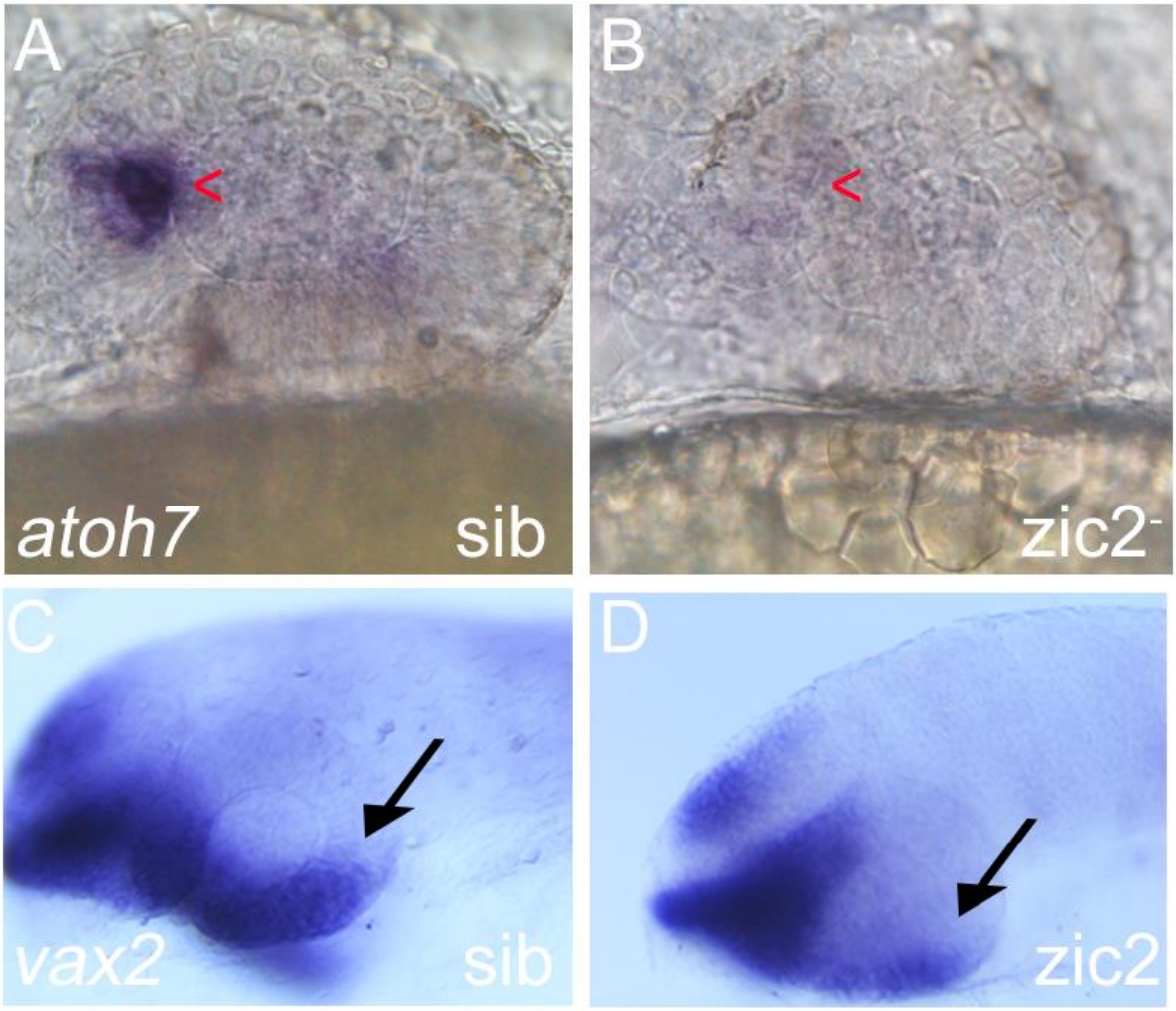

Supplemental Figure 4. *Aberrant expression of Atoh7 and vax2 in MZ-zic2 mutants.*

Embryos derived from zic2a^{gbt133}/+; zic2b^{t104}/zic2b^{t104} parents were stained for atoh7 (A,B) and vax2 (C,D) expression by WISH. A: normal *atoh7* expression in retinal precursor cells (arrowhead); B: depleted *atoh7* expression in 8 out of 33 embryos (24.2%). C: normal *vax2* expression in choroid fissure (arrow); D: depleted *vax2* expression. Embryos are shown in lateral views, anterior to the left.

Summary of coloboma ratios, scored at 1.5- 2 dpf

Date of Clutch	Cross	total	# coloboma	% coloboma	Exp'd % zic2a;zic2b homozygotes
9/25/14		400	32	8.0	
11/4/14		145	12	8.3	
1/10/15		192	20	10.4	
TOTAL	**1127 homo;het F x het;het**	**737**	**64**	**8.7**	**12.5%**
2/25/15		406	23	5.7	
TOTAL	**1127 het;het incross**	**406**	**23**	**5.7**	**6.25%**
11/26/14		71	4	5.6	
1/27/15		205	10	4.9	
3/11/16		138	6	4.3	
TOTAL	**1116 het;het incross**	**414**	**20**	**4.8**	**6.25%**
7/22/16		79	24	30.4	
10/28/16		132	29	22.0	
TOTAL	**t104 homo;het incross**	**211**	**53**	**25.1**	**25%**

Summary of coloboma ratios, scored at 4dpf

Date of Clutch	Cross	total	w/coloboma	severe col	% coloboma	% severe col
2/7/17		313	26	1	8.3	0.3
TOTAL	**1116 het;het incross**	**313**	**26**	**1**	**8.3**	**0.3**
2/7/1/7		106	56	26	52.8	24.5
TOTAL	**116 homo;het incross**	**106**	**56**	**26**	**52.8**	**24.5**

Supplementary Table 1. *Frequency of coloboma in zic2 mutant crosses*

Summary of cartilage defects, scored in Alcian blue-stained embryos at 5 dpf

Date of Clutch	Cross	Total embryos	# jaw defects	% jaw defect	Exp'd % zic2a;zic2b homozygotes
11/19/14		49	4	8.2	
3/9/17		87	10	11.5	
TOTAL	**1116 het;het incross**	**136**	**14**	**10.3**	**6.25%**
3/9/17		88	72	81.8	
TOTAL	**1116 homo;het incross**	**88**	**72**	**81.8**	**25%**

Supplementary Table 2. *Frequency of craniofacial defects in zic2 mutant crosses*

ID	FDR	c1.WT_3	c1.WT_4	c1.WT_6	c1.WT_7	c2.COL_3	c2.COL_4	c2.COL_5	c2.COL_6	c2.COL_7	avg.c1.WT	avg.c2.COL	c2.COL.vs.. c1.WT
AL935184.1	3.827E-71	5	4	5	5	0	0	0	0	0	5	0	-782.1
pdxka	2.464E-19	5	3	4	6	0	0	0	0	0	5	0	-13.8
cldn11a	6.609E-38	7	8	9	9	1	1	1	1	1	8	1	-9.6
si:ch211-63o20.10	4.643E-19	4	2	3	5	1	1	0	1	0	3	1	-6.0
crygm2d9	3.225E-23	48	16	24	46	0	4	13	5	10	33	6	-5.3
cyp27a1.4	1.059E-20	5	9	7	10	1	1	1	5	1	8	2	-4.7
slc15a2	2.467E-20	5	5	5	6	1	1	1	3	1	5	1	-4.6
RBBP6 (13 of 71)	2.16E-12	4	1	3	1	0	1	0	1	1	2	1	-4.5
PRTG (3 of 3)	1.414E-14	25	17	16	3	4	4	3	3	5	15	4	-4.0
si:dkey-59l11.7	3.855E-05	4	5	6	6	1	1	2	3	0	5	1	-3.7
BX321871.1	1.111E-06	1	1	2	3	1	1	0	0	1	2	1	-3.3
rnf17	4.186E-18	3	1	2	2	0	1	1	1	1	2	1	-3.1
si:dkey-66a8.7	1.999E-11	27	13	15	10	0	14	0	0	12	16	5	-3.1
si:ch211-67e16.2	6.687E-08	4	3	4	6	1	1	1	1	2	4	1	-3.1
crygmxl1	3.206E-07	3	1	3	5	0	1	1	1	2	3	1	-2.9
zgc:112970	2.755E-09	14	2	9	20	10	3	6	2	0	11	4	-2.8
cryaa	1.925E-08	6	4	4	6	0	2	1	2	4	5	2	-2.8
kctd4	2.923E-07	4	3	5	4	1	1	2	2	1	4	1	-2.6
si:dkeyp-106c3.1	1.291E-07	2	2	4	2	1	1	1	1	2	2	1	-2.6
itga10	2.905E-07	9	9	11	3	8	2	2	2	2	8	3	-2.5
CELA1 (1 of 7)	2.138E-10	23	6	12	2	2	3	10	4	3	11	4	-2.4
scrt1b	8.11E-06	3	3	3	2	2	1	1	1	1	3	1	-2.4
lhx6	3.694E-06	2	2	3	3	1	1	1	1	1	3	1	-2.4
CABZ01080435.1	1.265E-06	37	28	48	21	12	12	18	13	16	33	14	-2.3
wdr4	4.696E-06	10	6	12	11	4	4	5	5	4	10	4	-2.3
oacyl	2.344E-06	5	6	4	6	1	2	4	2	3	6	2	-2.3
cyb561a3b	5.59E-05	4	4	3	4	1	2	2	2	3	4	2	-2.2
COL18A1 (2 of 2)	0.0045631	2	1	2	3	2	1	0	0	1	2	1	-2.2
gngt2a	0.0046188	2	2	2	2	1	0	1	1	2	2	1	-2.2
rlbp1b	6.659E-05	6	2	6	6	1	2	2	2	4	5	2	-2.2
sprb	2.215E-05	8	9	8	7	5	4	3	3	4	8	4	-2.2
lmln	0.0004367	5	5	6	6	2	2	2	3	2	5	2	-2.2
ankrd44	2.105E-05	7	8	8	8	4	3	3	4	4	8	3	-2.2
si:dkey-251i10.2	1.419E-05	99	114	98	99	28	42	70	41	55	103	47	-2.2
hspb9	6.933E-06	150	36	21	12	23	17	22	29	36	55	25	-2.2
tmem130	3.444E-05	8	10	10	12	4	5	5	5	5	10	5	-2.2
zgc:173556	0.0001501	1	6	7	6	6	2	2	2	1	5	2	-2.2
tyrp1a	2.202E-05	11	13	10	6	4	5	3	4	7	10	5	-2.2
si:dkey-106n21.1	0.0001753	3	3	1	3	1	1	2	1	1	2	1	-2.1
fabp11b	0.0007643	1	2	8	12	0	2	4	3	5	6	3	-2.1
arr3a	0.0003077	3	2	2	2	3	1	0	1	1	2	1	-2.1
alx1	0.0003103	5	6	6	4	2	2	4	2	3	5	2	-2.1

CT573248.1	0.0054833	2	2	2	2	1	1	0	1	1	2	1	-2.1
xdh	6.365E-05	3	3	2	3	1	1	1	2	1	3	1	-2.1
RBBP6 (14 of 71)	0.0009726	2	2	3	3	2	2	0	0	3	3	1	-2.1
si:dkey-248g17.3	0.0009358	3	3	5	5	2	2	2	2	3	4	2	-2.1
pmepa1	0.0012551	8	5	7	4	2	3	3	3	3	6	3	-2.1
ldlrad4	0.0007702	5	4	5	2	2	2	1	2	2	4	2	-2.1
vax2	0.0013591	3	2	3	2	1	1	2	1	1	3	1	-2.1
foxl2	0.0030528	3	2	2	2	1	1	1	1	1	2	1	-2.0
RBBP6 (21 of 71)	0.0018102	4	2	3	2	2	2	0	0	3	3	2	-2.0
APOA4 (4 of 4)	0.0002658	21	26	14	7	22	9	6	3	2	17	9	-2.0
lactb2	0.0072195	7	8	7	5	5	4	2	5	3	7	3	-2.0
CT027576.1	0.0004487	9	2	8	5	0	4	2	4	5	6	3	-2.0
si:dkey-202l22.5	0.0009444	4	4	4	4	1	2	0	3	4	4	2	-2.0
cthrc1a	0.0002319	26	32	40	33	16	16	12	19	20	33	16	-2.0
foxf2a	0.0003867	9	7	7	6	3	3	4	3	3	7	4	-2.0
TMEM100 (2 of 2)	0.0308755	4	4	5	3	2	2	3	1	1	4	2	-2.0
slc2a11b	0.0002976	35	46	35	41	17	18	25	20	20	40	20	-2.0
dlx1a	0.0004336	26	20	24	19	4	15	16	14	8	22	11	-2.0
slc22a7a	0.0004336	22	21	21	23	8	10	15	10	13	22	11	-1.9
DRAXIN (2 of 2)	0.0094232	2	2	2	2	1	1	1	1	1	2	1	-1.9
PTGR1 (2 of 2)	0.0032498	5	2	2	2	0	0	3	3	0	3	1	-1.9
CD200 (1 of 5)	0.0016269	4	4	4	5	2	1	3	2	2	4	2	-1.9
si:dkey-238o13.4	0.0006947	9	11	9	13	3	4	5	6	9	10	5	-1.9
BX088718.1	0.0062917	3	3	2	2	1	1	1	1	2	3	1	-1.9
hbbe2	0.0004367	61	74	37	44	47	26	20	26	22	54	28	-1.9
gch2	0.0003801	212	231	203	206	106	102	105	117	120	213	110	-1.9
rpe65a	0.0022528	4	4	3	3	1	1	3	1	2	3	2	-1.9
aox3	0.0005042	18	20	17	20	8	10	12	9	10	19	10	-1.9
APOA4 (1 of 4)	0.0028434	602	621	457	334	303	237	348	231	196	503	263	-1.9
PLIN4	2.687E-05	2	2	2	2	1	1	0	1	1	2	1	-1.9
si:ch211-229b6.1	0.0085117	2	3	7	5	2	2	1	4	2	4	2	-1.9
nlgn4a	0.0022608	2	2	2	2	1	1	1	1	2	2	1	-1.9
slc2a15a	0.0008473	15	18	20	20	9	9	11	10	10	18	10	-1.9
C1QL4 (1 of 2)	0.0054941	4	3	4	2	2	2	2	1	2	3	2	-1.9
trim25	0.0025861	7	3	8	8	3	4	3	3	4	6	3	-1.9
ppp2r2bb	0.0032874	7	4	7	4	2	4	3	3	3	6	3	-1.9
scn1bb	0.0062909	6	5	4	2	4	2	1	3	2	4	2	-1.9
C9H3orf17	0.0139016	8	9	11	11	4	5	6	7	6	10	5	-1.8
cax1	0.0018272	10	12	10	11	5	6	6	6	7	11	6	-1.8
CABZ01108997.2	0.0042187	30	25	16	7	14	13	6	11	9	20	11	-1.8
crygm2d7	0.0028197	79	44	41	72	1	27	46	39	49	59	32	-1.8
scrt1a	0.0020137	29	26	33	19	19	14	12	12	16	27	15	-1.8
atoh7	0.0041985	13	5	22	17	2	7	13	6	12	14	8	-1.8
RNF213 (3 of 4)	0.0215417	2	2	1	2	1	2	0	1	2	2	1	-1.8

SAMD8	0.0215025	4	3	2	1	2	1	1	2	1	3	1	-1.8
nppa	0.0049194	5	6	6	4	2	3	4	3	2	5	3	-1.8
MREG	0.0037249	17	12	12	14	6	6	9	7	9	14	8	-1.8
pomcb	0.0475963	3	2	3	2	0	2	1	2	1	2	1	-1.8
pcdh2ab3	0.0099541	1	2	2	2	1	1	0	1	1	2	1	-1.8
ZGC:174357	0.0104758	4	3	4	4	4	2	0	1	4	4	2	-1.8
sfrp1b	0.0032117	8	16	9	10	3	9	6	5	8	11	6	-1.8
gc3	0.0143632	1	1	3	1	2	0	1	1	1	2	1	-1.8
si:dkey-211i20.3	0.0173128	2	2	2	2	2	1	0	2	1	2	1	-1.8
si:dkey-31f5.8	0.020756	2	2	2	3	1	1	1	1	2	2	1	-1.8
ncanb	0.0364528	12	8	11	8	6	5	6	4	5	9	5	-1.8
si:zfos-754c12.1	0.0037434	6	6	4	7	3	3	2	3	6	6	3	-1.8
cart4	0.0131648	7	6	6	5	3	4	3	3	3	6	3	-1.8
pcdh1g18	0.013639	1	1	2	2	1	1	1	1	1	2	1	-1.8
vax1	0.0051579	9	4	11	10	1	6	7	6	4	9	5	-1.8
her4.4	0.0039452	17	16	39	34	19	20	3	18	15	27	15	-1.8
gsc	0.0210693	3	2	2	3	2	1	2	1	1	2	1	-1.8
BX511129.1	0.0145193	5	3	5	5	3	3	3	2	2	5	3	-1.8
atoh1b	0.0048243	26	26	27	15	19	14	10	10	14	24	13	-1.8
RBBP6 (25 of 71)	0.0143632	14	6	11	3	10	2	0	7	5	9	5	-1.8
BX119910.9	0.0081674	4	3	5	4	2	2	2	3	2	4	2	-1.8
SLC22A23 (2 of 2)	0.0171639	6	4	4	2	2	3	1	3	2	4	2	-1.8
gpr37l1a	0.0135974	2	2	3	2	2	1	1	2	1	2	1	-1.8
CT990561.1	0.0098099	1	1	2	2	1	1	1	1	1	2	1	-1.8
hbbe1.2	0.0038425	1986	2471	1100	1877	1798	1351	495	636	1023	1859	1061	-1.8
PTS	0.0058771	89	96	79	85	54	46	45	51	54	87	50	-1.7
bscl2l	0.0076009	11	13	12	12	6	6	8	6	8	12	7	-1.7
RNF166 (2 of 2)	0.0373313	5	4	4	3	2	2	4	1	2	4	2	-1.7
si:ch211-165b10.3	0.0384382	2	2	1	2	2	1	1	1	1	2	1	-1.7
rgrb	0.0057752	44	33	22	13	20	16	12	19	14	28	16	-1.7
IGSF3	0.0084521	13	9	13	9	6	7	7	6	6	11	6	-1.7
atp1a1a.5	0.0170555	1	2	3	3	1	1	1	1	2	2	1	-1.7
rasef	0.0215576	2	3	2	2	1	1	2	1	1	2	1	-1.7
mitd1	0.0124996	7	7	8	7	3	5	3	4	5	7	4	-1.7
abcg2d	0.0305913	1	1	1	2	0	1	1	1	1	1	1	-1.7
si:ch211-5k11.12	0.0069529	2347	2725	1205	2054	1893	1459	706	921	1125	2083	1221	-1.7
cyp1c2	0.0323698	3	2	2	1	2	1	1	1	2	2	1	-1.7
dlx2a	0.0096941	30	26	28	32	12	21	17	21	14	29	17	-1.7
cerkl	0.0171639	4	3	3	2	2	2	1	2	2	3	2	-1.7
dlx4a	0.0133833	13	14	9	13	6	8	7	7	8	12	7	-1.7
zgc:172079	0.0350858	2	1	3	2	1	1	1	2	1	2	1	-1.7
zp3.2	0.0492148	1	3	3	3	3	1	1	1	1	3	1	-1.7
zgc:162322	0.019954	3	3	4	3	2	2	2	2	2	3	2	-1.7
npb	0.0200623	6	6	7	7	5	3	3	3	5	7	4	-1.7

gpr143	0.0198378	10	11	10	9	5	5	6	5	8	10	6	-1.7
si:ch211-5k11.2	0.0088544	4622	5373	2387	3639	3844	2707	1443	1825	2047	4005	2373	-1.7
rorb	0.0209295	9	7	11	9	2	5	9	5	6	9	5	-1.7
si:dkey-188k17.3	0.0170555	2	4	5	4	2	2	1	4	3	4	2	-1.7
slc10a4	0.0366655	3	3	2	2	2	2	1	1	1	2	1	-1.7
kctd12.1	0.0419249	2	2	3	2	2	1	1	2	1	2	1	-1.7
si:dkeyp-122d12.1	0.0223758	26	31	29	39	24	16	18	16	20	31	19	-1.7
rnf32	0.0458595	2	2	2	2	1	1	1	2	1	2	1	-1.7
zbtb18	0.016663	31	20	29	19	13	16	14	15	16	25	15	-1.7
RCVRN (2 of 2)	0.0308755	5	6	4	5	4	2	3	2	4	5	3	-1.7
nkx2.1a	0.0282213	9	8	7	3	1	5	7	4	3	7	4	-1.7
slc2a15b	0.0194926	20	22	21	25	11	13	16	12	14	22	13	-1.7
f7i	0.0194541	6	6	9	8	5	3	4	5	4	7	4	-1.7
hbae3	0.017068	2836	3696	1422	2337	2388	1695	1251	1333	1189	2573	1571	-1.6
zgc:101846	0.019945	334	249	274	215	180	137	152	206	146	268	164	-1.6
zgc:77391	0.0373495	14	10	9	5	6	6	5	6	6	10	6	-1.6
gpm6bb	0.0349944	64	54	107	82	49	49	51	44	41	77	47	-1.6
fbxo28	0.0228351	25	24	15	7	13	12	8	11	10	18	11	-1.6
hspb11	0.0218561	31	6	6	5	6	6	5	7	13	12	7	-1.6
prdm13	0.0239349	6	6	6	5	4	4	4	2	3	6	4	-1.6
alas2	0.0222645	38	55	22	44	34	29	20	21	19	40	25	-1.6
rx2	0.0215417	11	10	13	15	3	7	10	9	9	12	8	-1.6
nedd9	0.0308755	11	13	12	11	5	7	10	7	7	12	7	-1.6
slc4a1a	0.0235834	57	74	34	60	52	41	23	31	27	56	35	-1.6
plekho1a	0.0432916	4	3	4	4	3	2	2	2	2	4	2	-1.6
slc29a2	0.0449134	19	4	16	17	4	4	4	10	20	14	9	-1.6
g3bp2	0.0325632	17	17	30	26	13	16	8	17	16	22	14	-1.6
glb1l	0.0361872	9	11	11	11	5	7	7	6	8	10	6	-1.6
si:ch73-366i20.25	0.0472748	22	17	39	37	20	16	13	23	18	29	18	-1.6
evlb	0.0454952	22	12	23	12	12	10	9	11	12	17	11	-1.6
barx1	0.0449681	13	14	12	16	7	8	11	8	9	14	9	-1.6
RPS11 (2 of 2)	0.0455265	41	34	42	58	43	46	1	2	46	43	27	-1.6
inab	0.0457152	36	30	38	28	20	20	25	19	21	33	21	-1.6
si:dkey-259g19.1	0.0417897	4	5	8	11	6	3	5	4	4	7	4	-1.6
rnd3b	0.0348754	12	13	15	16	9	9	10	8	8	14	9	-1.6
cyp27a7	0.0122411	2	4	4	5	3	3	1	3	3	4	3	-1.5
smad7	0.0434621	14	12	13	9	9	9	4	8	9	12	8	-1.5
gdf10a	0.0224578	17	18	11	22	10	14	8	12	13	17	11	-1.5
si:ch211-278d18.4	0.0167556	5	6	5	4	5	6	7	6	9	5	7	1.3
dmd	0.0142881	28	32	31	29	44	37	42	43	46	30	42	1.4
GPA33 (1 of 2)	0.0104604	32	33	15	15	32	33	35	33	35	24	34	1.4
cacna2d1a	0.0492823	14	18	14	14	26	22	14	26	27	15	23	1.5
si:dkey-208k4.1	0.0258456	1	1	2	2	3	2	4	3	2	2	3	1.5
als2a	0.0225067	3	5	4	4	6	5	7	5	5	4	6	1.6

hfe2	0.0319615	6	8	8	9	16	11	7	15	14	8	13	1.6
ugt1a7	0.0445907	10	17	9	10	15	14	16	21	23	11	18	1.6
sytl4	0.0364989	7	3	2	2	4	6	12	3	4	4	6	1.6
si:ch211-271g18.1	0.0397611	2	2	1	2	2	3	3	2	3	2	3	1.6
ypel2b	0.0304971	1	2	1	1	3	1	1	2	2	1	2	1.6
agla	0.0406938	14	22	18	18	43	31	19	28	26	18	29	1.6
CABZ01080590.1	0.0429207	21	27	23	20	40	32	25	42	45	23	37	1.6
smyd1a	0.0493066	54	74	59	32	116	75	48	104	102	55	89	1.6
fam46c	0.0216275	12	13	12	11	25	18	10	25	19	12	19	1.6
fxr2	0.030184	56	65	73	57	129	81	54	130	112	62	101	1.6
mafa	0.0351058	3	5	5	4	9	6	4	9	9	4	7	1.6
FBXO40 (2 of 2)	0.0393762	1	2	2	2	3	2	3	3	3	2	3	1.6
actn3b	0.047022	96	133	121	85	225	145	120	208	192	109	178	1.6
si:dkey-269i1.3	0.0316855	1740	692	913	554	2037	1438	1592	1910	992	975	1594	1.6
CABZ01043311.1	0.0300213	12	15	29	21	44	27	10	41	34	19	31	1.6
zgc:136930	0.0406764	9	15	8	13	12	15	22	19	23	11	18	1.6
si:ch1073-100f3.2	0.0366655	5	7	6	7	14	11	5	13	10	6	10	1.7
dhrs7ca	0.0376956	10	8	8	12	16	12	13	23	12	9	15	1.7
si:ch211-213d14.2	0.0427931	7	8	6	6	9	10	14	8	12	6	11	1.7
ms4a17a.11	0.0352579	10	20	10	10	15	23	27	15	23	12	21	1.7
myhz1.2	0.0209295	589	583	551	461	762	928	853	887	1117	546	910	1.7
si:dkey-187j14.4	0.0493475	1	0	1	1	2	1	2	1	1	1	2	1.7
si:dkey-28n18.9	0.0250423	11	14	10	14	20	20	24	20	18	12	20	1.7
si:dkey-33c14.3	0.0219286	5	8	12	8	15	11	14	17	13	8	14	1.7
FHOD3 (2 of 2)	0.0209295	3	6	5	6	10	6	4	11	11	5	9	1.7
actc1a	0.0197358	715	708	730	673	1326	968	713	1450	1457	706	1183	1.7
slc26a6	0.0138961	2	2	1	1	2	4	2	3	2	2	3	1.7
gys1	0.0185195	10	10	12	9	23	16	10	20	17	10	17	1.7
zak	0.0388484	9	18	10	9	14	19	16	26	23	12	20	1.7
si:ch211-266g18.10	0.0115451	17	29	22	25	58	37	25	38	37	23	39	1.7
MYPN	0.0207142	4	6	5	4	9	7	4	9	11	5	8	1.7
cmya5	0.0182978	5	7	6	5	12	9	5	10	12	6	10	1.7
OBSCN (1 of 2)	0.0171899	14	21	16	14	31	24	15	34	33	16	28	1.7
si:dkeyp-41f9.3	0.0454378	1	2	2	2	2	3	4	2	4	2	3	1.7
ccdc125	0.030092	3	2	3	3	4	4	6	4	4	3	4	1.7
usp28	0.0168535	10	14	11	13	24	16	12	26	22	12	20	1.7
si:rp71-77l1.1	0.0200544	7	11	8	11	12	19	18	17	14	9	16	1.7
si:ch211-158m24.12	0.0317849	3	5	6	5	8	6	5	10	9	5	8	1.7
six2b	0.0209887	4	5	5	4	9	5	7	9	8	4	8	1.7
LIMD1 (2 of 2)	0.0284016	7	9	8	6	19	11	5	14	15	8	13	1.7
tenc1b	0.0314047	10	17	17	16	35	24	13	27	28	15	26	1.7
gpr137	0.0165476	4	6	4	4	7	11	7	7	6	4	8	1.7
adrb1	0.0316855	2	2	2	2	4	3	4	3	3	2	3	1.7
ppp2r3a	0.020756	9	15	17	14	25	19	13	31	32	14	24	1.7

HTRA2 (1 of 31)	0.0350235	6	5	5	0	6	5	13	2	9	4	7	1.7
si:dkey-23p11.4	0.0286054	5	11	5	10	12	11	10	17	18	8	14	1.7
ctsl.1	0.030915	1	1	1	1	2	1	2	2	2	1	2	1.7
mylpfb	0.0119407	813	1299	931	1008	2066	1493	1462	1728	2042	1013	1758	1.7
wu:fb15e04	0.0127558	4	12	3	6	11	11	10	11	10	6	11	1.7
mef2ca	0.017504	33	57	51	61	116	74	48	103	98	51	88	1.7
pvalb5	0.0113818	16	16	18	12	1	32	38	29	33	15	27	1.7
EHBP1L1 (1 of 2)	0.008029	2	5	4	4	8	5	3	9	8	4	6	1.8
MYH7B (3 of 3)	0.0115262	2	2	1	2	3	2	3	2	3	2	3	1.8
ptgdsb	0.0068591	87	57	52	44	80	101	99	112	141	60	107	1.8
MURC (1 of 2)	0.0060558	59	83	73	52	157	95	70	135	136	67	119	1.8
si:dkey-26g8.5	0.0043938	347	377	546	327	482	986	928	457	691	399	709	1.8
klhl31	0.0055742	73	104	111	98	240	137	80	211	192	97	172	1.8
CU571255.1	0.0075166	1	2	2	2	4	3	1	4	4	2	3	1.8
SPEG (1 of 2)	0.0049889	5	7	8	8	15	10	6	16	16	7	13	1.8
si:dkey-236a14.14	0.0133434	9	13	10	14	24	23	12	22	23	12	21	1.8
si:ch211-64i20.3	0.0107783	1	3	1	2	1	4	4	2	4	2	3	1.8
CABZ01072242.1	0.0085966	10	16	13	13	29	15	14	29	27	13	23	1.8
slc4a4a	0.0076009	9	10	6	5	10	15	9	16	16	7	13	1.8
si:dkey-32e6.6	0.0323632	0	1	1	1	2	1	2	1	1	1	1	1.8
MFAP4 (6 of 14)	0.0127752	7	10	10	7	15	28	8	10	17	9	15	1.8
pabpc4	0.0042578	55	90	88	82	187	122	64	169	166	79	142	1.8
btr20	0.0159175	1	0	1	1	2	1	2	2	2	1	2	1.8
igfn1.1	0.005649	32	57	43	45	111	64	54	80	90	44	80	1.8
BX511021.2	0.0046188	14	18	23	12	18	13	49	30	42	17	31	1.8
si:dkey-71b5.6	0.0416616	2	3	3	7	3	7	9	5	7	3	6	1.8
CABZ01066734.1	0.0255276	1	1	1	1	1	1	1	2	2	1	2	1.8
CABZ01088346.1	0.0075166	2	4	3	1	6	4	2	5	6	3	5	1.8
CR318603.2	0.0065175	2	3	2	2	4	5	5	2	4	2	4	1.8
METTL21C (2 of 2)	0.0050434	5	6	7	9	19	8	4	16	12	7	12	1.8
ckma	0.0030645	1248	2059	1564	904	3143	2159	1600	3086	3228	1443	2643	1.8
CU041398.1	0.0031408	2	3	4	3	11	3	1	7	6	3	6	1.8
abcb11a	0.0033672	2	2	1	1	2	5	2	2	2	1	3	1.8
nqo1	0.0010464	43	48	42	45	74	102	95	40	97	44	82	1.8
ehbp1l1b	0.0022773	3	4	5	5	12	6	4	10	8	4	8	1.8
pttg1ipb	0.0032498	6	13	7	9	15	18	13	18	15	9	16	1.9
srpk3	0.0025352	5	7	9	9	14	10	6	21	19	8	14	1.9
si:ch211-170p16.1	0.019945	0	3	1	1	3	3	2	2	3	1	2	1.9
si:dkey-121n8.4	0.0024453	2	4	3	3	7	5	3	6	6	3	5	1.9
ZACN (1 of 2)	0.0055926	3	3	1	5	3	7	7	6	4	3	6	1.9
CABZ01086825.1	0.0023168	10	13	11	8	27	15	7	26	23	11	20	1.9
pfkmb	0.0019506	19	22	21	15	64	40	16	29	30	19	36	1.9
si:dkey-192g7.3	0.0068184	2	2	2	3	4	4	5	3	4	2	4	1.9
obsl1b	0.0066106	5	11	8	9	21	13	8	18	17	8	15	1.9

si:ch211-233g6.8	0.0020137	27	28	31	1	53	30	33	32	55	22	41	1.9
kcnk5a	0.002053	6	16	7	7	17	19	19	6	23	9	17	1.9
CABZ01068324.1	0.0155075	3	7	5	8	8	4	21	12	11	6	11	1.9
si:dkey-241f21.6	0.0453162	1	1	2	2	3	2	5	2	2	1	3	1.9
lrrc58a	0.01139	2	2	2	1	3	4	3	2	2	2	3	1.9
si:dkey-53i3.1	0.002411	5	10	9	8	26	11	8	17	17	8	16	1.9
CD200 (5 of 5)	0.0038639	1	1	1	1	1	1	3	1	2	1	2	1.9
si:ch211-145b13.6	0.0034287	6	8	9	12	17	18	17	14	15	9	16	1.9
si:dkeyp-69b9.3	0.0017069	4	9	10	9	16	11	8	21	19	8	15	1.9
wu:fe11b02	0.004131	4	4	8	6	18	5	12	14	5	6	11	1.9
abrab	0.0014409	4	7	7	6	14	9	8	12	14	6	11	1.9
actc1b	0.0011334	3474	5431	4867	2572	11054	6133	3379	9280	9143	4086	7798	1.9
MFAP4 (5 of 14)	0.002106	7	6	8	5	14	11	13	7	17	6	12	1.9
CR847986.1	0.0015171	3	6	4	4	12	7	6	8	11	4	9	1.9
atp2a1l	0.0037434	9	27	13	5	28	18	19	23	40	13	26	1.9
slc8a3	0.0015737	2	3	3	2	6	4	2	7	5	3	5	1.9
CABZ01073112.1	0.0015584	3	5	4	2	9	5	4	9	8	4	7	1.9
cacng6b	0.0018393	4	5	4	3	11	7	3	9	8	4	8	1.9
si:dkey-27n6.1	0.0043574	1	1	1	1	2	3	2	1	3	1	2	1.9
ldb3a	0.0004833	37	66	56	43	124	80	43	124	119	51	98	1.9
hspbap1	0.0021156	2	2	2	2	3	3	4	3	4	2	3	1.9
g6pca.2	0.0086126	14	10	6	10	8	28	35	9	18	10	20	1.9
MFAP4 (11 of 14)	0.0018463	3	2	8	2	7	10	4	2	13	4	7	1.9
kbtbd12	0.0014409	2	4	2	2	5	3	4	6	5	2	5	1.9
si:dkey-239j18.2	0.0004597	155	181	222	127	232	460	447	234	300	171	335	2.0
pnpla4	0.0072593	1	1	1	2	2	2	3	1	3	1	2	2.0
ms4a17a.1	0.0055742	1	2	2	1	2	4	3	2	4	1	3	2.0
nanos3	0.0099541	2	1	0	1	2	3	1	2	2	1	2	2.0
cplx3a	0.018234	1	1	2	1	2	3	4	3	3	1	3	2.0
s100a11	0.0003863	47	63	52	45	119	104	106	117	71	52	103	2.0
si:dkey-190i10.1	0.0106001	1	2	2	2	4	3	4	3	4	2	4	2.0
zgc:171759	0.0009945	11	10	11	4	32	5	25	19	10	9	18	2.0
MFAP4 (10 of 14)	0.020416	8	6	2	2	6	3	15	8	12	4	9	2.0
prp	0.0002717	7	12	10	8	25	15	7	24	21	9	19	2.0
CR450793.1	0.0066745	0	1	1	2	3	2	3	3	2	1	3	2.0
SYNPO2L (1 of 2)	0.0002342	8	18	14	13	32	20	11	36	36	13	27	2.0
cox6b1	0.0002333	28	41	21	21	99	99	29	37	20	28	57	2.1
trpv6	0.0005663	3	3	3	2	6	6	6	6	3	3	5	2.1
si:dkey-265k11.2	0.0007524	1	1	1	1	1	2	3	2	2	1	2	2.1
jph1b	0.0004096	21	36	40	36	84	51	25	100	86	33	69	2.1
lmo7b	0.0006366	3	4	5	5	12	7	4	9	11	4	9	2.1
neb	0.0006366	81	121	119	95	270	183	98	256	282	104	218	2.1
cfl2	8.817E-05	13	20	29	28	44	40	19	71	62	22	47	2.1
CABZ01065679.1	0.000197	1	2	2	4	6	5	3	8	5	3	5	2.1

atp2a1	0.0009469	2084	3287	2663	1961	6331	4028	3456	6090	6344	2499	5250	2.1
MAL2 (2 of 2)	0.0016957	4	2	1	4	6	7	3	6	6	3	5	2.1
ryr3	8.901E-05	14	27	25	20	61	37	19	52	57	21	45	2.1
dnajb2	3.321E-05	12	12	11	12	23	24	22	28	28	12	25	2.1
ROCK2 (3 of 9)	0.0039176	1	2	2	1	4	1	1	4	4	1	3	2.2
hnmt	1.984E-05	9	17	11	19	37	33	25	33	28	14	31	2.2
MYOM2 (2 of 3)	2.078E-05	29	42	40	30	87	60	39	103	100	35	78	2.2
si:ch211-225h9.2	0.0037493	1	1	1	1	2	2	3	2	2	1	2	2.2
CABZ01099890.1	0.001631	1	3	2	0	5	2	2	4	4	2	4	2.2
BX511270.1	4.482E-05	3	6	6	5	10	13	6	15	11	5	11	2.2
daam2	0.0001981	1	1	2	1	4	2	1	4	3	1	3	2.2
ryr1b	1.908E-05	9	19	17	17	43	26	13	48	43	15	35	2.2
NEDD9 (2 of 2)	1.798E-05	3	0	3	3	4	6	2	7	6	2	5	2.3
si:ch211-226o13.2	6.258E-06	103	214	236	203	518	325	206	530	567	189	429	2.3
zgc:162780	2.429E-05	2	2	3	2	4	6	5	5	6	2	5	2.3
si:ch211-256e16.9	2.785E-05	12	6	6	6	5	20	18	18	23	7	17	2.3
ms4a17a.2	0.0010568	1	1	1	1	2	1	4	2	2	1	2	2.3
si:dkeyp-77c8.3	0.0001927	3	3	3	2	9	3	3	8	8	3	6	2.3
si:dkeyp-77c8.1	2.497E-05	4	5	6	6	16	8	6	14	18	5	12	2.4
mybphb	1.121E-06	106	182	175	135	457	261	144	438	493	149	359	2.4
hpx	2.941E-05	1	1	1	1	1	2	2	3	3	1	2	2.4
SYNPO2 (2 of 2)	9.479E-07	8	15	16	17	43	25	12	45	42	14	34	2.4
casp6l1	0.001288	2	3	13	4	17	3	20	12	14	5	13	2.4
xirp2b	3.23E-06	4	9	7	5	22	15	8	16	16	6	15	2.4
CR847973.1	3.801E-07	43	71	81	69	191	126	67	201	232	66	163	2.5
ttna	2.034E-07	19	35	27	27	91	45	24	85	88	27	67	2.5
mustn1a	4.444E-06	1	4	1	7	8	4	13	11	5	3	8	2.5
asmtl	1.521E-07	7	10	7	8	18	25	20	14	21	8	20	2.5
si:dkeyp-13a3.6	4.974E-05	2	1	2	2	5	4	2	4	5	2	4	2.5
RNF166 (1 of 2)	0.0034287	0	0	2	1	1	1	1	2	2	1	2	2.5
ponzr6	0.0007524	1	1	1	1	2	2	4	2	3	1	2	2.6
MYOM2 (3 of 3)	9.433E-08	28	50	46	31	119	73	44	118	150	39	101	2.6
ttnb	5.715E-09	56	96	101	94	285	154	70	282	371	87	233	2.7
si:ch73-36p18.4	0.0060017	1	1	1	1	3	1	2	3	2	1	2	2.8
im:7148925	3.922E-09	3	4	3	4	11	11	11	8	9	3	10	2.9
CABZ01064972.1	1.387E-09	11	12	5	9	20	24	50	25	16	9	27	2.9
dao.3	3.713E-08	3	2	2	1	5	11	9	2	2	2	6	2.9
si:dkey-15h8.10	3.801E-07	7	9	0	2	5	4	54	2	3	5	14	3.0
zgc:158463	4.279E-12	1117	1405	1913	923	9787	1229	3350	5268	1885	1340	4304	3.2
FP017279.3	2.62E-11	2	9	2	3	9	13	15	16	15	4	14	3.3
zgc:171452	2.989E-10	0	3	3	0	8	4	5	3	8	2	6	3.4
si:dkey-153m14.1	1.705E-13	931	1411	2236	1393	10349	1577	4054	7002	2591	1493	5115	3.4
btr22	2.489E-11	1	0	1	2	4	4	2	4	5	1	4	3.4
g6pca.1	1.202E-10	1	1	1	1	5	6	5	2	1	1	4	3.6

BX511021.4	2.829E-15	13	24	100	13	125	10	241	153	162	37	138	3.7
si:ch73-366i20.1	4.346E-10	0	1	1	1	2	3	3	4	4	1	3	4.0
dnah7	3.621E-14	1	0	0	1	2	2	2	3	3	1	2	4.0
si:dkey-281i8.1	1.446E-15	2	9	2	3	15	17	15	17	19	4	17	4.1
mtdhb	2.8E-18	3	3	4	6	16	21	20	24	6	4	17	4.4
si:dkey-111b14.2	4.161E-19	19	26	34	21	263	30	147	67	47	25	111	4.4
kcnh3	5.918E-19	1	1	1	1	6	4	3	5	5	1	5	4.8
dao.1	2.467E-20	14	19	10	8	59	143	80	14	14	13	62	4.9
si:dkey-100n23.4	1.138E-29	12	16	19	19	86	102	82	98	103	16	94	5.7
CT956064.3	8.967E-16	0	2	0	1	5	2	8	3	2	1	4	6.7
si:ch211-133d24.25	2.467E-20	1	1	0	0	3	3	2	5	6	1	4	6.8
kbtbd7	1.076E-26	0	2	0	0	4	5	6	4	4	1	4	7.8

Supplementary Table 3. *Gene expression data for the replicate RNA-Seq libraries representing wild type and coloboma zebrafish embryos.*

Genome-wide data ("All Data") and genes differentially expressed between coloboma and wild type samples, defined by FDR < 0.05 of edgeR differential expression test ("Responsive"). Column A, gene ID; column B, False Discover Rate from edgeR; columns C to F, gene expression (Transcript Per Million - TPM - values) for wildtype libraries; columns G to K, gene expression (TPM) for coloboma-representing libraries; columns L and M - average expression levels for wild type and coloboma libraries, respectively; column N, bidirectional fold change values for coloboma vs. wild type comparison (genes downregulated in coloboma are assigned negative fold change values); columns O and P, gene name and gene product description, where available.

Gene	Expression at 24 hpf	References
dlx2a	pharyngeal neural crest, telencephalon, ventral thalamus	(Akimenko et al., 1994)
dlx4a	pharyngeal neural crest	(Talbot et al., 2010)
barx1	pharyngeal neural crest	(Sperber et al., 2008)
aox5 (prev. names xdh, aox3)	xanthophore precursors	(Parichy et al., 2000)
gch2	xanthophore precursors	(Parichy et al., 2000)
cax1	xanthophore precursors, pharyngeal neural crest	(Manohar et al., 2010)

Supplementary Table 4. *Neural crest lineage genes with reduced expression in zic2 mutants*

Akimenko, M.A., Ekker, M., Wegner, J., Lin, W., Westerfield, M., 1994. Combinatorial expression of three zebrafish genes related to distal-less: part of a homeobox gene code for the head. The Journal of neuroscience : the official journal of the Society for Neuroscience 14, 3475-3486.

Manohar, M., Mei, H., Franklin, A.J., Sweet, E.M., Shigaki, T., Riley, B.B., Macdiarmid, C.W., Hirschi, K., 2010. Zebrafish (Danio rerio) endomembrane antiporter similar to a

yeast cation/H(+) transporter is required for neural crest development. Biochemistry 49, 6557-6566.

Parichy, D.M., Ransom, D.G., Paw, B., Zon, L.I., Johnson, S.L., 2000. An orthologue of the kit-related gene fms is required for development of neural crest-derived xanthophores and a subpopulation of adult melanocytes in the zebrafish, Danio rerio. Development 127, 3031-3044.

Sperber, S.M., Saxena, V., Hatch, G., Ekker, M., 2008. Zebrafish dlx2a contributes to hindbrain neural crest survival, is necessary for differentiation of sensory ganglia and functions with dlx1a in maturation of the arch cartilage elements. Developmental biology 314, 59-70.

Talbot, J.C., Johnson, S.L., Kimmel, C.B., 2010. hand2 and Dlx genes specify dorsal, intermediate and ventral domains within zebrafish pharyngeal arches. Development 137, 2507-2517.

Chapter III

Zebrafish alx1 and alx3 regulate craniofacial and ocular morphogenesis

This chapter is currently in prep for publication.

Authors: Yoon, B., Bluhm, L., Kawasaki, K., Yeung, P., Santistevan, N., Dubielzig, R.R., Liao, E.C., Grinblat, Y.

Introduction

Proper genetic and environmental regulation is critical for the development of craniofacial complex, including the anterior segment of the eyes (anterior segment) and anterior neurocranium. Frontonasal dysplasia (FND), linked with mutations of the ALX, aristaless-like homeobox protein, gene family (Pini et al., 2020; Uz et al., 2010), and fetal alcohol syndrome (FAS), associated with prenatal ethanol exposure (Kaminen-Ahola, 2020), are two major congenital defects that negatively affect craniofacial complex development. While the occurrence of hereditary FND is very rare (Pini et al., 2020), the occurrence of FAS is very common worldwide (Lovely et al., 2017). Genetic susceptibility to ethanol toxicity has been previously characterized (de la Morena-Barrio et al., 2018; Eberhart and Parnell, 2016; Kaminen-Ahola, 2020; Lovely et al., 2017); however, it remains not fully understood.

The formation of both the anterior segment and the anterior neurocranium is heavily influenced by anterior cranial neural crest (aCNC), a group of migratory stem cells from the posterior diencephalon and midbrain neural plate that migrates around the eyes (Kish et al., 2011; Serbedzija et al., 1992; Wada et al., 2005). aCNC differentiates into various anterior segment cell types (Cavodeassi et al., 2019; Cvekl and Tamm, 2004; Ma and Lwigale, 2019; Williams and Bohnsack, 2015), vascular pericytes of hyaloid vasculature (Gage et al., 2005; Trost et al., 2013), and anterior neurocranium (Kague et al., 2012; Kuratani, 2018). Despite the significance of aCNC in craniofacial complex development, little is known about how aCNC development is regulated genetically and environmentally.

The alx gene family plays essential roles in craniofacial complex development through regulating aCNC-derived lineages. The alx gene family is co-expressed in

aCNC that gives rise to anterior neurocranium (Dee et al., 2013; McGonnell et al., 2011; Qu et al., 1999; ten Berge et al., 1998), anterior segment (Ma and Lwigale, 2019), and periocular neural crest (Ma and Lwigale, 2019; Sedykh et al., 2017). In humans, ALX mutations are linked with FND and ocular defects (Pini et al., 2020; Uz et al., 2010). Alx gene function in craniofacial complex development is highly conserved throughout vertebrates as shown in the Burmese cat (Lyons et al., 2016), mouse (Beverdam et al., 2001; Forsthoefel, 1963; Lakhwani et al., 2010; Qu et al., 1999; Zhao et al., 1996), and zebrafish (Dee et al., 2013; Pini et al., 2020). A recent report demonstrates that *alx1* is required for regulating neural crest differentiation and migration *in vitro* and *in vivo* (Pini et al., 2020). While these data suggest that the alx gene family regulates aCNC lineages, the extent of alx gene family contribution to aCNC development is not well understood.

aCNC development is very sensitive to external oxidative stress (Sakai et al., 2016). Oxidative stress reduces the production of antioxidative defense genes in neural crest (Wentzel and Eriksson, 2011) and activates excessive apoptosis of neural crest (Wang et al., 2015), which, in both cases, threaten neural crest survival. In humans, dysregulation of oxidative state has been implicated in FAS (Brocardo et al., 2011; Dong et al., 2010; Eberhart and Parnell, 2016; Kaminen-Ahola, 2020; Lovely et al., 2017). Notably, mouse *alx3* is found to regulate oxidative stress through activating *foxo1*, which then promotes the oxidative stress defense response (Garcia-Sanz et al., 2017). It is necessary to have a robust animal model to fully understand the gene-environmental interaction on aCNC development.

Here we report that *ALX1* homozygous loss-of-function mutation is associated with severe ocular malformation in human. Likewise, we show that *alx1* mutant adult

fish develop with ocular impairments. We use CRISPR/Cas9-mediated mutagenesis to target the *alx3* locus in *alx1* mutant background to generate *alx1*; *alx3* double mutants to investigate the genetic interaction within the alx gene family members. We demonstrate a requirement for *alx1* and *alx3* in craniofacial cartilage development through regulating the migration of aCNC to the median element of anterior neurocranium. In addition, we show that *alx1* and *alx3* are required for anterior segment development, along with hyaloid and ocular vasculature formation. We find no evidence that *alx1* and *alx3* function are required for retinal ganglion cell differentiation and vision. Lastly, we identify that *alx1* confers genetic robustness against environmental perturbations, namely, alcohol exposure. Collectively, these data establish an *alx1* mutant and an *alx1; alx3* double mutant zebrafish model for dissecting the gene – environmental interactions of the alx gene family during craniofacial complex development.

Materials and Methods

Zebrafish strains and embryo manipulation

Adult zebrafish were maintained according to established methods (Westerfield, 1993). All experimental protocols using zebrafish, including adult euthanasia, were approved by the University of Wisconsin Animal Care and Use Committee and carried out in accordance with the institutional animal care protocols. Embryos were obtained from natural matings and staged according to Kimmel

(Kimmel et al., 1995). The following mutant strains of zebrafish were used: *alx1*^{uw2016} (Pini et al., 2020) and *alx1*^{uw2016}*; alx3*^{uw2113}, generated by CRISPR/Cas9 mutagenesis in the course of this study. *Alx1; alx3* double mutants were obtained by introducing alx3 CRISPR (GGAGTCCCCAGTCAAGCCGT) into *alx1*^{uw2016} mutant background. For adults, *alx1*^{uw2016} and *alx3*^{uw2113} mutant alleles were identified by PCR genotyping of genomic DNA extracted from tail clips.

Ethanol treatment was carried out as follows: Embryos were treated with 0.5% ethanol diluted in E3 starting at 6 hours post fertilization (hpf). At 2 days post fertilization (dpf), embryos were transferred to fresh E3 and raised until 5 dpf to score for craniofacial defects or until 2 months to score for ocular defects.

Sequencing and PCR genotyping of alx1, alx3, pappaa^{p170} *mutant alleles*

To determine *alx1* and *alx3* genotypes, DNA was extracted from individual embryos or adult fish and subjected to PCR with the following primers: *alx1* forward: 5’- CGTGACTTACTGCGCTCCTA – 3’ (Pini et al., 2020), *alx1* reverse: 5’- CGAGTTCGTCGAGGTCTGTT - 3’ (Pini et al., 2020), *alx3* forward: 5’- CTATCCCGCTCTGGACTCAG - 3', *alx3* reverse: 5’- TCCTCCAGTTGAAAGGTGCT - 3'. *Alx3* PCR fragments were subcloned via TA cloning into pGEMT-Easy (Promega) and sequenced to characterize the mutations. To determine *pappaa*^{p170} genotype, DNA was extracted from individual larvae and subjected to PCR with the following primers: *pappaa*^{p170} forward: 5’- CACTCTGGAGCCTCCAGCTTGCGGT– 3’ (Wolman et al., 2015), *pappaa*^{p170} reverse: 5’- TTGCTGACGTTGTGTACG– 3’ (Wolman et al.,

2015). The PCR product was digested with Mse1 (New England Biolabs), cleaving the mutant allele and producing a 245 bp fragment distinguishable from the 271 bp wild-type (WT) allele. Subsequently, metaphor (Lonza) gel electrophoresis was used to genotype individual embryos and adult fish.

Immunohistochemistry

Embryos were fixed in 4% paraformaldehyde (PFA)/ PBS overnight. After fixation, the embryos were bleached in 1% KOH/6% H_2O_2 and then washed with PBST-X (1X PBS with 0.5% TritonX-100). To enhance permeability, embryos were treated with proteinase-K (1:5000) for 5 minutes and post-fixed with 4% PFA/PBS for 30 minutes room-temperature (RT). Embryos were blocked with PBSTD-X (1X PBST-X mixed with 1% DMSO, 10% Bovine serum albumin mixed with 1X PBS, 10% goat serum) for 2 hours in RT before primary antibody incubation. Primary antibody mouse-anti zn5 antibody (Zebrafish International Resource Center; 1:100) was detected fluorescently with Alexa-488 goat anti-mouse antibodies (Invitrogen; 1:500). For nuclei staining, embryos were stained with DAPI (Molecular Probes; 1:5000). Embryos were mounted in VectaShield (Vector laboratories) and imaged on an Olympus IX81 inverted confocal microscope with the Fluoview 1000 confocal package, using a 60x water immersion objective (NA 1.10).

In situ hybridization and alcian blue staining

In situ hybridization was carried out as previously described (Gillhouse et al., 2004), using the following probes: col2a1a (Yan et al., 1995). After whole mount *in situ* hybridization (WISH), embryos were mounted in 100% glycerol and imaged on Leica MZ FLIII stereo microscopes equipped with Leica DFC310 FX camera and LAS v4.0 software. For cartilage staining, zebrafish larvae were fixed at 5 dpf in 4% PFA/PBS overnight and stained with alcian blue according to Kimmel (Kimmel et al., 1998). Stained zebrafish larvae were further dissected using forceps for imaging jaw cartilage and anterior neurocranium. Jaw cartilage and anterior neurocranium were imaged on NIKON eclipse E600 microscope equipped with Q Imaging QIclick 1.4MP CCD Monochrome Microscope camera and NIS-elements software.

O-dianisidine staining and alkaline phosphatase staining

Staining the hemoglobinized red blood cells with o-dianisidine was carried out as previous described (Paffett-Lugassy and Zon, 2005). To visualize the intraocular red blood cell population, embryos were bleached with 1% KOH/6% H_2O_2. Embryos were mounted in 100% glycerol and imaged on Leica MZ FLIII stereo microscopes equipped with Leica DFC310 FX camera and LAS v4.0 software.

Staining endogenous alkaline phosphatase activity of anterior segment and hyaloid vessels was previously described in (Goehlert et al., 1981; Lessell and Kuwabara, 1964). Zebrafish larvae were fixed at 5 dpf in 4% PFA/PBS overnight and

stained with alkaline phosphatase according to (Alvarez et al., 2007). Eyes were pierced with a tungsten microneedle and forceps as previously described (Vorontsova et al., 2019). Lens were imaged on NIKON eclipse E600 microscope equipped with Q Imaging QIclick 1.4MP CCD Monochrome Microscope camera and NIS-elements software.

Adult ocular histology

Adult *alx1*^{uw2016} zebrafish were euthanized and then preserved in 4% paraformaldehyde fixative. Each fish was photographed on both sides to document eye morphology, and the entire body was immersed for 30 minutes in a solution of 12% hydrochloric acid (Decal II, Surgipath) to decalcify the bone. Transverse sections were made through the head. The resulting head blocks containing the eyes were submitted for paraffin embedding and step sectioned at 100 microns to sample beyond the midway of the globes. Extra slides were saved at each step. The selected sections were stained using standard protocol with hematoxylin and eosin. Rough measurements were made of each globe in the axial plane and in the vertical plane using the histology slide.

Lineage tracing and fluorescent imaging

Embryos derived from *alx1*^{uw2016}; *Tg(sox10:kaede)* were injected with *alx3* CRISPR and raised until 20-somite stage, whereupon they were dechorionated, selected for strong fluorescent expression, and mounted in low melting agarose containing 0.013% tricane. Embryos were photoconverted using the 405nm UV laser on a Leica scanning confocal microscope, with regional selectivity accomplished by using region of interest features. Selected cells were exposed to the photoconverting laser at full power for 3-5 minutes, depending on the size of the region, or until red kaede was present. Embryos were raised until 4 day-post-fertilization when they were once again mounted in low melting agarose with tricane and imaged on the confocal microscope.

For fluorescent imaging of the ANC and Meckel's cartilage, both uninjected siblings and larvae at 4dpf with different genotype on a *Tg(sox10:kaede)* background were dissected and flat-mounted.

Behavior testing, video recording, and analysis

From 1 dpf, larvae were raised at 29°C in E3 on a 14:10 hr light/dark cycle. Larvae were behaviorally tested on 5 dpf and were held in 60mm-wide Petri dishes with 25 larvae/dish in 10mL E3, kept on a white light box (800 $\mu W/cm^2$) for at least 1 hour, and then transferred to a 4x4 grid. Larvae were illuminated from above with a mounted LED light (MCWHL5 6500 K LED, powered by LEDD1B driver, Thorlabs) and

below with an infrared light source (IR Illuminator CM-IR200B, C&M Vision Technologies). In the grid, larvae were acclimated to the illuminated testing stage (85$\mu W/cm^2$) for 5 min before exposure to a series of 10 dark flash stimuli. The O-bend behavior was elicited using an automated behavioral platform in which the mounted LED light and the timing of dark flashes could be controlled (Burgess and Granato, 2007; Wolman et al., 2011). Each stimulus lasted for 1 s and stimuli were presented at a 30 s interstimulus interval. Flote was used to analyze video images responses in an experimenter independent, automated manner (Burgess and Granato, 2007). Flote tracks the position of individual larvae frame by frame and characterizes locomotor maneuvers according to predefined kinematic parameters that distinguish these maneuvers. After testing in the 4 x 4 grid, larvae were transferred to a 96-well plate and genotyped for *alx1*, *alx3*, and *pappaa*^{p170} *post hoc.*

Statistics

Statistical analyses, including calculation of means, SEM, and ANOVA, Fisher's exact test, Chi-square test, were performed using GraphPad Prism software (GraphPad Software). P-values below 0.05 were considered statistically significant.

Result

Human ALX1 and zebrafish alx1 function in ocular development

Consanguineous parents had 13 children and 4 out of 13 children were born with complex FND (Fig. 1A). We previously carried out whole-exome sequencing and identified a missense L165F variant in *ALX1* homeodomain and identified that the FND phenotype was inherited in an autosomal recessive manner (Pini et al., 2020). Notably, all of the children affected with complex FND presented with ocular defects, such as anophthalmia, microphthalmia, and retinal coloboma, along with oblique facial cleft (Fig. 1B). The severity of the ocular defects varied among children. While subject 3 presented with unilateral microphthalmia and unilateral coloboma, subjects 4, 5, and 6 presented with bilateral anophthalmia with eyelid defects (Fig. 1C). This suggests that human *ALX1* is required for ocular development.

We next asked if zebrafish *alx1* function is required for ocular development. Previously, we showed zebrafish *alx1* mutant embryos developed with low-penetrant craniofacial malformations and were adult viable (Pini et al., 2020). While the phenotype was incompletely penetrant, 21% of *alx1* mutant adults (Fig. 2H) developed with ocular impairments, including aberrant pupils (Fig. 2A,C OS and 2B,D OD), aphakia (Fig. 2A,C OS), iridial dysplasia (Fig. 2B,D OD), coloboma (Fig. 2F), and mild ocular hemorrhaging (Fig. 2G), which are associated with anterior segment defects. *Alx1* mutants significantly exhibited these ocular impairments ($p < 0.0001$, Fisher's exact test; Fig. 2H). Together, these data support a conserved functional requirement

for *alx1* during ocular development but do not explain the difference in severity between human and zebrafish mutants.

Zebrafish alx1 and alx3 functions are required for craniofacial lineage formation

Previously, we hypothesized that the low penetrance of craniofacial malformations in *alx1* mutants is due to genetic compensation by other alx gene family members and demonstrated that *alx3* transcription was upregulated in *alx1* mutants (Pini et al., 2020). To understand the genetic interaction between *alx1* and *alx3*, we used CRISPR/Cas9 mutagenesis to generate a frameshift allele in the second exon of the *alx3* locus in the *alx1* mutant background. A mutant allele was isolated that contained a 13 nucleotides insertion (*alx3*^{uw2113}). A mutant allele triggered premature stop codons and lost homeodomain and transactivation domains; thus, its function was presumably null (Supp Fig. 1). In parallel, we adapted G0 knockout zebrafish (Wu et al., 2018) against *alx3* in *alx1* mutant background (*alx1 -/-; alx3* CRISPant) to rapidly evaluate the craniofacial phenotype (Supp Fig. 2).

We asked if both *alx1* and *alx3* functions were required for craniofacial lineage formation by assessing the craniofacial phenotypes in progeny from a cross between *alx1*^{uw2016}*; alx3*^{uw2113}/+ parents. At 5 dpf, *alx1; alx3* double mutants develop with shortened neurocranium and aberrant jaw cartilage formation (Fig. 3B). To visualize the ethmoid plates, we stained craniofacial cartilage with alcian blue and dissected the embryos. We found *alx1; alx3* double mutant embryos developed with abnormal ethmoid plate formation with various degrees of severity (Fig. 3D-F). Notably, *alx1;*

alx3 +/- embryos also developed with abnormal ethmoid plate formation (Fig. 3G). At the same time, we assessed the craniofacial phenotypes of *alx1 -/-; alx3* CRISPants. While *alx1* mutants and *alx3* CRISPants developed with normal craniofacial cartilage, *alx1 -/-; alx3* CRISPants exhibited midline cleft (Supp Fig. 2G) along with abnormal trabeculae and ethmoid plate formation (Supp Fig. 2O), consistent with the severe phenotype observed in *alx1; alx3* double mutants (Fig. 3F). These data suggest that both *alx1* and *alx3* are required for proper craniofacial development.

We next asked if cartilage precursors were mispatterned in *alx1; alx3* double mutants at 2 dpf, prior to the craniofacial abnormalities at 5 dpf. We examined *col2a1a*, a craniofacial cartilage precursor marker (Yan et al., 1995), expression in WT, *alx1* mutant, and *alx1; alx3* double mutant embryos using whole mount *in situ* hybridization (WISH). 88% of the embryos derived from *alx1 -/-* parents exhibited normal expression of col2a1a overall while only 24% from *alx1 -/-; alx3 +/-* parents did (Fig. 3M). *Alx1; alx3* double mutant embryos developed with truncated or depleted ethmoid plate precursors (Fig. 3I, I', L). The zebrafish scleral ring consists of a cartilaginous structure surrounding the anterior segment (Gestri et al., 2012). Notably, *col2a1a* expression in putative scleral precursors was reduced in *alx1* mutants and *alx1; alx3* double mutants (Fig. 3K, L). These data suggest an early requirement of *alx1* and *alx3* function in craniofacial lineage formation.

To further understand an early requirement of *alx1* and *alx3* in craniofacial lineage formation, we performed a lineage tracing analysis of cranial neural crest cells. We identified that in WT larvae, anterior and medial CNC labeled by kaede photoconversion (Fig. 4A, B) always migrated to the median element of anterior neurocranium (Fig. 4E,F). However, in *alx1 -/-; alx3* CRISPants, anterior and medial

CNC (Fig. 4C, D) failed to reach to the median element of anterior neurocranium and ectopically populated near the eyes (Fig. 4G, H). Collectively, these data indicate that *alx1* and *alx3* contribute to craniofacial lineage formation by regulating the migration of cranial neural crest cells.

Zebrafish alx1 and alx3 function are required for ocular morphogenesis

Ocular malformations were incompletely penetrant in *alx1* mutant adult fish (Fig. 2). To investigate if *alx3* function compensates during ocular morphogenesis, we observed the ocular phenotypes of progeny from a cross between *alx1 -/-; alx3 +/-* parents. Starting at 3 dpf, *alx1; alx3* double mutants exhibited obviously misshapen eyes. At 5 dpf, *alx1; alx3* double mutants exhibited both misshapen eyes and craniofacial abnormalities (Fig. 5B, D) and these phenotypes were not seen in progenies from WT incross ($p = 0.0009$, Fisher's exact test; Fig. 5E). Genotypic analysis revealed that this phenotype was restricted to *alx1; alx3* double mutants and *alx1; alx3* heterozygotes larvae (Fig. 5F).

Because alkaline phosphatase is expressed in anterior segment, such as ciliary epithelium, lens epithelium, and corneal endothelium of the fish (Lessell and Kuwabara, 1964), we examined endogenous alkaline phosphatase activity of progeny from a cross between WT or *alx1 -/-; alx3/+* parents at 5 dpf to elucidate whether anterior segment is malformed in *alx1; alx3* double mutants. In WT and *alx1* mutants, endogenous alkaline phosphatase is correctly expressed in anterior segment (Supp Fig. 3A, B). However, some *alx1; alx3* heterozygotes and all *alx1; alx3* double mutants

developed with aberrantly formed anterior segment shown as partially missing endogenous alkaline phosphatase expression (asterisk in Supp Fig. 3C), misshapen eyes (arrowhead in Supp Fig. 3C), and coloboma shown as two separately protruded hyaloid vessels, where endogenous alkaline phosphatase is also expressed (Alvarez et al., 2007) (arrow in Supp Fig. 3D). We found that the anterior segment defect is specific to some *alx1; alx3* heterozygotes and all *alx1; alx3* double mutants ($p < 0.0001$, Fisher's exact test; Supp Fig. 3E).

Alx1 mutants and *alx1; alx3* double mutants also exhibited intraocular (Fig. 6B, D) and/or periocular hemorrhaging (Fig. 6C, F). To visualize the red blood cell population within and surrounding the eyes, we stained embryos with o-dianisidine and bleached them. We found that the hemorrhaging phenotype was significantly increased in *alx1* mutants compared with WT ($p < 0.0001$, Fisher's exact test; Fig. 6G). Notably, we identified that the hemorrhaging phenotype is linked with misshapen eyes in *alx1; alx3* double mutants and both phenotypes were significantly increased compared with WT ($p < 0.0001$, Chi-square test; Fig. 6H).

In zebrafish, the hyaloid vessel starts to form a branched hyaloid network within the lens soon after the hyaloid loop is completely formed around the lens at 32 hpf, which stays until at least 5 dpf (Hartsock et al., 2014). To identify if the hyaloid network is abnormally formed in *alx1; alx3* double mutants, we scored for ocular and craniofacial defects in 5 dpf progeny from a cross between WT or *alx1 -/-; alx3*/+ parents, stained for endogenous alkaline phosphatase, and dissected the lens for imaging. WT embryos developed with normal hyaloid network formation (Supp Fig. 4A). Embryos derived from *alx1 -/-; alx3*/+ parents exhibited aberrant hyaloid network development regardless of the presence and the severity of ocular defects. Embryos

with normal eyes developed with reduced hyaloid network (Supp Fig. 4B), those with mildly misshapen eyes had unorganized hyaloid network (Supp Fig. 4C), and those with severely misshapen eyes had unorganized hyaloid network (Supp Fig. 4D) or no hyaloid network (Supp Fig. 4E).

We next asked if aberrant eye phenotypes in *alx1; alx3* double mutant embryos were associated with vision loss. Since retinal ganglion cell (RGC) neurons are required for sending visual information to the brain (Dhande and Huberman, 2014), we examined the differentiated RGC population through immunohistochemistry against zn5, a differentiated RGC marker (Lee et al., 2008), and imaged using a high-resolution confocal microscope. We identified that RGC differentiation was not impaired in absence of *alx1* or both *alx1* and *alx3* function (Fig. 7A-H).

In addition, we performed the dark flash assay to assess the behavioral response to a sudden change in visual field illumination (Burgess and Granato, 2007). In response to an abrupt absence of light, larval zebrafish execute a turning behavior termed the “O-bend” in which they turn their bodies ~180 degrees (Burgess and Granato, 2007) (Fig. 7I). As a negative control, we used *pappaa*^{p170} mutants which have been shown to exhibit a marked reduction in O-bend initiations compared to WT (Miller et al., 2018). We exposed 5 dpf WT, *alx1* homozygous mutants, *alx1; alx3* double mutants, *alx1;alx3* heterozygotes, and *pappaa*^{p170} mutant larvae to 10 dark flashes and evaluated the probability of larvae to initiate an O-bend maneuver in response to the abrupt absence of light. *Alx1* mutants, *alx1; alx3* double mutants, and *alx1; alx3* heterozygotes show no difference in O-bend initiations compared to WT ($p > 0.9999$; ANOVA with Kruskal-Wallis, Fig. 7J). *pappaa*^{p170} mutants, however, show a marked reduction in O-bend initiation compared to WT ($p < 0.0001$; ANOVA with

Kruskal-Wallis, Fig. 7J). These data suggest that vision is not significantly impaired in *alx1; alx3* double mutant larvae at 5 dpf as larvae are able to detect and respond to luminescence changes in their visual field.

Zebrafish alx function is required for protecting aCNC lineage against environmental perturbations.

Oxidative stress triggered by environmental assaults, such as prenatal ethanol exposure (Brocardo et al., 2011; Dong et al., 2010; Lovely et al., 2017) and maternal diabetes (Garcia-Sanz et al., 2017; Wang et al., 2015), is a major risk factor for congenital craniofacial and ocular malformations, which are typically caused by neural crest defects (Sakai et al., 2016). Because alx gene function is required for early neural crest development, we asked if zebrafish alx protects the aCNC lineages against environmental assaults. We exposed progenies derived from WT incross, *alx1* -/- and *alx1* +/- outcross, and *alx1* -/- incross to low concentration of ethanol (0.5%) so that most WT embryos were not affected by ethanol toxicity. Ethanol exposed *alx1* mutant embryos exhibited a mild reduction of the anterior element of ethmoid plates (Fig. 8B), with rare “stick” ethmoid plates (Fig. 8C). While only few ethanol exposed WT embryos develop with craniofacial defects, the penetrance of craniofacial defects significantly increased in ethanol exposed embryos derived from *alx1* -/- and *alx1* +/- outcross ($p = 0.0237$, Fisher’s exact test; Fig. 8D) and *alx1* -/- incross ($p = 0.0005$, Fisher’s exact test; Fig. 8D). Among ethanol exposed embryos, embryos from *alx1* -/- incross were

the most notably effected, suggesting that ethanol exposure has a greater impact on embryos that lack functional *alx1.*

We also observed the ocular morphology of embryos derived from WT incross and *alx1 -/-* incross after introducing low concentrations of ethanol. Ethanol exposed WT embryos and *alx1* mutants exhibit a mildly misshapen eye phenotype (Fig. 9B). The penetrance of ocular defects significantly increased in ethanol exposed embryos derived from *alx1 -/-* incross ($p = 0.0005$; Fisher's exact test; Fig. 9C). In addition, the penetrance of ocular defects significantly increased in both unexposed *alx1* mutants ($p = 0.0003$, Fisher's exact test; Fig. 9C) and ethanol exposed *alx1* mutants ($p < 0.0001$, Fisher's exact test; Fig. 9C) compared to unexposed WT and ethanol exposed WT, respectively. We performed the dark flash assay on ethanol exposed and unexposed WT and *alx1* mutants at 5 dpf. We observed no difference in O-bend initiations between ethanol exposed larvae and their unexposed siblings of the same genotype ($p > 0.9999$, ANOVA with Kruskal-Wallis; Supp Fig. 5), suggesting that low concentration ethanol exposure does not significantly impair vision in larvae at this developmental stage.

Next, we raised ethanol exposed embryos derived from *alx1 -/-* incross to 2 months and observed their ocular morphology. Ethanol exposed *alx1* adult mutants developed with ocular defects (Fig. 9D, E). The penetrance of ocular defects in ethanol exposed *alx1* adult fish increased compared with unexposed *alx1* adult fish, but not significantly ($p = 0.1022$, Fisher's exact test, Fig. 9F). Together, these data identified a protective role for the alx gene family in craniofacial and ocular lineages against environmental assaults.

DISCUSSION

Our work establishes alx mutants as a robust genetic model to study gene-environment interactions that influence anterior neural crest in zebrafish. We show a functional requirement of *alx1* for ocular morphogenesis is conserved between human and zebrafish and demonstrate an early requirement of zebrafish *alx1* and *alx3* function during craniofacial complex development through regulating aCNC migration. We also identify that alx gene family confers protection for aCNC-derived lineages against environmental assaults.

How does the alx gene family function during craniofacial development?

Although mutations in the ALX gene family are associated with FND in humans, the analysis of FND is very complicated as a wide spectrum of phenotypes and various modes of inheritance have been reported (Farlie et al., 2016). This correlates with the complexity of human craniofacial development and molecular mechanism involved with this development. To understand the complex roles of ALX gene during human craniofacial development, it is necessary to have various model organisms to study.

In mouse, *Alx1* and *Alx3* are required for early head mesenchyme survival and neural tube closure (Lakhwani et al., 2010; Zhao et al., 1996) and *Alx3* and *Alx4* function redundantly for facial midline development (Beverdam et al., 2001; Qu et al., 1999) While these phenotypes are not fully consistent with those reported in human cases, these data show that the alx gene family may have overlapping functions during

craniofacial development. Likewise, we demonstrated that zebrafish *alx1* mutants exhibit low penetrant craniofacial defects, likely due to genetic compensation by other alx gene family members (Pini et al., 2020).

To investigate the genetic interactions among the alx gene family during craniofacial development, we remove the functions of other alx gene family members along with *alx1*. We identify that *alx1*; *alx4b* double mutants do not exhibit more penetrant craniofacial defects than *alx1* mutants (data not shown), consistent with previous qPCR data showing *alx4b* transcript was not upregulated in *alx1* mutants (Pini et al., 2020). We remove both *alx1* and *alx3* function, which significantly enhances the penetrance and expressivity of craniofacial defects resulting from depleted cartilage precursors for the ethmoid plates. This shows that *alx1* and *alx3* function redundantly during craniofacial development. For future studies, it is necessary to design triple knockout alx zebrafish model (*alx1; alx3; alx4a* mutants) or quadruple knockout alx zebrafish model (*alx1; alx3; alx4a; alx4b* mutants) to fully understand the genetic interactions among the alx gene family.

A previous report shows that *alx1* regulates aCNC migration to the median element of the anterior neurocranium (Pini et al., 2020). While some aCNC population successfully migrates to the median element of the anterior neurocranium in alx1 mutants (Pini et al., 2020), here we show that the aCNC population fails to migrate to the destination but ectopically spreads around the eyes in *alx1 -/-; alx3* CRISPants. This indicates that both *alx1* and *alx3* are necessary for correct aCNC migration and facial midline formation. Because *alx1* has been characterized for its requirement in collective cell migration *in vivo* and *in vitro* (Saunders and McClay, 2014; Wu and McClay, 2007; Yao et al., 2015; Yuan et al., 2013) and neural crest migrates collectively

(Szabo and Mayor, 2018; Szabo et al., 2016), it is plausible that the alx gene family is required for collective cell migration of aCNC lineages. Future studies are needed to directly address the cell migration pattern of alx-expressing aCNC during embryogenesis, potentially through high resolution live imaging of alx knock-in zebrafish.

Our *alx1* mutants are susceptible to ethanol toxicity and, as a result, develop with more penetrant and severe craniofacial defects. Prenatal ethanol exposure has been shown to cause the production of reactive oxygen species (ROS), which increases oxidative stress (Brocardo et al., 2011; Dong et al., 2010; Lovely et al., 2017). Subsequently, oxidative stress reduces the antioxidative defense genes in neural crest (Wentzel and Eriksson, 2011) and activates excessive apoptosis of neural crest (Wang et al., 2015), which, in both cases, threaten neural crest survival. We hypothesize that *alx1* protects ocular and craniofacial lineages against ethanol toxicity through regulating oxidative stress defense mechanism. Comparative transcriptomic analysis between ethanol exposed and unexposed *alx1* mutants to identify oxidative stress defense mechanism regulators, such as *foxo1* (Garcia-Sanz et al., 2017), would be an approach to test our hypothesis.

How does the alx gene family function during ocular development?

In humans, defective periocular neural crest development is associated with anterior segment dysgenesis (ASD), a congenital disorder that leads to visual impairment and blindness (Evans and Gage, 2005; Hendee et al., 2018; Portal et al.,

2019; Reis and Semina, 2011). ASD is very difficult to cure because periocular neural crest cells populated in anterior segment are highly heterogenous (Van Der Meulen et al., 2020) and the functional requirement of many guidance molecules for periocular neural crest, such as pax6 and TGF-beta from lens (Takamiya et al., 2020), is not fully understood.

While *ALX1* mutation is often linked with ocular diseases, such as microphthalmia, anophthalmia, and ocular coloboma, in humans (Pini et al., 2020; Uz et al., 2010), nothing is known about how the alx gene family functions during anterior segment or posterior segment, such as retina, development. In mouse, anterior segment development seems normal in the absence of *Alx1*, *Alx3*, or *Alx4* function. The only reported ocular phenotype is open eyelids characterized in *Alx1* or *Alx4* mutant mice (Curtain et al., 2015; Zhao et al., 1996). In mouse, it is possible that the alx gene family members functionally compensate for ocular development. To test this, it is necessary to rigorously examine the ocular morphology in Alx double mutant mice. While zebrafish *alx1* morphants have reduced differentiation of lens fibers and disorganized corneal layers (Dee et al., 2013), this phenotype has not been rigorously examined in *alx1* mutant embryos.

Here we show that *alx1* mutant embryos develop with mildly misshapen eyes but normal retina, and they develop with more pronounced anterior segment defects, such as iridial dysplasia, aphakia, iridial coloboma, and aberrant pupils, in adulthood. However, all these phenotypes show incomplete penetrance. This suggests that *alx1* function for anterior segment development is likely compensated by other members of the alx gene family. Indeed, *alx1; alx3* double mutants exhibit a fully penetrant misshapen eye phenotype, consistent with our hypothesis. While periocular neural

crest that gives rise to anterior segment is very robust to ethanol toxicity (Eason et al., 2017), the genetic mechanism of how periocular neural crest resists to ethanol toxicity is not known. The appearance of ASD phenotypes in adult *alx1* mutants leads us to hypothesize that alx gene function is required for protecting the periocular neural crest cell lineages against environmental perturbations. We identify that ethanol-treated *alx1* mutant develop with higher penetrant ocular defects in both embryonic and adult stages, supporting our hypothesis.

Alx1 mutants and *alx1; alx3* double mutants exhibit intraocular and/or periocular hemorrhaging at 3 dpf. In addition, embryos derived from *alx1; alx3/+* incross exhibited reduced and mispatterned hyaloid network formation at 5 dpf. These suggest a potential requirement of *alx1* and *alx3* function during hyaloid vasculature formation. Both *alx1* and *alx3* are expressed in periocular neural crest (Dee et al., 2013) and vascular pericytes derived from periocular neural crest (Gage et al., 2005; Trost et al., 2013) stabilize the hyaloid vasculature (Jo et al., 2013). Therefore, we hypothesize that *alx1* and *alx3* function in periocular neural crest differentiation to vascular pericytes. For future studies, using a vascular pericyte marker, such as *pdgfr-b* (Wang et al., 2014), in alx-knock in zebrafish to visualize the differentiation of alx-expressing neural crest to vascular pericytes would test this hypothesis.

While *alx1* mutants and *alx1; alx3* double mutants exhibit ocular defects, their retinal ganglion cell differentiation at 2 dpf is normal and their vision at 5 dpf seems normal. Larval zebrafish are able to detect and behaviorally respond to changes in luminescence in their visual field by 5 dpf (Burgess and Granato, 2007). In addition, electroretinogram recordings of larvae at this age have demonstrated retinal function, where light input is processed, in response to changes in illumination (Chrispell et al.,

2015; Miller et al., 2018). Here we show that *alx1* mutants, *alx1; alx3* double mutants, and *alx1; alx3* heterozygotes larvae show normal initiation of O-bends following sudden flashes of darkness, suggesting that they are able to detect variation in luminescence and have functioning vision at this stage. The growing evidence in the mouse model shows that an early onset anterior segment dysgenesis is associated with the postnatal death of retinal ganglion cells (Mao et al., 2011; Mao et al., 2017; Martino et al., 2016). Therefore, it is possible that *alx1* mutants and *alx1; alx3* double mutants have visual impairments when they reach to adulthood. This hypothesis is partially supported by the appearance of ocular defects in adult *alx1* mutants, but additional studies are needed to investigate if they are visually impaired.

In addition, while hyaloid vessels are known to supply oxygen for developing retina (Sun and Smith, 2018), early retinal development in zebrafish is not dependent upon gas exchange from hyaloid vessels until 6 dpf (Dhakal et al., 2015; Pelster and Burggren, 1996). Therefore, it is plausible that abnormal hyaloid vasculature formation in *alx1* mutants and *alx1; alx3* double mutants may not influence their RGC differentiation at 2 dpf and visual perceptions at 5 dpf. However, zebrafish *cloche* mutants, which lacks hyaloid vessels, exhibit abnormal retinal neurogenesis (Dhakal et al., 2015) and zebrafish hyaloid vasculature does not regress for retinal angiogenesis but instead remains within the retina for angiogenic remodeling (Alvarez et al., 2007). Therefore, improper hyaloid vasculature formation in *alx1* mutants and *alx1; alx3* double mutants may negatively affect retinal neurogenesis and angiogenesis, leading to retinal degeneration in adults.

How does this study inform our understanding of craniofacial complex defects?

Different from humans, mouse and zebrafish alx gene family members genetically compensate one another during craniofacial complex development. In mouse, a single mutation of *Alx1* or *Alx3* does not generate phenotypes similar to FND (Lakhwani et al., 2010; Zhao et al., 1996) but *Alx1; Alx4* double mutant or *Alx3; Alx4* double mutant develop with midline fusion defects (Beverdam et al., 2001; Qu et al., 1999). In addition, *Alx1* mutant (Zhao et al., 1996) or *Alx4* mutant mouse (Curtain et al., 2015) develop with open eyelid, which does not fully recapitulate the ocular defects in human *ALX1*-related FND or *ALX4*-related FND (Pini et al., 2020; Uz et al., 2010). In zebrafish, *alx1* morphants largely recapitulate the craniofacial and ocular defects in human *ALX1*-related FND (Dee et al., 2013) but *alx1* mutants exhibit very low penetrance of craniofacial defects, likely due to transcriptional upregulation of other alx gene family members (Pini et al., 2020). *Alx1; alx3* double mutant phenotypes replicate the phenotypes observed in *alx1* morphants (Dee et al., 2013) while *alx1; alx4b* double mutants do not (data not shown), reflecting the complexity of functional compensation mechanisms among the zebrafish alx gene family during craniofacial complex development.

Because aCNC heavily contributes to both craniofacial cartilage and anterior segment development, human craniofacial abnormalities are often linked with ocular defects resulting from defective neural crest migration and differentiation. Our data show that human *ALX1*-related FND is associated with ocular defects, such as coloboma, microphthalmia, and anophthalmia. On the other hand, we show that zebrafish *alx1* mutants and *alx1; alx3* double mutants develop with anterior segment

defects besides their craniofacial abnormalities. Through lineage tracing experiments, we identify that *alx1* (Pini et al., 2020) and *alx1* and *alx3* are necessary for correct aCNC migration. It is important to note that our zebrafish *alx1; alx3* double mutants exhibit comparable ocular and craniofacial phenotypes found in zebrafish *pitx2* mutant, a model reflecting Axenfeld-Rieger syndrome (Bohnsack et al., 2012; Hendee et al., 2018; Liu and Semina, 2012). Because *pitx2* is known to function in the anterior segment, it might be a potential target or regulator of the alx gene family.

Interestingly, both *alx1* mutants and *alx1; alx3* double mutants exhibit intraocular and/or periocular hemorrhaging, reminiscent of the phenotype shown in *zic2* mutants (Sedykh et al., 2017). This hemorrhaging phenotype has not been characterized in humans diagnosed with either *ALX1*-related FND or *ZIC2*-linked holoprosencephaly and any other zebrafish models up to date. While the cause of this hemorrhaging phenotype remains unknown, we speculate that it is due to underpopulated periocular neural crest derived vascular pericytes, which maintain the vascular integrity of hyaloid vasculature (Jo et al., 2013). Because both *Zic2* and *Alx1* are expressed in periocular neural crest (Ma and Lwigale, 2019) and zebrafish *zic2* promotes *alx1* transcription at periocular neural crest (Sedykh et al., 2017), it is plausible that *zic2* and *alx1* functions in periocular neural crest regulate the differentiation of vascular pericytes, which would be a novel regulatory mechanism of maintaining the vascular integrity to alleviate or cure human ocular diseases.

Our data demonstrate the first alx zebrafish model to study the gene-environment interaction during craniofacial complex development. While, in mouse, *alx3* was found to regulate oxidative stress through activating *foxo1*, which then promotes oxidative stress defense mechanism (Garcia-Sanz et al., 2017), alx-

environment interaction has not been tested in other animal models. We show that ethanol treated *alx1* mutants develop with more penetrant and pronounced craniofacial and ocular defects, suggesting that the alx gene family protects aCNC lineages against environmental assaults. Interestingly, the penetrance of ocular defects is much lower than the penetrance of craniofacial defects in ethanol treated *alx1* mutant embryos. This can be explained by the fact that each neural crest lineage reacts to oxidative stress in varying degrees. While cranial neural crest that gives rise to craniofacial cartilage is highly susceptible to oxidative stress, periocular neural crest that forms anterior segment is much less affected (Eason et al., 2017). This explains that individuals diagnosed with FAS are frequently associated with craniofacial abnormalities but rarely with ASD.

Together, our data identify a genetic and environmental interaction of alx gene family for aCNC lineage development and establish new disease models to understand the interconnection of several human craniofacial and ocular defects caused by genetic and/or environmental factors, including FND, ASD, and FAS. Besides of its role in craniofacial development, we show a novel role for alx gene family contributing to anterior segment development and protecting aCNC lineage against environmental perturbations. These models should be useful for further investigating an early requirement of alx gene family for collective migration of neural crest (Szabo and Mayor, 2018; Szabo et al., 2016) and for exploring the genetic pathways that alx gene family regulates during craniofacial complex development.

Acknowledgements

We are grateful to Daniel North for fish husbandry. We thank Mary Halloran for the gift of zn5 antibody. We also thank the University of Wisconsin Biotechnology Center DNA Sequencing facility for providing sequencing facilities and services and the Comparative Ocular Pathology Laboratory of Wisconsin (COPLOW) for adult zebrafish histology.

Reference

Alvarez, Y., Cederlund, M.L., Cottell, D.C., Bill, B.R., Ekker, S.C., Torres-Vazquez, J., Weinstein, B.M., Hyde, D.R., Vihtelic, T.S., Kennedy, B.N., 2007. Genetic determinants of hyaloid and retinal vasculature in zebrafish. BMC Dev Biol 7, 114.

Beverdam, A., Brouwer, A., Reijnen, M., Korving, J., Meijlink, F., 2001. Severe nasal clefting and abnormal embryonic apoptosis in Alx3/Alx4 double mutant mice. Development 128, 3975-3986.

Bohnsack, B.L., Kasprick, D.S., Kish, P.E., Goldman, D., Kahana, A., 2012. A zebrafish model of axenfeld-rieger syndrome reveals that pitx2 regulation by retinoic acid is essential for ocular and craniofacial development. Invest Ophthalmol Vis Sci 53, 7-22.

Brocardo, P.S., Gil-Mohapel, J., Christie, B.R., 2011. The role of oxidative stress in fetal alcohol spectrum disorders. Brain Res Rev 67, 209-225.

Burgess, H.A., Granato, M., 2007. Modulation of locomotor activity in larval zebrafish during light adaptation. J Exp Biol 210, 2526-2539.

Cavodeassi, F., Creuzet, S., Etchevers, H.C., 2019. The hedgehog pathway and ocular developmental anomalies. Hum Genet 138, 917-936.

Chrispell, J.D., Rebrik, T.I., Weiss, E.R., 2015. Electroretinogram analysis of the visual response in zebrafish larvae. J Vis Exp.

Curtain, M., Heffner, C.S., Maddox, D.M., Gudis, P., Donahue, L.R., Murray, S.A., 2015. A novel allele of Alx4 results in reduced Fgf10 expression and failure of eyelid fusion in mice. Mamm Genome 26, 173-180.

Cvekl, A., Tamm, E.R., 2004. Anterior eye development and ocular mesenchyme: new insights from mouse models and human diseases. Bioessays 26, 374-386.

de la Morena-Barrio, M.E., Ballesta-Martinez, M.J., Lopez-Galvez, R., Anton, A.I., Lopez-Gonzalez, V., Martinez-Ribot, L., Padilla, J., Minano, A., Garcia-Algar, O., Del Campo, M., Corral, J., Guillen-Navarro, E., Vicente, V., 2018. Genetic predisposition to fetal alcohol syndrome: association with congenital disorders of N-glycosylation. Pediatr Res 83, 119-127.

Dee, C.T., Szymoniuk, C.R., Mills, P.E., Takahashi, T., 2013. Defective neural crest migration revealed by a Zebrafish model of Alx1-related frontonasal dysplasia. Hum Mol Genet 22, 239-251.

Dhakal, S., Stevens, C.B., Sebbagh, M., Weiss, O., Frey, R.A., Adamson, S., Shelden, E.A., Inbal, A., Stenkamp, D.L., 2015. Abnormal retinal development in Cloche mutant zebrafish. Dev Dyn 244, 1439-1455.

Dhande, O.S., Huberman, A.D., 2014. Retinal ganglion cell maps in the brain:

implications for visual processing. Curr Opin Neurobiol 24, 133-142.

Dong, J., Sulik, K.K., Chen, S.Y., 2010. The role of NOX enzymes in ethanol-induced oxidative stress and apoptosis in mouse embryos. Toxicol Lett 193, 94-100.

Eason, J., Williams, A.L., Chawla, B., Apsey, C., Bohnsack, B.L., 2017. Differences in neural crest sensitivity to ethanol account for the infrequency of anterior segment defects in the eye compared with craniofacial anomalies in a zebrafish model of fetal alcohol syndrome. Birth Defects Res 109, 1212-1227.

Eberhart, J.K., Parnell, S.E., 2016. The Genetics of Fetal Alcohol Spectrum Disorders. Alcohol Clin Exp Res 40, 1154-1165.

Evans, A.L., Gage, P.J., 2005. Expression of the homeobox gene Pitx2 in neural crest is required for optic stalk and ocular anterior segment development. Hum Mol Genet 14, 3347-3359.

Farlie, P.G., Baker, N.L., Yap, P., Tan, T.Y., 2016. Frontonasal Dysplasia: Towards an Understanding of Molecular and Developmental Aetiology. Mol Syndromol 7, 312-321.

Forsthoefel, P.F., 1963. The Embryological Development of the Effects of Strong's Luxoid Gene in the Mouse. J Morphol 113, 427-451.

Gage, P.J., Rhoades, W., Prucka, S.K., Hjalt, T., 2005. Fate maps of neural crest and mesoderm in the mammalian eye. Invest Ophthalmol Vis Sci 46, 4200-4208.

Garcia-Sanz, P., Mirasierra, M., Moratalla, R., Vallejo, M., 2017. Embryonic defence mechanisms against glucose-dependent oxidative stress require enhanced expression of Alx3 to prevent malformations during diabetic pregnancy. Sci Rep 7, 389.

Gestri, G., Link, B.A., Neuhauss, S.C., 2012. The visual system of zebrafish and its use to model human ocular diseases. Dev Neurobiol 72, 302-327.

Gillhouse, M., Wagner Nyholm, M., Hikasa, H., Sokol, S.Y., Grinblat, Y., 2004. Two Frodo/Dapper homologs are expressed in the developing brain and mesoderm of zebrafish. Dev Dyn 230, 403-409.

Goehlert, U.G., Ng Ying Kin, N.M., Wolfe, L.S., 1981. Biosynthesis of prostacyclin in rat cerebral microvessels and the choroid plexus. J Neurochem 36, 1192-1201.

Hartsock, A., Lee, C., Arnold, V., Gross, J.M., 2014. In vivo analysis of hyaloid vasculature morphogenesis in zebrafish: A role for the lens in maturation and maintenance of the hyaloid. Dev Biol 394, 327-339.

Hendee, K.E., Sorokina, E.A., Muheisen, S.S., Reis, L.M., Tyler, R.C., Markovic, V., Cuturilo, G., Link, B.A., Semina, E.V., 2018. PITX2 deficiency and associated human disease: insights from the zebrafish model. Hum Mol Genet 27, 1675-1695.

Jo, D.H., Kim, J.H., Heo, J.I., Kim, J.H., Cho, C.H., 2013. Interaction between pericytes and endothelial cells leads to formation of tight junction in hyaloid vessels. Mol Cells

36, 465-471.

Kague, E., Gallagher, M., Burke, S., Parsons, M., Franz-Odendaal, T., Fisher, S., 2012. Skeletogenic fate of zebrafish cranial and trunk neural crest. PLoS One 7, e47394.

Kaminen-Ahola, N., 2020. Fetal alcohol spectrum disorders: Genetic and epigenetic mechanisms. Prenat Diagn.

Kimmel, C.B., Ballard, W.W., Kimmel, S.R., Ullmann, B., Schilling, T.F., 1995. Stages of embryonic development of the zebrafish. Dev Dyn 203, 253-310.

Kimmel, C.B., Miller, C.T., Kruze, G., Ullmann, B., BreMiller, R.A., Larison, K.D., Snyder, H.C., 1998. The shaping of pharyngeal cartilages during early development of the zebrafish. Dev Biol 203, 245-263.

Kish, P.E., Bohnsack, B.L., Gallina, D., Kasprick, D.S., Kahana, A., 2011. The eye as an organizer of craniofacial development. Genesis 49, 222-230.

Kuratani, S., 2018. The neural crest and origin of the neurocranium in vertebrates. Genesis 56, e23213.

Lakhwani, S., Garcia-Sanz, P., Vallejo, M., 2010. Alx3-deficient mice exhibit folic acid-resistant craniofacial midline and neural tube closure defects. Dev Biol 344, 869-880.

Lee, J., Willer, J.R., Willer, G.B., Smith, K., Gregg, R.G., Gross, J.M., 2008. Zebrafish blowout provides genetic evidence for Patched1-mediated negative regulation of Hedgehog signaling within the proximal optic vesicle of the vertebrate eye. Dev Biol 319, 10-22.

Lessell, S., Kuwabara, T., 1964. Phosphatase Histochemistry of the Eye. Arch Ophthalmol 71, 851-860.

Liu, Y., Semina, E.V., 2012. pitx2 Deficiency results in abnormal ocular and craniofacial development in zebrafish. PLoS One 7, e30896.

Lovely, C., Rampersad, M., Fernandes, Y., Eberhart, J., 2017. Gene-environment interactions in development and disease. Wiley Interdiscip Rev Dev Biol 6.

Lyons, L.A., Erdman, C.A., Grahn, R.A., Hamilton, M.J., Carter, M.J., Helps, C.R., Alhaddad, H., Gandolfi, B., 2016. Aristaless-Like Homeobox protein 1 (ALX1) variant associated with craniofacial structure and frontonasal dysplasia in Burmese cats. Dev Biol 409, 451-458.

Ma, J., Lwigale, P., 2019. Transformation of the Transcriptomic Profile of Mouse Periocular Mesenchyme During Formation of the Embryonic Cornea. Invest Ophthalmol Vis Sci 60, 661-676.

Mao, M., Hedberg-Buenz, A., Koehn, D., John, S.W., Anderson, M.G., 2011. Anterior segment dysgenesis and early-onset glaucoma in nee mice with mutation of Sh3pxd2b. Invest Ophthalmol Vis Sci 52, 2679-2688.

Mao, M., Kiss, M., Ou, Y., Gould, D.B., 2017. Genetic dissection of anterior segment dysgenesis caused by a Col4a1 mutation in mouse. Dis Model Mech 10, 475-485.

Martino, V.B., Sabljic, T., Deschamps, P., Green, R.M., Akula, M., Peacock, E., Ball, A., Williams, T., West-Mays, J.A., 2016. Conditional deletion of AP-2beta in mouse cranial neural crest results in anterior segment dysgenesis and early-onset glaucoma. Dis Model Mech 9, 849-861.

McGonnell, I.M., Graham, A., Richardson, J., Fish, J.L., Depew, M.J., Dee, C.T., Holland, P.W., Takahashi, T., 2011. Evolution of the Alx homeobox gene family: parallel retention and independent loss of the vertebrate Alx3 gene. Evol Dev 13, 343-351.

Miller, A.H., Howe, H.B., Krause, B.M., Friedle, S.A., Banks, M.I., Perkins, B.D., Wolman, M.A., 2018. Pregnancy-Associated Plasma Protein-aa Regulates Photoreceptor Synaptic Development to Mediate Visually Guided Behavior. J Neurosci 38, 5220-5236.

Paffett-Lugassy, N.N., Zon, L.I., 2005. Analysis of hematopoietic development in the zebrafish. Methods Mol Med 105, 171-198.

Pelster, B., Burggren, W.W., 1996. Disruption of hemoglobin oxygen transport does not impact oxygen-dependent physiological processes in developing embryos of zebra fish (Danio rerio). Circ Res 79, 358-362.

Pini, J., Kueper, J., Hu, Y.D., Kawasaki, K., Yeung, P., Tsimbal, C., Yoon, B., Carmichael, N., Maas, R.L., Cotney, J., Grinblat, Y., Liao, E.C., 2020. ALX1-related frontonasal dysplasia results from defective neural crest cell development and migration. EMBO Mol Med, e12013.

Portal, C., Rompolas, P., Lwigale, P., Iomini, C., 2019. Primary cilia deficiency in neural crest cells models anterior segment dysgenesis in mouse. Elife 8.

Qu, S., Tucker, S.C., Zhao, Q., deCrombrugghe, B., Wisdom, R., 1999. Physical and genetic interactions between Alx4 and Cart1. Development 126, 359-369.

Reis, L.M., Semina, E.V., 2011. Genetics of anterior segment dysgenesis disorders. Curr Opin Ophthalmol 22, 314-324.

Sakai, D., Dixon, J., Achilleos, A., Dixon, M., Trainor, P.A., 2016. Prevention of Treacher Collins syndrome craniofacial anomalies in mouse models via maternal antioxidant supplementation. Nat Commun 7, 10328.

Saunders, L.R., McClay, D.R., 2014. Sub-circuits of a gene regulatory network control a developmental epithelial-mesenchymal transition. Development 141, 1503-1513.

Sedykh, I., Yoon, B., Roberson, L., Moskvin, O., Dewey, C.N., Grinblat, Y., 2017. Zebrafish zic2 controls formation of periocular neural crest and choroid fissure morphogenesis. Dev Biol 429, 92-104.

Serbedzija, G.N., Bronner-Fraser, M., Fraser, S.E., 1992. Vital dye analysis of cranial neural crest cell migration in the mouse embryo. Development 116, 297-307.

Sun, Y., Smith, L.E.H., 2018. Retinal Vasculature in Development and Diseases. Annu Rev Vis Sci 4, 101-122.

Szabo, A., Mayor, R., 2018. Mechanisms of Neural Crest Migration. Annu Rev Genet 52, 43-63.

Szabo, A., Melchionda, M., Nastasi, G., Woods, M.L., Campo, S., Perris, R., Mayor, R., 2016. In vivo confinement promotes collective migration of neural crest cells. J Cell Biol 213, 543-555.

Takamiya, M., Stegmaier, J., Kobitski, A.Y., Schott, B., Weger, B.D., Margariti, D., Cereceda Delgado, A.R., Gourain, V., Scherr, T., Yang, L., Sorge, S., Otte, J.C., Hartmann, V., van Wezel, J., Stotzka, R., Reinhard, T., Schlunck, G., Dickmeis, T., Rastegar, S., Mikut, R., Nienhaus, G.U., Strahle, U., 2020. Pax6 organizes the anterior eye segment by guiding two distinct neural crest waves. PLoS Genet 16, e1008774.

ten Berge, D., Brouwer, A., el Bahi, S., Guenet, J.L., Robert, B., Meijlink, F., 1998. Mouse Alx3: an aristaless-like homeobox gene expressed during embryogenesis in ectomesenchyme and lateral plate mesoderm. Dev Biol 199, 11-25.

Trost, A., Schroedl, F., Lange, S., Rivera, F.J., Tempfer, H., Korntner, S., Stolt, C.C., Wegner, M., Bogner, B., Kaser-Eichberger, A., Krefft, K., Runge, C., Aigner, L., Reitsamer, H.A., 2013. Neural crest origin of retinal and choroidal pericytes. Invest Ophthalmol Vis Sci 54, 7910-7921.

Uz, E., Alanay, Y., Aktas, D., Vargel, I., Gucer, S., Tuncbilek, G., von Eggeling, F., Yilmaz, E., Deren, O., Posorski, N., Ozdag, H., Liehr, T., Balci, S., Alikasifoglu, M., Wollnik, B., Akarsu, N.A., 2010. Disruption of ALX1 causes extreme microphthalmia and severe facial clefting: expanding the spectrum of autosomal-recessive ALX-related frontonasal dysplasia. Am J Hum Genet 86, 789-796.

Vaccaro, A., Patten, S.A., Ciura, S., Maios, C., Therrien, M., Drapeau, P., Kabashi, E., Parker, J.A., 2012. Methylene blue protects against TDP-43 and FUS neuronal toxicity in C. elegans and D. rerio. PLoS One 7, e42117.

Van Der Meulen, K.L., Vocking, O., Weaver, M.L., Meshram, N.N., Famulski, J.K., 2020. Spatiotemporal Characterization of Anterior Segment Mesenchyme Heterogeneity During Zebrafish Ocular Anterior Segment Development. Front Cell Dev Biol 8, 379.

Vorontsova, I., Hall, J.E., Schilling, T.F., 2019. Assessment of Zebrafish Lens Nucleus Localization and Sutural Integrity. J Vis Exp.

Wada, N., Javidan, Y., Nelson, S., Carney, T.J., Kelsh, R.N., Schilling, T.F., 2005. Hedgehog signaling is required for cranial neural crest morphogenesis and

chondrogenesis at the midline in the zebrafish skull. Development 132, 3977-3988.

Wang, X.Y., Li, S., Wang, G., Ma, Z.L., Chuai, M., Cao, L., Yang, X., 2015. High glucose environment inhibits cranial neural crest survival by activating excessive autophagy in the chick embryo. Sci Rep 5, 18321.

Wang, Y., Pan, L., Moens, C.B., Appel, B., 2014. Notch3 establishes brain vascular integrity by regulating pericyte number. Development 141, 307-317.

Wentzel, P., Eriksson, U.J., 2011. Altered gene expression in rat cranial neural crest cells exposed to a teratogenic glucose concentration in vitro: paradoxical downregulation of antioxidative defense genes. Birth Defects Res B Dev Reprod Toxicol 92, 487-497.

Westerfield, M., 1993. The zebrafish book : a guide for the laboratory use of zebrafish (Brachydanio rerio). M. Westerfield, Eugene, OR.

Williams, A.L., Bohnsack, B.L., 2015. Neural crest derivatives in ocular development: discerning the eye of the storm. Birth Defects Res C Embryo Today 105, 87-95.

Wolman, M.A., Jain, R.A., Liss, L., Granato, M., 2011. Chemical modulation of memory formation in larval zebrafish. Proc Natl Acad Sci U S A 108, 15468-15473.

Wolman, M.A., Jain, R.A., Marsden, K.C., Bell, H., Skinner, J., Hayer, K.E., Hogenesch, J.B., Granato, M., 2015. A genome-wide screen identifies PAPP-AA-mediated IGFR signaling as a novel regulator of habituation learning. Neuron 85, 1200-1211.

Wu, R.S., Lam, II, Clay, H., Duong, D.N., Deo, R.C., Coughlin, S.R., 2018. A Rapid Method for Directed Gene Knockout for Screening in G0 Zebrafish. Dev Cell 46, 112-125 e114.

Wu, S.Y., McClay, D.R., 2007. The Snail repressor is required for PMC ingression in the sea urchin embryo. Development 134, 1061-1070.

Xiang, Q., Xu, B., Ding, Y., Liu, X., Zhou, Y., Ahmad, F., 2018. Oxidative Stress Response Induced by Butachlor in Zebrafish Embryo/Larvae: The Protective Effect of Vitamin C. Bull Environ Contam Toxicol 100, 208-215.

Yan, Y.L., Hatta, K., Riggleman, B., Postlethwait, J.H., 1995. Expression of a type II collagen gene in the zebrafish embryonic axis. Dev Dyn 203, 363-376.

Yao, W., Liu, Y., Zhang, Z., Li, G., Xu, X., Zou, K., Xu, Y., Zou, L., 2015. ALX1 promotes migration and invasion of lung cancer cells through increasing snail expression. Int J Clin Exp Pathol 8, 12129-12139.

Yuan, H., Kajiyama, H., Ito, S., Yoshikawa, N., Hyodo, T., Asano, E., Hasegawa, H., Maeda, M., Shibata, K., Hamaguchi, M., Kikkawa, F., Senga, T., 2013. ALX1 induces snail expression to promote epithelial-to-mesenchymal transition and invasion of ovarian cancer cells. Cancer Res 73, 1581-1590.

Zhao, Q., Behringer, R.R., de Crombrugghe, B., 1996. Prenatal folic acid treatment suppresses acrania and meroanencephaly in mice mutant for the Cart1 homeobox gene. Nat Genet 13, 275-283.

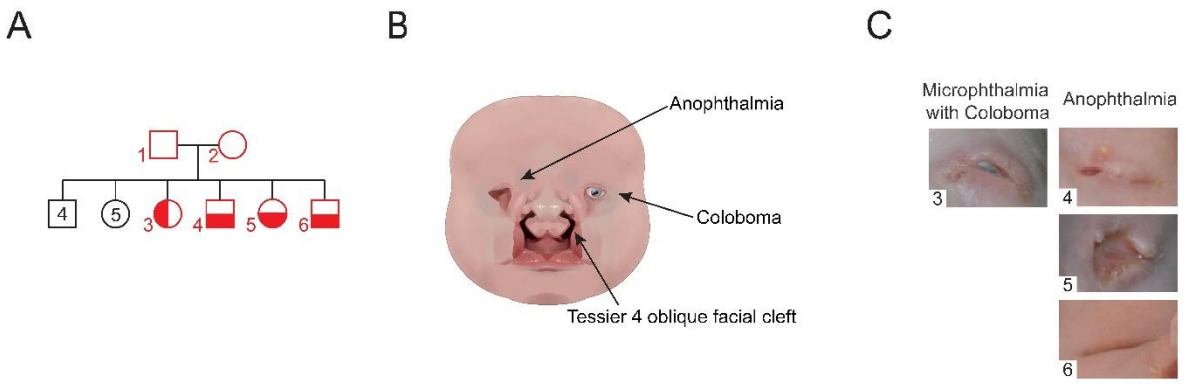

Figure 1. *Severe ocular malformations are associated with ALX1^{L165F} homozygosity.*

A: Consanguineous parents produced 13 children, 4 have complex frontonasal dysplasia (FND), subject numbers noted in red. Unaffected individuals do not have any eye or facial phenotypes suggestive of FND. B: Diagram summarizing the anophthalmia, coloboma and bilateral Tessier oblique facial clefts (ObFC). C: Human subjects displayed various severities of ocular malformation, ranging from microphthalmia with coloboma to anophthalmia. The eldest sibling (subject 3) with FND presented with right coloboma, left micro-ophthalmia and bilateral Tessier 4 oblique facial clefts (ObFC). The next child (subject 4) presented with bilateral anophthalmia with fused eyelids and shallow orbits, with bilateral ObFC. Subject 5 presented with bilateral anophthalmia with open shallow orbits and the upper and lower eyelids are absent, exposing the orbital mucosa, with bilateral ObFC. The nasal ala is also malformed with nodular skin tags. Subject 6 has bilateral anophthalmia, fused eyelids, shallow orbit and bilateral ObFC, similar to subject 4.

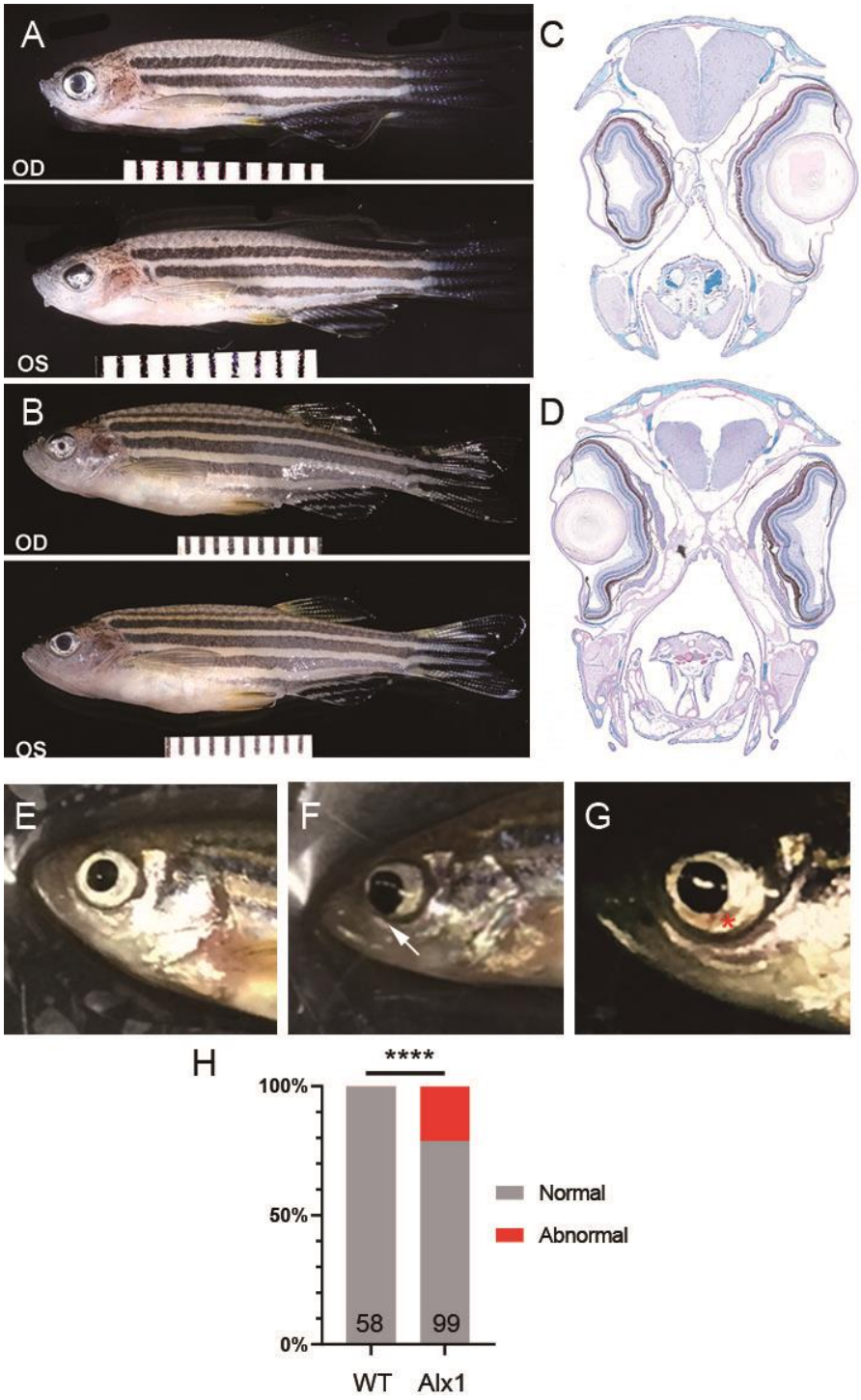

Figure 2. *Adult zebrafish alx1 mutants develop with ocular defects.*

A-B. Adult *alx1* mutant fish in each side of the eye (OD: *oculus dexter,* right eye, OS: *oculus sinister*, left eye) C: Transverse section of fish (A) with reduced pupil shows a normal right eye and aphakia (absent lens), displaced vitreous, and retinal

inflammation of the left eye. D: Transverse section of fish (B) shows a normal left eye and aphakia (absent lens), absent pupil, and iridal dysplasia in the right eye (1 trial). E: Majority of adult *alx1* mutants develop normally. F: Adult *alx1* mutants develop with coloboma (arrow, n = 2/99). G: Adult *alx1* mutants develop with hemorrhage (asterisk, n = 1/99) H: Several ocular defects, including abnormal pupil (n = 17/99), coloboma (n= 2/99), opaque lens (n= 1/99), and ocular hemorrhage (n= 1/99), appears in adult *alx1* mutant fish (****: $p < 0.0001$ using Fisher's exact test) (1 WT fish tank, 3 *alx1* mutant fish tanks combined) All fish are shown in lateral views, anterior to the left.

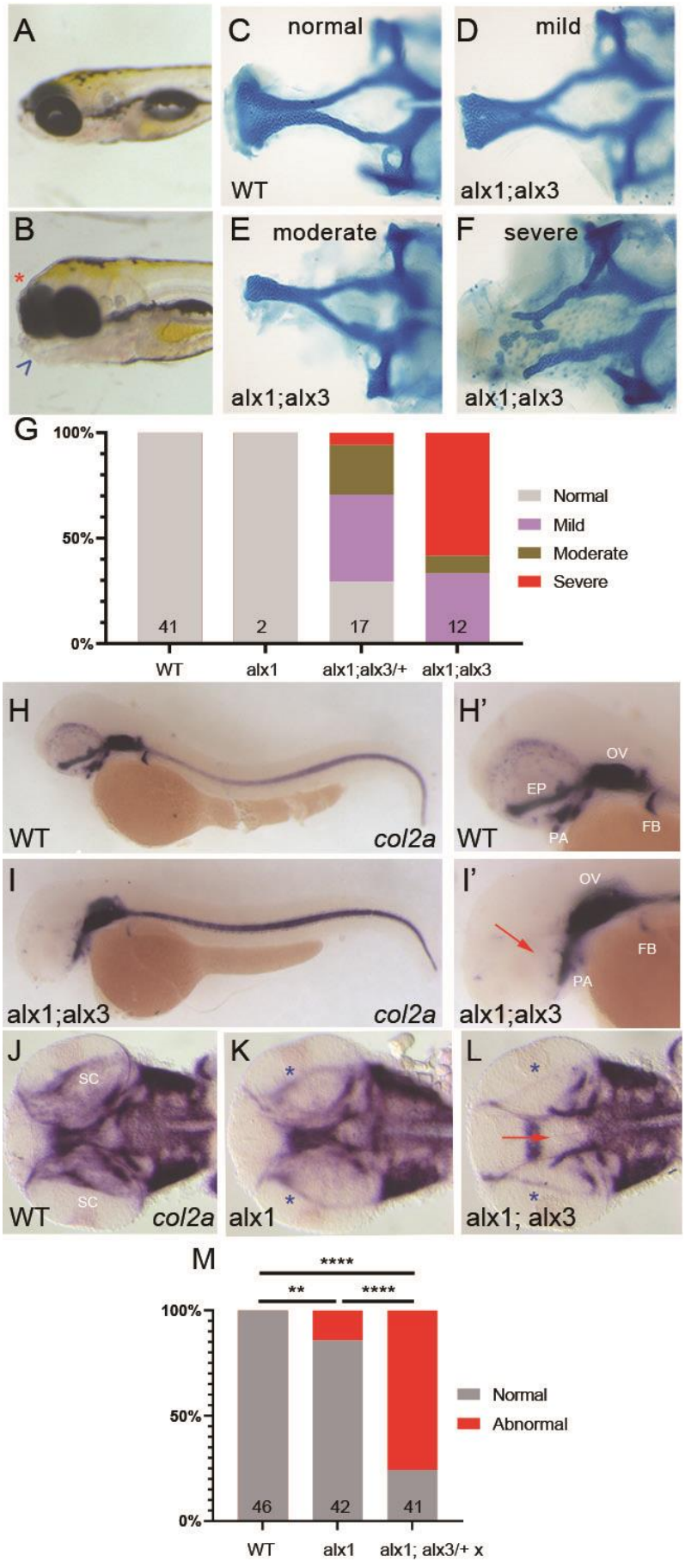
A
B
C normal
WT
D mild
alx1;alx3
E moderate
alx1;alx3
F severe
alx1;alx3
G
100%
50%
0%
41
2
17
12
WT
alx1
alx1;alx3/+
alx1;alx3
Normal
Mild
Moderate
Severe
H
WT
col2a
H'
WT
OV
EP
PA
FB
I
alx1;alx3
col2a
I'
alx1;alx3
OV
FB
PA
J
SC
WT
col2a
K
alx1
L
alx1; alx3
M
****
**
****
100%
50%
0%
46
42
41
WT
alx1
alx1; alx3/+ x
Normal
Abnormal

Figure 3. *Zebrafish alx1 and alx3 are required to control ethmoid plate formation.*

Embryos derived from *alx1; alx3/+* incross were fixed at 5 dpf for alcian blue staining (A-G) and embryos derived from WT, *alx1, alx1; alx3/+* were stained for *col2a1a* expression by WISH at 2 dpf. (H-M). A: Normal facial structure in wildtype embryos at 6 dpf. B: *Alx1; alx3* double mutants develop with shortened neurocranium (asterisk) and abnormal jaw cartilage (arrowhead) by 6 dpf. C - F: Alcian blue staining reveals mutant ethmoid plate (EP) morphologies that range from mildly (D) or moderately (E) reduced, to severely hypoplastic (F). G: Penetrance and severity of cartilage defects increase in *alx1; alx3* double mutants (2 trials). H, H'': Normal *col2a1a* expression in WT embryos. I, I': *alx1; alx3* double mutants develop with truncated ethmoid plates (arrow). J: Normal *col2a1a* expression in WT embryos. K: *Alx1* mutants develop with normal ethmoid plates but thinner sclera (asterisk). L: *Alx1; alx3* double mutants develop with abnormal ethmoid plate (arrow) and putative scleral precursors (asterisk) formation. Abbreviation: EP = ethmoid plates, OV = optic vesicle, PA = pharyngeal arches, FB= fin bud, SC= sclera. M: 75% of the embryos derived from *alx1; alx3/+* have aberrant EP and reduced cartilage precursors for sclera (**: $p = 0.0097$, ****: $p < 0.0001$ using Fisher's exact test) (2 separate trials for WT and *alx1; alx3*/+ incross and 1 trial for *alx1* incross). Embryos in A, B, H- I' are shown in lateral views, anterior to the left. Embryos in J - L are shown in ventral views, anterior to the left.

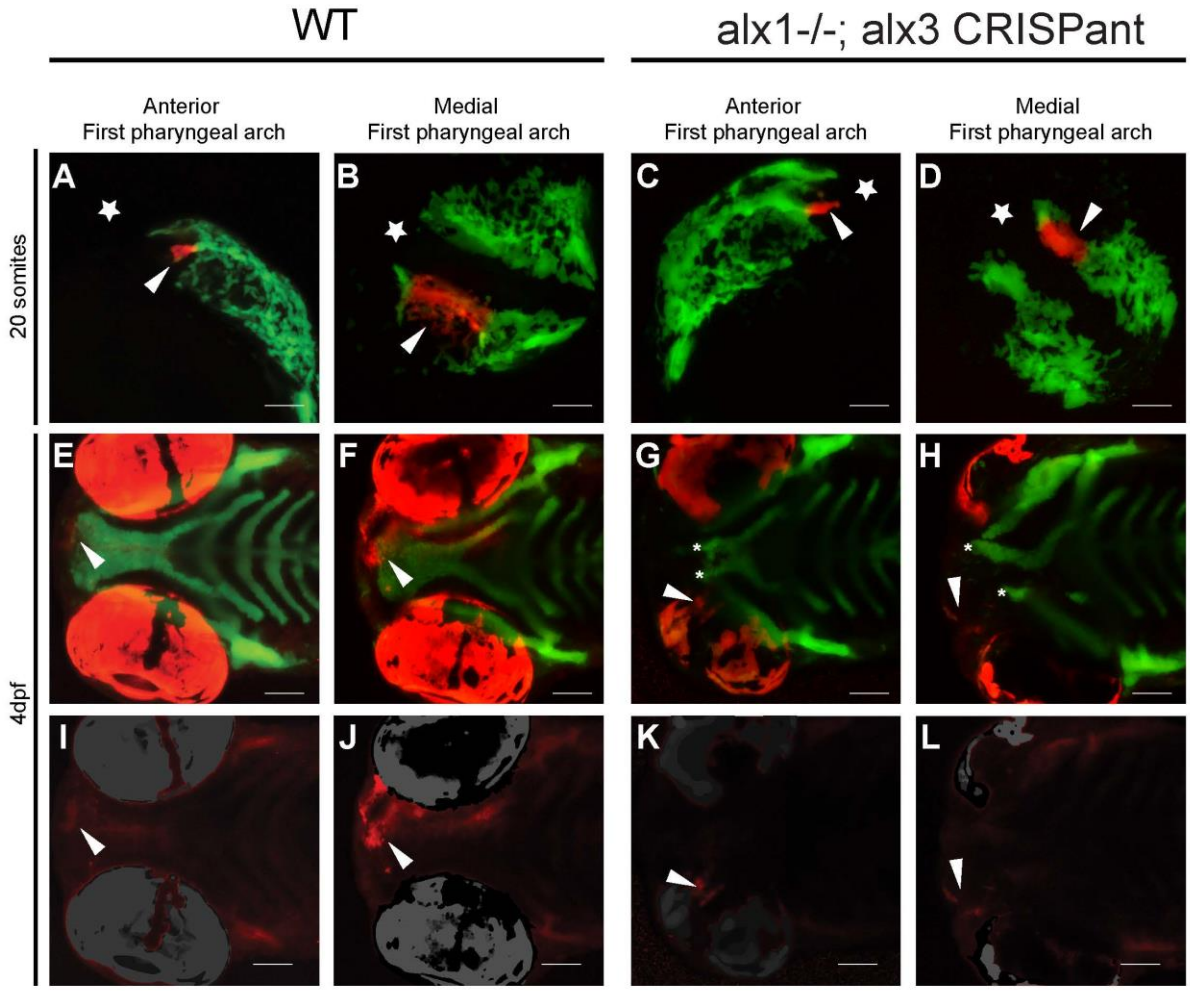

Figure 4. Zebrafish *alx1* and *alx3* are for correct migration of anterior cranial neural crest

Fate map of aCNC at the 20-somite stage (A-D, star sign marks the anterior) to the anterior neurocranium at 4 days post fertilization (E-H; I-L show red channel only with eye mask; anterior to the left) shows that aCNC labeled by kaede photoconversion (red cells, arrowheads in A,B and I,J) always contribute to the median element of the ethmoid plates (arrowheads in E,F) at 4dpf in WT. *Alx1 -/-; alx3* CRISPants exhibit a midline cleft (G,H) with the lateral elements (asterisks) separated as the median element is missing. In *alx1 -/-; alx3* CRISPants, aCNC fails to reach its destination and

ectopically populates near the eye (arrowheads in G,H and K,L). Note that the red color of the eye is due to autofluorescence from iridophores and not kaede photoconversion (E-H). Scale bar: 100μm.

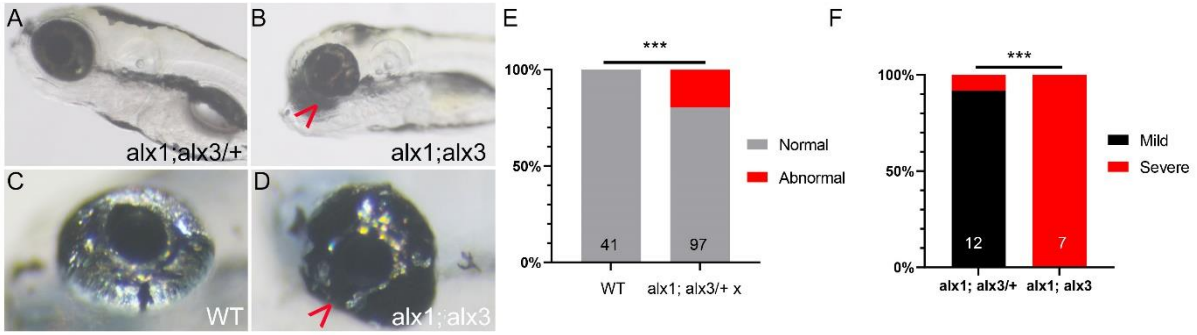

Figure 5. Zebrafish *alx1* and *alx3* are required for ocular morphogenesis

A-D: Larvae generated from *alx1;alx3/+* incross were scored at 5 dpf for ocular defects. Compared to normal siblings (A,C), *alx1; alx3* double mutants develop misshapen eyes (B,D, arrowhead). E: Misshapen eye phenotype is specific to the embryos derived from *alx1; alx3/+* incross (***: p = 0.0009 using Fisher's exact test) (2 trials). F: Genotypic analysis shows that the misshapen eye phenotype is linked with either *alx1; alx3* heterozygotes or *alx1; alx3* double mutants. Severity of the misshapen eye significantly increases in *alx1; alx3* double mutants (***: p = 0.0002 using Fisher's exact test) (2 trials). All embryos are shown in lateral views, anterior to the left.

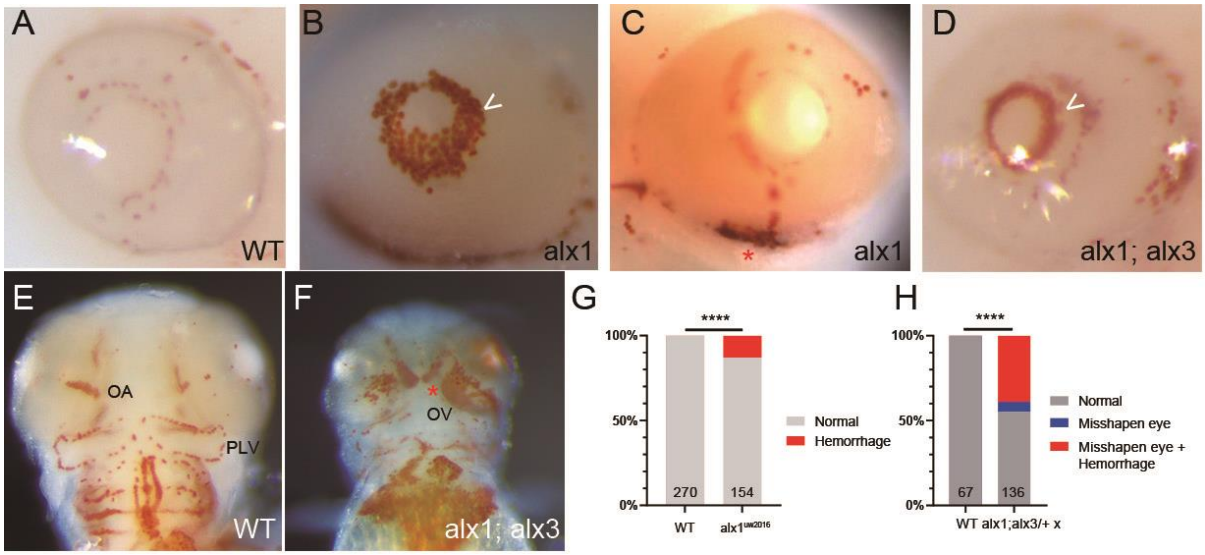

Figure 6. *alx1* and *alx3* are required for vascular integrity.

Embryos derived from WT or *alx1; alx3/+* incross were stained for red blood cells using o-dianisidine staining A: Normal retina morphology. B: *Alx1* mutants develop with ocular hemorrhage (arrowhead). C: *Alx1* mutants develop with periocular hemorrhage (asterisk). D: *Alx1; alx3* double mutants develop with ocular hemorrhage (arrowhead). E: Normal blood vessel patterning in WT. F: In *alx1; alx3* embryos, severe blood leakage occurs periocularly (asterisk) near the optic artery and optic vein and intraocularly. In addition, blood vessels surrounding the pharyngeal arch are not correctly formed. G: Hemorrhage phenotype is specific to *alx1* mutants (****: $p < 0.0001$, ns: $p = 0.3710$ using Fisher's exact test; 5 trials). H: Hemorrhage phenotype is specific to *alx1; alx3* heterozygotes or *alx1; alx3* double mutants developed with misshapen eye (****: $p < 0.0001$ using Chi-square test; 2 trials) and is more penetrant than *alx1* mutants (G). Embryos in A-D are shown in lateral views, anterior to the left. Embryos in E and F are shown in ventral views, anterior to the top. Abbreviation: OA = Optic artery, OV = Optic vein, PLV = Palatocerebral vein

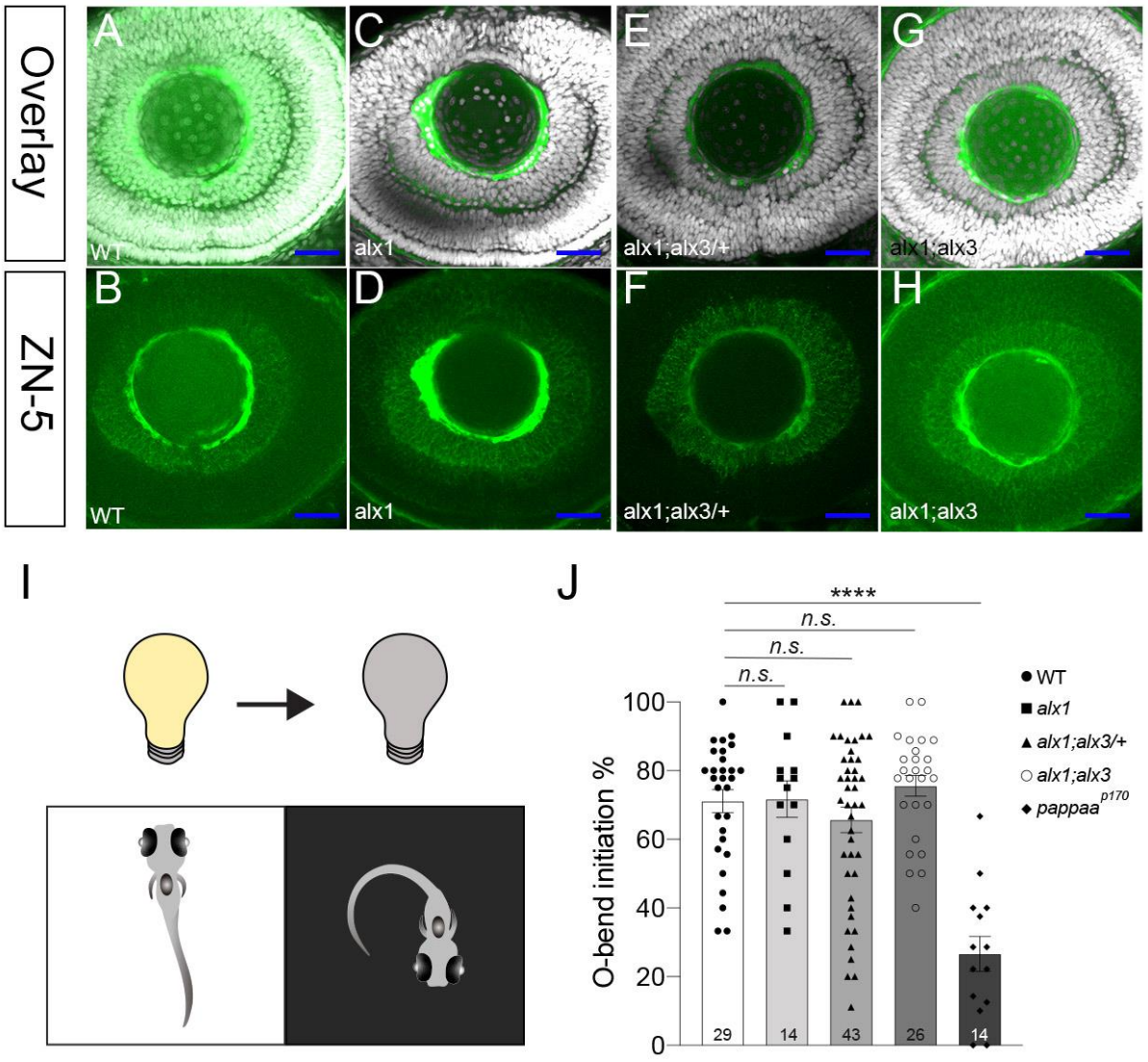

Figure 7. *alx1 mutants and alx1; alx3 double mutants have normal retinal development.*

Embryos derived from *WT* or *alx1; alx3/+* parents were stained with zn5, a differentiated retinal ganglion cell marker, using immunohistochemistry at 2 dpf (A-H). Normal differentiated RGC expression in WT (A,B; 4 embryos), *alx1* mutants (C,D; 2 embryos), *alx1; alx3* heterozygotes (E,F; 4 embryos), and *alx1; alx3* double mutants (G,H; 2 embryos). Left eyes of embryos were taken. All embryos are shown in lateral views, anterior to the left. Scale bar = 25μm. I: The dark flash stimulus elicits O-bend turn responses in 5 dpf larval zebrafish. J: Mean frequency of O-bend initiations to a

series of 10 dark flash stimuli (n.s.: $p > 0.9999$ vs WT control. ****: $p < 0.0001$ vs WT control. ANOVA with Kruskal-Wallis. Error bars indicate SEM.)

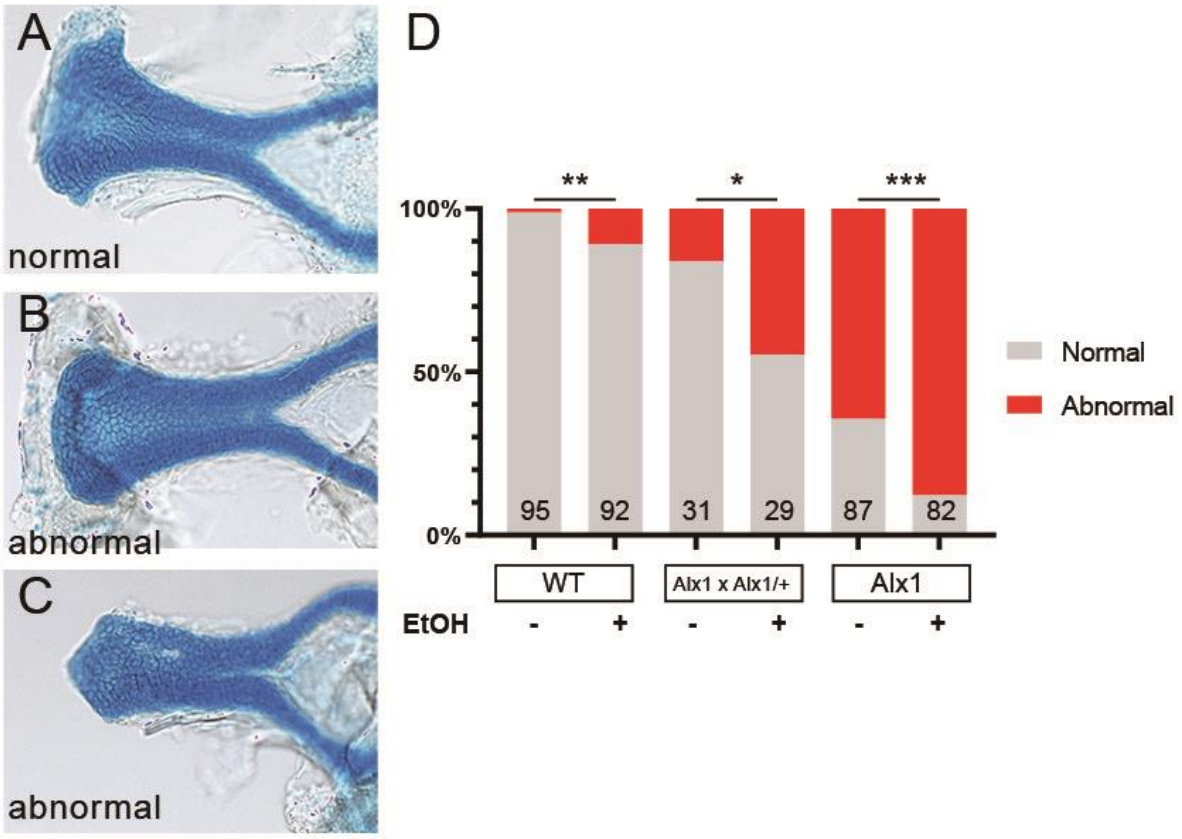

Figure 8. *Zebrafish alx1 protects facial lineages against ethanol toxicity.*

Embryos derived from WT incross, from a cross between *alx1* homozygotes and *alx1* heterozygotes (*alx1 x alx1/+*), or from *alx1* mutant incross were treated with ethanol and stained with alcian blue (A-C). A: Normal ethmoid plates. B, C: *alx1* mutants develop with mild ethmoid plate reduction (B) or “stick” palate (C). D: Penetrance of craniofacial defects is increased by transient exposure to ethanol in embryos derived from WT incross (**: p = 0.0045), *alx1 x alx1/+* cross (*: p = 0.0237), and *alx1* mutant incross (***: p = 0.0005). Fisher’s exact test was used to measure the statistical significance (3 trials for WT and 2 trials for *alx1 x alx1/+* and alx1 mutant).

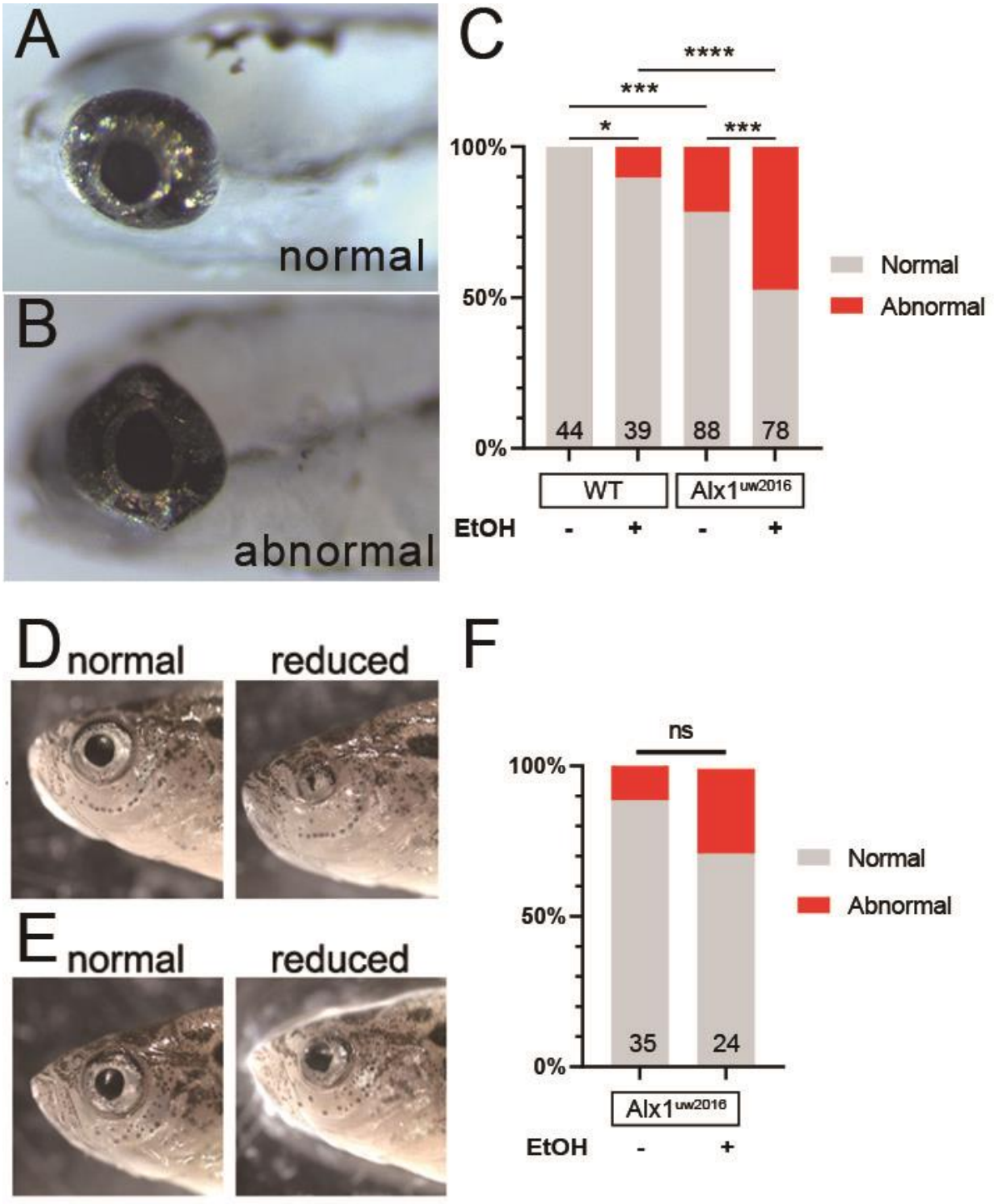

Figure 9. *Zebrafish alx1 protects ocular lineages against ethanol toxicity.*

A-C: Embryos derived from WT or *alx1* mutant incross were treated with 0.5% ethanol and scored for ocular defects at 5 dpf. A: Normal ocular morphology. B: Abnormal ocular morphology. C: Penetrance of abnormal ocular phenotype is increased by

transient exposure to EtOH in both WT (*: p = 0.0448) and *alx1* mutants (***: p = 0.0005). In addition, compared to WT, abnormal ocular phenotype is more penetrant in *alx1* mutants without EtOH (***: p = 0.0003) and with EtOH treatment (****: p < 0.0001). Fisher's exact test was used to measure the statistical significance (1 trial for WT and 2 trials for *alx1* mutants). D-F: Embryos derived from *alx1* mutant incross were treated with 0.5% ethanol and raised for 2 months to score for ocular defects. EtOH treated *alx1* mutant fish develop with microphthalmia (D) and coloboma (E). F: Penetrance of ocular phenotypes increases following embryonic exposure to alcohol but is not statistically significant (n.s.: p= 0.1022 using Fisher's exact test) (1 trial). All embryos and fish are shown in lateral views, anterior to the left.

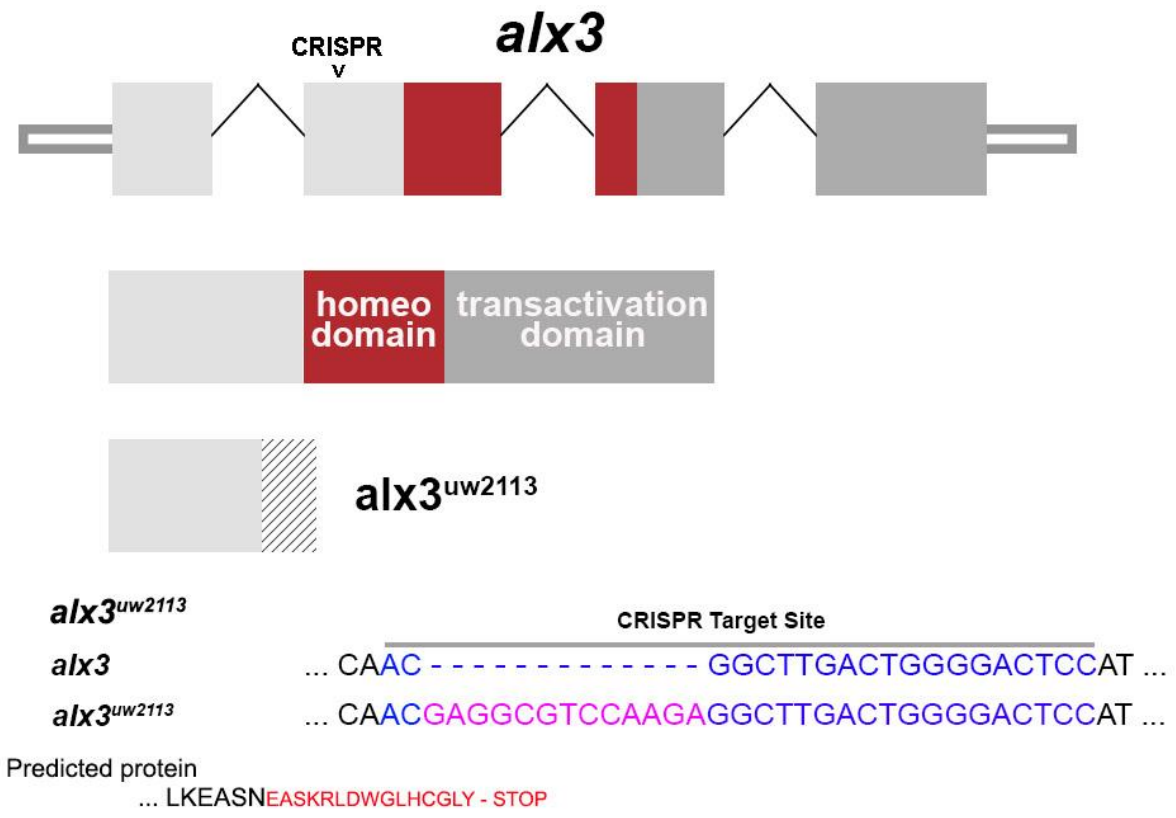

Supplementary Figure 1. *Generation of mutant alleles at the zebrafish alx3 locus*

Alx3 allele consists of 4 exons with homeobox (red) and transactivation (grey) domain. *Alx3* mutant allele was induced by CRISPR/Cas9 mutagenesis in the second exon. *Alx3*^{uw2113} allele has a net insertion of 13 nt. Red letters indicate abnormal sequence resulted from frameshift mutation.

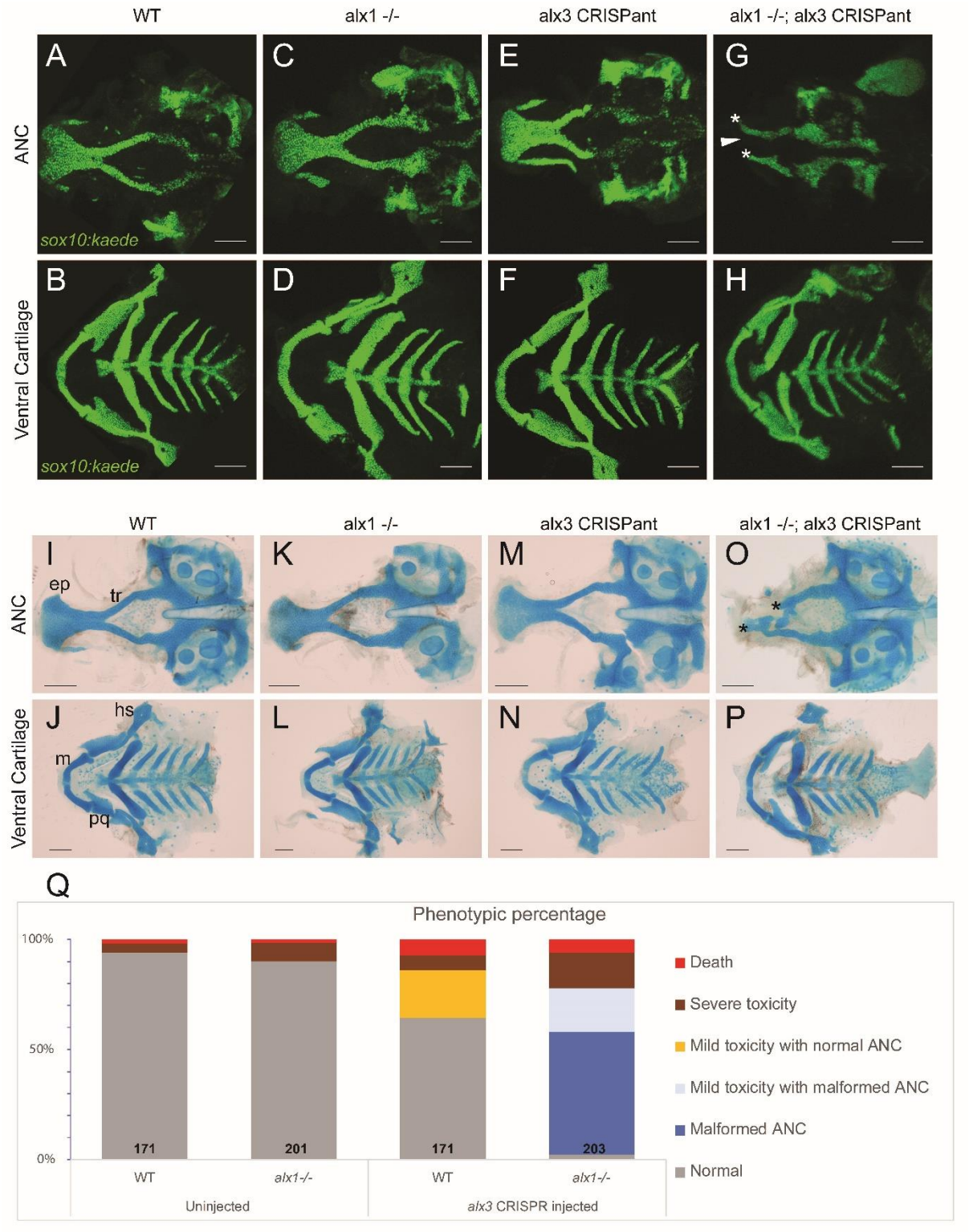

Supplementary Figure 2. *alx1 -/-; alx3 CRISPants phenocopy alx1; alx3 double mutants.*

Embryos derived from *Tg(sox10:kaede)* embryos or *alx1 -/-; Tg(sox10:kaede)* were injected with alx3 CRISPRs, dissected, and flat-mounted to fluorescently represent anterior neurocranium (ANC) and ventral cartilage at 4 dpf. *alx1 -/-; alx3* CRISPants develop with midline cleft (arrowhead in G), with the lateral elements (asterisks in G) separated as the median element is missing. I – P: Dissected flat-mount alcian blue stained cartilage in larvae of different genotype at 4 dpf, anterior to the left. While WT embryos develop with normal paired trabeculae (tr) and an ethmoid plate (ep) (I), *alx1 -/-; alx3* CRISPants exhibit defective trabeculae fusion (asterisks in O) and depleted ethmoid plate. Q: Percentage of embryos displaying malformed anterior neurocranium (ANC) phenotype in 4 dpf larvae of different genotype. All embryos were shown in anterior to the left. Scale bar: 100μm.

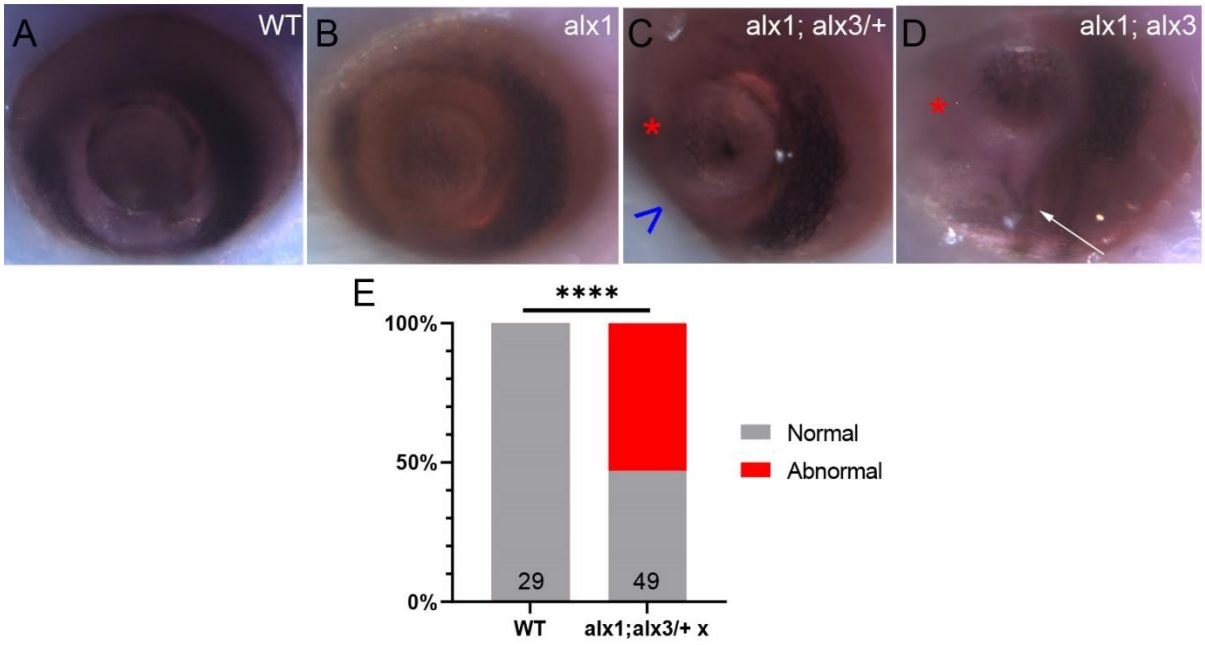

Supplementary Figure 3. *alx1 and alx3 are required for anterior segment development.*

Embryos derived from WT or *alx1; alx3/+* parental crosses were stained with alkaline phosphatase (AP) to visualize endogenous AP expression within the anterior segment at 5 dpf. A: Normal AP expression at anterior segment. B: *Alx1* mutants exhibit normal AP expression at anterior segment. C, D: *alx1; alx3* heterozygotes and *alx1; alx3* double mutants develop with anterior segment defects shown as partially missing AP expression at anterior segment (asterisk), misshapen eyes (arrowhead), and coloboma (arrow). E: The anterior segment defect is specific to some *alx1; alx3* heterozygotes and all *alx1; alx3* double mutants (****: $p < 0.0001$, Fisher's exact test, 2 trials). All embryos are shown in lateral view, anterior to the left.

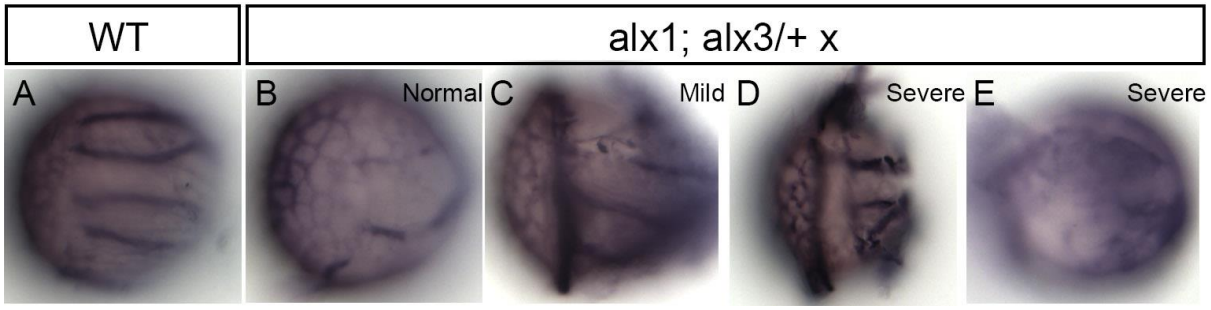

Supplementary Figure 4. *alx1 and alx3 are required for hyaloid network formation*

Embryos derived from WT (A) or *alx1; alx3/+* (B – E) were first scored for the presence of misshapen eyes and stained for alkaline phosphatase to visualize the hyaloid vasculature on lens at 5 dpf. A: Normal hyaloid network formation in WT (6/6 lens), B: Embryos with normal eyes have reduced hyaloid network formation (5/6 lens), C: Embryos with mild misshapen eyes have unorganized hyaloid network formation (5/6 lens). D-E: Embryos with severe misshapen eyes have unorganized hyaloid network (D; 2/5 lens) or no hyaloid network (E; 2/5 lens).

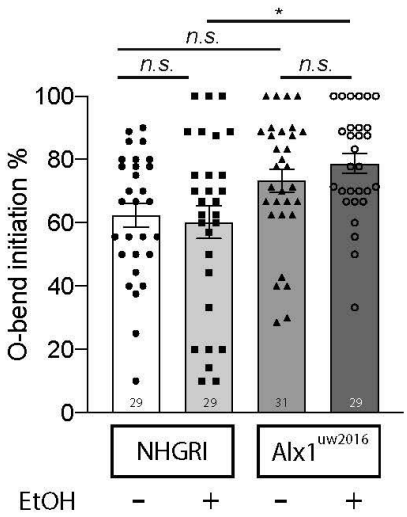

Supplementary Figure 5. *Ethanol treatment does not affect visually guided O-bend initiations*

Mean frequency of O-bend initiations to a series of 10 dark flash stimuli with and without ethanol treatment (n.s.: p>0.9999. *: p = 0.0305. ANOVA with Kruskal-Wallis. N at base of bars indicates number of larvae. Error bars indicate SEM).

Chapter IV

A novel gene regulatory network that controls ocular morphogenesis.

Introduction

Vertebrate eye morphogenesis begins when the neural retina evaginates from the forebrain and is shaped into bilayered optic cups (Chow and Lang, 2001; Fuhrmann, 2010). The optic cup is transiently attached to the forebrain through the optic stalk (later becoming optic nerve) and continues to develop as the choroid fissure, a transient opening in the ventral surface of retina, forms (Bibliowicz et al., 2011; Fuhrmann, 2010). Hyaloid vasculature, which is derived from mesoderm and anterior neural crest lineages (Gage et al., 2005), invades into the eyes guided by optic stalk through the choroid fissure prior to fusion (James et al., 2016; Morcillo et al., 2006; Tao and Zhang, 2014; Weaver et al., 2020). The choroid fissure must close for retinal vasculature development inside of the retina and for transmission of visual information to the brain (Alvarez et al., 2007; Patel and Sowden, 2019). In humans, failure of choroid fissure formation and closure is associated with coloboma, which leads to blindness and visual impairment worldwide (Eckert et al., 2019; Gordon et al., 2018; Gregory-Evans et al., 2004; Williamson and FitzPatrick, 2014). Despite the clinical significance, little is known about the regulatory mechanism of ventral retina morphogenesis.

The ventral retina is surrounded by various tissues and cell lineages including the ventral forebrain, optic stalk, hyaloid vessels, and neural crest-derived mesenchyme that gives rise to craniofacial cartilage and structures of the anterior segment of the eye, such as the cornea and lens. Future cartilage neural crest cells migrate around the eye on their way to their destination, oral ectoderm (Eberhart et al., 2008), and future anterior segment neural crest cells enter the eye through the choroid fissure (Takamiya et al., 2020; Van Der Meulen et al., 2020). Due to their proximity,

these lineages can signal one another to ensure the correct ventral retina formation, but the details of these signaling interactions are poorly understood.

Optic stalk is important for choroid fissure formation and closure (Bassett et al., 2010; Eckert et al., 2019; Wen et al., 2015), and hyaloid vasculature formation (Alvarez et al., 2007). Sonic hedgehog (Hh) signaling is the best-known regulator of their formation. Hh, which originated from the ventral midline of forebrain, induces optic stalk and choroid fissure formation while separating them from the retina (Chiang et al., 1996; Lee et al., 2008; Macdonald et al., 1995; Zhao et al., 2012). At this point, the genetic mechanism of how Hh regulates optic stalk and ventral retina development. Therefore, it is necessary to identify and examine the genetic regulators of Hh signaling.

Pax2 is one such important genetic regulator. Its transcription in presumptive optic nerve glia (Nornes et al., 1990) is induced by Hh signaling from the ventral midline of the forebrain (Chiang et al., 1996; Macdonald et al., 1995). Subsequently, it plays various roles during ventral retina morphogenesis, including retinal astrocyte migration and differentiation in the optic stalk (Chu et al., 2001; Sehgal et al., 2009), choroid fissure closure (Sehgal et al., 2008), optic nerve trajectory formation (Torres et al., 1996), and hyaloid vasculature recruitment (Weaver et al., 2020). In humans, dysregulation of *PAX2* is linked with coloboma (Okumura et al., 2015; Sanyanusin et al., 1995; Schimmenti, 2011). Together, these observations suggest that *pax2* is required for ventral retina development. To fully understand the mechanism of *pax2* functions in the developing embryo, it is essential to dissect these functions further while investigating potential regulators of *pax2*.

Our lab has previously shown that *zic2,* zinc-finger transcription factor, is

another target of Hh signaling that is important for optic stalk and ventral retina formation. Furthermore, it functions to restrict *pax2a* transcription at the optic stalk during retinal development (Sanek et al., 2009; Sedykh et al., 2017). In humans, mutations in *SHH* and *ZIC2* are associated with holoprosencephaly, a congenital forebrain malformation (Dubourg et al., 2004; Grinblat and Lipinski, 2019; Kruszka et al., 2018). Zic2 has been shown to interact with Hh signaling mediator gli proteins physically and functionally *in vitro* (Koyabu et al., 2001; Mizugishi et al., 2001). However, this interaction has not been tested *in vivo* to date. In zebrafish, *zic2* mutants exhibit ocular defects, namely coloboma and ocular hemorrhaging (Sedykh et al., 2017). I hypothesize that these ocular defects occur due to dysregulation of the Hh downstream target, *pax2a*. In this chapter, I further investigate the genetic regulations of ocular development focusing on *pax2a.*

Here, I present two novel genetic regulatory mechanisms of *pax2a* transcription mediated by *zic2* and highlight the role of *pax2a* during ocular and craniofacial development. I identify that zic2 cooperates with gli proteins to inhibit *pax2a* transcription at the optic stalk. I also identify that *cldn11*, a novel downstream target of zic2 (Sedykh et al., 2017), inhibits *pax2a* transcription expanding to ventral retina. After reducing *pax2a* transcription, I observe that coloboma, but not ocular hemorrhaging, is rescued in *zic2* mutants and *pax2a* function is required for hyaloid vasculature and craniofacial cartilage development.

Methods

Zebrafish husbandry and embryo manipulation

Adult zebrafish were maintained according to established methods (Westerfield, 1993). All experimental protocols using zebrafish were approved by the University of Wisconsin Animal Care and Use Committee and carried out in accordance with the institutional animal care protocols. Embryos were obtained from natural matings and staged according to Kimmel (Kimmel et al., 1995).

Embryos derived from NHGRI (WT) (LaFave et al., 2014), zic2a^{gbt133}/+; zic2b^{t104}/+, zic2b^{t104}, or zic2a^{gbt133}/+; zic2b^{t104} were injected with CRISPRs (Table 1) and Cas9 protein (IDT) accordingly. The final concentation for each CRISPR and Cas9 protein were adjusted to 5 μM.

Embryos derived from *Tg(hsp70l;gli2aDR-eGFP)* (Shen et al., 2013) were injected with zic2 CRISPRs (2.5 μM final concentration) (Table 1) and Cas9 protein (5 μM final concentration) at 1 cell stage and heat-shocked at 37^{o}C for an hour at 8 hours post fertilization (hpf).

O-dianisidine staining

Staining the hemoglobinized red blood cells with o-dianisidine was carried out as previous described (Paffett-Lugassy and Zon, 2005). To visualize the intraocular

red blood cell population, embryos were bleached with 1% KOH/6% H_2O_2. Embryos were mounted in 100% glycerol and imaged on Leica MZ FLIII stereo microscopes equipped with Leica DFC310 FX camera and LAS v4.0 software.

Immunohistochemistry

Embryos were fixed in 4% paraformaldehyde (PFA)/ PBS overnight. After fixation, the embryos were bleached in 1% KOH/6% H_2O_2 and then washed with PBST-X (1X PBS with 0.2% TritonX-100). To enhance permeability, embryos were dechorionated and deyolked. Embryos were blocked with PBSTD-X (1X PBST-X mixed with 1% DMSO, 10% Bovine serum albumin mixed with 1X PBS, 10% goat serum) for 2 hours in RT before primary antibody incubation. Rabbit-anti pax2a antibody (GeneTex; 1:500) and mouse-anti GFP antibody (Millipore; 1:500) were detected fluorescently with Alexa-594 goat anti-rabbit antibodies (Invitrogen; 1:500) and Alexa-488 goat anti-mouse antibodies (Invitrogen; 1:500), respectively. For F-actin and nuclei staining, embryos were stained with phalloidin Alexa-568 (Invitrogen; 1:100) and DAPI (Molecular Probes; 1:5000), respectively. Embryos were mounted in VectaShield (Vector laboratories) and imaged on an Olympus IX81 inverted confocal microscope with the Fluoview 1000 confocal package, using a 60x water immersion objective (NA 1.10).

In situ hybridization and alcian blue staining

In situ hybridization was carried out as previously described (Gillhouse et al., 2004), using the following probe: pax2a (Hoyle et al., 2004). After whole mount *in situ* hybridization (WISH), embryos were mounted in 100% glycerol and imaged on Leica MZ FLIII stereo microscopes equipped with Leica DFC310 FX camera and LAS v4.0 software. For cartilage staining, zebrafish larvae were fixed at 5 days post fertilization (dpf) in 4% PFA/PBS overnight and stained with alcian blue according to Kimmel (Kimmel et al., 1998). Stained zebrafish larvae were further dissected using forceps for imaging jaw cartilage and ethmoid plates. Jaw cartilage and ethmoid plates were imaged on NIKON eclipse E600 microscope equipped with Q Imaging QIclick 1.4MP CCD Monochrome Microscope camera and NIS-elements software.

Statistics

Statistical analyses, including Welch's t-test, Fisher's exact test, and Chi-square test, were performed using GraphPad Prism software (GraphPad Software). P-values below 0.05 were considered statistically significant.

Result and Discussion

Zebrafish zic2 is required for hyaloid vascular development.

Our lab previously generated a genetic model of zebrafish ZIC2-linked HPE model to examine the role of *zic2* during ventral retina morphogenesis (Sedykh et al., 2017). We found that zebrafish *zic2* mutants exhibit coloboma with intraocular and/or periocular hemorrhaging at 3 days post fertilization (dpf) (Fig. 1A-D; asterisk), suggesting that *zic2* may function in hyaloid vasculature development.

I next asked if hyaloid vasculature patterning and/or morphology were disrupted in *zic2* mutants at 28 hpf, when the hyaloid loop forms around the lens (Hartsock et al., 2014). Through whole mount immunohistochemistry, I examined hyaloid vasculature (marked with *fli1:GFP*) and optic stalk and choroid fissure (marked with *pax2a*) in *zic2* mutants. In *zic2* mutants, *pax2a* is ectopically expanded (Fig 1G, H; arrowhead) and hyaloid vasculature clusters ventrally and periocularly (Fig 1G, H; arrow).

Pax2a is regulated by the interaction between zic2 and glis

Hh signaling secreted from the ventral midline of the forebrain is required for patterning early vertebrate ocular morphogenesis such that it promotes *pax2* in the optic stalk but represses *pax6* in the retina to set the boundary between optic stalk

and retina (Chiang et al., 1996; Ekker et al., 1995; Macdonald et al., 1995; Zhao et al., 2012). Gli proteins are Hh signaling mediators that differentially activate or repress in various cellular contexts (Cavodeassi et al., 2019). For optic stalk development, *gli3* has been shown to restrict the expression of *pax2* at the optic stalk (Furimsky and Wallace, 2006; Wiegering et al., 2019). While the expression of Gli proteins overlaps at ventral forebrain in zebrafish (Sanek and Grinblat, 2008), an early functional requirement of Gli proteins for optic stalk development remains very poorly understood. In addition, while *zic2* restricts *pax2a* at optic stalk (Sanek et al., 2009; Sedykh et al., 2017) and gli proteins physically and functionally interacts with zic2 *in vitro* (Koyabu et al., 2001; Mizugishi et al., 2001), the interaction between zic2 and Gli proteins for optic stalk development has not been characterized and tested *in vivo* to date.

In zebrafish, *gli2* function can activate or repress Hh signaling downstream targets depending on the cellular context (Karlstrom et al., 2003), but its functional requirement for optic stalk development has not been tested. I first asked if *zic2* functionally interacts with *gli2* for optic stalk development. To test this, I overexpressed a dominant negative isoform of *gli2a* (*gli2*-DN) to deplete all gli functions (Karlstrom et al., 2003), while simultaneously abrogating *zic2* function. I mutagenized both *zic2a* and *zic2b* through CRISPR/Cas9 mutagenesis (Fig. 2A, B) in embryos derived from parental crosses of *Tg(hsp70l;gli2aDR-eGFP)* (Shen et al., 2013) and induced with heat-shock at 8 hpf for an hour (Fig. 2C). I observed that gli depleted embryos develop with U-shaped somites (Supp Fig. 1B, C), consistent with previous data (Shen et al., 2013). I next examined *pax2a* expression using WISH. WT embryos develop with normal *pax2a* expression at optic stalk and choroid fissure (Fig. 2D, n = 11/11) whereas *gli2*-DN embryos develop with mispatterned pax2a expression (Fig. 2E, n =

13/42). I observed a similar result in zic2 CRISPants (Fig. 2F, n = 9/12) and *gli2*-DN*; zic2* CRISPants (Fig. 2G, n = 5/7). Compared to WT, the proportion of mispatterned *pax2a* expression significantly increases in *gli2*-DN, *zic2* CRISPants, and *gli2*-DN*; zic2* CRISPants (Fig. 2H; p = 0.0474, p = 0.0003, p = 0.0025, respectively, Fisher's exact test). This suggests that both zic2 and glis inhibit *pax2a* transcription at optic stalk (Fig. 8).

In addition, to test a functional interaction between *zic2* and *gli3* for optic stalk development, I used CRISPR/Cas9 mutagenesis targeting exon 3, exon 6, and exon 7 of the *gli3* locus (Fig. 3A) in embryos derived from WT, *zic2a +/-; zic2b +/-* (Zygotic-*zic2*; Z-*zic2*), *zic2a +/+; zic2b -/-* (Maternal/zygotic-*zic2b*; MZ-*zic2b*), and *zic2a +/-; zic2b -/-* (Maternal/zygotic-*zic2*; MZ-*zic2*) and examined *pax2a* expression using WISH. While very few *gli3* CRISPants from WT and Z-*Zic2* develop with mispatterned *pax2a* expression (Fig. 3E, n= 4/76 from WT, n= 3/47 from Z-*zic2*), *gli3* CRISPants from MZ-*zic2b* (Fig. 3C) or MZ-*zic2* (Fig. 3D) parental incross significantly develop with mispatterned pax2a expression (Fig. 3E, n = 3/14 from MZ-zic2b and n = 40/64 from MZ-*zic2*). This finding suggests that *zic2* and *gli3* synergistically restrict *pax2a* transcription at the optic stalk (Fig. 8). While there is yet much to learn about the mechanism of the interaction between zic2 and gli proteins, investigating this interaction further would provide clues to how Hh signaling separates the fate of the optic stalk from the forebrain and retina.

Cldn11 represses pax2a transcription in retina.

Cldn11, a claudin gene family, is a tight junction protein that is enriched in myelinating sheath of the central nervous system and Sertoli cells in testes (Devaux and Gow, 2008; Morita et al., 1999; Tiwari-Woodruff et al., 2001). In zebrafish, *cldn11* has two homologs: *cldn11a* and *cldn11b*. Initially, zebrafish *cldn11a* was reported as a vascular endothelial marker (Cannon et al., 2013); however, we identified a novel domain of *cldn11a* expression, which overlaps with periocular neural crest, at 24 hpf (Sedykh et al., 2017). Through WISH and RNA-sequencing, we showed that *cldn11a* expression is significantly downregulated in zic2 mutants (Sedykh et al., 2017). On the other hand, *cldn11b* function and expression has not yet been reported to date.

While nothing is known about the role of *cldn11* during ventral retina morphogenesis, recent reports show that *cldn11* is required for epithelial-to-mesenchyme transition (EMT) and collective cell migration (Hutchins and Bronner, 2019; Li et al., 2019), which are the two requirements for neural crest migration. Because anterior neural crest-derived periocular mesenchyme contributes to ventral retinal morphogenesis (Gestri et al., 2018; Lupo et al., 2011; McMahon et al., 2009) and *cldn11a* expression overlaps with the domain where periocular neural crest presents (Sedykh et al., 2017), I investigated if *cldn11a* contributes to optic stalk development. To test this, I used CRISPR/Cas9 mutagenesis to target exon 1 and exon 3 of *cldn11a* locus (Fig. 4A). I found that all *cldn11a* CRISPants normally develop. Because a transcriptional adaptation mechanism is triggered by mutant mRNA degradation in the zebrafish genome (El-Brolosy et al., 2019), I reasoned that *cldn11b*, a paralog of *cldn11a*, may upregulate to compensate the loss of *cldn11a* function. I

next mutagenized two targets at exon 1 of *cldn11b* locus (Fig. 4B) along with same targets for *cldn11a*. Surprisingly, *cldn11a; cldn11b* double CRISPants develop with craniofacial and ocular defects (Supp. Fig. 2C, n = 24/42). Similar to *cldn11a* CRISPants, all *cldn11b* CRISPants develop normally.

To investigate if ventral retinal patterning is disrupted by loss of *cldn11a* and *cldn11b* function, I examined *pax2a* expression in *cldn11a; cldn11b* double CRISPants using WISH. Surprisingly, *pax2a* expression is ectopically expanded in *cldn11a; cldn11b* double CRISPants (Fig. 4E – G; $p < 0.0001$, Fisher's exact test, 1 trial), reminiscent of *zic2* mutants (Sedykh et al., 2017), *gli2*-DN*; zic2* CRISPants (Fig. 2), and *zic2; gli3* CRISPants (Fig. 3). Taken together, our data demonstrate that *cldn11* plays a critical early role during ventral retina morphogenesis through repression of *pax2a* transcript in the retina (Fig. 8). While the interaction between *cldn11* and *pax2a* and the role of *cldn11* in anterior neural crest migration need to be further investigated, this finding suggests the potential role of *cldn11* in optic stalk development. In addition, because cldn11 is a tight junction protein that shares a structural similarity with other claudin genes, such as *cldn5* expressed in hyaloid vasculature (Xie et al., 2010), *cldn11* might be a novel gene that regulates vascular integrity of hyaloid vasculature.

Reduction of pax2a transcription rescues coloboma but not ocular hemorrhaging in zic2 mutants.

Hh secreted from the ventral midline of the forebrain is required for ventral retina morphogenesis (Chiang et al., 1996; Lee et al., 2008; Macdonald et al., 1995;

Zhao et al., 2012). In the absence of *Hh* expression, *pax2a* expression is lost at the optic stalk (Varga et al., 2001). Conversely, ectopic *Hh* expression induces the expansion of *pax2a* at optic vesicle and optic stalk (Ekker et al., 1995). Likewise, mutation of *zic2* results in ectopic expansion of *pax2a* (Fig. 1G, H). Therefore, I hypothesized that coloboma and ocular hemorrhaging in zic2 mutants were due to aberrant *pax2a* transcriptional level.

To investigate if reduction of *pax2a* transcript rescues coloboma and ocular hemorrhaging, I used CRISPR/Cas9 mutagenesis targeting exon 2 and exon 4 of the *pax2a* locus (Fig. 5A). *Pax2a* CRISPants develop with no midbrain-hindbrain boundary (no isthmus, noi) (Supp Fig. 3B; asterisk) and mild coloboma (Supp Fig. 3D; arrow), consistent with previous findings in mutants (Kelly and Moon, 1995; Krauss et al., 1992; Lun and Brand, 1998; Macdonald et al., 1997; Pfeffer et al., 1998; Weaver et al., 2020). I conclude that *pax2a* CRISPRs effectively mutagenized *pax2a* transcript (Supp Fig. 3E; $p < 0.0001$, Chi-square test, 6 trials).

I introduced *pax2a* CRISPRs into *zic2* mutants and scored for coloboma and ocular hemorrhaging at 3 dpf in *zic2* mutants/*pax2a* CRISPants (going forward, I will refer to as *zic2; pax2a* CRISPants). The penetrance of coloboma significantly reduced in *zic2; pax2a* CRISPants (Fig. 5B, $p < 0.0001$, Chi-square test, 9 trials) as well as the severity (normal in Fig. 5C, $p = 0.003$; mild in Fig. 5D, $p = 0.0313$; moderate in Fig. 5E, $p = 0.0313$; severe in Fig. 5F, $p = 0.0001$, Welch's t-test. 9 trials). These findings are consistent with a significant alleviation of coloboma phenotype in *zic2* mutants treated with cyclopamine, a Hh inhibitor (Sedykh et al., 2017), suggesting that dysregulation of Hh signaling is associated with coloboma. However, the penetrance of ocular hemorrhaging did not significantly reduce in *zic2; pax2a* CRISPants (Fig. 5G, p =

0.1082; Fisher's exact test, 7 trials).

Pax2a is required for hyaloid vasculature formation.

I asked if ocular hemorrhaging *in zic2* mutants is associated with dysregulation of Hh signaling. Since ptch2 is a transmembrane protein serving as a Hh inhibitor (Cavodeassi et al., 2019), I used embryos derived from *ptch2 +/-; Tg(fli1:GFP)* parents to examine the hyaloid vasculature in overactivation of Hh signaling. I scored *ptch2* mutants by examining the mild coloboma phenotype at 2 dpf (Gordon et al., 2018; Lee et al., 2008) and immunostained for GFP. Both normal siblings and *ptch2* mutants develop with normal hyaloid vasculature formation at 2 dpf and 5 dpf (Fig. 6A – D).

Conversely, I investigated hyaloid vasculature formation in reduction of Hh signaling. I introduced *pax2a* CRISPRs into *Tg(fli1:*GFP), scored for noi phenotype to ensure CRISPR efficacy at 24 hpf, and stained for *pax2a* and GFP to visualize the optic stalk/choroid fissure and hyaloid vasculature, respectively, at 28 hpf. WT embryos develop with normal hyaloid loop formation (Fig. 6E) with normal *pax2a* expression at choroid fissure (Fig. 6F) whereas *pax2a* CRISPants exhibit partially incomplete hyaloid loop formation (Fig. 6G) with completely depleted pax2a expression (Fig. 6H). A recent report shows that *pax2a* mutants exhibit reduced hyaloid vascularization (Weaver et al., 2020), which is consistent with our data. Together, our data suggest that *pax2a* is required for hyaloid vasculature formation.

It is currently unclear whether *Hh* directly or indirectly influences hyaloid vasculature development. While previous reports show that *Hh* acts directly on

vascular endothelium of several cellular contexts (Chinchilla et al., 2010; Nagase et al., 2008), several reports demonstrate that *Hh* indirectly promotes angiogenesis through promoting vascular endothelium growth factor (VEGF) (Nagase et al., 2008; Pola et al., 2001; Weiss et al., 2017). Because zebrafish *pax2a* mutants show significant depletion of VEGF (Weaver et al., 2020) and *Hh*-dependent VEGF is required for ventral retinal vascular patterning (Weiss et al., 2017), it is likely that *Hh* indirectly influences initial hyaloid vasculature development through promoting VEGF. In addition, recent reports show that *Hh* regulates vascular integrity within the retina (Diaz-Coranguez et al., 2017; Pollock et al., 2020); hence, it is possible that *Hh* indirectly controls hyaloid vasculature development through promoting the differentiation of neural crest derived vascular pericytes that stabilize the hyaloid vasculature (Alvarez et al., 2007; Saint-Geniez and D'Amore, 2004). Additional studies are needed to investigate if *pax2a* function is required for regulating retinal vascular integrity.

Pax2a function is required for craniofacial development.

To investigate if *pax2a* function is required for craniofacial cartilage formation, Lauren and I examined the craniofacial structure following reducing *pax2a* transcription. I raised normal siblings and *pax2a* CRISPants until 5 dpf and Lauren used alcian blue staining to visualize craniofacial cartilage structure. Lauren further dissected the embryos to image the jaw cartilages and ethmoid plates. While all normal siblings develop with normal jaw cartilages and ethmoid plates (Fig. 7A, C),

pax2a CRISPants develop with reduced jaw cartilages and ethmoid plates (Fig. 7B, D). The craniofacial defects significantly appear in *pax2a* CRISPants (Fig. 7E; $p < 0.0001$, Fisher's exact test, 3 trials). This finding suggests *pax2a* function is required for craniofacial cartilage.

The craniofacial cartilage is derived from two different sources of cranial neural crest. Cranial neural crest that arises from diencephalon and midbrain migrates anteriorly to form the ethmoid plate (Wada et al., 2005) whereas cranial neural crest that arises from the hindbrain migrates in three separate streams ventrolaterally and develops into the jaw cartilages of the pharyngeal arches (Schilling and Kimmel, 1994, 1997; Trainor and Krumlauf, 2001). Anteriorly migrated cranial neural crest is influenced by the developing eyes as it requires signals from the eyes to start a directed migration (Langenberg et al., 2008). In the developing eyes, the optic stalk has been further characterized for its role in attracting anteriorly migrated cranial neural crest to optic stalk via platelet-derived growth factor (pdgf)-mediated cues. Without proper attractive cues, ethmoid plates abnormally form (Eberhart et al., 2008). Ventrolaterally migrated cranial neural crest and pharyngeal endoderm interact together to correctly form jaw cartilage and pattern pharyngeal arches, respectively (Trainor and Krumlauf, 2001). Morphogenesis and patterning of jaw cartilage depend upon the signals arising from pharyngeal endoderm (Couly et al., 2002; David et al., 2002; Swartz et al., 2012).

Although *pax2a* is not expressed in cranial neural crest, loss of *pax2a* function results in abnormal ethmoid plates and jaw cartilages (Fig. 7B, D). This suggests that *pax2a* function may non-cell-autonomously regulate both anteriorly and ventrolaterally migrated cranial neural crest. The molecular mechanism of *pax2a* for ethmoid plates

and jaw cartilage development is currently unknown. For future studies, it is necessary to examine if neural crest migration is disrupted in the absence of *pax2a* function through live imaging of *Tg(sox10:GFP)* embryos injected with pax2a CRISPRs.

Acknowledgements

I thank Lauren Bluhm for alcian blue staining, dissections, and imaging alcian blue stained embryos. I also thank Rolf Karlstrom for providing the *Tg(hsp70l;gli2aDR-eGFP)* zebrafish.

Reference

Alvarez, Y., Cederlund, M.L., Cottell, D.C., Bill, B.R., Ekker, S.C., Torres-Vazquez, J., Weinstein, B.M., Hyde, D.R., Vihtelic, T.S., Kennedy, B.N., 2007. Genetic determinants of hyaloid and retinal vasculature in zebrafish. BMC Dev Biol 7, 114.

Bassett, E.A., Williams, T., Zacharias, A.L., Gage, P.J., Fuhrmann, S., West-Mays, J.A., 2010. AP-2alpha knockout mice exhibit optic cup patterning defects and failure of optic stalk morphogenesis. Hum Mol Genet 19, 1791-1804.

Bibliowicz, J., Tittle, R.K., Gross, J.M., 2011. Toward a better understanding of human eye disease insights from the zebrafish, Danio rerio. Prog Mol Biol Transl Sci 100, 287-330.

Cannon, J.E., Place, E.S., Eve, A.M., Bradshaw, C.R., Sesay, A., Morrell, N.W., Smith, J.C., 2013. Global analysis of the haematopoietic and endothelial transcriptome during zebrafish development. Mech Dev 130, 122-131.

Cavodeassi, F., Creuzet, S., Etchevers, H.C., 2019. The hedgehog pathway and ocular developmental anomalies. Hum Genet 138, 917-936.

Chiang, C., Litingtung, Y., Lee, E., Young, K.E., Corden, J.L., Westphal, H., Beachy, P.A., 1996. Cyclopia and defective axial patterning in mice lacking Sonic hedgehog gene function. Nature 383, 407-413.

Chinchilla, P., Xiao, L., Kazanietz, M.G., Riobo, N.A., 2010. Hedgehog proteins activate pro-angiogenic responses in endothelial cells through non-canonical signaling pathways. Cell Cycle 9, 570-579.

Chow, R.L., Lang, R.A., 2001. Early eye development in vertebrates. Annu Rev Cell Dev Biol 17, 255-296.

Chu, Y., Hughes, S., Chan-Ling, T., 2001. Differentiation and migration of astrocyte precursor cells and astrocytes in human fetal retina: relevance to optic nerve coloboma. FASEB J 15, 2013-2015.

Couly, G., Creuzet, S., Bennaceur, S., Vincent, C., Le Douarin, N.M., 2002. Interactions between Hox-negative cephalic neural crest cells and the foregut endoderm in patterning the facial skeleton in the vertebrate head. Development 129, 1061-1073.

David, N.B., Saint-Etienne, L., Tsang, M., Schilling, T.F., Rosa, F.M., 2002. Requirement for endoderm and FGF3 in ventral head skeleton formation. Development 129, 4457-4468.

Devaux, J., Gow, A., 2008. Tight junctions potentiate the insulative properties of small CNS myelinated axons. J Cell Biol 183, 909-921.

Diaz-Coranguez, M., Chao, D.L., Salero, E.L., Goldberg, J.L., Antonetti, D.A., 2017.

Cell autonomous sonic hedgehog signaling contributes to maintenance of retinal endothelial tight junctions. Exp Eye Res 164, 82-89.

Dubourg, C., Lazaro, L., Pasquier, L., Bendavid, C., Blayau, M., Le Duff, F., Durou, M.R., Odent, S., David, V., 2004. Molecular screening of SHH, ZIC2, SIX3, and TGIF genes in patients with features of holoprosencephaly spectrum: Mutation review and genotype-phenotype correlations. Hum Mutat 24, 43-51.

Eberhart, J.K., He, X., Swartz, M.E., Yan, Y.L., Song, H., Boling, T.C., Kunerth, A.K., Walker, M.B., Kimmel, C.B., Postlethwait, J.H., 2008. MicroRNA Mirn140 modulates Pdgf signaling during palatogenesis. Nat Genet 40, 290-298.

Eckert, P., Knickmeyer, M.D., Schutz, L., Wittbrodt, J., Heermann, S., 2019. Morphogenesis and axis specification occur in parallel during optic cup and optic fissure formation, differentially modulated by BMP and Wnt. Open Biol 9, 180179.

Ekker, S.C., Ungar, A.R., Greenstein, P., von Kessler, D.P., Porter, J.A., Moon, R.T., Beachy, P.A., 1995. Patterning activities of vertebrate hedgehog proteins in the developing eye and brain. Curr Biol 5, 944-955.

El-Brolosy, M.A., Kontarakis, Z., Rossi, A., Kuenne, C., Gunther, S., Fukuda, N., Kikhi, K., Boezio, G.L.M., Takacs, C.M., Lai, S.L., Fukuda, R., Gerri, C., Giraldez, A.J., Stainier, D.Y.R., 2019. Genetic compensation triggered by mutant mRNA degradation. Nature 568, 193-197.

Fuhrmann, S., 2010. Eye morphogenesis and patterning of the optic vesicle. Curr Top Dev Biol 93, 61-84.

Furimsky, M., Wallace, V.A., 2006. Complementary Gli activity mediates early patterning of the mouse visual system. Dev Dyn 235, 594-605.

Gage, P.J., Rhoades, W., Prucka, S.K., Hjalt, T., 2005. Fate maps of neural crest and mesoderm in the mammalian eye. Invest Ophthalmol Vis Sci 46, 4200-4208.

Gestri, G., Bazin-Lopez, N., Scholes, C., Wilson, S.W., 2018. Cell Behaviors during Closure of the Choroid Fissure in the Developing Eye. Front Cell Neurosci 12, 42.

Gillhouse, M., Wagner Nyholm, M., Hikasa, H., Sokol, S.Y., Grinblat, Y., 2004. Two Frodo/Dapper homologs are expressed in the developing brain and mesoderm of zebrafish. Dev Dyn 230, 403-409.

Gordon, H.B., Lusk, S., Carney, K.R., Wirick, E.O., Murray, B.F., Kwan, K.M., 2018. Hedgehog signaling regulates cell motility and optic fissure and stalk formation during vertebrate eye morphogenesis. Development 145.

Gregory-Evans, C.Y., Williams, M.J., Halford, S., Gregory-Evans, K., 2004. Ocular coloboma: a reassessment in the age of molecular neuroscience. J Med Genet 41, 881-891.

Grinblat, Y., Lipinski, R.J., 2019. A forebrain undivided: Unleashing model organisms to solve the mysteries of holoprosencephaly. Dev Dyn 248, 626-633.

Hartsock, A., Lee, C., Arnold, V., Gross, J.M., 2014. In vivo analysis of hyaloid vasculature morphogenesis in zebrafish: A role for the lens in maturation and maintenance of the hyaloid. Dev Biol 394, 327-339.

Hoyle, J., Tang, Y.P., Wiellette, E.L., Wardle, F.C., Sive, H., 2004. nlz gene family is required for hindbrain patterning in the zebrafish. Dev Dyn 229, 835-846.

Hutchins, E.J., Bronner, M.E., 2019. Draxin alters laminin organization during basement membrane remodeling to control cranial neural crest EMT. Dev Biol 446, 151-158.

James, A., Lee, C., Williams, A.M., Angileri, K., Lathrop, K.L., Gross, J.M., 2016. The hyaloid vasculature facilitates basement membrane breakdown during choroid fissure closure in the zebrafish eye. Dev Biol 419, 262-272.

Karlstrom, R.O., Tyurina, O.V., Kawakami, A., Nishioka, N., Talbot, W.S., Sasaki, H., Schier, A.F., 2003. Genetic analysis of zebrafish gli1 and gli2 reveals divergent requirements for gli genes in vertebrate development. Development 130, 1549-1564.

Kelly, G.M., Moon, R.T., 1995. Involvement of wnt1 and pax2 in the formation of the midbrain-hindbrain boundary in the zebrafish gastrula. Dev Genet 17, 129-140.

Kimmel, C.B., Ballard, W.W., Kimmel, S.R., Ullmann, B., Schilling, T.F., 1995. Stages of embryonic development of the zebrafish. Dev Dyn 203, 253-310.

Kimmel, C.B., Miller, C.T., Kruze, G., Ullmann, B., BreMiller, R.A., Larison, K.D., Snyder, H.C., 1998. The shaping of pharyngeal cartilages during early development of the zebrafish. Dev Biol 203, 245-263.

Koyabu, Y., Nakata, K., Mizugishi, K., Aruga, J., Mikoshiba, K., 2001. Physical and functional interactions between Zic and Gli proteins. J Biol Chem 276, 6889-6892.

Krauss, S., Maden, M., Holder, N., Wilson, S.W., 1992. Zebrafish pax[b] is involved in the formation of the midbrain-hindbrain boundary. Nature 360, 87-89.

Kruszka, P., Martinez, A.F., Muenke, M., 2018. Molecular testing in holoprosencephaly. Am J Med Genet C Semin Med Genet 178, 187-193.

LaFave, M.C., Varshney, G.K., Vemulapalli, M., Mullikin, J.C., Burgess, S.M., 2014. A defined zebrafish line for high-throughput genetics and genomics: NHGRI-1. Genetics 198, 167-170.

Langenberg, T., Kahana, A., Wszalek, J.A., Halloran, M.C., 2008. The eye organizes neural crest cell migration. Dev Dyn 237, 1645-1652.

Lee, J., Willer, J.R., Willer, G.B., Smith, K., Gregg, R.G., Gross, J.M., 2008. Zebrafish blowout provides genetic evidence for Patched1-mediated negative regulation of

Hedgehog signaling within the proximal optic vesicle of the vertebrate eye. Dev Biol 319, 10-22.

Li, C.F., Chen, J.Y., Ho, Y.H., Hsu, W.H., Wu, L.C., Lan, H.Y., Hsu, D.S., Tai, S.K., Chang, Y.C., Yang, M.H., 2019. Snail-induced claudin-11 prompts collective migration for tumour progression. Nat Cell Biol 21, 251-262.

Lun, K., Brand, M., 1998. A series of no isthmus (noi) alleles of the zebrafish pax2.1 gene reveals multiple signaling events in development of the midbrain-hindbrain boundary. Development 125, 3049-3062.

Lupo, G., Gestri, G., O'Brien, M., Denton, R.M., Chandraratna, R.A., Ley, S.V., Harris, W.A., Wilson, S.W., 2011. Retinoic acid receptor signaling regulates choroid fissure closure through independent mechanisms in the ventral optic cup and periocular mesenchyme. Proc Natl Acad Sci U S A 108, 8698-8703.

Macdonald, R., Barth, K.A., Xu, Q., Holder, N., Mikkola, I., Wilson, S.W., 1995. Midline signalling is required for Pax gene regulation and patterning of the eyes. Development 121, 3267-3278.

Macdonald, R., Scholes, J., Strahle, U., Brennan, C., Holder, N., Brand, M., Wilson, S.W., 1997. The Pax protein Noi is required for commissural axon pathway formation in the rostral forebrain. Development 124, 2397-2408.

McMahon, C., Gestri, G., Wilson, S.W., Link, B.A., 2009. Lmx1b is essential for survival of periocular mesenchymal cells and influences Fgf-mediated retinal patterning in zebrafish. Dev Biol 332, 287-298.

Mizugishi, K., Aruga, J., Nakata, K., Mikoshiba, K., 2001. Molecular properties of Zic proteins as transcriptional regulators and their relationship to GLI proteins. J Biol Chem 276, 2180-2188.

Morcillo, J., Martinez-Morales, J.R., Trousse, F., Fermin, Y., Sowden, J.C., Bovolenta, P., 2006. Proper patterning of the optic fissure requires the sequential activity of BMP7 and SHH. Development 133, 3179-3190.

Morita, K., Sasaki, H., Fujimoto, K., Furuse, M., Tsukita, S., 1999. Claudin-11/OSP-based tight junctions of myelin sheaths in brain and Sertoli cells in testis. J Cell Biol 145, 579-588.

Nagase, T., Nagase, M., Machida, M., Fujita, T., 2008. Hedgehog signalling in vascular development. Angiogenesis 11, 71-77.

Nornes, H.O., Dressler, G.R., Knapik, E.W., Deutsch, U., Gruss, P., 1990. Spatially and temporally restricted expression of Pax2 during murine neurogenesis. Development 109, 797-809.

Okumura, T., Furuichi, K., Higashide, T., Sakurai, M., Hashimoto, S., Shinozaki, Y., Hara, A., Iwata, Y., Sakai, N., Sugiyama, K., Kaneko, S., Wada, T., 2015. Association

of PAX2 and Other Gene Mutations with the Clinical Manifestations of Renal Coloboma Syndrome. PLoS One 10, e0142843.

Paffett-Lugassy, N.N., Zon, L.I., 2005. Analysis of hematopoietic development in the zebrafish. Methods Mol Med 105, 171-198.

Patel, A., Sowden, J.C., 2019. Genes and pathways in optic fissure closure. Semin Cell Dev Biol 91, 55-65.

Pfeffer, P.L., Gerster, T., Lun, K., Brand, M., Busslinger, M., 1998. Characterization of three novel members of the zebrafish Pax2/5/8 family: dependency of Pax5 and Pax8 expression on the Pax2.1 (noi) function. Development 125, 3063-3074.

Pola, R., Ling, L.E., Silver, M., Corbley, M.J., Kearney, M., Blake Pepinsky, R., Shapiro, R., Taylor, F.R., Baker, D.P., Asahara, T., Isner, J.M., 2001. The morphogen Sonic hedgehog is an indirect angiogenic agent upregulating two families of angiogenic growth factors. Nat Med 7, 706-711.

Pollock, L.M., Perkins, B., Anand-Apte, B., 2020. Primary cilia are present on endothelial cells of the hyaloid vasculature but are not required for the development of the blood-retinal barrier. PLoS One 15, e0225351.

Saint-Geniez, M., D'Amore, P.A., 2004. Development and pathology of the hyaloid, choroidal and retinal vasculature. Int J Dev Biol 48, 1045-1058.

Sanek, N.A., Grinblat, Y., 2008. A novel role for zebrafish zic2a during forebrain development. Dev Biol 317, 325-335.

Sanek, N.A., Taylor, A.A., Nyholm, M.K., Grinblat, Y., 2009. Zebrafish zic2a patterns the forebrain through modulation of Hedgehog-activated gene expression. Development 136, 3791-3800.

Sanyanusin, P., McNoe, L.A., Sullivan, M.J., Weaver, R.G., Eccles, M.R., 1995. Mutation of PAX2 in two siblings with renal-coloboma syndrome. Hum Mol Genet 4, 2183-2184.

Schilling, T.F., Kimmel, C.B., 1994. Segment and cell type lineage restrictions during pharyngeal arch development in the zebrafish embryo. Development 120, 483-494.

Schilling, T.F., Kimmel, C.B., 1997. Musculoskeletal patterning in the pharyngeal segments of the zebrafish embryo. Development 124, 2945-2960.

Schimmenti, L.A., 2011. Renal coloboma syndrome. Eur J Hum Genet 19, 1207-1212.

Sedykh, I., Yoon, B., Roberson, L., Moskvin, O., Dewey, C.N., Grinblat, Y., 2017. Zebrafish zic2 controls formation of periocular neural crest and choroid fissure morphogenesis. Dev Biol 429, 92-104.

Sehgal, R., Karcavich, R., Carlson, S., Belecky-Adams, T.L., 2008. Ectopic Pax2 expression in chick ventral optic cup phenocopies loss of Pax2 expression. Dev Biol

319, 23-33.

Sehgal, R., Sheibani, N., Rhodes, S.J., Belecky Adams, T.L., 2009. BMP7 and SHH regulate Pax2 in mouse retinal astrocytes by relieving TLX repression. Dev Biol 332, 429-443.

Shen, M.C., Ozacar, A.T., Osgood, M., Boeras, C., Pink, J., Thomas, J., Kohtz, J.D., Karlstrom, R., 2013. Heat-shock-mediated conditional regulation of hedgehog/gli signaling in zebrafish. Dev Dyn 242, 539-549.

Swartz, M.E., Nguyen, V., McCarthy, N.Q., Eberhart, J.K., 2012. Hh signaling regulates patterning and morphogenesis of the pharyngeal arch-derived skeleton. Dev Biol 369, 65-75.

Takamiya, M., Stegmaier, J., Kobitski, A.Y., Schott, B., Weger, B.D., Margariti, D., Cereceda Delgado, A.R., Gourain, V., Scherr, T., Yang, L., Sorge, S., Otte, J.C., Hartmann, V., van Wezel, J., Stotzka, R., Reinhard, T., Schlunck, G., Dickmeis, T., Rastegar, S., Mikut, R., Nienhaus, G.U., Strahle, U., 2020. Pax6 organizes the anterior eye segment by guiding two distinct neural crest waves. PLoS Genet 16, e1008774.

Tao, C., Zhang, X., 2014. Development of astrocytes in the vertebrate eye. Dev Dyn 243, 1501-1510.

Tiwari-Woodruff, S.K., Buznikov, A.G., Vu, T.Q., Micevych, P.E., Chen, K., Kornblum, H.I., Bronstein, J.M., 2001. OSP/claudin-11 forms a complex with a novel member of the tetraspanin super family and beta1 integrin and regulates proliferation and migration of oligodendrocytes. J Cell Biol 153, 295-305.

Torres, M., Gomez-Pardo, E., Gruss, P., 1996. Pax2 contributes to inner ear patterning and optic nerve trajectory. Development 122, 3381-3391.

Trainor, P.A., Krumlauf, R., 2001. Hox genes, neural crest cells and branchial arch patterning. Curr Opin Cell Biol 13, 698-705.

Van Der Meulen, K.L., Vocking, O., Weaver, M.L., Meshram, N.N., Famulski, J.K., 2020. Spatiotemporal Characterization of Anterior Segment Mesenchyme Heterogeneity During Zebrafish Ocular Anterior Segment Development. Front Cell Dev Biol 8, 379.

Varga, Z.M., Amores, A., Lewis, K.E., Yan, Y.L., Postlethwait, J.H., Eisen, J.S., Westerfield, M., 2001. Zebrafish smoothened functions in ventral neural tube specification and axon tract formation. Development 128, 3497-3509.

Wada, N., Javidan, Y., Nelson, S., Carney, T.J., Kelsh, R.N., Schilling, T.F., 2005. Hedgehog signaling is required for cranial neural crest morphogenesis and chondrogenesis at the midline in the zebrafish skull. Development 132, 3977-3988.

Weaver, M.L., Piedade, W.P., Meshram, N.N., Famulski, J.K., 2020. Hyaloid vasculature and mmp2 activity play a role during optic fissure fusion in zebrafish. Sci

Rep 10, 10136.

Weiss, O., Kaufman, R., Mishani, E., Inbal, A., 2017. Ocular vessel patterning in zebrafish is indirectly regulated by Hedgehog signaling. Int J Dev Biol 61, 277-284.

Wen, W., Pillai-Kastoori, L., Wilson, S.G., Morris, A.C., 2015. Sox4 regulates choroid fissure closure by limiting Hedgehog signaling during ocular morphogenesis. Dev Biol 399, 139-153.

Westerfield, M., 1993. The zebrafish book : a guide for the laboratory use of zebrafish (Brachydanio rerio). M. Westerfield, Eugene, OR.

Wiegering, A., Petzsch, P., Kohrer, K., Ruther, U., Gerhardt, C., 2019. GLI3 repressor but not GLI3 activator is essential for mouse eye patterning and morphogenesis. Dev Biol 450, 141-154.

Williamson, K.A., FitzPatrick, D.R., 2014. The genetic architecture of microphthalmia, anophthalmia and coloboma. Eur J Med Genet 57, 369-380.

Xie, J., Farage, E., Sugimoto, M., Anand-Apte, B., 2010. A novel transgenic zebrafish model for blood-brain and blood-retinal barrier development. BMC Dev Biol 10, 76.

Zhao, L., Zevallos, S.E., Rizzoti, K., Jeong, Y., Lovell-Badge, R., Epstein, D.J., 2012. Disruption of SoxB1-dependent Sonic hedgehog expression in the hypothalamus causes septo-optic dysplasia. Dev Cell 22, 585-596.

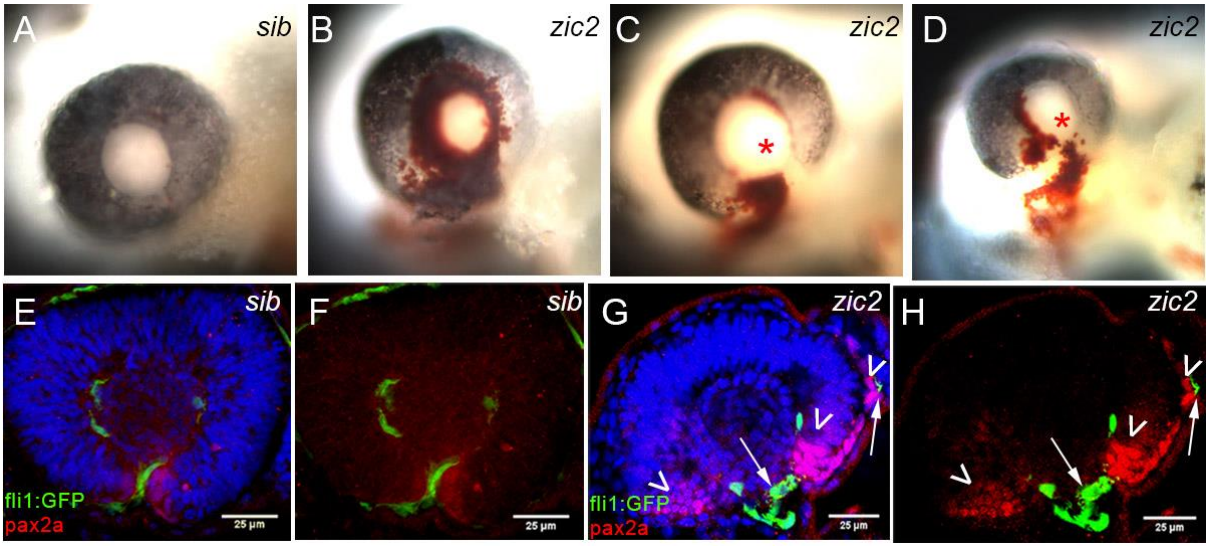

Figure 1. *Zic2 mutants exhibit ocular coloboma and hemorrhage.*

Embryos derived from *zic2a*^{gbt133}/+ ; *zic2b*^{t104} parents were stained with o-dianisidine to visualize the hemoglobinized red blood cells at 3 dpf (A-D) and those from *zic2a*^{gbt133}/+; *zic2b*^{t104}; *Tg(fli1:GFP/+)* parents were immunostained for GFP and *pax2a* at 28 hpf (E-H). A: Normal retina morphology. B-D: *Zic2* mutants exhibit intraocular hemorrhaging (B), coloboma (asterisk) with periocular (C) or both periocular and intraocular hemorrhaging (D). E, F: Single confocal stack of representative normal retina. G, H: Single confocal stack of representative *zic2* mutant retina. *Zic2* mutants exhibit abnormal *pax2a* expansion (arrowhead) and ectopic hyaloid vessel clustering ventrally and periocularly (arrow). red = *pax2a*; green = *fli1:GFP*; cyan = nuclei visualized by DAPI. All embryos are shown in lateral views, anterior to the left.

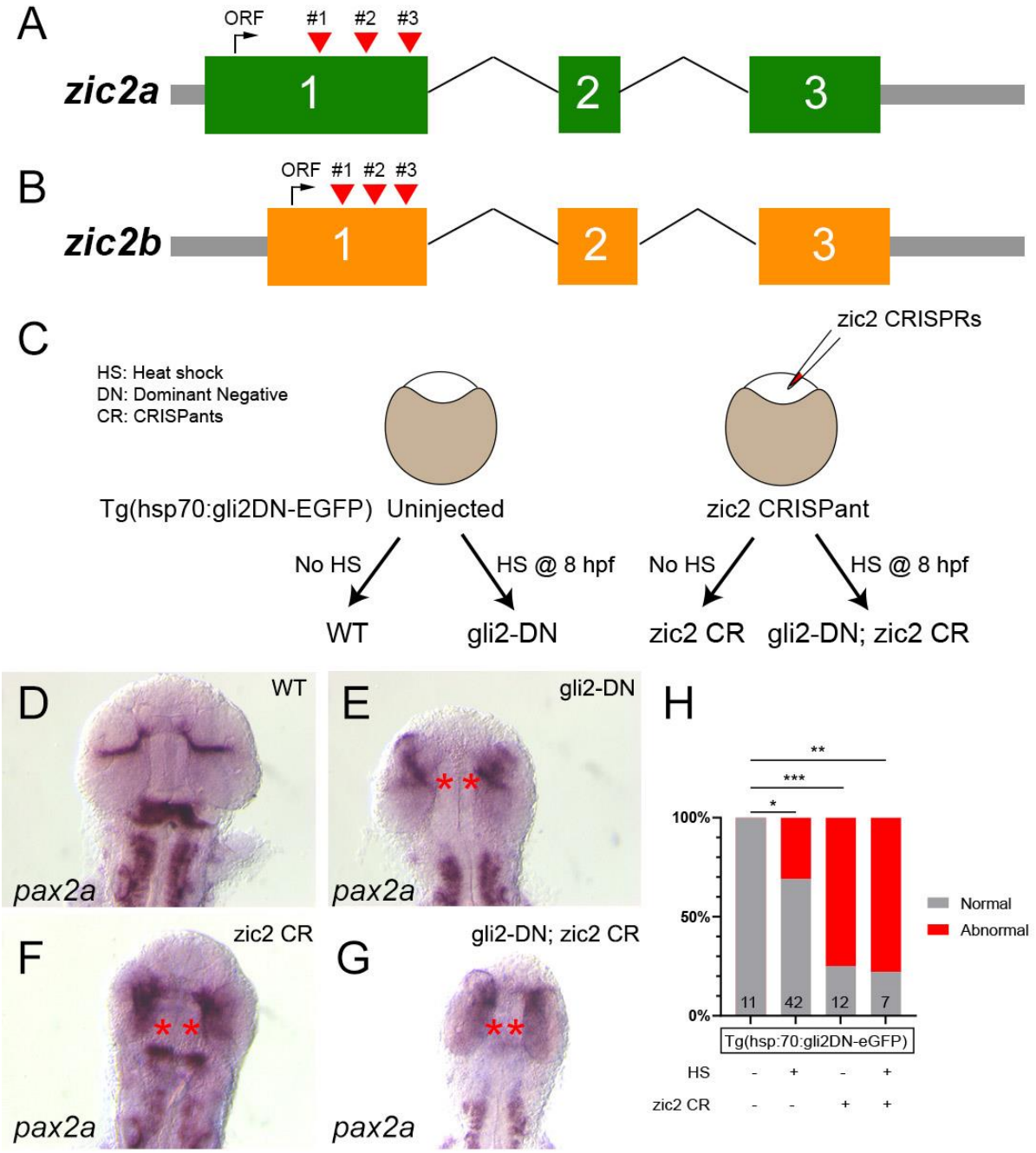

Figure 2. *Zic2 interacts with gli2 to restrict pax2a transcription at optic stalk*.

A, B: CRISPRs were designed to target three sites in exon 1 of *zic2a* locus (A) and three sites in exon 1 of *zic2b* locus (B). C: Schematic of the heat shock treatment between uninjected and zic2 CRISPants. D – G: Embryos were stained for *pax2a* expression using whole mount *in situ* hybridization (WISH) at 24 hpf. D: Normal

embryos have *pax2a* expression restricted at optic stalk (n = 11/11). E – G: *gli2*-DN (E, n = 13/42), *zic2* CRISPants (F, n = 9/12), and *gli2*-DN; *zic2* CRISPants (G, n = 5/7) have mispatterned *pax2a* expression (asterisk). H: Comparison of WT with *gli2*-DN, *zic2* CRISPants, and *gli2*-DN; *zic2* CRISPants (1 trial). WT – *gli2*:DN: p = 0.0474, WT – *zic2* CR: p = 0.0003, WT – *gli2*:DN; *zic2*-CR: p = 0.0025. P-values were calculated using Fisher's exact test.

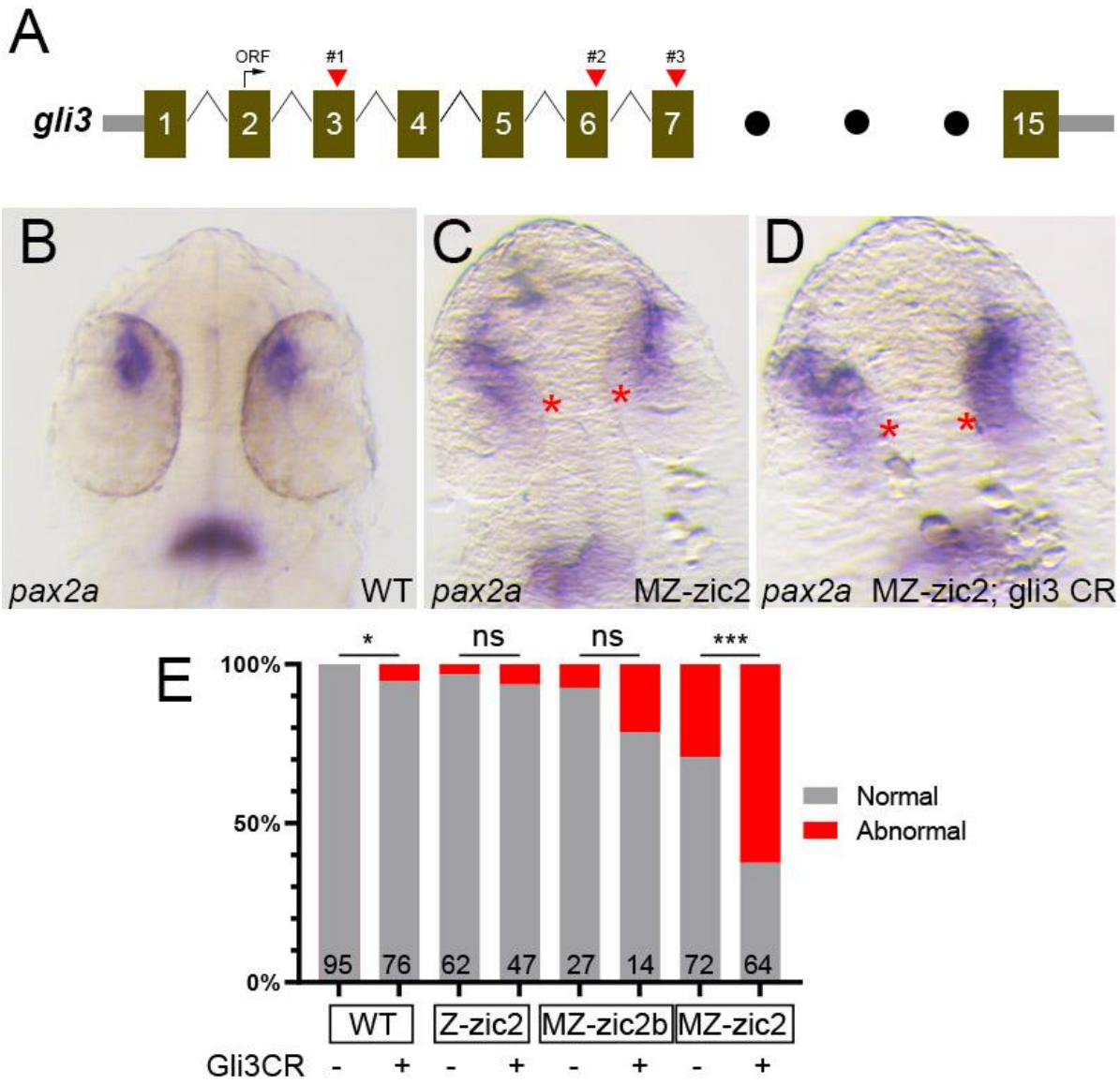

Figure 3. *Zic2 interacts with gli3 to restrict pax2a transcription at optic stalk*.

A: CRISPRs were designed to target three sites in exon 3, exon 6, and exon 7 of gli3 locus. B-E: Embryos derived from WT, *zic2a*^{gbt133}*/+; zic2b*^{t104}*/+* (Z-*zic2*), *zic2b*^{t104} (MZ-*zic2b*), or *zic2a*^{gbt133}*/+; zic2b*^{t104} (MZ-*zic2*) incrosses were injected with gli3 CRISPRs at one cell stage and stained for *pax2a* using WISH at 24 hpf. B: Normal embryos have *pax2a* expression restricted at optic stalk (n = 95/95). C,D: MZ-*zic2b* (B; n= 3/14) and MZ-*zic2* (C; n = 40/64) have mispatterned *pax2a* expression (asterisk). All

embryos are shown in ventral views, anterior to the top. E: Comparison between uninjected and CRISPants from each group. WT: p = 0.0373, 3 trials; Z-*zic2*: p = 0.6501, 2 trials; MZ-*zic2b*: p = 0.3170, 2 trials; MZ-*zic2*: p = 0.0001, 3 trials. P-values were calucluated using Fisher's exact test.

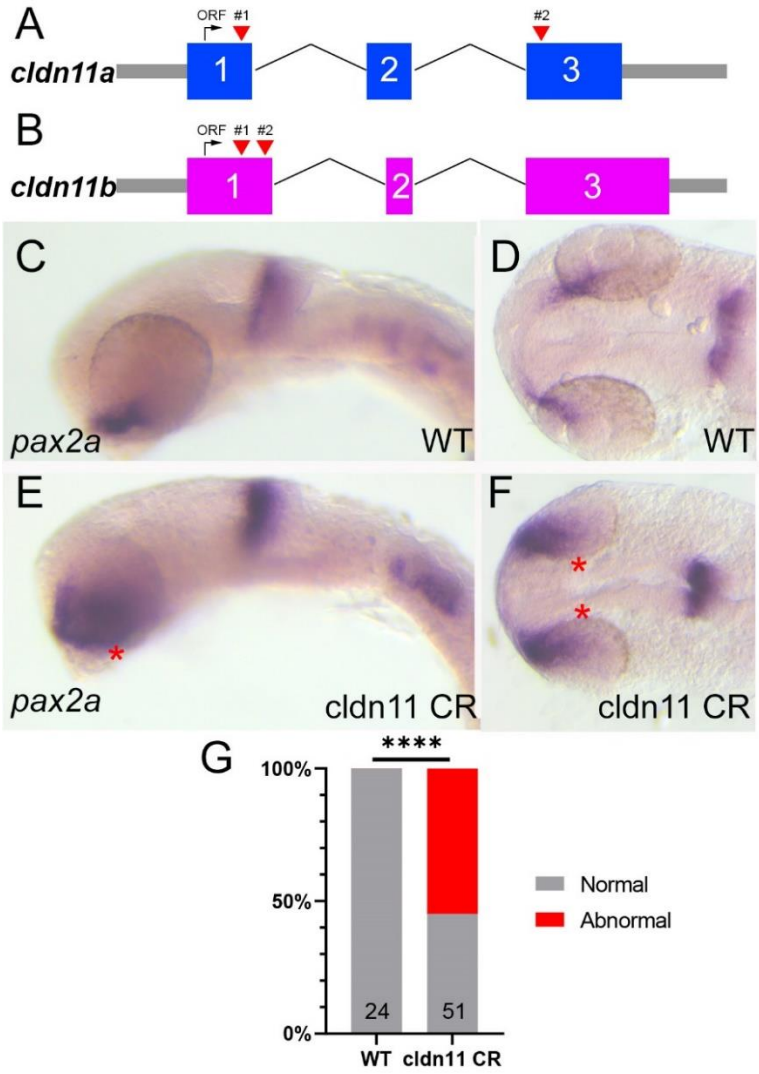

Figure 4. *cldn11a regulates pax2a transcription.*

A, B: CRISPRs were designed to target two sites in exon 1 and exon 3 of *cldn11a* locus (A) and two sites in exon 1 of *cldn11b* locus (B). Embryos derived from WT crosses were injected with *cldn11a* and *cldn11b* CRISPRs (*Cldn11* CRISPants) at one cell stage and stained for *pax2a* using WISH at 24 hpf. C, D: WT embryos have normal *pax2a* expression at optic stalk (n = 24/24). E, F: Cldn11 CRISPants develop with ectopic expansion of *pax2a* expression (arrowheads) (n = 28/51). G: *Cldn11* CRISPants develop with significantly abnormal *pax2a* expression (****: $p < 0.0001$, Fisher's exact test, 1 trial).

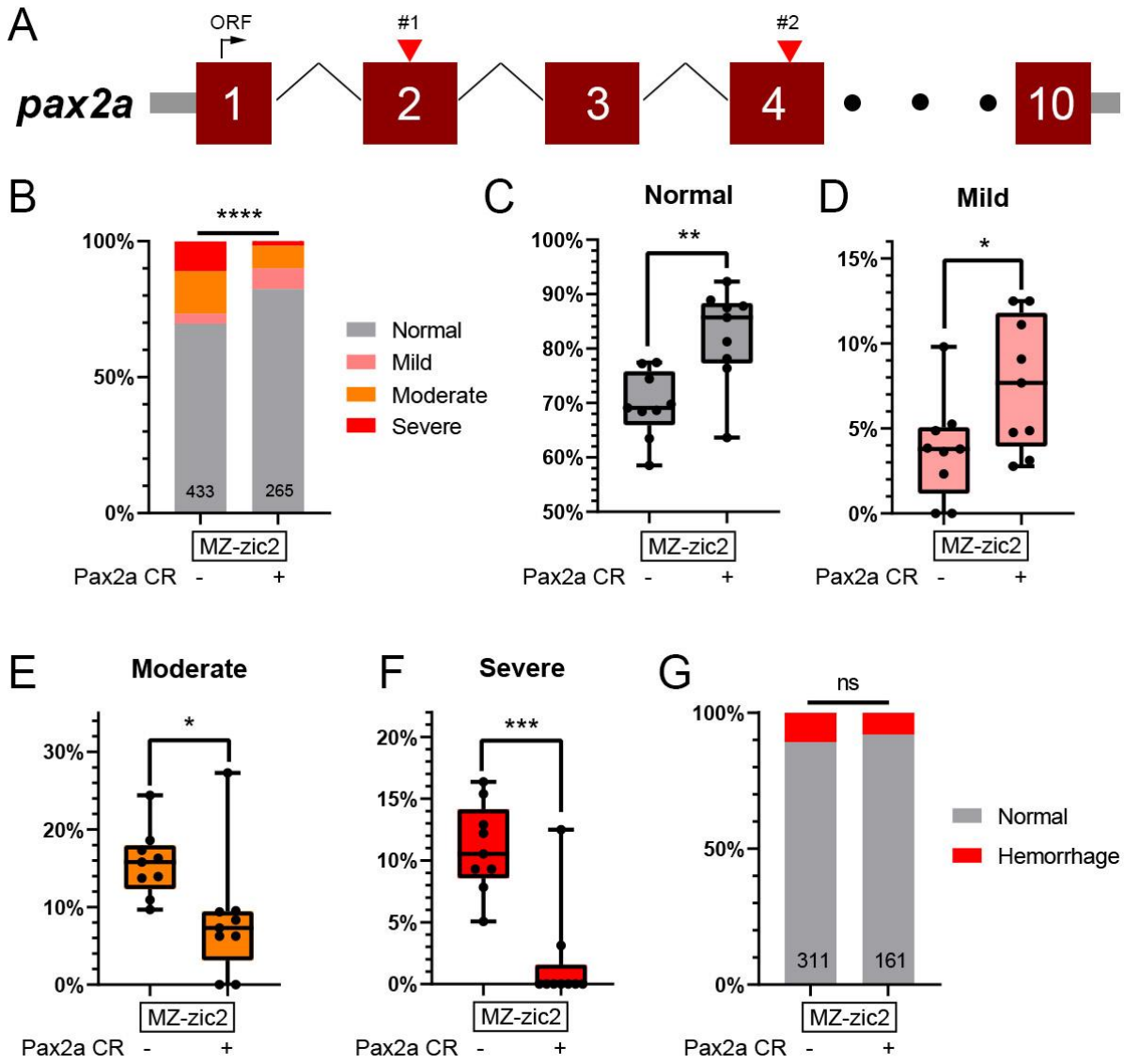

Figure 5. *Pax2a depletion rescues retinal coloboma but not hemorrhaging in zic2 mutants.*

A: CRISPRs were designed to target two sites in exon 2 and exon 4 of *pax2a* locus. B-G: Embryos derived from zic2b^{t104}; zic2a^{gbt133}/+ parents were injected with pax2a CRISPRs, stained with o-dianisidine at 3 dpf and scored for coloboma and hemorrhaging. Embryos with unilateral mild coloboma were scored as “mild”; embryos with bilateral mild coloboma were scored as “moderate”, and embryos with bilateral

moderate coloboma were scored as “severe.” B: Both penetrance and expressivity of coloboma decrease in *zic2*; *pax2a* CRISPant (****: $p < 0.0001$; Chi-square test; 9 trials). C: The penetrance of normal retinal morphology significantly increases in zic2 mutant; pax2a CRISPant (**: $p = 0.003$; Welch’s t-test; 9 trials). D: The penetrance of mild coloboma significantly increases in *zic2*; *pax2a* CRISPant (*: $p = 0.0313$; Welch’s t-test; 9 trials). E: The penetrance of moderate coloboma significantly decreases in *zic2*; *pax2a* CRISPant (*: $p = 0.0313$; Welch’s t-test; 9 trials). F: The penetrance of severe coloboma significantly decreases in *zic2*; *pax2a* CRISPant (***: $p = 0.0001$; Welch’s t-test; 9 trials). G: The penetrance of hemorrhaging does not significantly decrease in *zic2* mutant; *pax2a* CRISPant (ns: $p = 0.1082$; Fisher’s exact test; 7 trials).

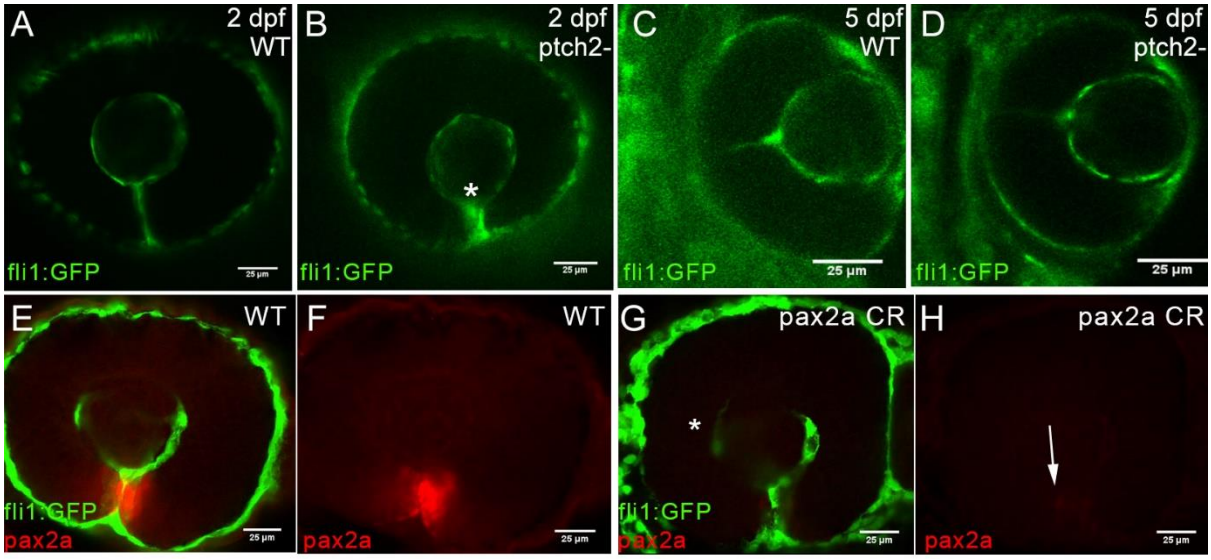

Figure 6. *Pax2a function is required for hyaloid vasculature development.*

Embryos derived from *ptch2 +/-; Tg(fli1:GFP)* incross (A-D) or *Tg(fli1:GFP) were* injected with pax2a CRISPRs (E-H) and immunostained for GFP. (A-D) *Fli1:GFP*, an endothelial marker, was visualized in both normal siblings (A and C) and *ptch2* mutants (B and D) at 2 dpf and 5 dpf. Normal siblings developed with normal hyaloid vessels at 2 dpf (A) and 5 dpf (C), while *ptch2* mutants developed with mild coloboma (asterisk in B, n = 4/4) at 2 dpf, hyaloid vessel formation is normal at both stages (B and D). (E-H) Both uninjected and *pax2a* CRISPants were stained for GFP (*fli1*) and *pax2a* at 28 hpf. Uninjected embryos have normal hyaloid loop formation (E, n = 2/2) and *pax2a* expression (F, n = 2/2). Pax2a CRISPants have partially incomplete hyaloid loop formation (G, asterisk, n = 4/5) and no *pax2a* expression (H, arrow, n = 5/5). green = *fli1:GFP*, red = *pax2a*. Embryos are shown in lateral views, anterior to the left (A, B, E-H) or in ventral views with anterior to the top (C, D).

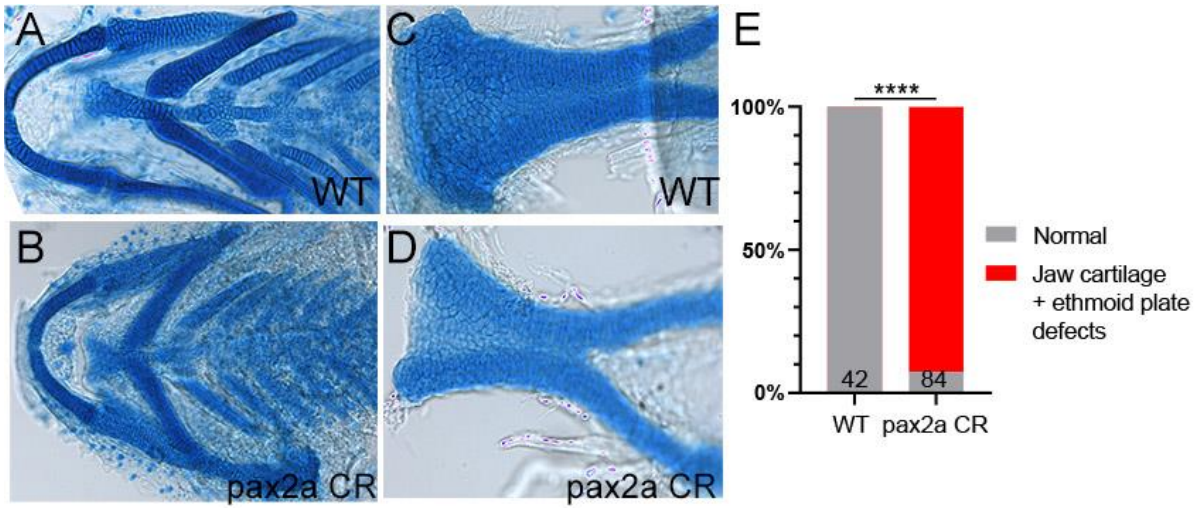

Figure 7. *Pax2a function is required for craniofacial cartilage development*.

Embryos derived from WT were injected with *pax2a* CRISPRs at one cell stage and stained for alcian blue to visualize craniofacial cartilage at 5 dpf. Embryos were dissected to visualize jaw cartilages (A, B) and ethmoid plates (C,D). A: Normal jaw cartilages in WT. B: Jaw cartilages are reduced in *pax2a* CRISPants. C: Normal ethmoid plates in WT. D: The anterior element of ethmoid plates is reduced or truncated in *pax2a* CRISPants. E: Both jaw cartilages and ethmoid plates are significantly abnormal in *pax2a* CRISPants. (****: $p < 0.0001$, Fisher's exact test, 2 trials).

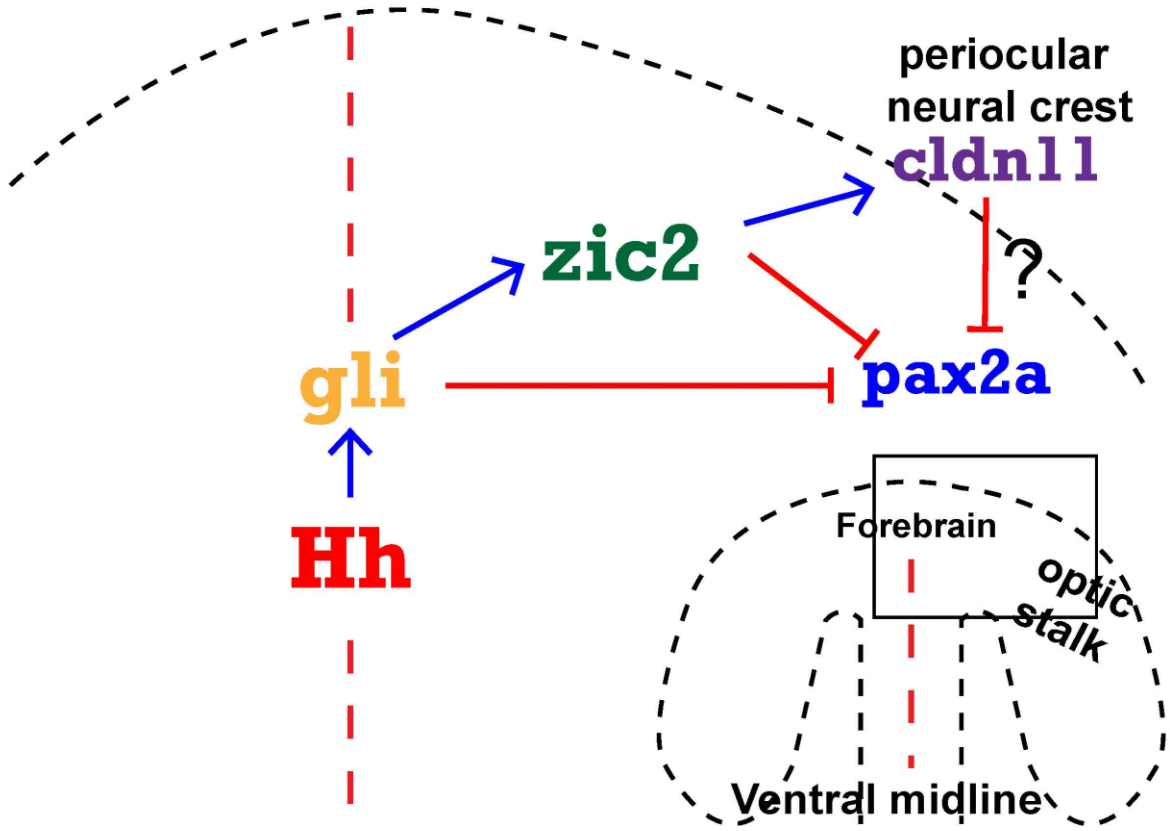

Figure 8. A model of *pax2a* regulation in the zebrafish optic stalk

Pax2a expression is restricted at optic stalk by two different genetic mechanisms: (1) *gli2/3* expressed in ventral forebrain inhibits *pax2a* transcription along with *zic2*. (2) *zic2* activates *cldn11*, a potential periocular neural crest marker, which subsequently inhibits *pax2a* transcription.

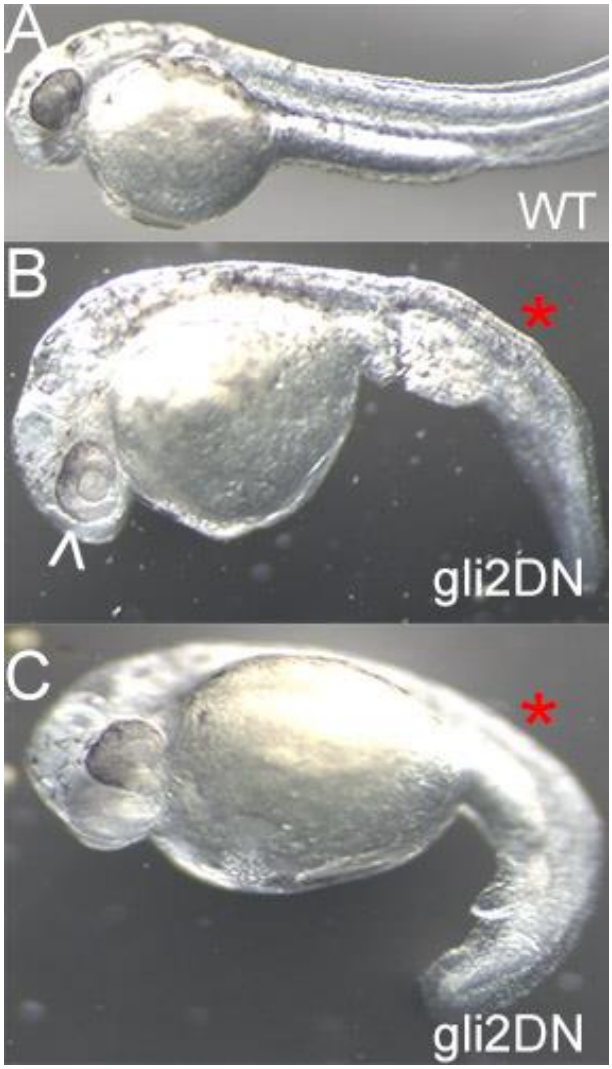

Supplementary Figure 1. *Heat shock inducible repression of Hh signaling*

Tg(hsp70l:gli2aDR-GFP) embryos were treated with 37°C heat shock at 8 hpf for an hour and imaged at 2 dpf. A: WT embryos without heat shock develop normally (n = 95/95, 2 trials). B-C gli2-DN embryos develop with U-shaped somites (asterisk; n= 101/115) and some without pigment at the eye (arrowhead in B; n = 19/101) (2 trials). Embryos are shown in lateral view, anterior to the left.

Supplementary Figure 2. *Cldn11 CRISPR efficacy*

A-C: WT embryos were injected with *cldn11a* + *cldn11b* CRISPRs (*cldn11* CRISPants) at one cell stage and imaged in group at 5 dpf for craniofacial defects. A: All WT embryos have normal craniofacial and ocular morphology (n = 24/24, 1 trial). B, C: *Cldn11* CRISPants with normal (B; n = 18/42) or abnormal craniofacial and ocular (C; n = 24/42) morphology (1 trial).

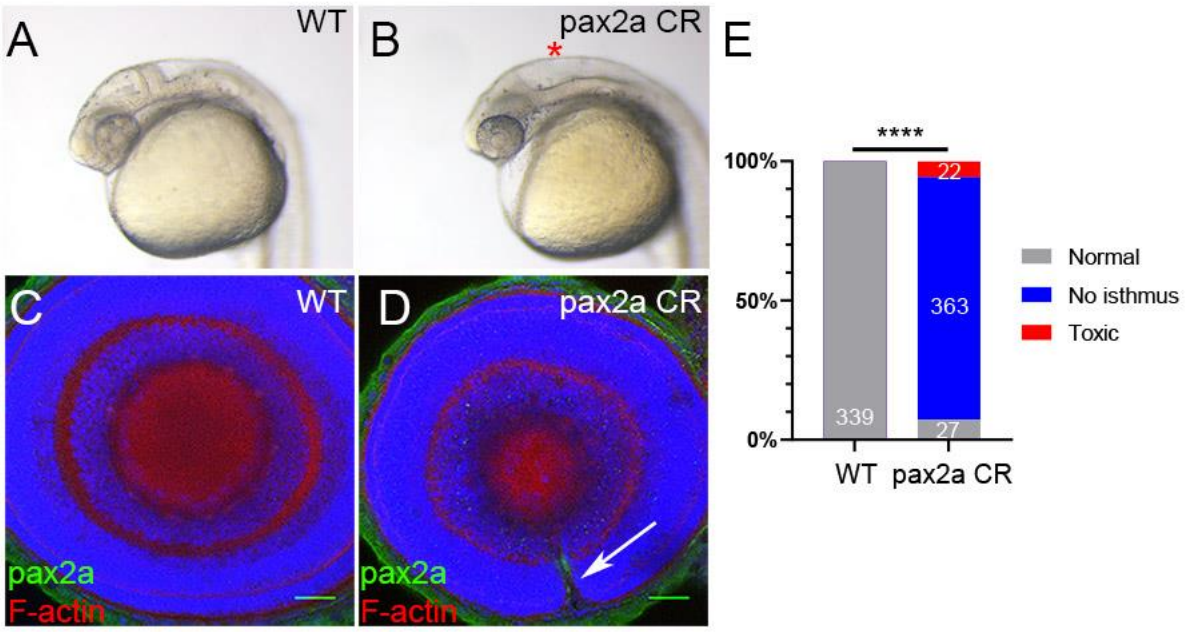

Supplementary Figure 3. *Pax2a CRISPRs effectively mutagenize pax2a in somatic cells.*

A, B: At 1 dpf, injected embryos were scored for the presence of midbrain-hindbrain boundary to determine efficacy of somatic mutagenesis. *Pax2a* CRISPants develop no midbrain-hindbrain boundary (no isthmus; noi) (asterisk in B). C, D: Single confocal stack through representative retina of normal (C) and *pax2a* CRISPants (D) at 2.5 dpf. *Pax2a* CRISPants exhibit coloboma (white arrow). Green = *pax2a*, Red = F-actin visualized by phalloidin, Blue = nuclei visualized by DAPI. Scale bar = 25 um. F: All the uninjected embryos develop normally while 88% of *pax2a* CRISPants develop no isthmus (****: $p < 0.0001$; Chi-square test, 6 trials). Embryos are shown in lateral view, anterior to the left.

CRISPR	Sequence	Source
pax2a CRISPR #1	ATCGTGGAGCTCGCACACCA	IDT
pax2a CRISPR #2	CACCATCCTCCGACGGCAC	
cldn11a CRISPR #1	AGGGGTTGTGGGCAGACTGT	
cldn11a CRISPR #2	CTGTGTGGTTTCCCATCGGG	
cldn11b CRISPR #1	CGCGACCTCCACAAATGATT	
cldn11b CRISPR #2	GGAGACCAAAGGCTTGTGGA	
zic2a CRISPR #1	AGATGCGACTCGGACTACCA	
zic2a CRISPR #2	AAGGTGCCCACTCCCAAACC	
zic2a CRISPR #3	CAAGGCCACATTCTGTTCCC	
zic2b CRISPR #1	TCACCAGGTGCCCAATACGC	
zic2b CRISPR #2	GTAGGTGACCCTGACCTTCT	
zic2b CRISPR #3	TAGGGGTTGGCACGTTCACA	
gli3 CRISPR #1	CGGTTTATCAGCCTAGGACT	Synthego
gli3 CRISPR #2	CCCTCAGTGGGGTCCACAAC	
gli3 CRISPR #3	GACCACACCCTGCCCTATCG	

Table 1. *CRISPR sequence information*

Chapter V

Summary and Future Directions

In the preceding chapters, I discussed several genetic controls regulating vertebrate ocular and craniofacial cartilage development (Fig. 1). Chapter 2 focused on *zic2*. We showed that zebrafish zic2 mutants develop with several craniofacial complex defects. This led us to hypothesize that *zic2* is required for ventral retina morphogenesis through restricting *pax2a*, a Hh-downstream target. Through RNA sequencing analysis, we found that *zic2* activates *alx1* transcription at the periocular neural crest. We also found that *zic2* activates *cldn11a* transcription at the anterior to the retina where the periocular neural crest is likely populated. This work begins to elucidate the molecular mechanism of how *zic2* regulates ventral retina morphogenesis and illustrates a novel role of *zic2* for periocular neural crest formation.

Chapter 3 focused on the alx gene family. We presented two zebrafish models (*alx1* mutants and *alx1; alx3* double mutants). Both *ALX1* mutation in humans and *alx1* zebrafish mutants are associated with ocular defects. To investigate the genetic interaction among the alx gene family, *alx1; alx3* double mutants were generated. *Alx1; alx3* double mutants develop with truncated ethmoid plates resulting from abnormal migration of the anterior neural crest. Along with craniofacial abnormalities, *alx1; alx3* double mutants also develop with ocular defects. Despite ocular defects, we found that *alx1; alx3* double mutant embryos develop with normal retinal function. Through ethanol exposure at early embryonic stages, we identified that *alx1* protects the neural crest from environmental perturbations. This work establishes the first zebrafish alx model for dissecting conserved genetic-environmental interactions during craniofacial complex development.

Chapter 4 focused on *pax2a*. *Pax2a* transcription at the optic stalk is restricted by *zic2* in two different genetic mechanisms: cooperative inhibition through the

interaction between zic2 and gli proteins, Hh signaling mediators, and inhibition by *cldn11*, which is activated by *zic2*. Coloboma in *zic2* mutants was rescued after reduction of *pax2a* transcription. We identified that *pax2a* function is required for hyaloid vascular formation and craniofacial cartilage development. This work dissects the genetic regulatory mechanisms of *pax2a* transcription and demonstrates the role of *pax2a* during ocular development. In addition, this work characterizes a novel requirement of *pax2a* function for craniofacial development.

In this final chapter, I address some of the most urgent questions raised by this work and provide suggestions for future experiments.

How does the alx gene family mediate the role of zic2 in craniofacial complex development?

In chapter 3, we showed that both anterior neural crest (aCNC)-derived structures (anterior neurocranium and anterior segment of the eye) are aberrantly formed in *alx1; alx3* double mutants. Through lineage tracing experiment, we identified that aCNC abnormally migrates in the absence of normal *alx1* and *alx3* function, suggesting that *alx1* and *alx3* control craniofacial complex development through regulating aCNC migration. To further elucidate an early requirement of the alx gene family for aCNC migration, *alx1* knock-in reporter will be introduced to *Tg(sox10:GFP)* zebrafish line, which labels the neural crest (Clay and Halloran, 2013), using GeneWeld targeted integration (Wierson et al., 2020). This knock-in zebrafish line will be useful to observe an early migration pattern of *alx1*-expressing aCNC through live

imaging between 13 hpf (hours post fertilization), when aCNC begins migration (Rocha et al., 2020), and 24 hpf, when aCNC passes the optic stalk to localize at presumptive anterior neurocranium (Eberhart et al., 2008). Introducing *alx3*, *alx4a*, or *alx4b* knock-in reporter to *Tg(sox10:GFP)* will be helpful to further elucidate where each alx gene is expressed during aCNC migration.

To fully understand the functional interactions among the alx gene family, it is ideal to knock out the entire alx gene family. Because both *alx1* mutant and *alx1; alx3* double mutant embryos do not fully recapitulate ocular defects found in *ALX1*-related FND patients, such as microphthalmia and retinal coloboma, we hypothesize that the zebrafish alx gene family functionally compensates for early ocular morphogenesis. We are currently generating *alx1; alx3; alx4a; alx4b* mutant/CRISPant hybrids through mutagenizing both *alx3* and *alx4a* alleles in already established *alx1; alx4b* double mutants. We are expecting to observe early ocular defects in *alx1; alx3; alx4a; alx4b* mutant/CRISPant hybrids that are comparable to those found in human ALX-related FND if our hypothesis is true.

To further dissect the genetic regulation of the alx gene family for craniofacial and anterior segment development, it is necessary to perform RNA-seq analysis on *alx1; alx3* double mutants and investigate the role of *alx1* and *alx3* during early neural crest migration. To identify the downstream effectors of *alx1* and *alx3*, embryos derived from *alx1; alx3/+* parental incross will be used and lysed at 16 hpf and 24 hpf, two representative developmental stages when aCNC migrates anteriorly from the dorsal surface to the eye (DeLaurier et al., 2012) and aCNC populates at optic stalk and localizes at presumptive anterior neurocranium (Eberhart et al., 2008), respectively. Because *alx1; alx3* double mutants do not exhibit obvious phenotypes until 3 dpf (days

post fertilization), a lot of individual embryos at 16 hpf and 24 hpf will be sequenced and their genotypes will be deduced from *alx3* transcriptional level. Both *alx1* and *alx3* are expressed in chondrogenic and periocular neural crest in zebrafish (Dee et al., 2013; Sedykh et al., 2017). This led us to hypothesize that alx gene family directly controls craniofacial development through regulating chondrogenic neural crest development and indirectly regulates ocular development through functioning in periocular neural crest development. Identifying the downstream chondrogenic and periocular neural crest markers through RNA-seq will test this hypothesis.

How does pax2a control neural crest migration and craniofacial complex development?

In chapter 4, we showed that both anterior neurocranium and jaw cartilage are aberrantly formed in *pax2a* CRISPants, suggesting that *pax2a* function may be required for cranial neural crest migration. Because *pax2a* is not expressed in the neural crest, we hypothesize that *pax2a* regulates cranial neural crest lineages in a non-cell-autonomous manner. To investigate whether *pax2a*-expressing optic stalk and/or midbrain-hindbrain boundary interacts with cranial neural crest, *pax2a* knock-in reporter will be introduced to *Tg(sox10:GFP*) zebrafish line. This zebrafish line will be used to elucidate when and where the cranial neural crest interacts with *pax2a*-expressing optic stalk and/or midbrain-hindbrain boundary through live imaging between 13 hpf and 24 hpf.

Pax2a CRISPants develop with abnormal ethmoid plates and jaw cartilages, which led us to hypothesize that *pax2a* function is required for correct cranial neural

crest migration. In order to test this, a lineage tracing experiment will be performed on *Tg(sox10:kaede)* zebrafish line (Dougherty et al., 2012) injected with *pax2a* CRISPRs. Photoconverted cranial neural crest populated in anteromost domain at 10 cell stage migrates to the median element of the anterior neurocranium at 4 dpf while photoconverted cranial neural crest in the first pharyngeal arch migrates to jaw elements of the pharyngeal arches at the same developmental stages (Dougherty et al., 2012). If our hypothesis is correct, cranial neural crest ectopically migrates in *pax2a* CRISPants.

While we showed that *pax2a* is required for the optic stalk and ventral retinal morphogenesis, how *pax2a* regulates this process remains elusive. Therefore, it is critical to investigate the downstream effectors of *pax2a* that are specifically expressed at the optic stalk and choroid fissure. *Pax2a* CRISPRs will be injected into WT embryos. At 24 hpf, RNA will be extracted for RNA-seq and the transcriptional level will be compared between uninjected siblings and *pax2a* CRISPants to find out potential candidate target genes of *pax2a.*

How do zic2 and the alx gene family regulate hyaloid vasculature development?

In chapter 2 and 4, we showed that *zic2* mutants develop with periocular and/or intraocular hemorrhaging. Although *zic2* expression has not been reported in endothelial cells, it is possible that it is expressed there at low levels or transiently. Thus, it is premature to rule out a cell-autonomous *zic2* function in endothelial lineage. To test this, we propose a rescue experiment. *Tg(UAS:zic2a-YFP),* which allows for

zic2a overexpression by introducing tissue-specific Gal4 (Teslaa et al., 2013), will be introduced into *zic2* mutant background. *Tg(kdrl:Gal4),* which is restricted to the endothelium (Totong et al., 2011; Uemura et al., 2016), will be introduced into *Tg(UAS:zic2a-YFP);zic2* embryos. This will lead to specific expression of *zic2a* only in the endothelium. The embryos will be examined for (1) expression of *zic2a-YFP* and (2) hemorrhage and vascular network using the o-dianisidine assay at 3 dpf and alkaline phosphatase assay at 5 dpf to determine if *zic2a* expressed in endothelium is sufficient to rescue periocular and intraocular hemorrhaging.

It is also possible that *zic2* regulates hyaloid vasculature development indirectly via a primary function in the periocular neural crest. In chapter 3, our data indicated that *alx1* mutants and *alx1; alx3* double mutants exhibited periocular and intraocular hemorrhaging, reminiscent of the phenotypes shown in *zic2* mutants (chapter 2, 4). We also showed that some *alx1; alx3* heterozygotes and all *alx1; alx3* double mutants develop with aberrant hyaloid vasculature network. Because *zic2* promotes *alx1* in periocular neural crest (Sedykh et al., 2017) and abnormal hyaloid vasculature formation can result from underpopulated vascular pericytes, which stabilize vascular endothelium (Jo et al., 2013), we hypothesize that the alx gene family regulates vascular pericyte development. To test this hypothesis, *alx1* or *alx3* knock-in reporter will be introduced into *Tg(pdgfrb:mCherry*) zebrafish line, which visualizes vascular pericytes by 3 dpf (Ando et al., 2016). This will allow us to examine if *alx1*-expressing or *alx3*-expressing periocular neural crest differentiates to vascular pericytes. If *alx1* and/or *alx3*-expressing periocular neural crest differentiates to vascular pericytes, *Tg(pdgfrb:mCherry*); *alx1; alx3* double mutants will be generated to investigate whether *alx1* and *alx3* function are required for vascular pericyte

development. The vascular pericyte population at 3 dpf will be compared and embryos will be genotyped post-hoc. If our hypothesis is correct, we are expecting to observe a significant reduction of vascular pericytes in *alx1; alx3* double mutants.

How do pax2a and cldn11a regulate hyaloid vasculature development?

In chapter 4, I showed that pax2a CRISPants develop with improper hyaloid vasculature formation. While a recent finding suggests that *pax2a* is necessary for hyaloid vasculature recruitment (Weaver et al., 2020), whether *pax2a* exerts its function for vascular integrity has not been characterized. Although *cldn11* has structural similarity with other claudin gene family such as *cldn5*, expressed in hyaloid vasculature (Xie et al., 2010), and zebrafish *cldn11a* was initially reported as a vascular endothelial marker (Cannon et al., 2013), it is unknown whether *cldn11* is required for hyaloid vasculature. In both *pax2a* CRISPants and *cldn11* CRISPants, alkaline phosphatase will be stained at 5 dpf to observe the hyaloid vascular network. If there is a defect, *pax2a* or *cldn11* will be mutagenized in *Tg(pdgfrb:mCherry*) zebrafish line (Ando et al., 2016) and the vascular pericyte population in each CRISPant will be examined. As a quantitative analysis, some of the known hyaloid vasculature markers, such as *tln1*, a regulator for vascular endothelium migration through choroid fissure (James et al., 2016), cldn5, a tight junction protein of hyaloid vasculature (Xie et al., 2010), and VEGF, a growth factor for vascular endothelium (Garcia et al., 2009), will be quantified and analyzed through qPCR analysis in *pax2a* CRISPants and *cldn11* CRISPants.

How does the alx gene family protect aCNC lineages from oxidative stress?

The interaction between the alx gene family and environment has not been characterized until recently when *alx3* was found to promote *foxo1*, which subsequently activates oxidative stress defense mechanism against hyperglycemia in mouse (Garcia-Sanz et al., 2017). In chapter 3, we showed that ethanol exposed *alx1* mutant embryos develop with more penetrant ocular and craniofacial defects, suggesting *alx1* function for protecting aCNC lineages against oxidative stress. Because oxidative stress disrupts the survival of the neural crest by triggering neural crest cell death (Wang et al., 2015), we hypothesize that *alx1* function is required to prevent neural crest cell death in response to oxidative stress. To test this hypothesis, embryos derived from *Tg(sox10:GFP)* and *alx1; Tg(sox10:GFP)* will be exposed with ethanol and stained for GFP and activated caspase 3, an apoptotic cell marker (Sorrells et al., 2013). Through colocalization analysis, the number of dead neural crest cells between ethanol exposed and unexposed groups will be scored. If our hypothesis is correct, we are expecting to observe an extensive neural crest cell death in ethanol exposed *alx1* mutants.

Because oxidative stress also diminishes the production of antioxidant genes from neural crest (Wentzel and Eriksson, 2011), we hypothesize that *alx1* promotes an oxidative stress defense mechanism. The simplest approach to test this hypothesis is to incubate *alx1* mutants in antioxidants. We are currently treating ethanol exposed and unexposed *alx1* mutants with methylene blue (Vaccaro et al., 2012) and unexposed *alx1* mutants with vitamin C (Xiang et al., 2018) to observe if the ocular

and craniofacial defects in *alx1* mutants are alleviated after antioxidant treatment. However, the expressivity and the penetrance of ocular and craniofacial defects in *alx1* mutants were not significantly reduced after introducing antioxidants. These data are preliminary and will be confirmed in additional trials. As an alternative approach, RNA-seq analysis will be done on *alx1* mutants exposed with or without ethanol at multiple developmental stages ranged from 2 dpf to 5 dpf. Analysis of oxidative stress defense mechanism regulators, such as *foxo1* (Garcia-Sanz et al., 2017), *nrf2* (nuclear factor erythroid 2-related factor) (Hahn et al., 2015), and *oxr1* (oxidation resistance gene 1) (Xu et al., 2020), and antioxidant genes, such as *Gpx* (glutathione peroxidase), *Cat* (catalase), *Gst* (gluthione-S-transferase) and *SOD* (superoxide dismutase) (Arnold et al., 2016; Jin et al., 2010; Xu et al., 2020), between ethanol exposed and unexposed alx1 mutants will elucidate whether *alx1* promotes oxidative defense regulators, which then activate antioxidant genes.

How does the alx family contribute to retinal development?

In chapter 3, we showed that *alx1* mutants, *alx1; alx3* heterozygotes, and *alx1; alx3* double mutants develop with anterior segment defects and ocular hemorrhaging. Despite their ocular defects, their retinal ganglion cell differentiation and visual perception are normal. We showed that *alx1* mutant embryos develop with mildly misshapen eyes and they exhibit more pronounced anterior segment defects, such as aphakia, iridial dysplasia, iridial coloboma, and aberrant pupils, in adulthood. While there is growing evidence showing the correlation of early on-set anterior segment defects and retinal degeneration (Mao et al., 2011; Mao et al., 2017; Martino et al.,

2016), whether *alx1* and *alx3* function are required for retinal function in has not been characterized in a preceding chapter.

Electoretinogram (ERG), an electrophysiological instrument to evaluate the function of the retina, has been optimized in zebrafish larva and adults (Chrispell et al., 2015; Tanvir et al., 2018). The eyeballs of adult *alx1* mutants, *alx1; alx3* heterozygotes, and *alx1; alx3* double mutants with or without ocular defects (3 months to 1 year old) will be dissected and these eyeballs will be prepared for ERG as described in Tanvir (Tanvir et al., 2018). Through ERG, the function of each retinal cell types can be analyzed by recording the ERG waveforms, such as photoreceptors (a-wave), ON-bipolar cells (b-wave), Müller glial cells (c-wave), and OFF-bipolar cells (d-wave), (Chrispell et al., 2015). The waveform patterns between the fish with ocular defects and the one without will be compared to identify the retinal cell types that are defective in fish with ocular defects. This method can also be applicable for adult *alx1* mutants with ethanol treatment to elucidate whether the alx gene family protects the retina from environmental perturbations since it has been optimized to understand the effects of environmental stress to retinal function in adult zebrafish (Tanvir et al., 2018).

What are the other transcriptional targets of zic2?

In chapter 2, we performed RNA-seq experiments from normal siblings and zic2 mutants derived from *zic2a +/-; zic2b +/-* parental incross (Z-*zic2* mutants). Although we found several chondrogenic neural crest markers and few ventral retina/optic stalk markers were significantly downregulated in Z-*zic2* mutants, we have

likely missed several known targets of *zic2* in the context of developing embryos. For example, *zic2* has been shown to interact with nodal (Houtmeyers et al., 2016) and canonical wnt signaling (Fujimi et al., 2012; Nyholm et al., 2009; Pourebrahim et al., 2011). *Zic2* synergistically interacts with *cdx1*, caudal-related homeobox, to activate a neural crest enhancer from the 5'-flanking region of *pax3* in the caudal neuroectoderm (Sanchez-Ferras et al., 2014). In addition, *zic2* modulates the chromatin remodeling as an enhancer-binding factor (Frank et al., 2015; Luo et al., 2015; Matsuda et al., 2017). In the future, embryos derived from *zic2a +/-; zic2b -/-* parental incross (MZ-*zic2* mutants) will be used for RNA-seq analysis. MZ-*zic2* mutant will be useful to identify maternal *zic2b* function dependent downstream targets, which we missed from Z-*zic2* mutants.

Recently, single cell RNA-seq technique has been optimized for zebrafish to understand the cell-type specific transcriptional changes during early development (Farnsworth et al., 2020; Farrell et al., 2018; Raj et al., 2018). Considering *zic2* functions in many cell lineages, single cell RNA-seq analysis would be useful to identify cell-type specific downstream targets of *zic2* in several different developmental stages. Because *zic2a* mutant allele can be selected by RFP fluorescence screening (Clark et al., 2011; Sedykh et al., 2017), RFP-positive cells will be isolated by fluorescence-activated cell sorting (FACs) from heterozygous and homozygous *zic2a; zic2b* mutant embryos derived from MZ-*zic2* parental incross. RFP-positive cells will be sequenced, and cell types will be identified via unsupervised clustering of transcriptomic data. Differential gene expression analysis between heterozygous and homozygous *zic2a; zic2b* mutant embryos will identify the cell-type specific downstream targets of *zic2*.

Reference

Ando, K., Fukuhara, S., Izumi, N., Nakajima, H., Fukui, H., Kelsh, R.N., Mochizuki, N., 2016. Clarification of mural cell coverage of vascular endothelial cells by live imaging of zebrafish. Development 143, 1328-1339.

Arnold, M.C., Forte, J.E., Osterberg, J.S., Di Giulio, R.T., 2016. Antioxidant Rescue of Selenomethionine-Induced Teratogenesis in Zebrafish Embryos. Arch Environ Contam Toxicol 70, 311-320.

Cannon, J.E., Place, E.S., Eve, A.M., Bradshaw, C.R., Sesay, A., Morrell, N.W., Smith, J.C., 2013. Global analysis of the haematopoietic and endothelial transcriptome during zebrafish development. Mech Dev 130, 122-131.

Chrispell, J.D., Rebrik, T.I., Weiss, E.R., 2015. Electroretinogram analysis of the visual response in zebrafish larvae. J Vis Exp.

Clark, K.J., Balciunas, D., Pogoda, H.M., Ding, Y., Westcot, S.E., Bedell, V.M., Greenwood, T.M., Urban, M.D., Skuster, K.J., Petzold, A.M., Ni, J., Nielsen, A.L., Patowary, A., Scaria, V., Sivasubbu, S., Xu, X., Hammerschmidt, M., Ekker, S.C., 2011. In vivo protein trapping produces a functional expression codex of the vertebrate proteome. Nat Methods 8, 506-515.

Clay, M.R., Halloran, M.C., 2013. Rho activation is apically restricted by Arhgap1 in neural crest cells and drives epithelial-to-mesenchymal transition. Development 140, 3198-3209.

Dee, C.T., Szymoniuk, C.R., Mills, P.E., Takahashi, T., 2013. Defective neural crest migration revealed by a Zebrafish model of Alx1-related frontonasal dysplasia. Hum Mol Genet 22, 239-251.

DeLaurier, A., Nakamura, Y., Braasch, I., Khanna, V., Kato, H., Wakitani, S., Postlethwait, J.H., Kimmel, C.B., 2012. Histone deacetylase-4 is required during early cranial neural crest development for generation of the zebrafish palatal skeleton. BMC Dev Biol 12, 16.

Dougherty, M., Kamel, G., Shubinets, V., Hickey, G., Grimaldi, M., Liao, E.C., 2012. Embryonic fate map of first pharyngeal arch structures in the sox10: kaede zebrafish transgenic model. J Craniofac Surg 23, 1333-1337.

Eberhart, J.K., He, X., Swartz, M.E., Yan, Y.L., Song, H., Boling, T.C., Kunerth, A.K., Walker, M.B., Kimmel, C.B., Postlethwait, J.H., 2008. MicroRNA Mirn140 modulates Pdgf signaling during palatogenesis. Nat Genet 40, 290-298.

Farnsworth, D.R., Saunders, L.M., Miller, A.C., 2020. A single-cell transcriptome atlas for zebrafish development. Dev Biol 459, 100-108.

Farrell, J.A., Wang, Y., Riesenfeld, S.J., Shekhar, K., Regev, A., Schier, A.F., 2018.

Single-cell reconstruction of developmental trajectories during zebrafish embryogenesis. Science 360.

Frank, C.L., Liu, F., Wijayatunge, R., Song, L., Biegler, M.T., Yang, M.G., Vockley, C.M., Safi, A., Gersbach, C.A., Crawford, G.E., West, A.E., 2015. Regulation of chromatin accessibility and Zic binding at enhancers in the developing cerebellum. Nat Neurosci 18, 647-656.

Fujimi, T.J., Hatayama, M., Aruga, J., 2012. Xenopus Zic3 controls notochord and organizer development through suppression of the Wnt/beta-catenin signaling pathway. Dev Biol 361, 220-231.

Garcia-Sanz, P., Mirasierra, M., Moratalla, R., Vallejo, M., 2017. Embryonic defence mechanisms against glucose-dependent oxidative stress require enhanced expression of Alx3 to prevent malformations during diabetic pregnancy. Sci Rep 7, 389.

Garcia, C.M., Shui, Y.B., Kamath, M., DeVillar, J., Johnson, R.S., Gerber, H.P., Ferrara, N., Robinson, M.L., Beebe, D.C., 2009. The function of VEGF-A in lens development: formation of the hyaloid capillary network and protection against transient nuclear cataracts. Exp Eye Res 88, 270-276.

Hahn, M.E., Timme-Laragy, A.R., Karchner, S.I., Stegeman, J.J., 2015. Nrf2 and Nrf2-related proteins in development and developmental toxicity: Insights from studies in zebrafish (Danio rerio). Free Radic Biol Med 88, 275-289.

Houtmeyers, R., Tchouate Gainkam, O., Glanville-Jones, H.A., Van den Bosch, B., Chappell, A., Barratt, K.S., Souopgui, J., Tejpar, S., Arkell, R.M., 2016. Zic2 mutation causes holoprosencephaly via disruption of NODAL signalling. Hum Mol Genet 25, 3946-3959.

James, A., Lee, C., Williams, A.M., Angileri, K., Lathrop, K.L., Gross, J.M., 2016. The hyaloid vasculature facilitates basement membrane breakdown during choroid fissure closure in the zebrafish eye. Dev Biol 419, 262-272.

Jin, Y., Zhang, X., Shu, L., Chen, L., Sun, L., Qian, H., Liu, W., Fu, Z., 2010. Oxidative stress response and gene expression with atrazine exposure in adult female zebrafish (Danio rerio). Chemosphere 78, 846-852.

Jo, D.H., Kim, J.H., Heo, J.I., Kim, J.H., Cho, C.H., 2013. Interaction between pericytes and endothelial cells leads to formation of tight junction in hyaloid vessels. Mol Cells 36, 465-471.

Luo, Z., Gao, X., Lin, C., Smith, E.R., Marshall, S.A., Swanson, S.K., Florens, L., Washburn, M.P., Shilatifard, A., 2015. Zic2 is an enhancer-binding factor required for embryonic stem cell specification. Mol Cell 57, 685-694.

Mao, M., Hedberg-Buenz, A., Koehn, D., John, S.W., Anderson, M.G., 2011. Anterior segment dysgenesis and early-onset glaucoma in nee mice with mutation of Sh3pxd2b.

Invest Ophthalmol Vis Sci 52, 2679-2688.

Mao, M., Kiss, M., Ou, Y., Gould, D.B., 2017. Genetic dissection of anterior segment dysgenesis caused by a Col4a1 mutation in mouse. Dis Model Mech 10, 475-485.

Martino, V.B., Sabljic, T., Deschamps, P., Green, R.M., Akula, M., Peacock, E., Ball, A., Williams, T., West-Mays, J.A., 2016. Conditional deletion of AP-2beta in mouse cranial neural crest results in anterior segment dysgenesis and early-onset glaucoma. Dis Model Mech 9, 849-861.

Matsuda, K., Mikami, T., Oki, S., Iida, H., Andrabi, M., Boss, J.M., Yamaguchi, K., Shigenobu, S., Kondoh, H., 2017. ChIP-seq analysis of genomic binding regions of five major transcription factors highlights a central role for ZIC2 in the mouse epiblast stem cell gene regulatory network. Development 144, 1948-1958.

Nyholm, M.K., Abdelilah-Seyfried, S., Grinblat, Y., 2009. A novel genetic mechanism regulates dorsolateral hinge-point formation during zebrafish cranial neurulation. J Cell Sci 122, 2137-2148.

Pourebrahim, R., Houtmeyers, R., Ghogomu, S., Janssens, S., Thelie, A., Tran, H.T., Langenberg, T., Vleminckx, K., Bellefroid, E., Cassiman, J.J., Tejpar, S., 2011. Transcription factor Zic2 inhibits Wnt/beta-catenin protein signaling. J Biol Chem 286, 37732-37740.

Raj, B., Wagner, D.E., McKenna, A., Pandey, S., Klein, A.M., Shendure, J., Gagnon, J.A., Schier, A.F., 2018. Simultaneous single-cell profiling of lineages and cell types in the vertebrate brain. Nat Biotechnol 36, 442-450.

Rocha, M., Singh, N., Ahsan, K., Beiriger, A., Prince, V.E., 2020. Neural crest development: insights from the zebrafish. Dev Dyn 249, 88-111.

Sanchez-Ferras, O., Bernas, G., Laberge-Perrault, E., Pilon, N., 2014. Induction and dorsal restriction of Paired-box 3 (Pax3) gene expression in the caudal neuroectoderm is mediated by integration of multiple pathways on a short neural crest enhancer. Biochim Biophys Acta 1839, 546-558.

Sedykh, I., Yoon, B., Roberson, L., Moskvin, O., Dewey, C.N., Grinblat, Y., 2017. Zebrafish zic2 controls formation of periocular neural crest and choroid fissure morphogenesis. Dev Biol 429, 92-104.

Sorrells, S., Toruno, C., Stewart, R.A., Jette, C., 2013. Analysis of apoptosis in zebrafish embryos by whole-mount immunofluorescence to detect activated Caspase 3. J Vis Exp, e51060.

Tanvir, Z., Nelson, R.F., DeCicco-Skinner, K., Connaughton, V.P., 2018. One month of hyperglycemia alters spectral responses of the zebrafish photopic electroretinogram. Dis Model Mech 11.

Teslaa, J.J., Keller, A.N., Nyholm, M.K., Grinblat, Y., 2013. Zebrafish Zic2a and Zic2b

regulate neural crest and craniofacial development. Dev Biol 380, 73-86.

Totong, R., Schell, T., Lescroart, F., Ryckebusch, L., Lin, Y.F., Zygmunt, T., Herwig, L., Krudewig, A., Gershoony, D., Belting, H.G., Affolter, M., Torres-Vazquez, J., Yelon, D., 2011. The novel transmembrane protein Tmem2 is essential for coordination of myocardial and endocardial morphogenesis. Development 138, 4199-4205.

Uemura, M., Nagasawa, A., Terai, K., 2016. Yap/Taz transcriptional activity in endothelial cells promotes intramembranous ossification via the BMP pathway. Sci Rep 6, 27473.

Vaccaro, A., Patten, S.A., Ciura, S., Maios, C., Therrien, M., Drapeau, P., Kabashi, E., Parker, J.A., 2012. Methylene blue protects against TDP-43 and FUS neuronal toxicity in C. elegans and D. rerio. PLoS One 7, e42117.

Wang, X.Y., Li, S., Wang, G., Ma, Z.L., Chuai, M., Cao, L., Yang, X., 2015. High glucose environment inhibits cranial neural crest survival by activating excessive autophagy in the chick embryo. Sci Rep 5, 18321.

Weaver, M.L., Piedade, W.P., Meshram, N.N., Famulski, J.K., 2020. Hyaloid vasculature and mmp2 activity play a role during optic fissure fusion in zebrafish. Sci Rep 10, 10136.

Wentzel, P., Eriksson, U.J., 2011. Altered gene expression in rat cranial neural crest cells exposed to a teratogenic glucose concentration in vitro: paradoxical downregulation of antioxidative defense genes. Birth Defects Res B Dev Reprod Toxicol 92, 487-497.

Wierson, W.A., Welker, J.M., Almeida, M.P., Mann, C.M., Webster, D.A., Torrie, M.E., Weiss, T.J., Kambakam, S., Vollbrecht, M.K., Lan, M., McKeighan, K.C., Levey, J., Ming, Z., Wehmeier, A., Mikelson, C.S., Haltom, J.A., Kwan, K.M., Chien, C.B., Balciunas, D., Ekker, S.C., Clark, K.J., Webber, B.R., Moriarity, B.S., Solin, S.L., Carlson, D.F., Dobbs, D.L., McGrail, M., Essner, J., 2020. Efficient targeted integration directed by short homology in zebrafish and mammalian cells. Elife 9.

Xiang, Q., Xu, B., Ding, Y., Liu, X., Zhou, Y., Ahmad, F., 2018. Oxidative Stress Response Induced by Butachlor in Zebrafish Embryo/Larvae: The Protective Effect of Vitamin C. Bull Environ Contam Toxicol 100, 208-215.

Xie, J., Farage, E., Sugimoto, M., Anand-Apte, B., 2010. A novel transgenic zebrafish model for blood-brain and blood-retinal barrier development. BMC Dev Biol 10, 76.

Xu, H., Jiang, Y., Li, S., Xie, L., Tao, Y.X., Li, Y., 2020. Zebrafish Oxr1a Knockout Reveals Its Role in Regulating Antioxidant Defenses and Aging. Genes (Basel) 11.

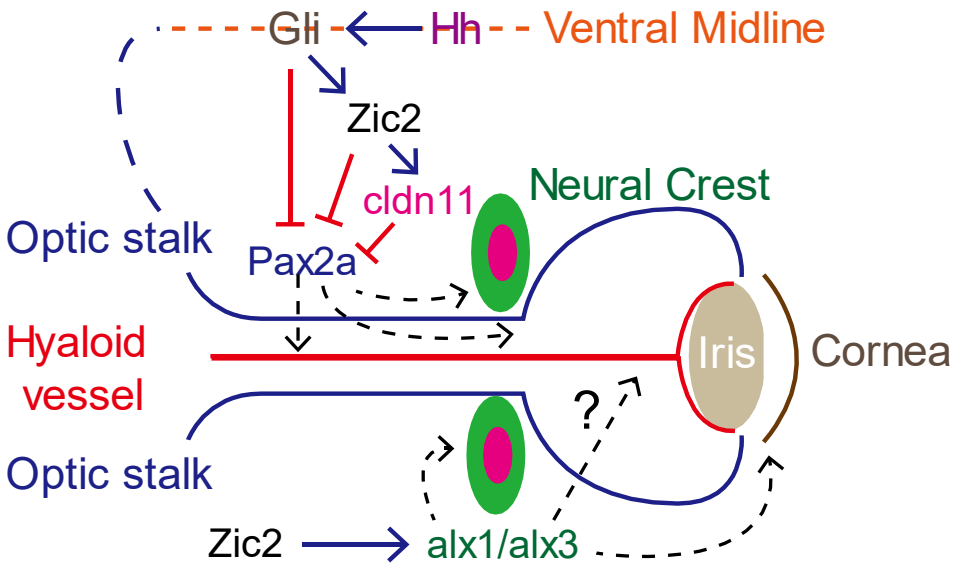

Figure 1. *Model representation of several general factors for zebrafish craniofacial complex development*

Chapter 2 describes the role of *zic2* for restricting *pax2a* at the optic stalk, activating *alx1* at the periocular neural crest, and activating *cldn11a* at the potential periocular neural crest.

Chapter 3 describes *alx1* and *alx3* function in aCNC lineages, which differentiates into several cell types of anterior segment, craniofacial cartilages, and potentially vascular pericytes for hyaloid vasculature.

Chapter 4 describes *pax2a* at the optic stalk is restricted by gli-zic2 interaction and *cldn11*. *Pax2a* is required for choroid fissure, hyaloid vasculature, and craniofacial cartilage development.

Appendix

Alx1-related frontonasal dysplasia results from defective neural crest cell development and migration

Pini, J., Kueper, J., Hu, Y.D., Kawasaki, K., Yeung, P., Tsimbal, C., Yoon, B., Carmichael, N., Maas, R.L., Cotney, J., Grinblat, Y., Liao, E.C., 2020. ALX1-related frontonasal dysplasia results from defective neural crest cell development and migration. EMBO Mol Med, e12013.

Preface

As a 7th co-author, I conducted zebrafish alx1 mutant experiments and my data contributed figure 6 and supplementary figures 4 and 5.

Abstract

A pedigree of subjects presented with frontonasal dysplasia (FND). Genome sequencing and analysis identified a p.L165F missense variant in the homeodomain of the transcription factor ALX1 which was imputed to be pathogenic. Induced pluripotent stem cells (iPSC) were derived from the subjects and differentiated to neural crest cells (NCC). NCC derived from ALX1L165F/L165F iPSC were more sensitive to apoptosis, showed an elevated expression of several neural crest progenitor state markers, and exhibited impaired migration compared to wild-type controls. NCC migration was evaluated in vivo using lineage tracing in a zebrafish model, which revealed defective migration of the anterior NCC stream that contributes to the median portion of the anterior neurocranium, phenocopying the clinical presentation. Analysis of human NCC culture media revealed a change in the level of bone morphogenic proteins (BMP), with a low level of BMP2 and a high level of BMP9.

Soluble BMP2 and BMP9 antagonist treatments were able to rescue the defective migration phenotype. Taken together, these results demonstrate a mechanistic requirement of ALX1 in NCC development and migration.

Introduction

The central part of the human face contains key anatomic features and sensory organs that enable us to interact with the environment and each other. The embryologic processes that form midface structures, including the eyes, nose, upper lip, and maxilla, are tightly regulated (Johnston, 1966; Minoux & Rijli, 2010; Rada-Iglesias *et al*, 2012). The midface structures form as the centrally located frontonasal prominence extends anteriorly, coalescing with elements derived from the paired maxillary prominences (Johnston, 1966, 1975; Le Lièvre & Le Douarin, 1975; Le Lièvre, 1978; Sadaghiani & Thiébaud, 1987). The embryonic facial prominences are derived from distinct migrating streams of cranial neural crest cells (NCC) that are conserved across vertebrates (Le Douarin *et al*, 1993; Schilling *et al*, 1996; Chai *et al*, 2000; Olsson, *et al*, 2002; Trainor *et al*, 2002; Barrallo-Gimeno *et al*, 2004; Wada, 2005; Dougherty *et al*, 2012). NCC migration and differentiation are highly coordinated and are associated with dynamic gene expression patterns (Simoes-Costa & Bronner, 2015). Key signaling pathways that regulate NCC development involve BMP, Wnt, FGF, or Notch which activate the expression of transcription factors such as *PAX3*, *ZIC1*, *TFAP2a*, *MSX1/2,* and *DLX5* (Meulemans & Bronner-Fraser, 2002; Khudyakov & Bronner-Fraser, 2009; Stuhlmiller & Garcia-Castro, 2012; Rada-Iglesias *et al*, 2013; Simoes-Costa & Bronner, 2015). Disruptions of NCC development contribute to a number of congenital malformations such as Waardenburg syndrome (WS), velocardiofacial syndrome/DiGeorge syndrome, Hirschsprung's disease, congenital heart conditions, and craniofacial anomalies (Sedano *et al*, 1970; Fox *et al*, 1976; Pierpont *et al*, 2007; Uz *et al*, 2010).

Frontonasal dysplasia (FND) is considered a rare “orphan” disease

(ORPHA250), with very few cases reported in the literature. The true prevalence of FND and its etiology remain unknown. To date, six genetic causes of subtypes of FND with varying patterns of inheritance have been described in individual case reports: *EFNB1* (MIM 300035) in X-linked craniofrontonasal syndrome (MIM 304110*);* *ALX3* (MIM 606014) in FND type 1 (MIM 136760); *ALX4* (MIM 605420) in FND type 2 (MIM 613451); *ALX1* (MIM 601527) in FND type 3 (MIM 613456)*; ZSWIM6* (MIM 615951) in dominant acromelic frontonasal dysostosis (MIM 603671); and *SPECC1L* (MIM 614140) in Teebi syndrome (MIM 145420; Bhoj *et al*, 2015; Kayserili *et al*, 2009; Smith *et al*, 2014; Twigg *et al*, 2004, 2009; Ullah *et al*, 2016; Uz *et al*, 2010; Wieland *et al*, 2004). The heterogeneity of clinical phenotypes, including a wide range of possible ocular and craniofacial components, likely corresponds to different underlying genetic variants, genetic environments, and epigenetic modifications.

This study examined a pedigree of FND and identified a pathogenic variant in the homeodomain of transcription factor ALX1 resulting in a likely loss of function. A human stem cell model of FND was generated in order to investigate the effect of *ALX1* mutations on NCC behavior. Cellular and molecular characterizations identified a number of differences between subject-derived and control NCC that shed light on the developmental processes that are disrupted in FND. *In vivo* characterization of *alx1* in zebrafish revealed defective migration of the most anterior cranial NCC. This study underscores the utility of complementary human iPSC and zebrafish models to gain mechanistic insight into the molecular and cellular basis of *ALX1*-related FND.

Materials and Methods

Approvals to perform research with human samples and zebrafish

The collection of human blood and discard specimens, genome sequencing, and generation of iPSC was approved by the Institutional Review Board of Partners Healthcare (IRB No. 2015P000904). Informed consent was obtained from the parents of the patients prior to all sample collections. All experimental protocols using zebrafish were approved by the Animal Care and Use Committees of Massachusetts General Hospital (IACUC No. 2010N000106) and the University of Wisconsin and carried out in accordance with institutional animal care protocols.

iPSC and EB generation

Peripheral blood mononuclear cells were isolated using whole blood from two individuals (subjects 5 and 6: *ALX1*$^{165F/165F}$), the unaffected father (subject 1: *ALX1*$^{165L/165F}$), and three unrelated healthy individuals (controls: *ALX1*$^{165L/165L}$). Samples were diluted in an equal volume of PBS and gently transferred to a tube containing 4 ml of FICOLL. After centrifuging the sample for 10 min at 350 *g*, the FICOLL-plasma interface containing the PBMCs was recovered and washed several times in PBS. After 24 h of recovery in StemPro-34 SFM medium (Invitrogen) supplemented with 100 ng/ml Stem Cell Factor (SCF, PeproTech, Rocky Hill, NJ),

100 ng/ml Fms-related tyrosine kinase 3 ligand (Flt3L, PeproTech), 20 ng/ml Interleukin-3 (IL-3, PeproTech) and 20 ng/ml IL-6 (PeproTech), 1 million PBMC were processed using the CytoTune-iPS 2.0 Sendai Reprogramming Kit (Invitrogen, Carlsbad, CA), following manufacturers instruction, for iPSC generation. One million PBMCs were infected with three different Sendai Viruses containing the Yamanaka reprogramming factors, *OCT4, SOX2, KLF4,* and *c-MYC*, in StemPro-34 SFM medium supplemented with cytokines. Starting on day 21, individual iPSC clones were picked based on morphologic criteria. Subsequently, the iPSC were maintained in StemFlex medium and passaged 1–2 a week using ReLSR (STEMCELL Technologies, Vancouver, BC, Canada) dissociation buffer. Since iPSC can exhibit genetic instability after reprogramming, the clones were expanded up to passage 10 before characterizing each cell line. The genetic stability of the cells was assessed analyzing copy number variants through genome-wide microarray analysis (Thermo Fisher). Epigenetic differences were controlled for in a limited manner by ensuring that all major experiments were performed in both biologic and technical triplicate at the identical passage number.

To form embryoid bodies (EB), iPSC were harvested using ReLSR dissociation buffer and clumps were transferred to a low adherent 6-well plate in differentiation medium containing 80% DMEM-F12, 20% Knock out Serum Replacer (Invitrogen), 1 mM nonessential amino acids, 1 mM Penicillin/Streptomycin, and 100 μM 2-mercaptoethanol. The medium was changed daily. After 14 days of differentiation, cells were recovered for RNA extraction and subsequent qPCR analysis of markers of the ectoderm, endoderm, and mesoderm.

Derivation of NCC and multilineage differentiation

In order to derive NCC, a previously published protocol for mesenchymal differentiation was adapted (Pini *et al*, 2018). iPSC medium was replaced by NCC-inducing medium containing DMEM-F12, 10% fetal bovine serum (FBS), 1 mM sodium pyruvate, 1 mM Penicillin/Streptomycin, 1 mM nonessential amino acid, 110 µM 2-mercaptoethanol, and 10 ng/ml epidermal growth factor (EGF). The medium was changed every 2 days. After 1 week, cells were recovered using 0.25% trypsin-EDTA and transferred to new cultureware for an additional week. Following this, cells were harvested, phenotypically characterized by flow cytometry for their expression of NCC markers and assayed for their mesenchymal differentiation ability.

Schwann cell differentiation was performed as previously described (Kawano *et al*, 2017). NCC were plated on glass coverslips in 24-well tissue culture plates (0.2×10^5 cells per well) in neuronal differentiation medium consisting of a 3:1 ratio of DMEM-F12 and neurobasal medium supplemented with 0.25× B-27, 1 mM glutamine, and 1 mM Penicillin/Streptomycin for 5 weeks. The medium was changed weekly. At the end of the differentiation, cells were fixed in 4% formaldehyde and analyzed by immunohistochemistry for S100B (Thermo Fisher, Waltham, MA) and GFAP expression (Abcam, Cambridge, United Kingdom).

Adipocyte and chondrocyte differentiation was performed as previously described (Pini *et al*, 2018). Adipogenesis was investigated using the StemPro adipogenesis differentiation kit (Life Technologies, Carlsbad, CA). NCC were seeded at 5×10^4 per well, in a 24-well plate, and cultured for 2 weeks, in complete

adipogenesis differentiation medium. Lipid deposits were observed following staining with Oil Red O (MilliporeSigma, St. Louis, MO), according to manufacturers' instructions. After washing, cells were counterstained with Mayer's hematoxylin.

Chondrogenic differentiation was performed using the StemPro chondrogenesis differentiation kit (Life Technologies). NCC were seeded in a 12-well plate, in aggregates containing 8×10^4 cells, in 5 µl of NCC medium, and placed in a 37°C, 5% CO_2 incubator for 1 h. Following this, the NCC medium was replaced by chondrogenesis differentiation medium, and cultured for 20 days. The medium was changed once a week. Chondrogenic matrix formation was observed following Alcian blue, Safranin O and Toluidine Blue staining.

Osteoblast differentiation was performed using the StemPro osteogenesis differentiation kit (Life Technologies). NCC were plated in 12-well tissue culture plates (5×10^5 cells per well) in osteogenesis differentiation medium for 14 days. At the end of the differentiation, the presence of mineralized nodules was assessed using Alizarin Red S, Von Kossa (silver nitrate) and Alkaline Phosphatase staining.

Images were acquired using the RETIGA OEM fast camera and Qcapture software (Teledyne QImaging, Surrey, BC, Canada).

Genomic DNA extraction and sequencing

Genomic DNA was extracted with the REDExtract-N-Amp tissue PCR kit (MilliporeSigma), following the manufacturer's instructions. Sanger sequencing of *ALX1* to ensure *ALX1* sequence integrity in all iPSCs clones was carried out as previously described (Umm-e-Kalsoom *et al*, 2012). The four *ALX1* exons encoding the open reading frame were amplified using the CloneAmp HiFi PCR premix (Takara Bio Inc., Kusatsu, Shiga, Japan) and exon-specific *ALX1* oligonucleotides. All exon-specific PCR products were purified using the Qiaquick PCR purification kit (Qiagen, Hilden, Germany) prior to sequencing.

Whole-exome sequencing and analysis

Whole-exome sequencing (WES) of the affected subjects 3 and 4, an unaffected sibling, and the parents was performed and analyzed assuming a recessive mode of inheritance given the presence of multiple affected siblings. Three compound heterozygous variants and one homozygous recessive variant were identified in the affected siblings (*ALX1* c.493C>T). This variant was predicted to be causative of the phenotype based on known gene function, the previously identified role of *ALX1* in frontonasal development, and the effect of the variant (substitution of phenylalanine for the highly conserved leucine in a DNA-binding domain). Polymorphism Phenotyping v2, Sorting Intolerant from Tolerant, MutationTaster, and Functional

Analysis through Hidden Markov Models (v2.3) were used for functional variant consequence prediction (Lowe, 1999; Adzhubei *et al*, 2010; Schwarz *et al*, 2014; Shihab *et al*, 2014). The gnomAD platform was used to identify any other missense variants at the location identified in the subjects (preprint: Karczewski *et al*, 2019). Clustal Omega was used for multiple sequence alignment (Sievers *et al*, 2011). Domain Graph was used to create the annotated schematic diagrams of *ALX1* and ALX1 (Ren *et al*, 2009).

RNA extraction and processing

RNA was isolated using the RNAeasy Plus mini kit (Qiagen), following the manufacturer's recommendations. One µg of RNA was reverse-transcribed using the SuperScript III first-strand synthesis system (Thermo Fisher). All PCR reactions on cDNA were performed using the GoTaq DNA polymerase (Promega, Madison, WI) unless otherwise noted. For zebrafish RNA extraction, 24 hpf Tübingen zebrafish embryos were harvested and homogenized using a micropestle in TRIzol reagent (Thermo Fisher), following manufacturer's instructions. Total RNA was then purified using phenol-chloroform. One µg of total RNA was reverse-transcribed using the SuperScript III First-Strand Synthesis Kit (Thermo Fisher), following manufacturer's recommendations.

Flow cytometry analysis

Neural crest cells were harvested and suspended in FACS buffer solution consisting of PBS with Ca^{2+} and Mg^{2+}, 0.1% bovine serum albumin (BSA), and 0.1% sodium azide. Approximately 2×10^5 cells were incubated with the desired cell surface marker antibodies or isotype controls at 4°C for 15 min. Specific antibodies for CD90, CD73, CD105, and CD57 (BD Biosciences, San Jose, CA), and isotype control immunoglobulin IgG1 (BD Biosciences) were used for labeling. Antibodies were diluted in FACS buffer. After three washes in FACS buffer, samples were fixed in 0.4% formaldehyde and processed using an LSR II flow cytometer (BD Biosciences). The data acquired were analyzed using FlowJo software (FlowJo, LLC).

Immunohistochemical analysis of iPSC

Cells were fixed with 4% formaldehyde in PBS for 15 min at room temperature, permeabilized with 1% saponin in PBS, and blocked using 3% BSA in PBS for 30 min at room temperature. The cells were then incubated with the primary antibodies for 3 h at room temperature. The following primary antibodies and dilutions were used: rabbit anti-OCT4 (1:100, Life Technologies), mouse anti-SSEA4 (1:100, Life Technologies); rat anti-SOX2 (1:100, Life Technologies), mouse anti-TRA-1-60 (1:100, Life Technologies), rabbit anti-GFAP (1:500, Abcam), and rabbit anti-S100B (1:500, Thermo Fisher). The cells were then incubated with the secondary antibodies (1:1,000,

MilliporeSigma) for 1 h at room temperature, washed with PBS, and counterstained with DAPI (MilliporeSigma). Secondary antibodies were Alexa 594 donkey anti-rabbit, Alexa 488 goat anti-mouse, and Alexa 488 donkey anti-rat and Alexa 594 goat anti-mouse (Thermo Fisher). Images were acquired using the RETIGA OEM fast camera and Qcapture software (Teledyne QImaging).

Staining of iPSC and mesenchymal NCC derivatives

Alkaline phosphatase activity was measured using the leukocyte alkaline phosphatase staining kit (MilliporeSigma), following the manufacturer instructions. Cells were first fixed using a citrate/acetone/formaldehyde solution for 30 s, washed several times, and stained with Fast Blue for 30 min. After further washing, these cells were counter stained with Mayer's hematoxylin. Alizarin Red S., Von Kossa, Alcian Blue, and Toluidine Blue staining were performed as previously described (Pini *et al*, 2018). Cells were first fixed in 4% formaldehyde at room temperature for 15 min. Following a wash, cells were incubated in either 1% Alizarin Red, 1% Silver nitrate, 0.1% Toluidine Blue, 0.02% Alcian Blue, or 0.1% Safranine O solution. For Von Kossa staining, cells were exposed to UV light until dark staining appeared. Images were acquired using the RETIGA OEM fast camera and Qcapture software (Teledyne QImaging).

Quantitative and nonquantitative polymerase chain reaction

Real-time PCR assays were conducted on a StepOnePlus real-time PCR system, using PowerUp SYBR Green Master Mix (Applied Biosystems, Waltham, MA). Transcript expression levels were evaluated using a comparative CT process (ΔΔCT) with human *RPLP0* and *GAPDH* used as reference genes. For zebrafish, *elfa* and *18S* were used as reference genes. Specific primers were used for amplification as noted (Table EV1).

Apoptosis assay

2×10^5 cells were incubated for 30 min in the dark in 1× Fixable Viability Dye (FVD, Invitrogen) solution. After two washes in FACS buffer and one wash in binding buffer, cells were incubated 10–15 min in 1× Annexin V (BioLegend, San Diego, CA) solution in binding buffer composed of 0.1 M HEPES (pH 7.4), 1.4 M NaCl, and 25 mM $CaCl_2$. After one wash in binding buffer, cells were suspended in 200 µl of binding buffer and immediately processed using an LSR II flow cytometer (BD Biosciences) and analyzed using FlowJo software (FlowJo LLC, Ashland, OR). Apoptosis was induced by placing the cell suspension in a water bath at 55°C for 10 min.

Wound healing assay and analysis

Migration was investigated using the Radius™ 48-Well Cell Migration Assay (Cell Biolabs, Inc., San Diego, CA), following manufacturer's instructions. Control or *ALX1*$^{165F/165F}$ NCC (1×10^5 cells/well) were plated in a 48-well plate containing a Radium™ Gel spot. Before beginning the migration assay, cells were washed three times with medium and incubated with gel removal solution for 30 min at 37°C. Following three subsequent washes in medium, the NCC were placed in a culture chamber for live cell imaging at 37°C and 5% CO_2. Rescue experiments were performed through the addition of soluble BMP2, CV2, or a combination of the two at a concentration of 10, 50, or 100 ng/ml to the medium at the beginning of the assay. For fluorescent pictures, cells were stained in serum-free media containing 3.6 μM CellTracker Green CMFDA (Life Technologies) for 30 min at 37°C and allowed to recover for 30 min before starting the experiment. All images were acquired using a Keyence BZ-X800 microscope. The time-lapse film was made by acquiring images every 15 min for 24 h. The fluorescent images were acquired every 6 h. Surface area analyses and percentages of recovery were measured using ImageJ software (NIH, Bethesda, MD).

Multiplex analysis of BMP concentration

The concentration of the BMP family in the supernatant of *ALX1*$^{165F/165F}$ NCC was measured using a bead-based multiplex array (Forsyth Institute, Cambridge, MA). Manufacturers' protocols were followed for all panels. Reagents were prepared as per kit instructions. Assay plates (96-well) were loaded with assay buffer, standards, supernatant from the *ALX1*$^{165F/165F}$ NCC, and beads and then covered and incubated on a plate shaker (500 rpm) overnight at 4°C. After primary incubation, plates were washed twice. Following this, the detection antibody cocktail, consisting of BMP-specific antibody with biotin (1:10) and the detection antibody streptavidin conjugated with PE (1:25), was added to all wells; the plates were covered and left to incubate at room temperature for 1 h on a plate shaker. After the incubation, streptavidin-phycoerythrin fluorescent reporter was added to all wells, and the plate was covered and incubated for 30 min at room temperature on a plate shaker. Plates were then washed twice, and beads were resuspended in sheath fluid, placed on shaker for 5 min, and then read on a Bio-Plex® 200 following manufacturers' specifications and analyzed using Bio-Plex Manager software v6.0 (Bio-Rad, Hercules, CA).

Plasmid construct generation

The In-Fusion Cloning Kit (Takara) and the In-Fusion Cloning primer design tool were used for primer design. Tübingen zebrafish *alx1* was amplified via PCR. Zebrafish *alx1* as cloned into the SpeI and PacI (NEB, Ipswich, MA) restriction sites of pCS2 + 8 (Promega). The subsequent reaction product was used to transform One Shot TOP10 competent cells (Thermo Fisher) or Stellar competent cells (Takara).

For the generation of truncated *alx1* constructs, the genes were divided into N-terminal and C-terminal sections, with aa181 being designated as the beginning of the C-terminal portion in zebrafish *alx1*.

For all plasmid constructs, individual clones were picked, DNA purified (Qiagen), and validated using Sanger and Next Generation whole plasmid sequencing.

CRISPR-Cas9 directed mutagenesis of zebrafish

A CRISPR site on exon 2 of the *alx1* gene was selected using the Burgess lab protocol (Varshney *et al*, 2015, 2016). The single guide RNA (sgRNA) targeting this site (sequence: GGAGAGCAGCCTGCACGCGA), and Cas9 or nCas9n mRNA, were prepared as previously described (Gagnon *et al*, 2014; Shah *et al*, 2016a,b). Genetically defined wild-type (NIHGRI-1; LaFave *et al*, 2014) embryos were injected at the one-cell stage with 50–100 pg of sgRNA and 360–400 pg of Cas9 or nCas9n

mRNA. Adult F0 animals were intercrossed to produce the F1 generation. F1 mutant carriers were identified by PCR using forward primer CGTGACTTACTGCGCTCCTA and reverse primer CGAGTTCGTCGAGGTCTGTT. The PCR products were resolved on a MetaPhor gel (Lonza, Basel, Switzerland) and sequenced. A frameshift allele was identified: a deletion of 16 nucleotides, termed *alx1*^{uw2016} (Fig EV4).

Alx1DN expression in zebrafish embryos

The validated Alx1DN (N-terminal portion of protein product containing homeodomain and nuclear localization domains) clones in pCS2+8 were purified via miniprep (Qiagen) alongside a control (C-terminal portion containing transactivation domain) and digested using NotI (NEB), before being gel purified using the Zymoclean Gel DNA Recovery Kit (Zymo Research, Irvine, CA). Five hundred microgram of purified, digested plasmid DNA served as the input for the mMessage mMachine SP6 Transcription Kit (Thermo Fisher). The resulting mRNA was then further purified using the RNeasy Mini Kit (Qiagen) and frozen in 100 ng/µl aliquots at −80°C. mRNA overexpression was accomplished using microinjections. mRNA stock aliquots were first diluted to the desired concentration with 0.125% Phenol Red in ultrapure water (Invitrogen). A 2 nl drop was then injected into fertilized Tübingen embryos at the single cell stage. At 4 h post-fertilization (hpf), all unfertilized and visibly damaged embryos were removed.

Alcian blue staining

All injected and uninjected zebrafish were incubated at 28.5°C for 5 dpf in E3 buffer with 0.0001% methylene blue. At 4 days post-fertilization (dpf), injected and uninjected embryos were fixed overnight at 4°C in 4% formaldehyde, washed stepwise with 1 × PBS and 50% EtOH in PBS before being stained in a solution of 0.02% Alcian blue, 70% EtOH, and 190 mM $MgCl_2$ overnight at room temperature on a rotating platform. Following this, embryos were washed with ddH_2O before being bleached in a solution of 0.9% H_2O_2, 0.8% KOH, and 0.1% Tween20 for 20 min. Stained embryos were then imaged in 4% methylcellulose in E3 solution and stored in 4% PFA at 4°C. Images were captured using a Nikon DS-Fi3 digital camera.

Lineage tracing

The application of *Tg:sox10;kaede* in cell labeling has previously been reported, where photoconversion of the kaede protein from green to red in selected cells under confocal microscopy can be used to follow distinct NCC migration patterns across time.

Alx1DN injected or control *sox10:*KAEDE transgenic embryos were imaged using a Leica SP8 confocal microscope at 19 to 20-somite stage to identify neural crest structures in a manner previously described (Dougherty *et al*, 2012, 2013). The

most distal population of the migrating stream of cranial neural crest cells was excited for 15 s for photoconversion with the FRAP module and a 405 nm laser at 25% power. Embryos were then placed back into a 28.5°C incubator. Both the photoconverted red (488 nm) and nonphotoconverted green (572 nm) neural crest populations were captured at 4 days post-fertilization (dpf) using a Leica Sp8 and analyzed with the Leica Application Suite X (Leica Microsystems, Buffalo Grove, IL) software for image capturing. A composite image was subsequently generated using ImageJ (NIH; Fig 8D, Film 3).

Statistical analysis

Each experiment was performed on six independent healthy control *ALX1*$^{165L/165L}$ clones, three heterozygous *ALX1*$^{165L/165F}$ clones, and nine homozygous *ALX1*$^{165F/165F}$ clones, and repeated at least three times. The qualitative craniofacial analysis of *alx1*$^{-/-}$ zebrafish and Alx1DN injections was performed three times, on three different clutches of embryos. For RT–qPCR experiments, data from each clone were pooled and the mathematical mean was calculated. SEM was used to determine the standard error. To test statistical significance, Student's *t*-test for paired data was used. Statistical analysis of the significance of the qPCR results was performed with an ANOVA test. A *P*-value < 0.05 was considered to be statistically significant. Statistical analysis was performed using GraphPad Prism 7.0 software. The D'Agostino and Pearson normality test was performed to verify normality. For groups that fulfilled normality and equal variance requirements, a one-way ANOVA

with a Sidak comparison test (95% confidence interval to compare all the different groups) was performed. For data sets that did not fulfill normality and equal variance requirements, a Kruskal–Wallis test was performed. Mean values for each group were compared using two-tailed Student's test for comparisons of two independent groups.

Result

Clinical features of ALX1-related FND in a consanguineous pedigree

A family with four children born of consanguineous parents of Amish heritage presented with complex FND. The FND phenotype was inherited in a Mendelian recessive fashion. Both parents, one unaffected sibling and three affected children (one male and two females), were consented and enrolled in the study (Fig 1A, subject numbers indicated in red). The parents (subjects 1 and 2) and nine unaffected siblings (including subject 3) had normal facial structures without clinical stigmata suggestive of mild FND. All four affected children presented with bilateral oblique facial clefts, extending from either side of the nasal bone, involving both the primary and secondary palate. Among the affected children, there was some variability of the ocular phenotype, where the older affected girl (subject 4) presented with bilateral coloboma and asymmetric microphthalmia, whereas the three other affected children (including subjects 5 and 6) exhibited bilateral anophthalmia, with deficient upper and lower eyelids covering a shallow orbit. Subject 6 was the most severely affected and presented with bilateral oblique facial clefts and anophthalmia as well as no upper and

lower eyelids, leaving the mucous membranes of both orbits exposed. Her nasal remnant also lacked the lateral alar subunits and is surrounded by several nodular skin tags.

Identification of pathogenic ALX1 variant

Whole-exome sequencing (WES) was performed on blood samples collected from subjects 1–5, which corresponded to both parents, one unaffected sibling, and two affected children. A missense p.L165F variant (c.493C>T) was identified in the homeodomain of *ALX1*, which was heterozygous in the parents ($ALX1^{165L/165F}$), wild type in the unaffected sibling ($ALX1^{165L/165L}$), and homozygous in both affected subjects ($ALX1^{165F/165F}$; Fig 1B). WES results were confirmed by Sanger sequencing of the entire *ALX1* coding sequence. The ALX1 p.L165F missense variant has not been reported in connection with an *ALX1*-related instance of FND in the literature nor been recorded as a variant in the gnomAD database (preprint: Karczewski *et al*, 2019; Fig 1C and D). The ALX1 p.L165F amino acid substitution was predicted to be damaging and disease causing by *in silico* tools (Sift, Polyphen, muttaster, fathmm) and consistent with the observed autosomal recessive inheritance pattern of this pedigree (Lowe, 1999; Adzhubei *et al*, 2010; Schwarz *et al*, 2014; Shihab *et al*, 2014).

Generation of patient-derived iPSC model of ALX1-related FND

Induced pluripotent stem cell lines were generated using peripheral blood mononuclear cells (PBMC) obtained from whole blood samples that were collected from three unrelated wild-type individuals (*ALX1*$^{165L/165L}$), the heterozygous father (*ALX1*$^{165L/165F}$), and two of the four affected children (Subjects 5 and 6; *ALX1*$^{165F/165F}$). PBMC were subsequently reprogrammed into iPSC (Fig EV1). Overall, 22 mutant *ALX1*$^{165F/165F}$ iPSC clones were successfully isolated and expanded from the two affected subjects, 13 *ALX1*$^{165L/165F}$ clones were isolated and expanded from the heterozygous father, and 35 *ALX1*$^{165L/165L}$ clones were isolated and expanded from healthy controls. Six *ALX1*$^{165F/165F}$ mutant clones (3 for each affected subject), 3 *ALX1*$^{165L/165F}$ clones from the heterozygous father, and 9 *ALX1*$^{165L/165L}$ clones from healthy controls (3 from each control) were fully characterized to confirm their pluripotency (Fig 1E) and ability to generate the three germ layers (Fig 1F). Sanger sequencing confirmed that the affected *ALX1*$^{165F/165F}$ and the heterozygous *ALX1*$^{165L/165F}$ -derived iPSC clones retained the *ALX1* p.L165F variant through reprogramming. Copy number variant analysis did not show any amplifications or deletions.

Generation and characterization of iPSC-derived NCC

Given the primary role of neural crest cells in midface morphogenesis, the iPSC clones were differentiated into NCC using a protocol adapted from a previous

study (Pini *et al*, 2018; Fig 2A). All NCC displayed similar morphological features and were indistinguishable at the colony level immediately following differentiation at passage 1 (Fig 2B).

Overexpression of neural plate border specifier genes in ALX1$^{165F/165F}$ NCC

A panel of marker genes at the center of the gene regulatory network required for NCC development and differentiation was selected to be examined in detail across the 14 days of the neural crest differentiation protocol (Fig 3; Barrallo-Gimeno *et al,* 2004; Sauka-Spengler & Bronner-Fraser, 2008; Sauka-Spengler *et al,* 2007; Simoes-Costa & Bronner, 2015). The NCC gene expression results can broadly be divided into three groups. The first group includes genes that did not significantly differ between affected, heterozygous, and unaffected controls. This group of genes comprises the neural crest specifiers *FOXD3* and *P75,* as well as the lineage specifier *HAND2*. The second group includes genes where the affected cells exhibited expression patterns that differed significantly from the heterozygous and the unaffected control cells, with no difference between the heterozygote and the control. This group of genes includes the neural plate border specifiers *ZIC1, PAX7, PAX3, MSX1,* and *DLX5* and the neural crest specifiers *SNAI2* and *TWIST1* ($P < 0.05$ between days 2–8 when comparing subjects', father, and control NCC for *ZIC1, PAX7, DLX5*; $P < 0.05$ between days 2–14 when comparing subjects', father, and control NCC for *PAX3, MSX1, SNAI2*, and *TWIST1*). The final group includes genes that were significantly differentially expressed between the affected homozygous, heterozygous, and unaffected control cells. This group comprised the neural plate border

specifier *MSX2, DLX5,* and the neural crest specifier *TFAP2A* (*P* < 0.05 between days 2-14 when comparing subjects' father and control NCC for *MSX2*, *DLX5,* and *TFAP2A*). Of note, all significantly differentially expressed genes in the affected cells were overexpressed above the levels observed in the heterozygous and unaffected control cells, consistent with a putative role of ALX1 as a transcriptional repressor.

ALX1 itself was found to be differentially expressed between affected cells when compared to the heterozygous and unaffected control cells at day 8 during NCC differentiation. The unaffected control and heterozygous cells exhibited similar *ALX1* expression levels*,* with peak expression level reached at day 8 where unaffected cells exhibited a plateaued, lower level of expression. The greatest difference in gene expression levels was observed early in the NCC differentiation process, around days 2–8 (such as in the cases of *ZIC1*, *PAX3*, *PAX7*, *DLX5*, and *TWIST1*). This characterization suggests an early function for ALX1 in NCC differentiation and identifies the 2–8 day window for in-depth transcriptome analysis in future studies.

Increased sensitivity to apoptosis in ALX1165F/165F NCC

Since anomalies in cell cycle progression predispose cells to apoptosis and given the importance of apoptosis in regulating craniofacial development, the impact of the ALX1$^{165F/165F}$ gene variant on the sensitivity of the iPSC-derived NCC to apoptosis was analyzed. Basal apoptosis levels, determined by the percentage of Annexin V-positive cells, did not differ between control NCC (4 ± 0.2%) and *ALX1$^{165F/165F}$* NCC (4.82 ± 0.65%; Fig 4A). After apoptosis induction via heat

shock, the percentage of Annexin V-positive cells significantly increased specifically in *ALX1*$^{165F/165F}$ NCC (87.97 ± 2.44%) versus control NCC (24.15 ± 0.96%). These findings suggest that the affected subject's *ALX1*$^{165F/165F}$ NCC are more sensitive to apoptosis.

These findings also indicate that *ALX1* functions in proliferating NCC. To determine whether *ALX1* function is required for cell cycle progression, we investigated expression of Cyclin D1 (CCND1), required for the cell cycle G1/S transition, and Cyclin A2 (CCNA2), required for the DNA synthesis during the S-phase. Both cyclins are expressed throughout the active cell cycle, from the G1/S transition to the G2/M transition (Pagano *et al,* 1992; Minarikova *et al,* 2016). Expression levels of CCND1 and CCNA2 were compared between control and ALX1$^{165F/165F}$ NCC at passages 2 and 3 post-differentiation. The *ALX1*$^{165F/165F}$ NCC were found to express significantly more CCNA2 and CCND1 at both passage 2 and passage 3 compared to the control NCC, consistent with a greater degree of active cellular proliferation (Fig 4B).

ALX1$^{165F/165F}$ *NCC do not undergo mesenchymal marker transition*

As NCC clones derived from the control *ALX1*$^{165L/165L}$, heterozygous *ALX1*$^{165L/165F}$, and homozygous *ALX1*$^{165F/165F}$ iPSC were maintained in culture, consistent qualitative morphologic differences were observed across cell passages. While control-derived NCC became progressively spindle-shaped and elongated, the mutant *ALX1*$^{165F/165F}$ NCC remained rounded (Fig 2B). In order to investigate these differences more fully, flow cytometry was performed across different

cell passage cycles in order to investigate the effect of the *in vitro* maturation of the NCC via an examination of NCC marker expression. At passage cycles 1–4, a number of key surface markers were examined. Expression of CD57 (synonym: HNK-1), indicative of NCC precursors before their commitment to downstream cell lineages (Minarcik & Golden, 2003), as well as markers of mesenchymal differentiation, CD105, CD73, and CD90, was assessed (Fig 4C).

Table 1 contains the precise percentage values of the FACS analysis of NCC at varying passage numbers. At passage 1 following differentiation, control and homozygous *ALX1*$^{165F/165F}$ NCC expressed similar levels of neural crest precursor marker CD57. The control and homozygous ALX1$^{165F/165F}$ NCC also expressed similar levels of mesenchymal markers CD90, CD105, and CD73. No significant differences were observed in marker expression between control and homozygous *ALX1*$^{165F/165F}$ NCC at this stage ($P > 0.05$). However, by passage 4, control NCC exhibited decreased CD57 expression and increased expression of CD90, CD105, and CD73, consistent with a progression to MSC differentiation. In contrast, homozygous *ALX1*$^{165F/165F}$ NCC displayed a similar expression of the aforementioned NCC and MSC markers at passage 4 as they did at passage 1 (Fig 4C).

The persistent CD57 expression in the homozygous *ALX1*$^{165F/165F}$ NCC, taken together with the elevated expression of neural crest specifier genes *ZIC1, PAX7, PAX3, MSX1, MSX2, and DLX5,* suggests that the mutant NCC may be unable to progress from the progenitor to the differentiating state. To understand whether the persistent CD57 expression had an effect on the ability of the homozygous *ALX1*$^{165F/165F}$ NCC to differentiate into downstream cell types, multilineage differentiation experiment was performed. Control and

homozygous *ALX1*$^{165F/165F}$ NCC demonstrated equal ability to differentiate into Schwann cells (GFAP and S100B-positive expression), adipocytes (oil Red O. staining), chondrocytes (Alcian Blue, Safranin O. and Toluidine Blue staining), and osteoblasts (Alizarin Red S., Von Kossa staining and strong alkaline phosphatase activity; Fig EV2). The maintenance of CD57 and lack of elevation of CD90 / CD105 / CD73 and the same ability to differentiate into NCCs derivatives suggest that the homozygous *ALX1*$^{165F/165F}$ failed to progress through the process of NCCs differentiation despite multiple cell passages and are blocked into the progenitor state.

Homozygous ALX1$^{165F/165F}$ *NCC display a migration defect*

During embryonic development, NCC migrate to specific locations in order to form the prominences that coalesce to shape the face. To investigate the migratory properties of the iPSC-derived NCC *in vitro,* a wound healing assay with a central clearing was used. A significant migration defect was observed in the homozygous *ALX1*$^{165F/165F}$ NCC when compared with control NCC (Fig 5A, Movie EV1). Control NCC were able to migrate and fully cover the central clearing area of the wound healing assay after 24 h (recovery of 95.99 ± 3.22% of the surface area). In contrast, the homozygous *ALX1*$^{165F/165F}$ NCC covered less than half of the central clearing surface area (38.79 ± 3.22% for *ALX1*$^{165F/165F}$ NCC).

ALX1$^{165F/165F}$ *NCC show differences in BMP secretion*

The family of BMP family of growth factors plays a critical role in NCC migration (Tribulo *et al*, 2003; Sato *et al*, 2005). This, in combination with the increased

expression of *TWIST1* in *ALX1*$^{165F/165F}$ NCC, a known BMP inhibitor, led to us to hypothesize that *ALX1*$^{165F/165F}$ NCC might display abnormal levels of secreted BMP when compared to healthy control NCC (Hayashi *et al*, 2007). To test this hypothesis, the levels of secreted BMP in the culture medium of *ALX1*$^{165F/165F}$ and control NCC were measured via multiplex analysis. The concentration of BMP2 was found to be significantly reduced in control *ALX1*$^{165F/165F}$ NCC (11.9 ± 0.65 pg/ml) compared to control NCC (19.52 ± 0.9 pg/ml; $P < 0.05$; Fig 5B). In contrast, the BMP9 concentration was significantly increased in mutant *ALX1*$^{165F/165F}$ NCC (3.72 ± 0.85 pg/ml) compared to control NCC (0.25 ± 0.02 pg/ml). BMP4, BMP7, and BMP10 levels were undetectable.

To follow-up on the observed dysregulation of BMPs, we hypothesized that treatments to counteract BMP2 reduction or BMP9 elevation could result in an improved migration phenotype. The *ALX1*$^{165F/165F}$ NCC were treated with different concentrations of soluble BMP2, the BMP9 antagonist Crossveinless (CV2), or a combination of the two (Fig 5C, Fig EV3, Movies EV2 and EV4). Treatment with an increasing concentration of BMP2 from 10 to 50 ng/ml was able to restore the migration of homozygous *ALX1*$^{165F/165F}$ NCC in a dose-dependent manner. However, no difference was observed between 50 and 100 ng/ml of BMP2, suggesting a saturation effect (64.53 ± 3.17% for 50 ng/ml BMP2, and 67.31 ± 3.25% for 100 ng/ml BMP2).

Likewise, treatment with the BMP9 antagonist CV2 was able to partially rescue the migration defect of homozygous ALX1$^{165F/165F}$ NCC. The low dose of 10 ng/ml of CV2 did not show a significant effect on the migration defect of treated and untreated *ALX1*$^{165F/165F}$ NCC (37.5 ± 2.5% for 10 ng/ml CV2). As observed with BMP2, treatments with both 50 ng/ml and 100 ng/ml of CV2 were able to partially restore the

ability of the homozygous *ALX1*$^{165F/165F}$ NCC to migrate, with no difference found between these two concentrations (57.6 ± 4.77% for 50 ng/ml of CV2, and 64.64 ± 3.36% for 100 ng/ml of CV2). Finally, we asked whether treatment with a combination of BMP2 and CV2 would exert an additive or synergistic effect to restore cell migration than single compound treatment. No additive effect was identified, as BMP2 and CV2 cotreatment at 100 ng/ml was able to rescue the migration defect phenotype of mutant *ALX1*$^{165F/165F}$ NCC at a similar level to what was observed with the individual treatments (73 ± 5.89% for BMP2 and CV2 cotreatment).

Evaluation of alx1 function in the zebrafish

We and others previously showed that the zebrafish anterior neurocranium (ANC) forms from the convergence of the frontonasal prominence and the paired maxillary prominences (Wada, 2005; Eberhart, 2006; Dougherty *et al*, 2012). Since FND malformation is characterized by facial cleft affecting fusion of the frontonasal and maxillary structures, examination of the ANC morphology in zebrafish would be a sensitive assay for frontonasal development.

To generate an *in vivo* model of *alx1*, we employed CRISPR/Cas9-mediated targeted mutagenesis of the *alx1* locus in zebrafish. This approach produced a frameshift mutation harboring a 16-base pair (bp) deletion in exon 2 of *alx1* (NM_001045074), named *alx1*^{uw2016} (Fig 6A, Fig EV4). The *alx1*^{uw2016} mutation is likely to cause complete loss of function since the encoded truncated protein lacks both the homeobox and transactivation domains. While the majority of *alx1*^{uw2016} homozygous zebrafish developed normally and were viable as adults,

approximately 5% displayed specific craniofacial defects (Fig EV5). Alcian blue staining of *alx1*^{uw2016} homozygous larvae at 5 days post-fertilization (dpf) revealed that the posterior neurocranium and ventral cartilages and Meckel's cartilage were formed but smaller in size in a subset of zebrafish. In contrast, the ANC appeared dysmorphic, i.e., narrower in the transverse dimension and linear, rather than fan-shaped (Fig 6A). The chondrocytes of the ANC appeared cuboidal in mutant larvae, whereas wild-type ANC chondrocytes were lenticular and stacked in an intercalated pattern (Fig 6A).

The low penetrance of the ANC defect suggests the possibility of gene compensation by other *alx* family members (also see Discussion). To test this hypothesis, *alx* transcripts were quantified by qRT–PCR at several stages of embryogenesis in *alx1*^{uw2016} homozygotes. We observed that *alx1* mRNA level was significantly decreased in *alx1*^{uw2016} mutants across several time points, likely because the mutation triggers nonsense-mediated decay (Fig 6B; El-Brolosy *et al*, 2019). Consistent with transcriptional gene compensation, *alx3* and *alx4a* mRNA levels were significantly increased in the *alx1*^{uw2016} mutant embryos compared to wild-type embryos ($P < 0.05$ for 10 ss, 24 hpf and 36 hpf embryos for *alx3*; $P < 0.05$ for 24 hpf and 36 hpf embryos for *alx4a*). These data suggest that *alx3* and *alx4a* functions may compensate for the loss of *alx1* during zebrafish development (Fig 6B).

Given the likely genetic compensation between different *alx* family members, we utilized a dominant-negative approach to interrogate the function of *alx* genes in embryonic development. It has been reported that ALX1 protein homodimerizes to be fully functional (Furukawa *et al*, 2002). In order to circumvent the genetic compensation by *alx3* and *alx4a*, a truncated form of *alx1* containing the N-terminal domain (Alx1DN) was generated. The Alx1DN truncation contains the DNA-binding

homeodomain but is missing the transactivation domain (Herskowitz, 1987). Additionally, an alternative truncated protein that lacks the DNA-binding homeodomain and contains the transactivation domain, termed Alx1CT, was generated. We reasoned that, if a truncated Alx1 protein can occupy its binding sites but fail to dimerize or associate with its coactivators, it may function in a dominant-negative manner.

When Alx1DN was overexpressed by mRNA injection in wild-type zebrafish embryos, embryos displayed significant craniofacial defects (Fig 6C), while Alx1CT-expressing embryos developed normally. On closer inspection with Alcian blue staining, Alx1DN-expressing embryos showed complete abrogation of the frontonasal-derived median section of the ANC and Meckel's cartilage, a similar but more severe phenotype as expected due to the interference with all alx proteins than that observed in *alx1*^{uw2016} mutant embryos. Both *alx1*^{uw2016} and the Alx1DN mutant phenotypes suggest that alx1 regulates the migration of the anterior frontonasal NCC stream that contributes to the median portion of the ANC.

Lineage tracing reveals migration defect of NCC

To elucidate whether anterior cranial NCC migration is specifically affected in Alx1DN embryos, lineage tracing of the migrating NCC was carried out using the *Tg(sox10:kaede*) reporter line (Wada, 2005; Eberhart, 2006; Dougherty *et al,* 2012; McGurk *et al.* 2014). The anterior most stream of NCC in wild-type and Alx1DN

injected embryos was labeled at the 10-somites stage and followed to 96 h post-fertilization (Fig 6D). In the wild-type embryos, at 4 days post-fertilization (dpf), the NCC were able to migrate into the frontonasal region of the palate (Fig 6D). In contrast, the anterior cranial NCC of Alx1DN injected embryos were unable to reach their final location of the median ANC. Instead, the NCC in the AlxDN injected zebrafish were found in an ectopic anterior location outside of the frontonasal domain (Fig 6D, Movie EV3). While it is possible that increased cell death and altered cell division that were observed in the iPSC model are also operating here in the embryo, these cellular derangements are likely minor contributors to explain the ectopic localization of the cranial NCC, whereas altered cell migration is the dominant mechanism.

Discussion

We report the identification of a novel missense variant of human *ALX1* associated with FND. Analysis of this putative loss-of-function variant in patient-derived iPSC and NCC showed a lack of cellular maturation, an increase in apoptosis, and a migration defect. We identified an overexpression of neural plate border specifiers in subject-derived cells, and an imbalance of BMP levels which, when addressed, was capable of mitigating the migration defect discovered in the subject's NCC. A delay of NCC migration was also recognized as key to the morphologic consequences of a loss of *alx1* in zebrafish models. We could identify genetic compensation between different members of the *alx* gene family.

Human genetics of ALX1

Genes of the *ALX* family encode homeodomain transcription factors and are associated with craniofacial malformations. Like other members of this family, the ALX1 protein is composed of two main functional domains: the N-terminal portion containing the DNA-binding homeodomain with two nuclear localization signals, and the C-terminal portion containing an OAR/aristaless domain required for transactivation and protein interaction (Furukawa *et al*, 2002). In this study's pedigree, a novel missense variant p.L165F within the conserved homeodomain was identified. Leucine is an aliphatic, branched amino acid, while phenylalanine is an aromatic, neutral, and nonpolar amino acid. Due to properties of leucine, the substitution itself is likely disruptive to helix II in the DNA-binding element of the homeodomain within which it resides. Disruptive leucine to phenylalanine substitutions have been described in a number of published, genotyped disorders (Miller *et al*, 1992; Gomez & Gammack, 1995). Pathogenic missense variants within the homeodomains of both *ALX3* and *ALX4* have previously been identified as the causes of FND types 1 and 2, respectively (Wuyts *et al*, 2000; Kayserili *et al*, 2009; Twigg *et al*, 2009).

Pathogenic *ALX1* gene variants in FND have been reported in two case studies in the literature. The first study described two families (Uz *et al*, 2010). In the first, three siblings of consanguineous parents were described to suffer from a midline defect of the cranium, bilateral extreme microphthalmia, bilateral oblique cleft lip and palate, a caudal appendage in the sacral region, and agenesis of the corpus callosum. A homozygous 3.7 Mb deletion spanning *ALX1* was identified in all affected subjects. In

a second family, one affected subject was born with a midline defect of the cranium, bilateral microphthalmia, bilateral oblique cleft lip and palate, and a thin corpus callosum. A donor splice-site mutation c.531+1G>A of *ALX1,* homozygous in the child and heterozygous in the parents, was identified to be the likely cause of the child's phenotype.

None of the affected subjects from the pedigree reported in this study demonstrated midline defects of the cranium or a cerebral phenotype. This is in spite of the fact that the missense mutation of the affected subjects in our study lies just proximal to that of family 2, within helix II, within the homeodomain.

A second case report described one family with FND (Ullah *et al*, 2016). It reported on four children born of consanguineous parents that presented with a broad nasal root, smooth philtrum, and mouth protrusion. An *ALX1* gene variant c.661-1G>C was found to be heterozygous in the parents and homozygous in the affected children. The skipping of the exon via alternative splicing likely resulted in a mutant protein with some residual function, explaining the relatively mild phenotype.

The ALX gene family: ALX1, ALX3, and ALX4

The *ALX* gene family consists of three members: *ALX1, ALX3,* and *ALX4* (McGonnell *et al.* 2011). In humans, mutations of each *ALX* gene have been associated with craniofacial malformations of the frontonasal-derived structures with variable phenotypic severity (Wu *et al.,* 2000; Wuyts *et al.,* 2000; Mavrogiannis *et al.,*

2001; Kayserili *et al*, 2009; Twigg *et al*, 2009; Uz *et al*, 2010). FND is a descriptive term that broadly describes a number of malformations of the midface. Previously classified based on appearance (see Tessier, Sedano, De Myer classifications), FND related to variants within the *ALX* gene family has recently been reordered on the basis of genetics: Type I is caused by mutations of *ALX3*; type 2 is caused by mutations of *ALX4*; and type 3 is caused by mutations of *ALX1*. FND types 1 and 2 appear milder than type 3, frequently presenting with altered appearance of the nasal soft tissue (Twigg *et al*, 2009).

In mouse and zebrafish, *Alx1, Alx3,* and *Alx4* have been shown to be expressed in spatiotemporally restricted regions of the craniofacial mesenchyme (Zhao *et al*, 1994; Qu *et al*, 1997; ten Berge *et al*, 1998; Beverdam & Meijlink, 2001; Dee *et al*, 2013; Lours-Calet *et al*, 2014). Evidence of gene compensation has previously been reported in animal studies (Beverdam *et al*, 2001; Dee *et al*, 2013). In studies of sea urchins, *Alx4* was shown to directly regulated by *Alx1* (Rafiq *et al*, 2012; Khor *et al*, 2019). The question remains how the different *ALX* family members regulate craniofacial development, through transcriptional activation or repression of shared and unique target genes.

iPSC-derived NCC for craniofacial disease modeling

Most craniofacial structures are derived from a transient multipotent embryonic population called NCC. The NCC progenitors give rise to a wide variety of cell lineages

including peripheral neurons, melanocytes, and craniofacial mesenchyme (Betancur *et al*, 2010; Stuhlmiller & Garcia-Castro, 2012). NCC exhibit a restricted expression of *ALX1* in the rostral domain during early developmental stages (Zhao *et al*, 1996; Dee *et al*, 2013). Cellular and genetic mechanisms that drive frontonasal NCC formation are poorly understood. In order to gain insight into the functional consequences of the clinically pathogenic *ALX1* gene variant identified in this study's pedigree, iPSC were differentiated into NCC.

While a number of sophisticated protocols using chemically defined mediums and a combination of adherent and/or suspension culturing approaches have been published in recent years, no consensus has been established on a number of controversial issues (Bajpai *et al*, 2010; Leung *et al*, 2016; Tchieu *et al*, 2017).

First, the definition of what a NCC in fact is remains based entirely on the transcriptomic profiling performed in animal studies. While we succeeded in identifying distinctive differences between the *ALX1*$^{165F/165F}$ NCC and healthy controls, the results suffer from an obvious limitation: a lack of understanding which stage of development the NCC represent. The central challenge of the work with iPSC models of human disease remains the lack of available human transcriptomic cell data to allow for an understanding which stage of development is modeled by the cellular lineages derived. NCC are characterized *in vitro* by the expression of markers identified to be specific to this cell population, namely P75, CD57, CD90, CD73, and CD105 (Minarcik & Golden, 2003; Billon *et al*, 2007; Kawano *et al*, 2017) as well as their multilineage differentiation ability. NCC formation is a stepwise process coordinated by a spatiotemporally specific gene expression pattern. In this study, a putative loss of *ALX1* function did not impair NCC differentiation itself or the ability of NCC to

differentiate into multiple cell lineages. Rather, it appeared that the clinically pathogenic *ALX1*$^{165F/165F}$ variant maintained the NCC in a precursor state. While control cells progressively became craniofacial mesenchymal cells by CD57 downregulation and increases in MSC associated marker expression, *ALX1*$^{165F/165F}$ NCC did not undergo changes of their morphology or show a transition of progenitor to mesenchymal markers. Second, a lack of a 3D representation of NCC migration *in vitro* based studies force scientists to either transplant human iPSC-derived NCC into model organisms or retain a 2D system of representation (Bajpai *et al*, 2010; Okuno *et al*, 2017). We focused on the validation of the findings in human iPSC in zebrafish. Third, the development of craniofacial mesenchyme is a product of the interactions of derivatives of all three germ layers. This left the role of *ALX1* in other developmental derivatives unexplored in this study.

To allow for some insight into the expression profile of key NCC markers during the *in vitro* differentiation process, we surveyed relative expression via qPCR every 2 days throughout our differentiation protocol. We found the greatest differences between the unaffected father and the affected children in the expression of *PAX7, PAX3, DLX5, SNAI2*, and *TWIST1*. *ALX1* has been described as a transcription modulator capable of both activating and repressing target gene expression, adapting its activity to different cell types and environments (Gordon *et al*, 1996; Cai, 1998; Damle & Davidson, 2011). Its activity as a repressor, for example, has been documented with prolactin, as *ALX1* binds directly to the prolactin promoter (Gordon *et al*, 1996). In this study, all of the genes were substantially upregulated in the affected children, with the greatest changes found in the earlier time points of

differentiation. ALX1 appears to play the role of a transcriptional repressor in NCC-based craniofacial development.

Neural crest cells delamination and migration depend on signals from the surrounding epidermis, including BMPs, which induce expression of neural plate border specifier genes such as *PAX3*, *TFAP2a*, *MSX1/2* or *ZIC1* (Tribulo *et al*, 2003; Sato *et al*, 2005; Garnett *et al*, 2012; Dougherty *et al*, 2013; Simoes-Costa & Bronner, 2015). Fine temporospatial regulation of the level of these signaling molecules is critical to allow for delamination and migration of NCC craniofacial development. BMPs belong to the transforming growth factor beta (TGFβ) superfamily and can be divided into several subcategories based on molecular similarities. The two BMPs showing dysregulation in this study, BMP2 and BMP9, belong to different subcategories which exhibit different expression patterns and receptors. BMP2 was identified as an important factor in migratory NCC development, with a depletion of mobile NCC in knockout models in transgenic mice resulting in hypomorphic branchial arches. (Kanzler *et al*, 2000). In a complementary mouse model, BMP2 increased migration of NCC when added as a supplement to culture medium (Anderson *et al*, 2006). BMP2 was also found to be required for the migration of NCC in the enteric nervous system in the zebrafish and to be significantly decreased in the gut of patients affected by Hirschsprung's disease, a disease characterized by deficient enteric NCC migration (Huang *et al*, 2019a). BMP9 on the other hand was shown to be required for tooth development in mice (Huang *et al*, 2019b). It was previously identified as a potent inducing factor of osteogenesis, chondrogenesis, and adipogenesis during development (Luther *et al*, 2011; Lamplot *et al*, 2013). Opposed

to other BMPs, including BMP2, BMP9 was found to be resistant to feedback inhibition by BMP3 and noggin (Wang *et al*, 2013).

The relationship of BMP2 and BMP9 in NCC development, migration, and differentiation has yet to be examined. Why BMP2 and BMP9 appeared to play antagonistic roles in the NCC modeling of *ALX1*-related FND presented in this study remains unclear. On the basis of the qPCR data and the multiplex assay revealing a decrease in BMP2 and an increase in BMP9 in NCC supernatant, we hypothesized that a lack of fully functional ALX1 may account for the overexpression of neural plate border specifiers, and the change of BMP signaling. In substituting or repressing BMP2 and BMP9, respectively, an almost complete rescue of the migration defect of the mutant *ALX1*$^{165F/165F}$ NCC was achieved. Pretreatment of subject-derived NCC could perhaps result in a complete rescue of migration.

Animal models of ALX1-related FND

Studies in sea urchins have contributed meaningful knowledge to the regulatory functions of Alx1 as a transcription factor. In the sea urchin *Strongylocentrotus puparatus,* the *alx1* gene was found to activate itself in a self-regulatory loop at lower levels. Once its level exceeds a certain threshold, *alx1* reverses its activity and becomes a repressor of its own transcription (Damle & Davidson, 2011). As a transcription factor, alx1 was found to be essential

for the regulation of epithelial–mesenchymal transition, a process of great importance for the ability of NCC to delaminate and initiate migration (Ettensohn *et al*, 2003).

The specific role of *Alx1* in craniofacial development was investigated in different animal models. Targeted gene ablation of *Alx1* in mice resulted in neural tube closure defects in the majority of the pups, a phenotype not observed in any reported case report of *ALX1*-related FND type 3 (Zhao *et al*, 1996). A previously published morpholino knockdown of *alx1* in zebrafish suggested that the gene is essential for the migration of NCC into the frontonasal prominence, with a disorganization of NCC in the frontonasal stream, and reduction both in the number of NCC and its cellular projections (Dee *et al*, 2013). A major weakness of morpholino gene disruption is nonspecific or off target effects. This study utilized germline *alx1* mutant allele to investigate the effect of *alx1* loss-of-function, complemented by a dominant-negative disruption approach to address gene compensation of other *alx* family members. These approaches corroborate a requirement for alx1 in median ANC morphogenesis, corresponding to formation of the midface in humans.

In summary, this work describes a novel *ALX1* gene variant associated with FND. Using complementary human iPSC and zebrafish models, this study showed that *ALX1* is required for coordinated NCC differentiation and migration. Discordance of NCC differentiation from cell migration during midface morphogenesis results in FND. Future work will be directed at identifying *ALX1* downstream targets and characterize the ALX regulated pathways in craniofacial development.

Data availability

The raw sequencing data sets produced in this study are available in the following database: FaceBase Record ID: 25J0 Accession: FB00000907 (https://www.facebase.org/).

Acknowledgements

We are grateful for Shriners Hospital for Children (85112) and National Institute of Health (U01DE024443) for funding that supported this work. ECL is a recipient of the Massachusetts General Laurie and Mason Tenaglia Research Scholar award. JK is a recipient of the Shiners Hospital Research Fellowship (84701-BOS-19). We thank Jessica Bathoney for excellent management of our aquatics facility.

Author contributions

JP, JK, and ECL conceived of the project and designed the research studies. JP, JK, YDH, CT, KK, PY, BY, NC, RM, JC, and YG conducted the experiments. JP, JK, CT, NC, RM, JC, YG, and ECL prepared the manuscript. JK, CT, and ECL worked on the revision of the manuscript.

Conflict of Interest

The author declares that he has no conflict of interest.

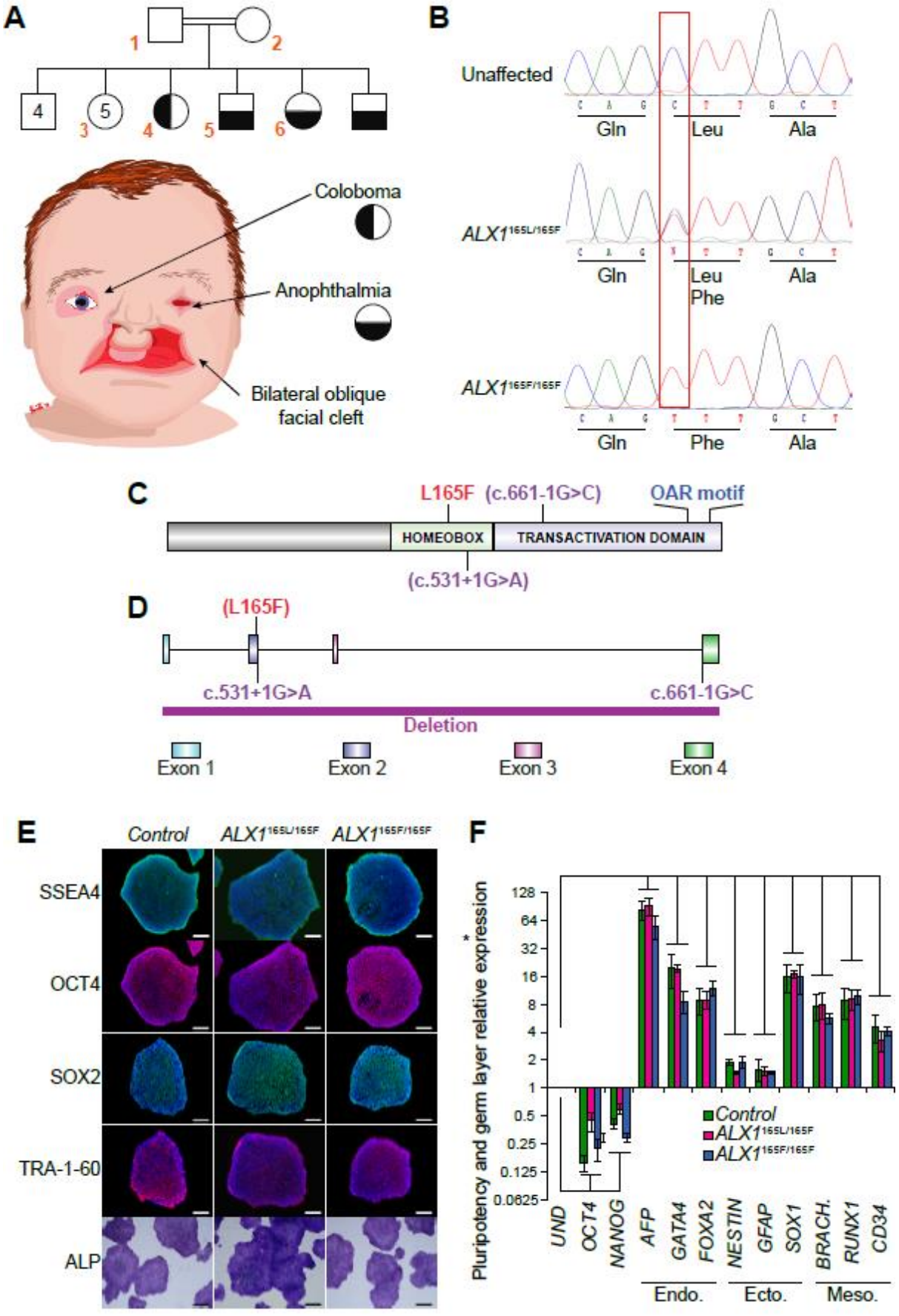
A
1
2
4
3
5
4
5
6
Coloboma
Anophthalmia
Bilateral oblique facial cleft
B
Unaffected
Gln
Leu
Ala
ALX1165L/165F
Gln
Leu
Phe
Ala
ALX1165F/165F
Gln
Phe
Ala
C
L165F (c.661-1G>C)
OAR motif
HOMEOBOX
TRANSACTIVATION DOMAIN
(c.531+1G>A)
D
(L165F)
c.531+1G>A
c.661-1G>C
Deletion
Exon 1
Exon 2
Exon 3
Exon 4
E
Control
ALX1165L/165F
ALX1165F/165F
SSEA4
OCT4
SOX2
TRA-1-60
ALP
F
Pluripotency and germ layer relative expression
128
64
32
16
8
4
2
1
0.5
0.25
0.125
0.0625
Control
ALX1165L/165F
ALX1165F/165F
UND
OCT4
NANOG
AFP
GATA4
FOXA2
NESTIN
GFAP
SOX1
BRACH.
RUNX1
CD34
Endo.
Ecto.
Meso.

Figure 1. *Clinical presentation of the FND pedigree and generation of control, father, and subject-derived iPSC*

A: The pedigree family tree includes two unaffected parents, four unaffected male siblings, five unaffected female siblings, and two each female and male affected sibling. Subjects 1–6, indicated in red, were enrolled in the study. Subjects 4–6 show complex FND with ocular involvement. The eldest affected sibling (subject 4) presented with right coloboma, left microphthalmia, and bilateral Tessier 4 oblique facial clefts. Subject 5 presented with bilateral anophthalmia with fused eyelids and shallow orbits, with bilateral oblique facial clefts. Subject 6 presented with bilateral anophthalmia with open shallow orbits, absent upper and lower eyelids, exposed orbital mucosa, bilateral oblique facial clefts, and malformed nasal ala with nodular skin tags. iPSCs were generated using blood samples collected from subjects 1, 5, and 6.

B: Whole-exome sequencing was carried out and analysis revealed a missense p.L165F variant (c.493 C>T) in the *ALX1* homeodomain, heterozygous in the parents (*ALX1*$^{165L/165F}$), wild type in the unaffected sibling (*ALX1*$^{165L/165L}$), and homozygous in both affected subjects (*ALX1*$^{165F/165F}$).

C: Schematic of the ALX1 protein structure showing the position of the L165F substitution described here (red) and the locations of exon borders affected by two reported pathogenic variants (purple; Ullah *et al*, 2016; Uz *et al*, 2010).

D: Schematic of the *ALX1* genomic sequence, showing the locations of the three reported pathogenic variants. The purple bar at the bottom represents a FND-associated homozygous *ALX1* deletion previously reported in the literature (Uz *et al*, 2010; Ullah *et al*, 2016).

E: Immunofluorescence staining for pluripotent markers *SSEA4*, *OCT4*, *SOX2*, and *TRA-1-60* and alkaline phosphatase staining of iPSC clones. One representative iPSC clone is shown for each genotype. Scale bar: 400 µm.

F: Expression of pluripotent (OCT4, NANOG), endoderm (Endo., AFP, GATA4, FOXA2), ectoderm (Ecto., NESTIN, GFAP, SOX1), and mesoderm (Meso., BRACH. (BRACHYURY), RUNX1, CD34) gene markers for *ALX1*$^{165I/165L}$ (green), *ALX1*$^{165L/165F}$(red), and *ALX1*$^{165F/165F}$ (blue) iPSC relative to undifferentiated cells (UND). Data are represented as pooled mean ± SEM of three experiments on three clones from each genotype. Significance: $P = 0.0167$ for OCT4, $P = 0.0005$ for NANOG, $P = 0.000004$ for AFP, $P = 0.0082$ for GATA4, $P = 0.0137$ for FOXA2, $P = 0.00002$ for NESTIN, $P = 0.0167$ for GFAP, $P = 0.0014$ for SOX1, $P = 0.0117$ for BRACHYURY, $P = 0.0008$ for RUNX1 and $P = 0.0068$ for CD34 when comparing undifferentiated and differentiated *ALX1*$^{165L/165L}$ iPSC. $P = 0.0013$ for OCT4, $P = 0.0011$ for NANOG, $P = 0.0000003$ for AFP, $P = 0.0003$ for GATA4, $P = 0.0063$ for FOXA2, $P = 0.0001$ for NESTIN, $P = 0.027$ for GFAP, $P = 0.000002$ for SOX1, $P = 0.000009$ for BRACHYURY, $P = 3e^{-9}$ for RUNX1 and $P = 0.000006$ for CD34 when comparing undifferentiated and differentiated ALX1$^{165F/165L}$ iPSC. $P = 0.0201$ for OCT4, $P = 0.006$ for NANOG, $P = 1 \times 10^{-12}$ for AFP, $P = 5 \times 10^{-13}$ for GATA4, $P = 0.0031$ for FOXA2, $P = 0.0292$ for NESTIN, $P = 0.00001$ for GFAP, $P = 6 \times 10^{-7}$ for SOX1, $P = 0.0204$ for BRACHYURY, $P = 0.0009$ for RUNX1 and $P = 0.000003$ for CD34 when comparing undifferentiated and differentiated *ALX1*$^{165F/165F}$ iPSC. Data from each clone were pooled, and the mathematical mean was calculated. SEM was used to determine the

standard error. To test statistical significance, an ANOVA test was performed. A *P*-value < 0.05 was considered to be statistically significant.

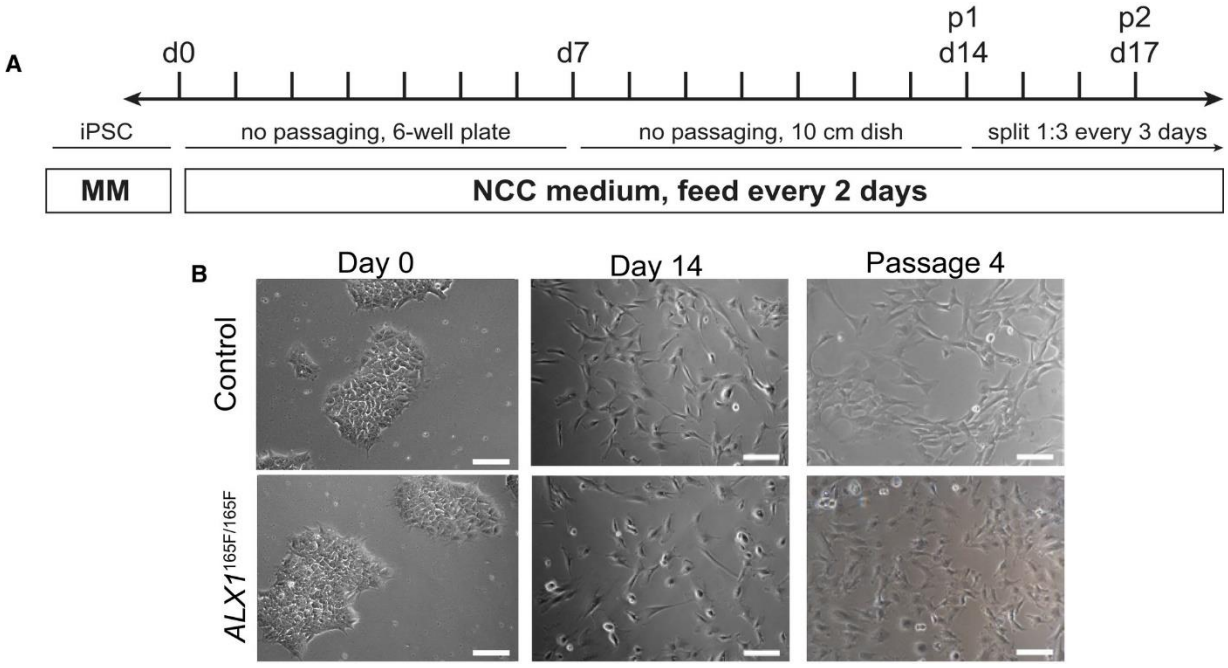

Figure 2. *Generation of iPSC-derived NCC*

A: Schematic of the differentiation protocol timeline. Maintenance Medium (MM) = iPSC medium (StemFlex with 1× penicillin/streptomycin), NCC differentiation medium = DMEM-F12, 10% fetal bovine serum, 1 mM sodium pyruvate, 1 mM penicillin/streptomycin, 1 mM nonessential amino acids, 110 μM 2-mercaptoethanol, 10 ng/ml epidermal growth factor.

B: Images of iPSC and iPSC-derived NCC at Days 0, 14, and passage 4 following differentiation. Scale bars: 400 μm (Day 0), 200 μm (Day 14, passage 4).

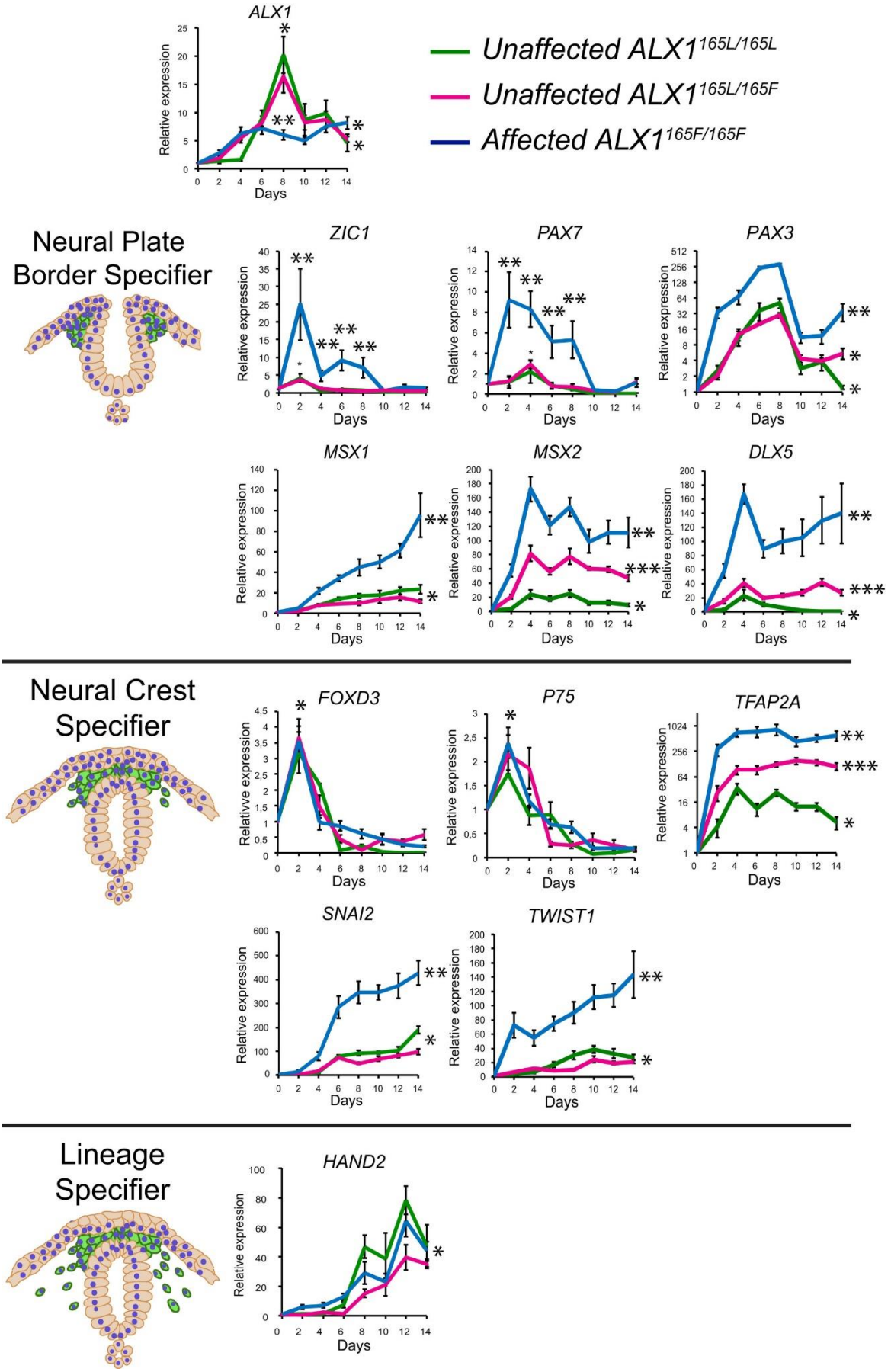
ALX1
Relative expression
Days
Unaffected ALX1165L/165L
Unaffected ALX1165L/165F
Affected ALX1165F/165F
Neural Plate Border Specifier
ZIC1
PAX7
PAX3
MSX1
MSX2
DLX5
Neural Crest Specifier
FOXD3
P75
TFAP2A
SNAI2
TWIST1
Lineage Specifier
HAND2

Figure 3. *Timeline of key NCC-associated genes during differentiation*

Gene expression analysis across NCC differentiation of unaffected control *ALX1*$^{165L/165L}$ (green), heterozygous *ALX1*$^{165L/165F}$ (magenta), and homozygous *ALX1*$^{165F/165F}$ iPSC; *ALX1,* neural plate border specifier genes *ZIC1, PAX7, PAX3, MSX1, MSX2, DLX5;* neural crest specifier genes *FOXD3, P75, TFAP2A, SNAI2, TWIST1;* and lineage specifier gene *HAND2*. The RT–qPCR relative expression values were normalized to *RPLP0* and *GAPDH* expression. Data are represented as pooled mean ± SEM of three experiments on three clones from each genotype. Exact *P*-values are provided in Table EV1. Data from each clone were pooled, and the mathematical mean was calculated. SEM was used to determine the standard error. To test statistical significance, an ANOVA test was performed. A *P*-value < 0.05 was considered to be statistically significant.

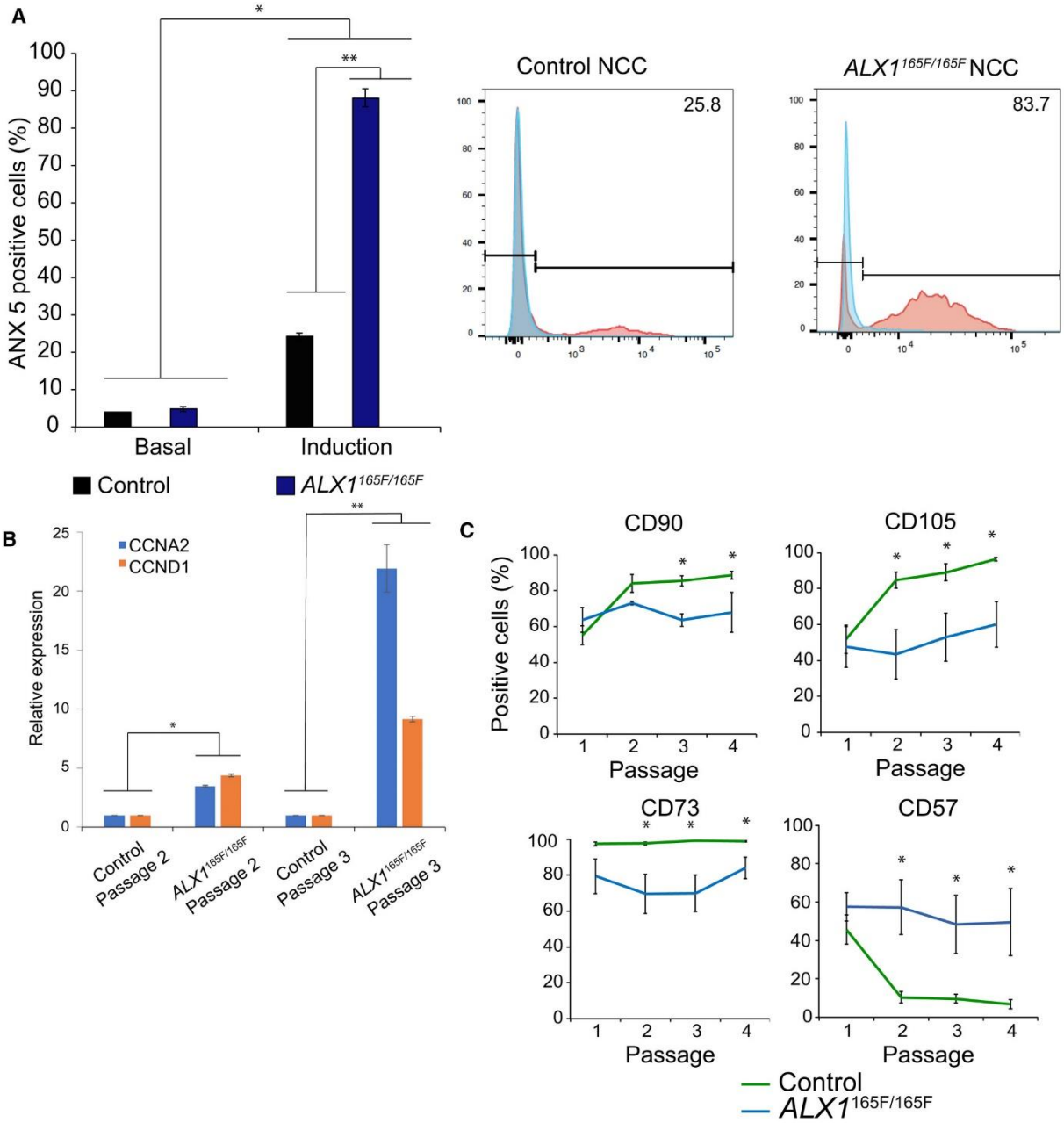

Figure 4. *NCC apoptosis, cell cycle, and differentiation*

A: Homozygous *ALX1*$^{165F/165F}$ NCC (blue) showed an increase in sensitivity to apoptosis when compared to control *ALX1*$^{165L/165L}$ NCC (black). The data on the left represent the mean percentage of Annexin V-positive cells, indicative of apoptosis, as determined by FACS analysis, with the data on the right being an example of one such experiment. Apoptosis was induced by immersion in a 55°C water bath for 10 min.

Representative experiment for each condition is shown. Data are represented as pooled mean ± SEM of three independent experiments. Data obtained of each clone from three independent experiments were pooled, and the mathematical mean was calculated. SEM was used to determine the standard error. To test statistical significance, an ANOVA test was performed. A *P*-value < 0.05 was considered to be statistically significant. *: Significantly different from the basal apoptosis rate: $P = 3 \times 10^{-12}$ between control NCC basal apoptosis and induced apoptosis, and between *ALX1*$^{165F/165F}$ NCC basal apoptosis and induced apoptosis. **Significantly different from control NCC ($P = 0.0004$).

B: Expression levels of cyclins *CCNA2* (blue) and *CCND1* (orange) in NCC at passages 2 and 3 of *ALX1*$^{165L/165L}$ and *ALX1*$^{165F/165F}$ NCC. The RT–qPCR relative expression values were normalized to *RPLP0* and *GAPDH* expression. Data are represented as pooled mean ± SEM of three experiments on three clones from each genotype. *Significantly different from control NCC at passage 2 ($P = 0.001$ between control and *ALX1*$^{165F/165F}$ NCC at passage 2 for CCNA2, $P = 0.0052$ for CCND1). **Significantly different from control NCC at passage 3 ($P = 0.0494$ between control and *ALX1*$^{165F/165F}$ NCC for CCNA2, $P = 0.0008$ for CCND1).

C: Fluorescence activated cell sorting (FACS) experiments showed that control *ALX1*$^{165L/165L}$ NCC (green) exhibited increased expression of mesenchymal markers CD90, CD105, and CD73 with culture time (passages 1 through 4), whereas homozygous *ALX1*$^{165F/165F}$ NCC (blue) showed a consistent expression of the markers expressed at passage 1 throughout. Further, control *ALX1*$^{165L/165L}$ NCC showed a downregulation of CD57 expression with culture time, while *ALX1*$^{165F/165F}$ NCC maintained the same level of CD57 across passages. Data are presented as the mean

percentage of positive-stained cells across passage numbers. Data obtained of each clone from three independent experiments were pooled, and the mathematical mean was calculated. SEM was used to determine the standard error. To test statistical significance, an ANOVA test was performed. A *P*-value < 0.05 was considered to be statistically significant. *Significantly different from control NCC. For CD90, $P = 0.0013$ at passage 3 and $P = 0.0207$ at passage 4. For CD105, $P = 0.0016$ at passage 2, $P = 0.00004$ at passage 3 and $P = 0.0021$ at passage 4. For CD73, $P = 0.0060$ at passage 2, $P = 0.00004$ at passage 3 and $P = 0.0114$ at passage 4. For CD57, $P = 0.0026$ at passage 2, $P = 0.000003$ at passage 3 and $P = 0.000007$ at passage 4.

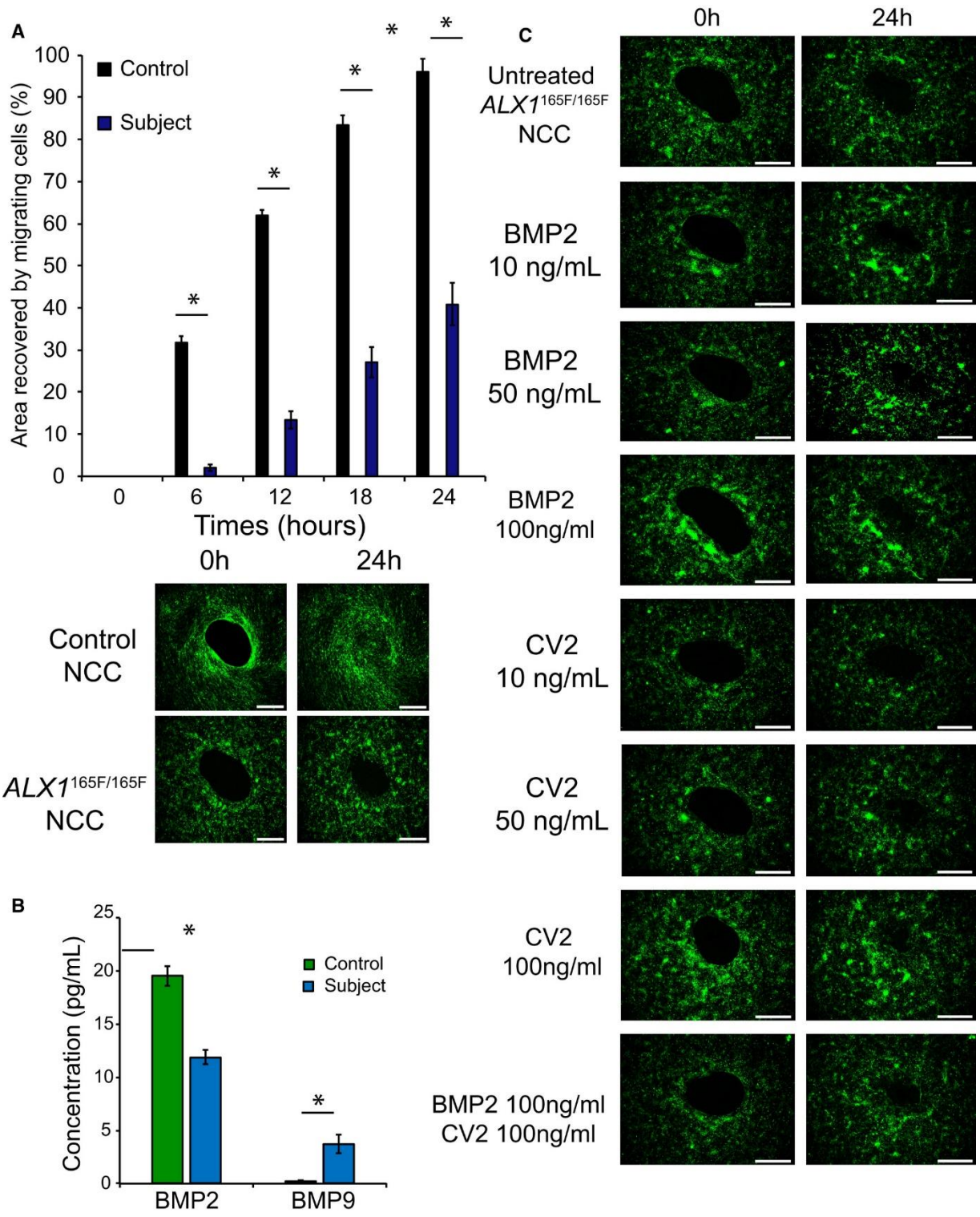
A
Area recovered by migrating cells (%)
Control
Subject
Times (hours)
0
6
12
18
24
0h
24h
Control NCC
ALX1165F/165F NCC
B
Concentration (pg/mL)
Control
Subject
BMP2
BMP9
C
0h
24h
Untreated ALX1165F/165F NCC
BMP2 10 ng/mL
BMP2 50 ng/mL
BMP2 100ng/ml
CV2 10 ng/mL
CV2 50 ng/mL
CV2 100ng/ml
BMP2 100ng/ml CV2 100ng/ml

Figure 5. *ALX1*$^{165F/165F}$ *NCC show a migration defect and a difference in BMP secretion*

A: Mutant *ALX1*$^{165F/165F}$ NCC (blue) exhibited a migration defect in timed coverage of the central clearing of the wound assay when compared with control *ALX1*$^{165L/165L}$ NCC (black). Data are presented as percent area recovery of the central circular clear area of the wound assay by migrating NCC at the end of a 24-h period. For fluorescent pictures, cells were stained in serum-free media containing 3.6 µM CellTracker Green CMFDA (Life Technologies) for 30 min at 37°C and allowed to recover for 30 min before starting the experiment. Images were acquired every 6 h using a Keyence BZ-X800 microscope. Surface area analyses and percentages of coverage were measured using ImageJ software (NIH). The NCC were monitored over 24 h. The data are represented as the average of the percentage of closure ± SEM. Scale bar = 200 µm. Data obtained of each clone from three independent experiments were pooled, and the mathematical mean was calculated. SEM was used to determine the standard error. To test statistical significance, an ANOVA test was performed. A *P*-value < 0.05 was considered to be statistically significant. *Significantly different from control NCC ($P < 0.0001$).

B: Multiplex analysis of BMP2 and BMP9 in the supernatant of cultured NCC showed that *ALX1*$^{165F/165F}$ NCC (blue) secrete less BMP2 and more BMP9 compared to control *ALX1*$^{165L/165L}$ NCC (green). Data are represented as pooled mean ± SEM of three clones from each genotype. Statistical significance was determined with an ANOVA test. A *P*-value < 0.05 was considered significant. *Significantly different from control NCC ($P = 0.0424$ for BMP2 and $P = 0.0192$ for BMP9).

C: Addition of soluble BMP2 or CV2, a BMP9 antagonist, to the culture medium could partially rescue the migration defect of *ALX1*$^{165F/165F}$ NCC. At the beginning of the assay, 10, 50, or 100 ng/ml of soluble BMP2, CV2, or a combination of the two at 100 ng/ml each were added to the culture medium, and the cells were monitored over the next 24 h. The data are represented as the average of the percentage of closure ± SEM. Scale bar: 400 μm.

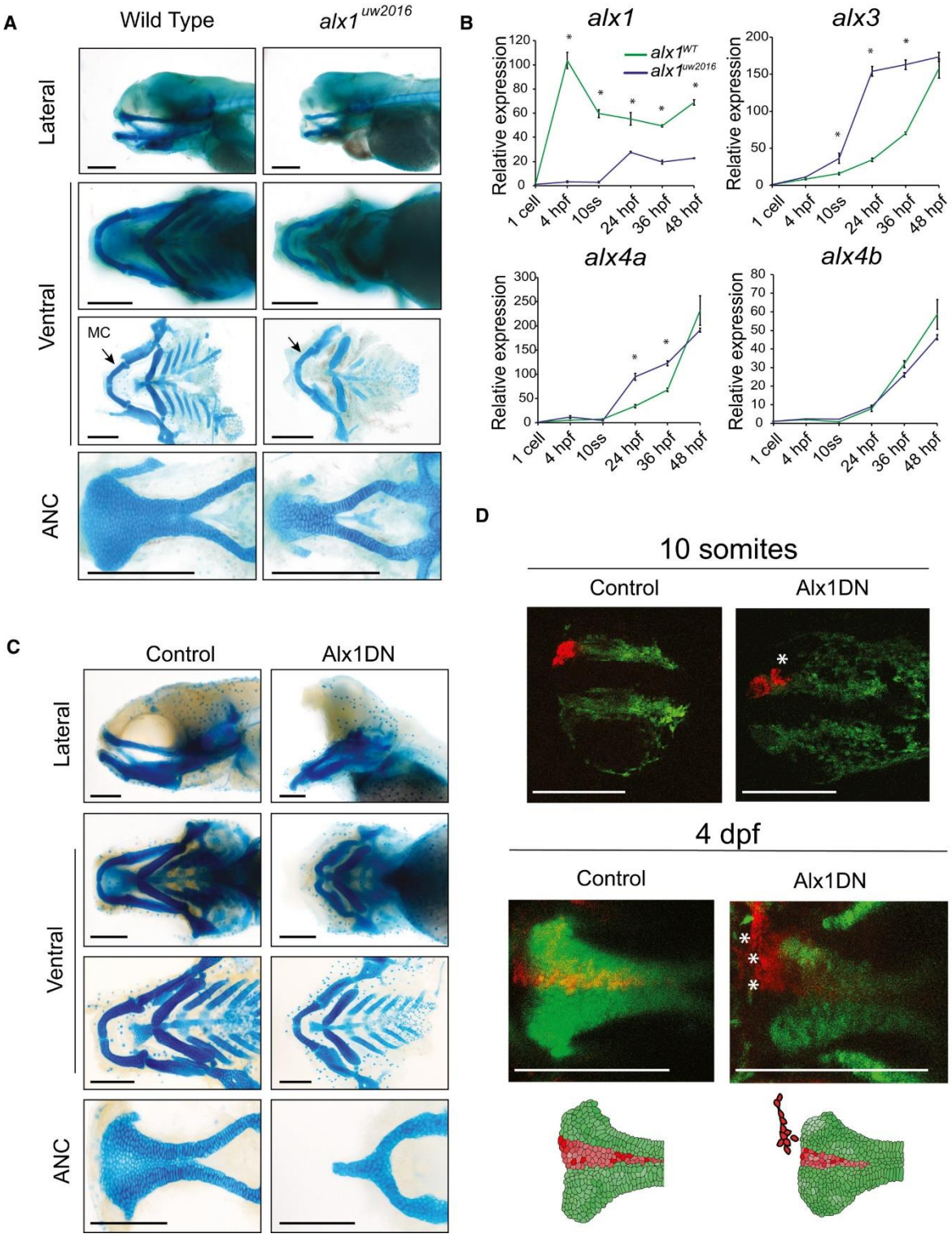

Figure 6. *Alx1 function in zebrafish*

A: Dissected flatmount wild-type and *alx1*$^{-/-}$ zebrafish larvae craniofacial cartilages after Alcian blue staining, the anterior points to the left of the page in all images. The

ventral cartilages appear normal, but the *alx1*$^{-/-}$ anterior neurocranium (ANC) appears narrow, with the midline element that is derived from the frontonasal NCC being absent. Meckel's cartilage (arrow, MC) is also diminutive. Scale bar: 200 μm.

B: Zebrafish *alx1* mutants (blue) show reduced detectable expression of *alx1* but increased expression of *alx3, alx4a* compared to wild-type controls (green). *alx4b* expression levels are similar between wild-type and *alx1*$^{-/-}$ lines. Data are represented as the mean of all pooled embryos from three different clutches. The RT–qPCR relative expression values were normalized to *elfa* and *18S* expression using the ΔΔCT method. Data from each clutch were pooled, and the mathematical mean was calculated. SEM was used to determine the standard error. To test statistical significance, an ANOVA test was performed. A *P*-value < 0.05 was considered to be statistically significant. Statistical significance denoted by *; *P* < 0.0001 between WT zebrafish and *alx1*$^{-/-}$ at all measured time points; at 10 ss, 24 hpf and 36 hpf for *alx3*; and at 24 hpf and 36 hpf for *alx4a*. Refer to Table EV2 for *P*-values.

C: Dissected flatmount of zebrafish embryos injected with Alx1DN, after Alcian blue staining. The embryos developed an absence of the frontonasal-derived median portion of the anterior neurocranium (ANC) and a profound hypoplasia of Meckel's and ventral cartilages. In the most severely affected zebrafish, a nearly abrogated ANC was observed. Scale bar: 200 μm.

D: Lineage tracing experiments in control and Alx1DN mutant embryos revealed aberrant migration of anterior cranial NCC when *alx1* is disrupted. In the control animal, the anterior cranial NCC always migrate to contribute to the median portion of the ANC. In contrast, the anterior cranial NCC labeled in the Alx1DN animals fail to migrate to

the median ANC, where the ANC structure is narrower and the labeled cranial NCC are found in an anterior and lateral ectopic location (white asterisks). Scale bar: 250 μm.

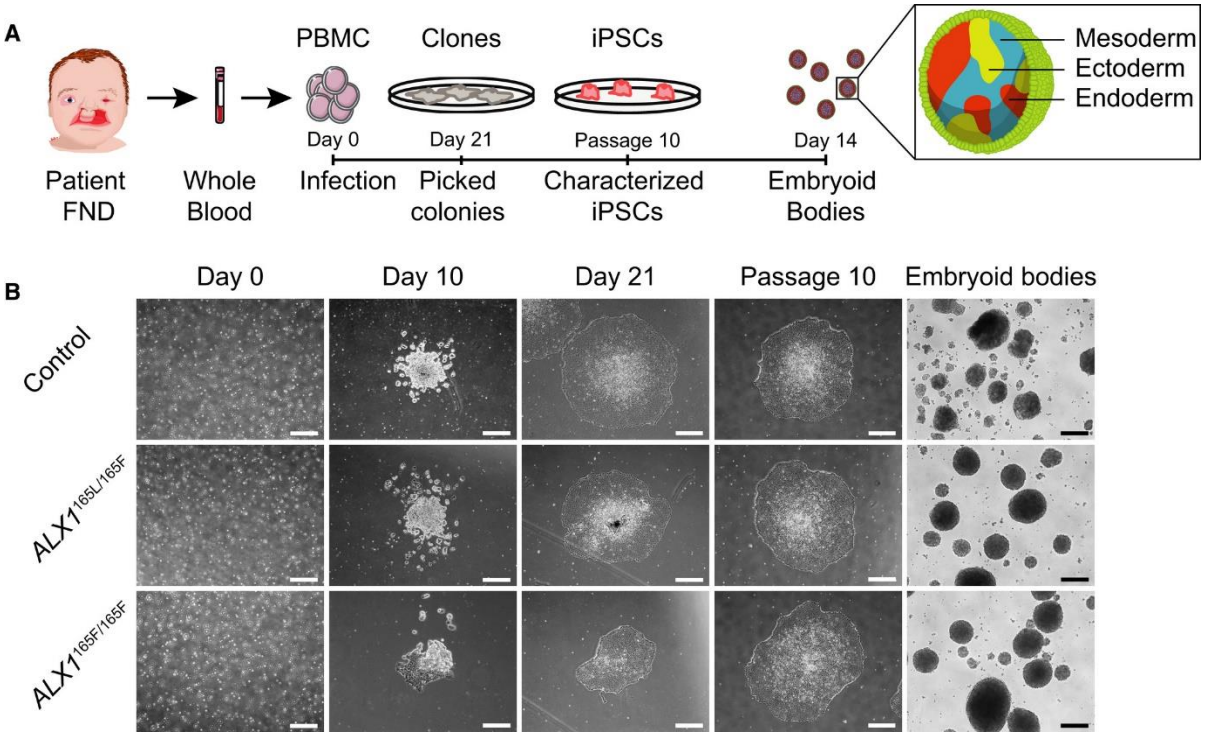

Supplementary Figure 1. *Induced pluripotent stem cells (iPSC) derivation and EB generation*

A: Schematic representation of the strategy used to generate iPSC. Blood samples from an unrelated normal individual, unaffected father (subject 1), and two of the affected children (subjects 5 and 6) were processed. Isolated PBMC were infected with Sendai virus, and individual clones were picked 21 days after the infection. Following expansion until passage 10, iPSC were characterized and embryoid bodies were formed by suspension culture for 14 days.

B: The reprogramming process of the PBMC showed that all cells underwent similar morphological changes leading to the formation of iPSC clones by day 21. These clones still displayed embryonic stem cells morphology at passage 10, indicating that the cells are able to self-renew. All iPSC clones were able to form EBs. One clone of each subject is represented. Scale bar is 400 µm.

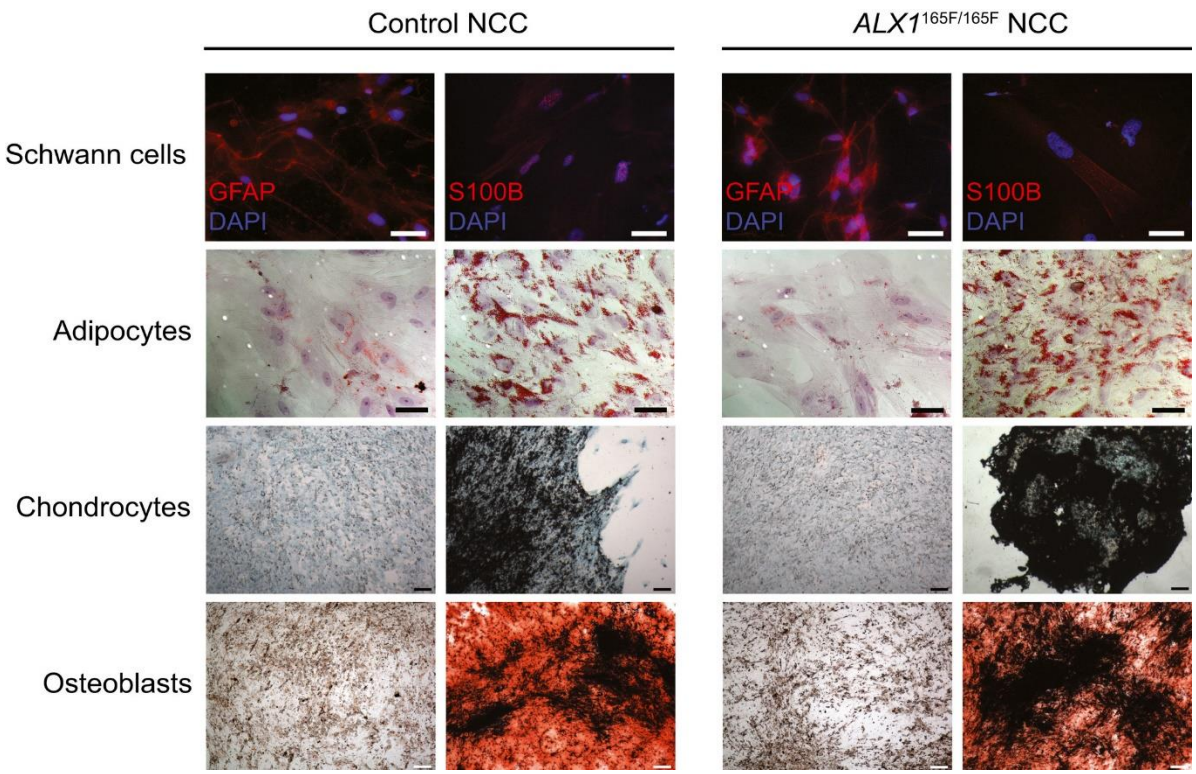

Supplementary Figure 2. *Characterization of NCC*

Multilineage differentiation experiments revealed that both control and subject-derived NCC are able to differentiate into Schwann cells, shown by the GFAP and S100B-positive immunofluorescence staining; adipocytes, demonstrated by the Oil Red O. positive lipidic droplets; osteoblasts, shown by Alizarin Red S. positive mineralized nodules and chondrocytes, assessed by Alcian Blue-positive cartilaginous matrix. Scale bar is 200 µm for images of Schwann cells and adipocytes, and 400 µm for images of chondrocytes and osteoblasts.

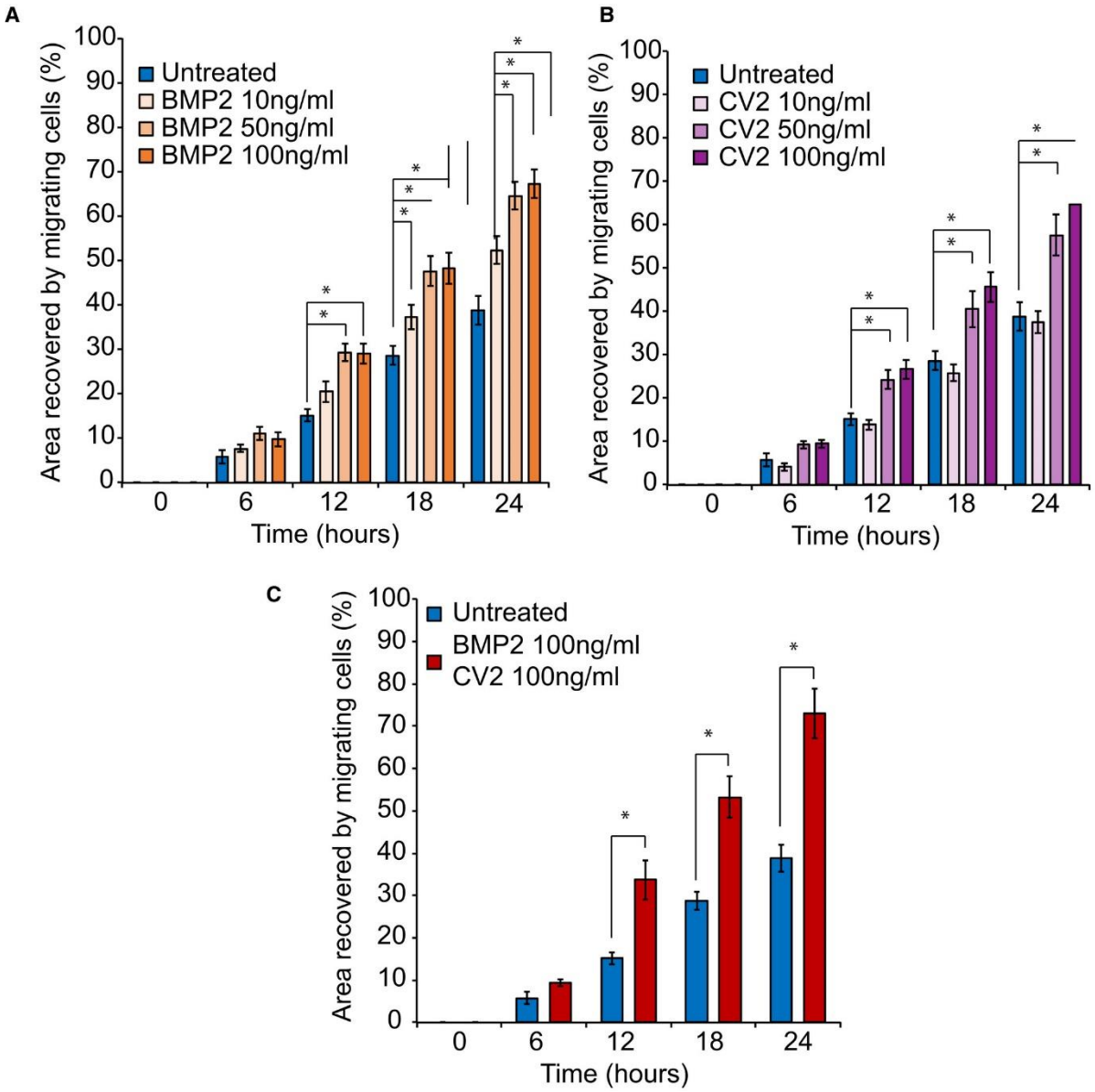

Supplementary Figure 3. *Effect of BMP and CV2 on NCC migration*

A: 10, 50, or 100 ng/ml of soluble BMP2 was added to the culture medium. Surface area analyses and percentages of coverage were measured using ImageJ software (NIH). The data of NCC migration following the treatment with 10, 50, and 100 ng/ml soluble BMP2 are represented as the average of the percentage of closure ± SEM from three independent experiments performed with each clone. To test statistical significance, an ANOVA test was performed. A *P*-value < 0.05 was considered to be

statistically significant *: Significantly different from untreated *ALX1*$^{165F/165F}$ NCC: at 12 h, *P* = 0.0038 when comparing BMP2 50 ng/ml and untreated *ALX1*$^{165F/165F}$ NCC, and *P* = 0.0045 when comparing BMP2 100 ng/ml and untreated *ALX1*$^{165F/165F}$ NCC. At 18 h, *P* = 0.0337 when comparing BMP2 10 ng/ml and untreated *ALX1*$^{165F/165F}$ NCC; *P* = 0.0009 when comparing BMP2 50 ng/ml and untreated *ALX1*$^{165F/165F}$ NCC; and *P* = 0.0006 when comparing BMP2 100 ng/ml and untreated *ALX1*$^{165F/165F}$ NCC. At 24 h, *P* = 0.005 when comparing BMP2 10 ng/ml and untreated *ALX1*$^{165F/165F}$ NCC; *P* < 0.0001. when comparing BMP2 50 ng/ml and untreated *ALX1*$^{165F/165F}$ NCC; and *P* < 0.0001 when comparing BMP2 100 ng/ml and untreated *ALX1*$^{165F/165F}$ NCC.

B: 10, 50, or 100 ng/ml of soluble CV2 was added to the culture medium. Surface area analyses and percentages of coverage were measured using ImageJ software (NIH). The data of NCC migration following the treatment with 10, 50, and 100 ng/ml soluble CV2 are represented as the average of the percentage of closure ± SEM. Scale bar = 400 µm. *: Significantly different from untreated *ALX1*$^{165F/165F}$ NCC: at 12 h, *P* = 0.0146 when comparing CV2 50 ng/ml and untreated *ALX1*$^{165F/165F}$ NCC, and *P* = 0.0262 when comparing CV2 100 ng/ml and untreated *ALX1*$^{165F/165F}$ NCC. At 18 h, *P* = 0.0028 when comparing CV2 50 ng/ml and untreated *ALX1*$^{165F/165F}$ NCC, and *P* = 0.0035 when comparing CV2 100 ng/ml and untreated *ALX1*$^{165F/165F}$ NCC. At 24 h, *P* = 0.0002 when comparing CV2 50 ng/ml and untreated *ALX1*$^{165F/165F}$ NCC, and *P* < 0.0001 when comparing CV2 100 ng/ml and untreated *ALX1*$^{165F/165F}$ NCC.

C: Recovery of subject-derived NCC migration in a migration assay following the combined treatment with 100 ng/ml each of soluble BMP2 and CV2. The data are represented as the average of the percentage of closure ± SEM from three

independent experiments performed with each clone. To test statistical significance, an ANOVA test was performed. A *P*-value < 0.05 was considered to be statistically significant * : Significantly different from *ALX1*$^{165F/165F}$ NCC: at 12 h, *P* = 0.0031, at 18 h *P* = 0.0001, and at 24 h *P* < 0.0001).

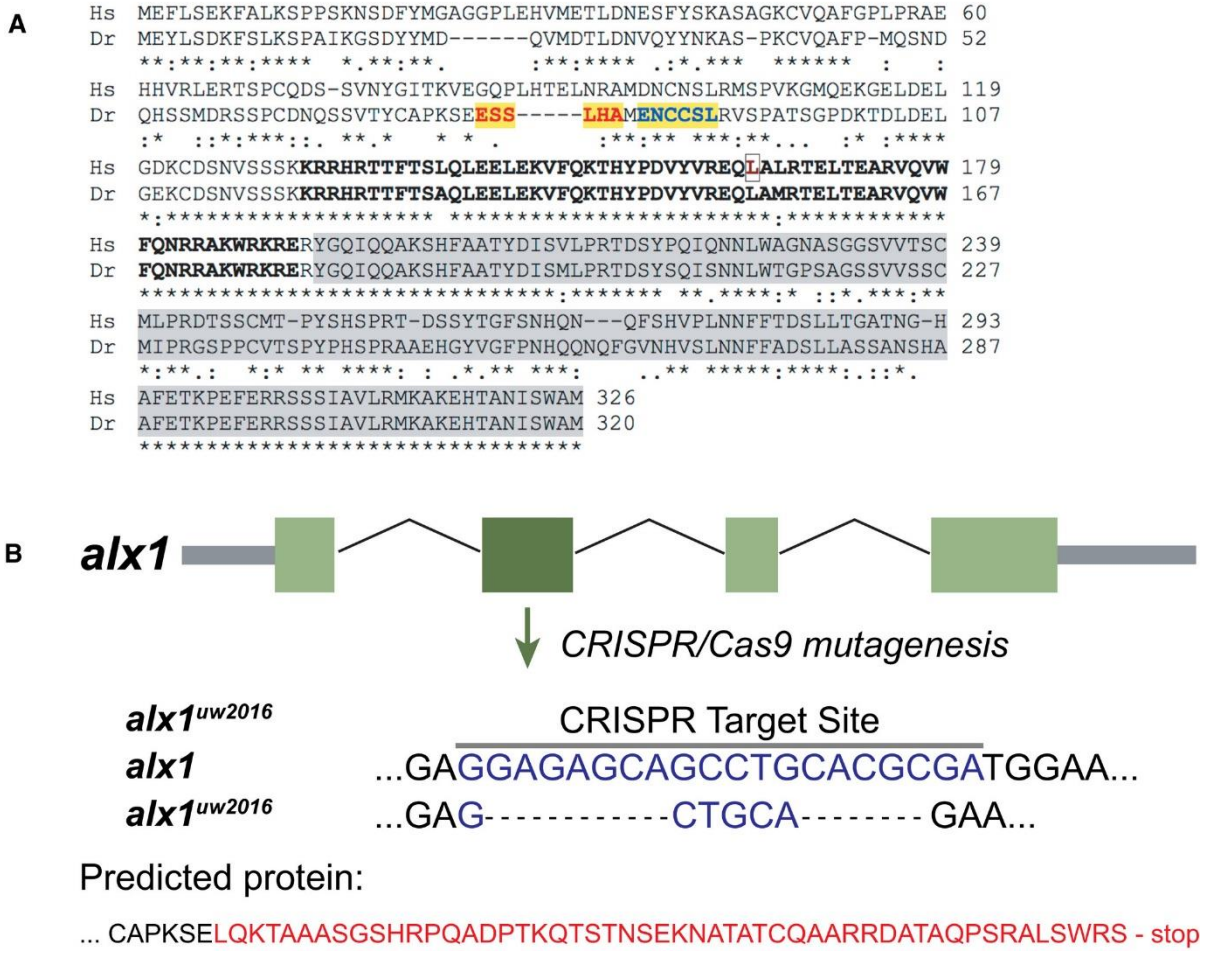

Supplementary Figure 4. *CRISPR/Cas9 targeted mutagenesis of alx1 in zebrafish*

A: Human ALX1 and zebrafish alx1 protein sequences were obtained from Ensembl and aligned using Clustal Omega (https://www.ebi.ac.uk/Tools/msa/clustalo/) under the default settings. The homeobox DNA-binding domain is shown in bold, with the amino acid residue mutated in the subjects indicated by an outline. The transactivation domain is shaded in gray. Zebrafish *alx1* CRISPR sites #1 and #2 are highlighted in yellow. The red and blue letters visually demarcate the sites.

B: Schematic diagram shows the effect of the mutant allele resulting from our choice of target site #1. The allele, termed, *alx1*^{uw2016}, has a net deletion of 16 nucleotides. Red letters denote the abnormal sequence that results from the frameshift mutation.

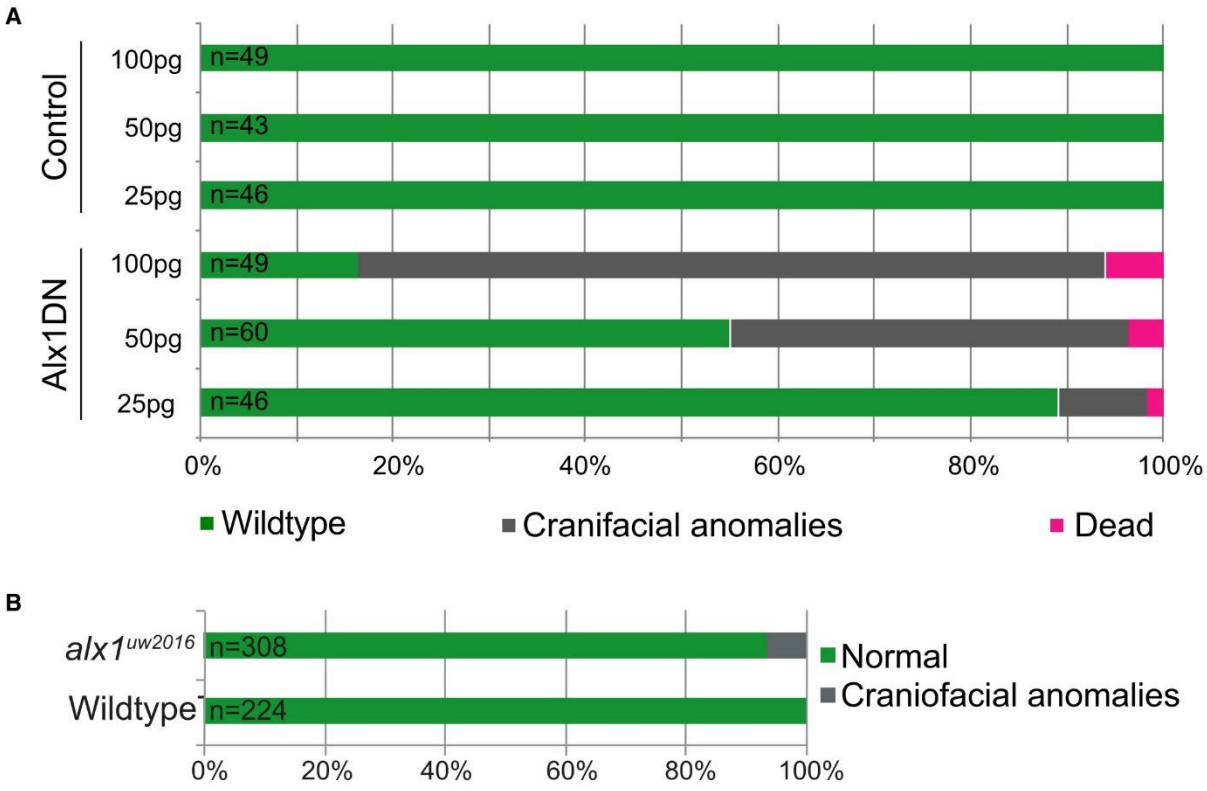

Supplementary Figure 5. *Qualitative and quantitative characterization of zebrafish mutants*

A: The number of embryos displaying craniofacial phenotypes increased with increasing concentration of Alx1DN mRNA injected into the single cell stage embryo. Overview of the relationship of the results of injections of 25, 50, and 100 pg of control mRNA and Alx1DN mRNA with the outcomes of wild-type zebrafish (green), a craniofacial phenotype (gray), and dead zebrafish (magenta).

B: The number of embryos displaying craniofacial phenotypes injected with *alx1*^{uw2016} mRNA was very low. Overview of the percent of injected wild-type zebrafish displaying a craniofacial phenotype (gray), compared with uninjected wild-type zebrafish from the identical clutches (gray). Data of the injections are presented as a comparative percentage.

Table 1. Comparative FACS analysis of subject-derived *ALX1*$^{165F/165F}$ and control NCC at passages 1 and 4

	Passage 1		Passage 4	
	Control (*ALX1*$^{165L/165L}$)	*ALX1*$^{165F/165F}$	Control (*ALX1*$^{165L/165L}$)	*ALX1*$^{165F/165F}$
CD57	45.6 ± 7.7%	57.4 ± 7.3%	6.78 ± 2.36%	49.55 ± 17.53%
CD90	55.05 ± 5.24%	63.6 ± 6.9%	88.46 ± 2.05%	67.8 ± 11.07%
CD105	51.7 ± 7.8%	47.6 ± 11.4%	96.31 ± 0.95%	60.02 ± 12.66%
CD73	97.4 ± 1.08%	79.2 ± 9.6%	98.8 ± 0.44%	83.95 ± 6.05%

Reference

Adzhubei IA, Schmidt S, Peshkin L, Ramensky VE, Gerasimova A, Bork P, Kondrashov AS, Sunyaev SR (2010) A method and server for predicting damaging missense mutations. Nat Methods 7: 248 – 249

Anderson RM, Stottmann RW, Choi M, Klingensmith J (2006) Endogenous bone morphogenetic protein antagonists regulate mammalian neural crest generation and survival. Dev Dyn 235: 2507 – 2520

Bajpai R, Chen DA, Rada-Iglesias A, Zhang J, Xiong Y, Helms J, Chang CP, Zhao Y, Swigut T, Wysocka J (2010) CHD7 cooperates with PBAF to control multipotent neural crest formation. Nature 463: 958 – 962

Barrallo-Gimeno A, Holzschuh J, Driever W, Knapik EW (2004) Neural crest survival and differentiation in zebrafish depends on mont blanc/tfap2a gene function. Development 131: 1463 – 1477

ten Berge D, Brouwer A, el Bahi S, Guenet JL, Robert B, Meijlink F (1998) Mouse Alx3: an aristaless-like homeobox gene expressed during embryogenesis in ectomesenchyme and lateral plate mesoderm. Dev Biol 199: 11 – 25

Betancur P, Bronner-Fraser M, Sauka-Spengler T (2010) Assembling neural crest regulatory circuits into a gene regulatory network. Annu Rev Cell Dev Biol 26: 581 – 603

Beverdam A, Brouwer A, Reijnen M, Korving J, Meijlink F (2001) Severe nasal clefting and abnormal embryonic apoptosis in Alx3/Alx4 double mutant mice. Development 128: 3975 – 3986

Beverdam A, Meijlink F (2001) Expression patterns of group-I aristaless-related genes during craniofacial and limb development. Mech Dev 107: 163 – 167

Adzhubei IA, Schmidt S, Peshkin L, Ramensky VE, Gerasimova A, Bork P, Kondrashov AS, Sunyaev SR (2010) A method and server for predicting damaging missense mutations. Nat Methods 7: 248 – 249

Anderson RM, Stottmann RW, Choi M, Klingensmith J (2006) Endogenous bone morphogenetic protein antagonists regulate mammalian neural crest generation and survival. Dev Dyn 235: 2507 – 2520

Bajpai R, Chen DA, Rada-Iglesias A, Zhang J, Xiong Y, Helms J, Chang CP, Zhao Y, Swigut T, Wysocka J (2010) CHD7 cooperates with PBAF to control multipotent neural

crest formation. Nature 463: 958 – 962

Barrallo-Gimeno A, Holzschuh J, Driever W, Knapik EW (2004) Neural crest survival and differentiation in zebrafish depends on mont blanc/tfap2a gene function. Development 131: 1463 – 1477

ten Berge D, Brouwer A, el Bahi S, Guenet JL, Robert B, Meijlink F (1998) Mouse Alx3: an aristaless-like homeobox gene expressed during embryogenesis in ectomesenchyme and lateral plate mesoderm. Dev Biol 199: 11 – 25

Betancur P, Bronner-Fraser M, Sauka-Spengler T (2010) Assembling neural crest regulatory circuits into a gene regulatory network. Annu Rev Cell Dev Biol 26: 581 – 603

Beverdam A, Brouwer A, Reijnen M, Korving J, Meijlink F (2001) Severe nasal clefting and abnormal embryonic apoptosis in Alx3/Alx4 double mutant mice. Development 128: 3975 – 3986

Beverdam A, Meijlink F (2001) Expression patterns of group-I aristaless-related genes during craniofacial and limb development. Mech Dev 107: 163 – 167

Bhoj EJ, Li D, Harr MH, Tian L, Wang T, Zhao Y, Qiu H, Kim C, Hoffman JD, Hakonarson H et al (2015) Expanding the SPECC1L mutation phenotypic spectrum to include Teebi hypertelorism syndrome. Am J Med Genet A 167A: 2497 – 2502

Billon N, Iannarelli P, Monteiro MC, Glavieux-Pardanaud C, Richardson WD, Kessaris N, Dani C, Dupin E (2007) The generation of adipocytes by the neural crest. Development 134: 2283 – 2292

Cai RL (1998) Human CART1, a paired-class homeodomain protein, activates transcription through palindromic binding sites. Biochem Biophys Res Comm 250: 305 – 311

Chai Y, Jiang X, Ito Y, Bringas P Jr, Han J, Rowitch DH, Soriano P, McMahon AP, Sucov HM (2000) Fate of the mammalian cranial neural crest during tooth and mandibular morphogenesis. Development 127: 1671 – 1679

Damle S, Davidson EH (2011) Precise cis-regulatory control of spatial and temporal expression of the alx-1 gene in the skeletogenic lineage of S. purpuratus. Dev Biol 357: 505 – 517

Dee CT, Szymoniuk CR, Mills PE, Takahashi T (2013) Defective neural crest migration revealed by a Zebrafish model of Alx1-related frontonasal dysplasia. Hum Mol Genet 22: 239 – 251

Dougherty M, Kamel G, Shubinets V, Hickey G, Grimaldi M, Liao EC (2012) Embryonic fate map of first pharyngeal arch structures in the sox10:kaede zebrafish transgenic model. J Craniofac Surg 23: 1333 – 1337

Dougherty M, Kamel G, Grimaldi M, Gfrerer L, Shubinets V, Ethier R, Hickey G, Cornell RA, Liao EC (2013) Distinct requirements for wnt9a and irf6 in extension and integration mechanisms during zebrafish palate morphogenesis. Development 140: 76 – 81

Eberhart JK (2006) Early Hedgehog signaling from neural to oral epithelium organizes anterior craniofacial development. Development 133: 1069 – 1077

El-Brolosy MA, Kontarakis Z, Rossi A, Kuenne C, Gunther S, Fukuda N, Kikhi K, Boezio GLM, Takacs CM, Lai SL et al (2019) Genetic compensation triggered by mutant mRNA degradation. Nature 568: 193 – 197

Ettensohn CA, Illies MR, Oliveri P, De Jong DL (2003) Alx1, a member of the Cart1/Alx3/Alx4 subfamily of Paired-class homeodomain proteins, is an essential component of the gene network controlling skeletogenic fate specification in the sea urchin embryo. Development 130: 2917 – 2928

Fox JW, Golden GT, Edgerton MT (1976) Frontonasal dysplasia with alar clefts in two sisters. Genetic considerations and surgical correction. Plast Reconstr Surg 57: 553 – 561

Furukawa K, Iioka T, Morishita M, Yamaguchi A, Shindo H, Namba H, Yamashita S, Tsukazaki T (2002) Functional domains of paired-like homeoprotein Cart1 and the relationship between dimerization and transcription activity. Genes Cells 7: 1135 – 1147

Gagnon JA, Valen E, Thyme SB, Huang P, Akhmetova L, Pauli A, Montague TG, Zimmerman S, Richter C, Schier AF (2014) Efficient mutagenesis by Cas9 protein-mediated oligonucleotide insertion and large-scale assessment of single-guide RNAs. PLoS ONE 9: e98186

Garnett AT, Square TA, Medeiros DM (2012) BMP, Wnt and FGF signals are integrated through evolutionarily conserved enhancers to achieve robust expression of Pax3 and Zic genes at the zebrafish neural plate border. Development 139: 4220 – 4231

Gomez CM, Gammack JT (1995) A leucine-to-phenylalanine substitution in the acetylcholine receptor ion channel in a family with the slow-channel syndrome.

Neurology 45: 982 – 985

Gordon DF, Wagner J, Atkinson BL, Chiono M, Berry R, Sikela J, Gutierrez-Hartmann A (1996) Human Cart-1: structural organization, chromosomal localization, and functional analysis of a cartilage-specific homeodomain cDNA. DNA Cell Biol 15: 531 – 541

Hayashi M, Nimura K, Kashiwagi K, Harada T, Takaoka K, Kato H, Tamai K, Kaneda Y (2007) Comparative roles of Twist-1 and Id1 in transcriptional regulation by BMP signaling. J Cell Sci 120: 1350 – 1357

Herskowitz I (1987) Functional inactivation of genes by dominant negative mutations. Nature 329: 219 – 222

Huang S, Wang Y, Luo L, Li X, Jin X, Li S, Yu X, Yang M, Guo Z (2019a) BMP2 is related to Hirschsprung's disease and required for enteric nervous system development. Front Cell Neurosci 13: 523

Huang X, Wang F, Zhao C, Yang S, Cheng Q, Tang Y, Zhang F, Zhang Y, Luo W, Wang C et al (2019b) Dentinogenesis and tooth-alveolar bone complex defects in BMP9/GDF2 knockout mice. Stem Cells Dev 28: 683 – 694

Johnston MC (1966) A radioautographic study of the migration and fate of cranial neural crest cells in the chick embryo. Anat Rec 156: 143 – 155

Johnston MC (1975) The neural crest in abnormalities of the face and brain. Birth Defects Orig Artic Ser 11: 1 – 18

Kanzler B, Foreman RK, Labosky PA, Mallo M (2000) BMP signaling is essential for development of skeletogenic and neurogenic cranial neural crest. Development 127: 1095 – 1104

Karczewski KJ, Francioli LC, Tiao G, Cummings BB, Alföldi J, Wang Q, Collins RL, Laricchia KM, Ganna A, Birnbaum DP et al (2019) The mutational constraint spectrum quantified from variation in 141,456 humans. BioRxiv https://doi.org/10.1101/531210 [PREPRINT]

Kawano E, Toriumi T, Iguchi S, Suzuki D, Sato S, Honda M (2017) Induction of neural crest cells from human dental pulp-derived induced pluripotent stem cells. Biomed Res 38: 135 – 147

Kayserili H, Uz E, Niessen C, Vargel I, Alanay Y, Tuncbilek G, Yigit G, Uyguner O, Candan S, Okur H et al (2009) ALX4 dysfunction disrupts craniofacial and epidermal development. Hum Mol Genet 18: 4357 – 4366

Khor JM, Guerrero-Santoro J, Ettensohn CA (2019) Genome-wide identification of binding sites and gene targets of Alx1, a pivotal regulator of echinoderm skeletogenesis. Development 146: dev180653

Khudyakov J, Bronner-Fraser M (2009) Comprehensive spatiotemporal analysis of early chick neural crest network genes. Dev Dyn 238: 716 – 723

LaFave MC, Varshney GK, Vemulapalli M, Mullikin JC, Burgess SM (2014) A defined zebrafish line for high-throughput genetics and genomics: NHGRI-1. Genetics 198: 167 – 170

Lamplot JD, Qin J, Nan G, Wang J, Liu X, Yin L, Tomal J, Li R, Shui W, Zhang H et al (2013) BMP9 signaling in stem cell differentiation and osteogenesis. Am J Stem Cells 2: 1 – 21

Le Douarin NM, Ziller C, Couly GF (1993) Patterning of neural crest derivatives in the avian embryo: in vivo and in vitro studies. Dev Biol 159: 24 – 49

Le Lièvre CS, Le Douarin NM (1975) Mesenchymal derivatives of the neural crest: analysis of chimaeric quail and chick embryos. J Embryol Exp Morphol 34: 125 – 154

Le Lièvre CS (1978) Participation of neural crest-derived cells in the genesis of the skull in birds. J Embryol Exp Morphol 47: 17 – 37

Leung AW, Murdoch B, Salem AF, Prasad MS, Gomez GA, Garcia-Castro MI (2016) WNT/beta-catenin signaling mediates human neural crest induction via a pre-neural border intermediate. Development 143: 398 – 410

Lours-Calet C, Alvares LE, El-Hanfy AS, Gandesha S, Walters EH, Sobreira DR, Wotton KR, Jorge EC, Lawson JA, Kelsey Lewis A et al (2014) Evolutionarily conserved morphogenetic movements at the vertebrate head-trunk interface coordinate the transport and assembly of hypopharyngeal structures. Dev Biol 390: 231 – 246

Lowe D (1999) Object recognition from local scale-invariant features. In Proceedings of the International Conference on Computer Vision 2

Luther G, Wagner ER, Zhu G, Kang Q, Luo Q, Lamplot J, Bi Y, Luo X, Luo J, Teven C et al (2011) BMP-9 induced osteogenic differentiation of mesenchymal stem cells: molecular mechanism and therapeutic potential. Curr Gene Ther 11: 229 – 240

Mavrogiannis LA, Antonopoulou I, Baxova A, Kutilek S, Kim CA, Sugayama SM, Salamanca A, Wall SA, Morriss-Kay GM, Wilkie AO (2001) Haploinsufficiency of the human homeobox gene ALX4 causes skull ossification defects. Nat Genet 27: 17 – 18

McGonnell IM, Graham A, Richardson J, Fish JL, Depew MJ, Dee CT, Holland PWH, Takahashi T (2011) Evolution of the Alx homeobox gene family: parallel retention and independent loss of the vertebrate Alx3 gene: Evolution of vertebrate Alx homeobox genes. Evol Dev 13: 343 – 351

McGurk PD, Lovely CB, Eberhart JK (2014) Analyzing craniofacial morphogenesis in zebrafish using 4D confocal microscopy. J Vis Exp 83: e51190

Meulemans D, Bronner-Fraser M (2002) Amphioxus and lamprey AP-2 genes: implications for neural crest evolution and migration patterns. Development 129: 4953 – 4962

Miller JL, Lyle VA, Cunningham D (1992) Mutation of leucine-57 to phenylalanine in a platelet glycoprotein Ib alpha leucine tandem repeat occurring in patients with an autosomal dominant variant of Bernard-Soulier disease. Blood 79: 439 – 446

Minarcik JC, Golden JA (2003) AP-2 and HNK-1 define distinct populations of cranial neural crest cells. Orthod Craniofac Res 6: 210 – 219

Minarikova P, Benesova L, Halkova T, Belsanova B, Tuckova I, Belina F, Dusek L, Zavoral M, Minarik M (2016) Prognostic importance of Cell Cycle Regulators Cyclin D1 (CCND1) and Cyclin-Dependent Kinase Inhibitor 1B (CDKN1B/p27) in sporadic gastric cancers. Gastroenterol Res Pract 2016: 9408190

Minoux M, Rijli FM (2010) Molecular mechanisms of cranial neural crest cell migration and patterning in craniofacial development. Development 137: 2605 – 2621

Okuno H, Renault Mihara F, Ohta S, Fukuda K, Kurosawa K, Akamatsu W, Sanosaka T, Kohyama J, Hayashi K, Nakajima K et al (2017) CHARGE syndrome modeling using patient-iPSCs reveals defective migration of neural crest cells harboring CHD7 mutations. eLife 6: e21114

Olsson L, Moury DJ, Carl TF, Hastad O, Hanken J (2002) Cranial neural crest cell migration in the direct-developing frog, Eleutherodactylus coqui: molecular heterogeneity within and among migratory streams. Zoology 105: 3 – 13

Pagano M, Pepperkok R, Verde F, Ansorge W, Draetta G (1992) Cyclin A is required at two points in the human cell cycle. EMBO J 11: 961 – 971

Pierpont ME, Basson CT, Benson DW Jr, Gelb BD, Giglia TM, Goldmuntz E, McGee G, Sable CA, Srivastava D, Webb CL et al (2007) Genetic basis for congenital heart defects: current knowledge: a scientific statement from the American Heart Association Congenital Cardiac Defects Committee, Council on Cardiovascular

Disease in the Young: endorsed by the American Academy of Pediatrics. Circulation 115: 3015 – 3038

Pini J, Giuliano S, Matonti J, Gannoun L, Simkin D, Rouleau M, Bendahhou S (2018) Osteogenic and chondrogenic master genes expression is dependent on the Kir2.1 potassium channel through the bone morphogenetic protein pathway. J Bone Miner Res 33: 1826 – 1841

Qu S, Li L, Wisdom R (1997) Alx-4: cDNA cloning and characterization of a novel paired-type homeodomain protein. Gene 203: 217 – 223

Rada-Iglesias A, Bajpai R, Prescott S, Brugmann SA, Swigut T, Wysocka J (2012) Epigenomic annotation of enhancers predicts transcriptional regulators of human neural crest. Cell Stem Cell 11: 633 – 648

Rada-Iglesias A, Prescott SL, Wysocka J (2013) Human genetic variation within neural crest enhancers: molecular and phenotypic implications. Philos Trans R Soc Lond B Biol Sci 368: 20120360

Rafiq K, Cheers MS, Ettensohn CA (2012) The genomic regulatory control of skeletal morphogenesis in the sea urchin. Development 139: 579 – 590

Ren J, Wen L, Gao X, Jin C, Xue Y, Yao X (2009) DOG 1.0: illustrator of protein domain structures. Cell Res 19: 271 – 273

Sadaghiani B, Thiébaud CH (1987) Neural crest development in the Xenopus laevis embryo, studied by interspecific transplantation and scanning electron microscopy. Dev Biol 124: 91 – 110

Sato T, Sasai N, Sasai Y (2005) Neural crest determination by co-activation of Pax3 and Zic1 genes in Xenopus ectoderm. Development 132: 2355 – 2363

Sauka-Spengler T, Meulemans D, Jones M, Bronner-Fraser M (2007) Ancient evolutionary origin of the neural crest gene regulatory network. Dev Cell 13: 405 – 420

Sauka-Spengler T, Bronner-Fraser M (2008) A gene regulatory network orchestrates neural crest formation. Nat Rev Mol Cell Biol 9: 557 – 568

Schilling TF, Walker C, Kimmel CB (1996) The chinless mutation and neural crest cell interactions in zebrafish jaw development. Development 122: 1417 – 1426

Schwarz JM, Cooper DN, Schuelke M, Seelow D (2014) MutationTaster2: mutation prediction for the deep-sequencing age. Nat Methods 11: 361 – 362

Sedano HO, Cohen MM Jr, Jirasek J, Gorlin RJ (1970) Frontonasal dysplasia. J Pediatr 76: 906 – 913

Shah AN, Davey CF, Whitebirch AC, Miller AC, Moens CB (2016a) Rapid reverse genetic screening using CRISPR in zebrafish. Zebrafish 13: 152 – 153

Shah AN, Moens CB, Miller AC (2016b) Targeted candidate gene screens using CRISPR/Cas9 technology. Methods Cell Biol 135: 89 – 106

Shihab HA, Gough J, Mort M, Cooper DN, Day IN, Gaunt TR (2014) Ranking non-synonymous single nucleotide polymorphisms based on disease concepts. Hum Genomics 8: 11

Sievers F, Wilm A, Dineen D, Gibson TJ, Karplus K, Li W, Lopez R, McWilliam H, Remmert M, Soding J et al (2011) Fast, scalable generation of high quality protein multiple sequence alignments using Clustal Omega. Mol Syst Biol 7: 539

Simoes-Costa M, Bronner ME (2015) Establishing neural crest identity: a gene regulatory recipe. Development 142: 242 – 257

Smith JD, Hing AV, Clarke CM, Johnson NM, Perez FA, Park SS, Horst JA, Mecham B, Maves L, Nickerson DA et al (2014) Exome sequencing identifies a recurrent de novo ZSWIM6 mutation associated with acromelic frontonasal dysostosis. Am J Hum Genet 95: 235 – 240

Stuhlmiller TJ, Garcia-Castro MI (2012) Current perspectives of the signaling pathways directing neural crest induction. Cell Mol Life Sci 69: 3715 – 3737

Tchieu J, Zimmer B, Fattahi F, Amin S, Zeltner N, Chen S, Studer L (2017) A modular platform for differentiation of human PSCs into all major ectodermal lineages. Cell Stem Cell 21: 399 – 410

Trainor PA, Sobieszczuk D, Wilkinson D, Krumlauf R (2002) Signalling between the hindbrain and paraxial tissues dictates neural crest migration pathways. Development 129: 433 – 442

Tribulo C, Aybar MJ, Nguyen VH, Mullins MC, Mayor R (2003) Regulation of Msx genes by a Bmp gradient is essential for neural crest specification. Development 130: 6441 – 6452

Twigg SR, Kan R, Babbs C, Bochukova EG, Robertson SP, Wall SA, Morriss-Kay GM, Wilkie AO (2004) Mutations of ephrin-B1 (EFNB1), a marker of tissue boundary formation, cause craniofrontonasal syndrome. Proc Natl Acad Sci USA 101: 8652 – 8657

Twigg SR, Versnel SL, Nurnberg G, Lees MM, Bhat M, Hammond P, Hennekam RC, Hoogeboom AJ, Hurst JA, Johnson D et al (2009) Frontorhiny, a distinctive

presentation of frontonasal dysplasia caused by recessive mutations in the ALX3 homeobox gene. Am J Hum Genet 84: 698 – 705

Ullah A, Kalsoom UE, Umair M, John P, Ansar M, Basit S, Ahmad W (2016) Exome sequencing revealed a novel splice site variant in the ALX1 gene underlying frontonasal dysplasia. Clin Genet 91: 494 – 498

Umm-e-Kalsoom BS, Kamran-ul-Hassan Naqvi S, Ansar M, Ahmad W (2012) Genetic mapping of an autosomal recessive postaxial polydactyly type A to chromosome 13q13.3–q21.2 and screening of the candidate genes. Hum Genet 131: 415 – 422

Uz E, Alanay Y, Aktas D, Vargel I, Gucer S, Tuncbilek G, von Eggeling F, Yilmaz E, Deren O, Posorski N et al (2010) Disruption of ALX1 causes extreme microphthalmia and severe facial clefting: expanding the spectrum of autosomal-recessive ALX-related frontonasal dysplasia. Am J Hum Genet 86: 789 – 796

Varshney GK, Sood R, Burgess SM (2015) Understanding and editing the zebrafish genome. Adv Genet 92: 1 – 52

Varshney GK, Zhang S, Pei W, Adomako-Ankomah A, Fohtung J, Schaffer K, Carrington B, Maskeri A, Slevin C, Wolfsberg T et al (2016) CRISPRz: a database of zebrafish validated sgRNAs. Nucleic Acids Res 44: D822 – D826

Wada N (2005) Hedgehog signaling is required for cranial neural crest morphogenesis and chondrogenesis at the midline in the zebrafish skull. Development 132: 3977 – 3988

Wang Y, Hong S, Li M, Zhang J, Bi Y, He Y, Liu X, Nan G, Su Y, Zhu G et al (2013) Noggin resistance contributes to the potent osteogenic capability of BMP9 in mesenchymal stem cells. J Orthop Res 31: 1796 – 1803

Wieland I, Jakubiczka S, Muschke P, Cohen M, Thiele H, Gerlach KL, Adams RH, Wieacker P (2004) Mutations of the ephrin-B1 gene cause craniofrontonasal syndrome. Am J Hum Genet 74: 1209 – 1215

Wu YQ, Badano JL, McCaskill C, Vogel H, Potocki L, Shaffer LG (2000) Haploinsufficiency of ALX4 as a potential cause of parietal foramina in the 11p11.2 contiguous gene-deletion syndrome. Am J Hum Genet 67: 1327 – 1332

Wuyts W, Cleiren E, Homfray T, Rasore-Quartino A, Vanhoenacker F, Van Hul W (2000) The ALX4 homeobox gene is mutated in patients with ossification defects of the skull (foramina parietalia permagna, OMIM 168500). J Med Genet 37: 916 – 920

Zhao GQ, Eberspaecher H, Seldin MF, de Crombrugghe B (1994) The gene for the

homeodomain-containing protein Cart-1 is expressed in cells that have a chondrogenic potential during embryonic development. Mech Dev 48: 245 – 254

Zhao Q, Behringer RR, de Crombrugghe B (1996) Prenatal folic acid treatment suppresses acrania and meroanencephaly in mice mutant for the Cart1 homeobox gene. Nat Genet 13: 275 – 283